Optimizing Battery Use for a More Sustainable Energy System

by

Joonho Bae

A dissertation submitted in partial fulfillment
of the requirements for the degree of
Doctor of Philosophy
(Business Administration)
in the University of Michigan
2026

Doctoral Committee:

Professor Roman Kapuscinski, Co-Chair
Assistant Professor John Silberholz, Co-Chair
Professor Xiuli Chao
Associate Professor Eric Schwartz

Joonho Bae
baejh@umich.edu
ORCID iD: 0000-0002-0836-8083

© Joonho Bae 2026

ACKNOWLEDGEMENTS

This dissertation marks an opportunity to reflect on and bring closure to more than six years of my doctoral journey. From settling in Ann Arbor in 2019 to beginning a new chapter in Indiana in 2025, this journey would not have been possible without the unwavering support, guidance, and encouragement of my advisors, as well as the friendship and love of my friends and family.

First and foremost, I would like to express my deepest gratitude to my advisors, Dr. Roman Kapuscinski and Dr. John Silberholz. I still vividly remember my one-on-one admissions interview with Roman in the winter of 2019, during which we spoke for over an hour. The strong positive impression I had from that meeting led me to choose Roman as my advisor, a decision that I now consider one of the best I made during my PhD. Despite his busy schedule, he always made time for me—often meeting late into the evening—and for that I am truly grateful. His relentless curiosity and passion for research will remain a guiding motto throughout my academic career. While rigorous in his expectations, he consistently showed deep care for my personal well-being and my family, which I sincerely appreciate.

John, without you, I am confident that I would not be where I am today. You taught me, step by step, how to conduct research—from the smallest details to the broader vision—and in doing so, you shaped me into the scholar I have become. I truly believe that I found the best mentor possible at Michigan. As I have shared with you on several occasions, your influence extends far beyond research. Your perspective on life, and especially your priceless advice on finding joy and meaning as a father to Jared and Rodney, has had a profound and lasting impact on me.

I am also deeply grateful to my wonderful cohort: Zijin (Jean), Fan, and Clare. From the moment we first met in August 2019, we shared countless memories—celebrating after exams, sharing office space and everyday conversations, attending classes together, and supporting one another through the challenges of the pandemic. I feel incredibly fortunate to have grown alongside you and to begin our careers as researchers at the same time. I am proud that ours was not only the largest cohort at Ross, but also one of the closest-knit.

My deepest gratitude goes to my family. I am profoundly thankful to my parents and my parents-in-law for repeatedly traveling to the United States and providing tremendous

support with childcare, which allowed me to focus on my research. Being able to share good news with them brings me great joy. Among the happiest moments of my doctoral journey were the births of my two sons, Jared and Rodney. The memories of raising them in Northwood Housing will remain with me forever. Thank you for coming into my life as healthy and warm-hearted boys.

Finally, I extend my heartfelt thanks to my beloved wife, Kyungjin (Jinny). Thank you for being my greatest source of comfort and my best friend throughout this journey. I am deeply grateful for your love and support, and I love you more than words can express.

TABLE OF CONTENTS

ACKNOWLEDGEMENTS ii

LIST OF FIGURES vi

LIST OF TABLES x

LIST OF APPENDICES xi

ABSTRACT xii

CHAPTER

1 Introduction 1

2 Cost-Saving Synergy: Energy Stacking in Battery Energy Storage Systems 5

2.1 Introduction 5
2.1.1 Results and Contributions 8
2.2 Literature Review 9
2.2.1 Energy Storage Research in Operations Management 9
2.2.2 Stacking 9
2.3 The Preliminaries 10
2.3.1 Key Services: Arbitrage and Frequency Regulation 11
2.3.2 Battery Degradation Cost 12
2.4 Model 14
2.4.1 Cost of Degradation 17
2.4.2 Formulation 18
2.5 Properties 19
2.5.1 Stacking 20
2.6 Generalizations/Extensions 25
2.6.1 Correlated Prices 25
2.6.2 Operations with Energy Loss: Round-Trip Energy Efficiency (η^2) . 27
2.6.3 Non-Uniform Regulation Signal 30
2.6.4 Power Capacity is Binding 32
2.6.5 Summary of the Generalizations and Extensions 34
2.7 Closing Remarks 36

3 Dynamic Valuation of A Battery Under Performance Degradation . . . 37

3.1 Introduction . . . 37
3.2 Background and Setting . . . 41
3.2.1 Battery Application: (Day-Ahead) Energy Arbitrage . . . 41
3.2.2 Battery Performance Degradation . . . 41
3.2.3 Commonly-Used Heuristics . . . 43
3.3 Literature Review . . . 45
3.3.1 Degradation-Aware Models in OR/MS: Machine Replacement and Non-Renewable Resource Extraction . . . 46
3.3.2 Optimal Control of (Battery) Energy Storage . . . 47
3.4 Optimal Control Problem . . . 49
3.4.1 Capacity-Degradation-Only . . . 49
3.4.2 Unified Model (In the Presence of Efficiency Degradation) . . . 58
3.5 Generalization/Extension . . . 67
3.5.1 Alternative Degradation Functions . . . 67
3.5.2 Multiple Prices . . . 68
3.5.3 Summary of Generalization . . . 69
3.6 Numerical Study . . . 70
3.6.1 Calibration of Model Parameters with Data . . . 70
3.6.2 Effect of Grid/Market Environments . . . 70
3.6.3 How Costly Ignoring Efficiency Degradation Can Be? . . . 72
3.7 Conclusion . . . 74

4 Choice of Battery Portfolios and Benefits of Heterogeneity . . . 76

4.1 Introduction and Literature Review . . . 76
4.2 Preliminaries for the Model . . . 81
4.2.1 Renewable-plus-Storage with PPA . . . 81
4.2.2 Battery Performance Degradation . . . 82
4.3 Model . . . 83
4.3.1 Optimal Control Problem (Profit Maximization) . . . 85
4.3.2 Dynamic Program for Numerical Exploration . . . 86
4.3.3 Numerical Experiments . . . 88
4.4 The Protection Effect . . . 95
4.4.1 Deterministic Setting: Characterizing Preferred Workload Trajectories 95
4.4.2 Stochastic Setting: Even Workload Allocation under Unbalanced Workloads . . . 97
4.4.3 Static Analytical Model for Stochastic Setting . . . 98
4.5 Future Directions and Concluding Remarks . . . 101

APPENDICES . . . 104

BIBLIOGRAPHY . . . 255

LIST OF FIGURES

FIGURE

1.1 Dissertation structure. 2

2.1 Different strategies to use a battery — (a): arbitrage alone; (b): arbitrage with frequency regulation during the otherwise idle periods (time-exclusive stacking); and (c): combined arbitrage and regulation throughout the day (simultaneous stacking). 6

2.2 A simple illustration of rainflow-counting algorithm (Example B.44) 14

2.3 SOC profiles of arbitrage (top), regulation (middle), and stacking (bottom), where the stacking profiles are established by superimposing the arbitrage and regulation profiles. 17

2.4 Comparative statics: optimal stacking actions in Theorem 2.1 ($T = 24,\ T_H = 8,\ c_0^b = 100,\ E = 1$). 23

2.5 $S = \frac{\Pi^*_{stk}}{\max(\Pi^*_{arb}, \Pi^*_{reg})}$ over different service price ratios $\frac{p^a}{p^r}$ ($T = 18$). 25

2.6 Stacking's energy flow with round-trip efficiency $\eta^2 \in [0, 1]$. 27

2.7 Stacking performance with energy loss ($T = 16, T_H = 4, \bar{p} = 100, \underline{p} = 30, p^r = 12, c_0^b = 160$). 30

2.8 Illustration of optimal stacking for inefficient batteries when $p^r < \underline{p}$: green (free regulation; $a_H^* > 0,\ x_L^* = x_H^* = 0$), black (no battery use), red (regulation only; $a_H^* = 0$), and gray (excess regulation; $a_H^* > 0,\ x_L^* > 0$ and/or $x_H^* > 0$). Parameters: $T_L = 16,\ T_H = 4, \underline{p} = 20,\ p^r = 10$, and $c_0^b = 160$, with η and p^a varied. 31

2.9 Stacking's performance with power binding ($P < \infty$) versus power not binding ($P = \infty$). (a): $P/E = 0.25$ (blue), $c_0^b = 100, \frac{T_H}{T} = \frac{1}{24}$, (b): $P/E = 0.15$ (blue), $c_0^b = 100, \frac{T_H}{T} = \frac{1}{8}$. 34

3.1 Two types of battery performance degradation: (a) Energy capacity degradation—a reduction in the maximum amount of energy a battery can store; and (b) Energy efficiency degradation—a decrease in the amount of retrievable energy per unit of energy charged. 38

3.2 Illustration of Observation 3.1. (a) Discounted: $\delta = 0.02$ ($t_A = 82.75$); (b) Undiscounted: $\delta = 0$ ($t_A = 86.13$). Other parameters: $\bar{p} = 40,\ \underline{p} = 10,\ k = 0.05,\ x_0 = 1,\ T = 100$. 52

3.3 Comparison of the fixed-DOD heuristic and the optimal policy. (a) $T = 30$ ($\bar{u} = 0.91$); (b) $T = 100$ ($\bar{u} = 0.50$). Other parameters: $\bar{p} = 40,\ \underline{p} = 10,\ k = 0.05,\ x_0 = 1,\ \delta = 0$. 56

3.4 Performance of the fixed-DOD heuristic: Illustration of the worst-case performance across a range of power function exponents $\beta \geq 1$ (Corollary B.2). $\min S(\beta) \approx 0.898$ is achieved at $\beta \approx 1.64$ (dashed line). 57
3.5 Motivating example: Comparison of the full DOD and optimal policies. Under the optimal policy, $x^*(T) = 0.57 > 0.35 = \underline{x}, E^*(T) = 0.39 > 0.07 = \underline{E} := \frac{\underline{x}-\alpha_0}{\alpha_1}$, and the revenue ratio is $S = \frac{R^{DOD}_{cum}}{R^*_{cum}} = 0.62$. The following parameters are used: $\alpha_1 = 0.7, \alpha_0 = 0.3, k = 0.1, \bar{p} = 80, \underline{p} = 10$, $\delta = 0$, and $T^s = 25.70$. 60
3.6 Strictly reduced utilization in the presence of efficiency degradation (Corollary 3.4). Battery 1's efficiency x_1 is fixed at 0.875. For Battery 2, its efficiency $x_2(t)$ evolves as follows: (a) $x_2(t) \in [0.9, 1]$ (i.e., $x_2(t) > x_1$ for all t) with $\alpha_1 = 0.1$ and $\alpha_0 = 0.9$; (b): $x_2(t) \in [0.87, 1]$ with $\alpha_1 = 0.2$ and $\alpha_0 = 0.8$. Other parameters are: $\bar{p} = 40, \underline{p} = 30, k = 1$, with $\delta = 0.6$ for (a) and $\delta = 2$ for (b). 65
3.7 Optimal system dynamics under multiple prices (Theorems B.8 and B.10): (a) capacity degradation only ($\alpha_1 = 0$), and (b) unified degradation ($\alpha_1 = 0.4$). Other parameters: $\underline{p}_1 = 42,\ \bar{p}_1 = 79,\ \underline{p}_2 = 57,\ \bar{p}_2 = 152,\ p_1 = 0.62, \delta = 0.02, k = 0.05, T = 120$. 71

4.1 Illustration of a battery energy storage system: (a) homogeneous system, composed of identical packs (and cells), and (b) hybrid system, composed of two different pack types (Cell A and Cell B). Reproduced from [22]. 77
4.2 Stationary deterministic workload: $d_H(t) = 1, p_H(t) = 1$ for all t. 90
4.3 Illustration of the CAISO duck curve: (a) net load and (b) average hourly price [27]. 91
4.4 Illustration of "High" and "Low" days: (a) daily solar generation and (b) average hourly capacity factors. 93
4.5 Stationary stochastic workload. 93
4.6 Non-stationary deterministic workload: $d_H(t) = 1.1 - 0.2t$. 94

A.1 Illustration of Theorem 2.1 – The shaded region denotes the optimal excess regulation: $x^* = 0$ (orange) and $x^* > 0$ (blue). Energy capacity is binding on the red line and above for stacking (solid) and standalone arbitrage (dashed). . . . 114
A.2 Illustration of Theorem A.1 – The shaded region denotes the optimal excess regulation: $x^*_H > x^*_L > 0$ (green), $x^*_H = x^*_L = 0$ (orange), and $x^*_H = x^*_L > 0$ (blue). Energy capacity is binding on the red line and above for stacking (solid) and standalone arbitrage (dashed). 124
A.3 Illustration of Corollary A.4: (a) $A^*_{stk} > A^*_{arb}$ (blue), $R^*_{stk} > R^*_{reg}$ (yellow), (b) positive cost-saving (orange), (c) $\Pi^*_{stk} > \Pi^*_{arb} + \Pi^*_{reg}$ (purple). Adapted from Figure 2.8 (green: free regulation; black: no battery use; red: regulation-only; gray: excess regulation). 141
A.4 Illustration of Theorem A.5 – Colors denote discrete regions: $A^* = 0$ (green), $A^* > 0,\ x^* = 0$ (orange), and $A^* > 0,\ x^* > 0$ (blue). Energy capacity is binding on the red line and above for stacking (solid) and standalone arbitrage (dashed). The subregion within the blue dashed lines denotes where $A^*_{stk} < A^*_{arb}$. 143

A.5 Illustration of Lemma A.5. The colored regions denote $x_L^* = x_H^* > 0$ (pink), $x_L^* = x_H^* = 0$ (gray), and $x_L^* > x_H^*$ (white). $A_1 = (\frac{T_H}{T}, \frac{T_H(T-2)}{T})$, $A_2 = (\frac{T_H}{T_L}, T_H)$, $A_3 = \Big\{(\frac{2T_H}{T_L}, 2T_H),\ T_L \geq 2T_H(1, T_L),\ T_L \leq 2T_H \quad$, $A_4 = (1, 0)$ where $T_L = 20, T_H = 8$ and $T_L = 20, T_H = 12$ are used for (a) and (b), respectively. 148

A.6 Illustration of Proposition A.1. The shaded regions denote $x_L^* = x_H^* > 0$ (pink), $x_L^* = x_H^* = 0$ (gray), and $x_L^* > x_H^*$ (white). The subregions within colored lines denote where each property holds: $A_{stk}^* > A_{arb}^*$ (red), $R_{stk}^* > R_{reg}^*$ (yellow), $\frac{R^*}{A^*} \geq 2$ (blue), positive cost-saving (orange), and superlinear profit (purple). . . 152

A.7 Illustration of optimal battery operations ($T_L \geq 2T_H$). Power is unconstrained within the yellow line, power is constrained in both time periods within the green line, and otherwise, power is constrained only in the high-price period. Energy is constrained within the red line. Maximum free regulation is used in both time periods within the black dashed area. The blue area denotes regulation alone ($A^* = 0$). $T_L = 20$ and $T_H = 8$ are used. 154

A.8 Illustration of the optimal battery operation ($T_L < 2T_H$). Power is unconstrained within the yellow line, power is constrained in both time periods within the green line, and otherwise, power is constrained only in the high-price period. Energy is constrained within the red line. Maximum free regulation is used in both time periods within the black dashed area. The blue area denotes regulation alone ($A^* = 0$). $T_L = 20$ and $T_H = 14$ are used. 155

A.9 Illustration of Propositions A.1 – A.2 ($T_L \geq 2T_H$). The limited energy capacity shifts the range where each of the properties holds, as seen by comparing the regions in solid lines ($E/P < \frac{T_H}{2}$) and the regions in dotted lines (unconstrained setting). Colors denote properties $A_{stk}^* > A_{arb}^*$ (red), $R_{stk}^* > R_{reg}^*$ (yellow), positive cost-saving (orange), and superlinear profit (purple). Energy is constrained within the black dashed line for the $E/P < \frac{T_H}{2}$ case. 156

A.10 Comparative statics (p^a effect). The backgrounds for $x_L^* = x_H^* > 0, x_L^* = x_H^* = 0$, and $x_L^* > x_H^* > 0$ are colored pink, gray, and white, respectively, and the dotted vertical lines show when the power capacity starts to bind in the high-price (left vertical line) and low-price (right vertical line) regions ($T_H = 8, T = 24, E = 2$). 163

A.11 Comparative statics (c_0^b effect). The backgrounds for $x_L^* = x_H^* > 0, x_L^* = x_H^* = 0$, and $x_L^* > x_H^* > 0$ are colored pink, gray, and white, respectively, and the dotted vertical lines show when the power capacity starts to bind in the high-price (left vertical line) and low-price (right vertical line) regions. 164

A.12 Stacking performance under the two misspecified models ($\rho_0 = \frac{\Pi_{no}^*}{\Pi_{quad}^*}, \rho_1 = \frac{\Pi_{lin}^*}{\Pi_{quad}^*}$). (a): $E = 1, P = 2, p^r = 10, p^a = 80, c_0^b = 150, c_{lin}^b = 75$, (b): $E = 1, P = 2, T_H = 4, T = 10, p^r = 20, c_0^b = 150, c_{lin}^b = 75$, (c): $E = 1, P = 0.25, T_H = 12, T = 40, p^r = 10, p^a = 60$, and $l = 0.5$ are used as parameters. 167

A.13 Day-ahead (hourly) energy and regulation prices: (top) summer, (bottom) winter. Gray lines represent realized price patterns. The blue solid line and blue region specify the average prices and confidence interval, respectively (source: [135]). 169

A.14 Regulation signals and the corresponding net energy change under a unit capacity commitment: (top) ISO-NE trinary; (middle) ISO-NE continuous; (bottom) PJM regD. 170
A.15 Illustration of actual dispatching profile: each row sequentially represents arbitrage-only, regulation-only, time-exclusive stacking, and simultaneous stacking. The left, middle, and right columns represent the SOC levels (three realizations), provision rates for arbitrage/regulation, and the histogram of DOD sizes (the number of half cycles) from the rainflow counting algorithm for the blue realization of the regulation signal, respectively. 175
A.16 Power and energy utilization density plot for Table A.10 under different degradation exponents $\beta = 1.7, 2.0, 2.3$. 178
A.17 Stacking's relative profit $S = \frac{\Pi^*_{stk}}{\max(\Pi^*_{arb}, \Pi^*_{reg})}$ with various grid/market environments. The NYISO 2021 – 2022 dataset (winter) is used. Other parameters are summarized in Table A.9. The p^r multiplier in pane (a) operates by multiplying historical regulation prices by some constant value while keeping historical energy prices fixed. The energy neutrality guarantees $2\Delta^c$ in pane (b) is varied by assuming the regulation signal is updated every $(4 \times \Delta)$ seconds for $\Delta = \{1/i | i = 1, \cdots, 8\}$ while using the historical regulation signal. 181
A.18 Stacking's relative profit $S = \frac{\Pi^*_{stk}}{\max(\Pi^*_{arb}, \Pi^*_{reg})}$ with various battery types. $\beta = 2, \eta^2 \in [0.72, 1]$, and the NYISO 2021 – 2022 price dataset (winter) are used. Other parameters are summarized in Table A.9. $N \in [100, 4000]$ indicates the battery's remaining cycle count, while $P/E \in [0.125, 2.5]$ indicates the battery's power-to-energy ratio. 183

B.1 Different performance degradation patterns 188
B.2 Experimental/empirical evidence on the linear relationship between ΔE and Δx. 190
B.3 Figures for the proof of Lemma 3.2 201
B.4 Optimal system dynamics under multiple prices (Theorems B.8 and B.10): (a) capacity degradation only ($\alpha_0 = 1, \alpha_1 = 0$), and (b) unified degradation ($\alpha_0 = 0.3, \alpha_1 = 0.7$). Other parameters: $\bar{p}_1 = 80, \bar{p}_2 = 120, \underline{p} = 40, p_1 = p_2 = 1/2, \delta = 0.03, k = 0.07, T = 120$. 244
B.5 Illustration of the optimal dynamic policy versus the optimal fixed-A heuristic. $T = 100, \delta = 0.03, \alpha_1 = 0.3, \underline{p} = 40, \bar{p} = 100$. 246

LIST OF TABLES

TABLE

2.1 Optimal stacking. 21
2.2 Key properties under the generalizations considered when c_0^b is sufficiently large. 35

3.1 Related literature: Modeling battery performance degradation. 45
3.2 Capacity-degradation-only (Finite horizon). 51
3.3 Sensitivity analysis (Corollary 3.3). For the degradation intercept α_0, we vary its value while keeping $\alpha_0 + \alpha_1$ fixed, thereby maintaining the same initial battery efficiency ($x_0 = \alpha_0 + \alpha_1$). 64
3.4 Summary of the model parameters used in Section 3.6. 70
3.5 Comparison of lifelong revenue ratios under different benchmark models and parameter settings. (a) $\underline{p}_1 = 54, \bar{p}_1 = 79, \underline{p}_2 = 63, \bar{p}_2 = 151, p_1 = 0.63$, (b) $\underline{p}_1 = 58, \bar{p}_1 = 82, \underline{p}_2 = 61, \bar{p}_2 = 124, p_1 = 0.71$. Other parameters used: $T = 120,\ k = 0.07,\ \delta = 0.01$. 73

4.1 Degradation functions in the industry and literature 90

A.1 Degradation functions in the industry and literature 106
A.2 Optimal stacking (correlated prices). 123
A.3 Optimal degradation cost $deg(A, X)$. 132
A.4 Optimal standalone regulation. 134
A.5 Optimal stacking with energy loss. 135
A.6 Optimal stacking (trinary signal). 142
A.7 Properties of the optimal power-constrained solution for fixed arbitrage amount A when $T_L > T_H$. 150
A.8 Key properties under the extensions considered (when c_0^b is sufficiently large). . 168
A.9 Summary of the model parameters used in Appendix A.4. 174
A.10 Sensitivity analysis: NYISO dataset ($\eta^2 = 0.8$) 184
A.11 Profitability analysis: NYISO dataset ($\eta^2 = 0.7$) 185

B.1 Capacity-degradation-only (finite horizon). 194
B.2 Capacity-degradation-only (finite horizon; $\beta > 1$) 217

LIST OF APPENDICES

A Proofs in Chapter 2 . . . . . **104**

Justifications of Key Assumptions 104
Proofs of Statements (Main) 112
Generalizations/Extensions and Proofs 123
Numerical Results 169

B Proofs in Chapter 3 . . . . . **186**

Empirical Evidence of Performance Degradation 186
Proofs of Statements (Main) 190
Generalization/Extension 215
Additional Numerical Results 245

C Proofs in Chapter 4 . . . . . **247**

Proof of Statements (Main) 247

ABSTRACT

Battery Energy Storage Systems (BESS) play a crucial role in integrating renewable energy into sustainable grid systems. This dissertation aims to optimize BESS operational policies to enhance profitability. In the first chapter, I investigate energy stacking, a strategy providing multiple services from a single BESS. While existing literature identifies scenarios where stacking can be numerically shown to enhance profitability, the precise mechanism remains unclear—despite boosting revenue, stacking may accelerate battery wear due to increased usage compared to a single service. I use a theoretical framework, as opposed to scenario-based approaches, to explain the source of this boost in profitability. Using two popular battery services, this research establishes the mechanism I refer to as "*cost-saving synergy,*" whereby a battery can provide multiple services simultaneously (increasing revenue) with limited increases in costs (energy losses plus wear and tear), and demonstrates its impact on profitability. The second chapter focuses on dynamically managing battery operations throughout their lifespan, considering different types of battery degradation (energy capacity degradation and energy efficiency degradation). Due to the complexities involved in modeling these trade-offs, a significant portion of existing research relies on naive heuristics, without conducting a systematic profitability analysis. This essay develops an analytical framework for studying the optimal dynamic policy that accounts for both capacity and efficiency degradation and provides practical heuristics with performance guarantees. In the third essay, I explore the benefits of hybrid battery systems, considering rapid technological advancements and the growing availability of batteries. This essay establishes the mechanism I refer to as the "*protection effect,*" whereby a hybrid portfolio can improve profits (relative to a homogeneous portfolio) by allocating work across batteries based on their degradation patterns, which are driven by battery chemistry. Under this mechanism, the "more convex" battery is assigned a workload that maximizes its energy revenue (or minimizes degradation and energy loss), while the remaining work is handled by the "less convex" battery, which is more flexible with respect to its workload pattern. I use stylized models to analytically characterize the "preferred trajectories" through which a hybrid system improves overall profit. I systematically highlight the advantages of diversification within battery portfolios and establish guiding principles for decision-making in this evolving landscape.

CHAPTER 1

Introduction

The global transition toward low-carbon energy systems has accelerated in recent years, driven by growing concerns over climate change, policy mandates, and technological advancements. Renewable energy sources, such as solar and wind, offer promising, cleaner alternatives for our energy systems. Nevertheless, the increased use of these resources amplifies existing challenges faced by electrical grids due to their intermittent nature; they generate electricity only when the sun is shining or the wind is blowing. This on-and-off pattern complicates grid reliability and the alignment of power supply with demand.

Battery Energy Storage Systems (BESS) offer a potential solution to mitigate several of these challenges by enabling the storage of electricity generated at one time for later use. Consequently, BESS have been recognized as a crucial component in integrating renewable energy into the grid. However, despite their immense potential, batteries often remain unprofitable [111]. A key driver of this challenge is the high upfront capital cost combined with limited operational lifespans, which together make it difficult to recover these investments. This economic barrier poses a significant obstacle to the widespread adoption of BESS.

Battery degradation plays a central role in this challenge. It is an irreversible process that reduces battery performance over time and is strongly influenced by the intensity and patterns of charging and discharging. As a result, operational decisions directly affect long-term costs. In particular, when a battery is deployed for a single service, the resulting degradation costs can be substantial—often comparable to, or even exceeding, the revenue generated from that service. This imbalance underscores the need for more efficient operational strategies.

In my dissertation, I conduct a series of studies focused on optimizing BESS usage, as illustrated in Figure 1.1, with the aim of increasing profitability. The first essay (Chapter 2) introduces an analytical framework exploring energy stacking. Stacking leverages a single BESS to offer multiple grid services, such as arbitrage and frequency regulation. Arbitrage involves buying energy at a low price and selling at a high price, while frequency regulation corrects short-term imbalances between supply and demand. While existing literature identifies scenarios where stacking can be numerically shown to enhance profitability, the precise

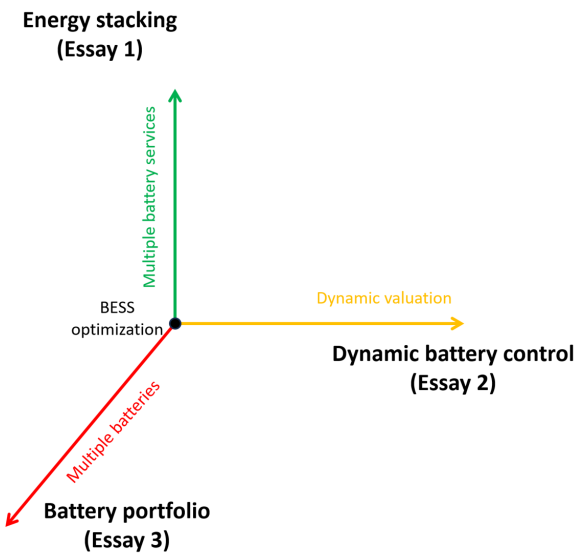


Figure 1.1: Dissertation structure.

mechanism remains unclear—despite boosting revenue, stacking may accelerate battery wear due to increased usage compared to a single service. I use a theoretical framework, as opposed to scenario-based approaches, to explain the source of this boost in profitability. Using two popular battery services, I analytically show that there often exists *cost-saving synergy* — the cost of performing both services at the same time (simultaneous stacking) is smaller than the sum of individual costs if I had performed each service alone — which allows for *bigger profits*. Under this synergy, the provision of one service creates incentives to increase the use of the other service. I show that (1) the optimal quantity of each service is increasing in both service prices, (2) stacking always increases the optimal service quantities relative to standalone operations, and (3) it is always optimal to provide both services jointly. I further analyze the benefits of simultaneous stacking under various grid and market conditions and characterize the conditions under which these benefits are larger or smaller. I also derive a theoretical upper bound on its profitability, showing that stacking can approximately double the profit of the best standalone service. I explore several generalizations of the base model, including inefficient batteries (energy loss) and correlated service prices. Not only do the main insights continue to hold under these extensions, but in several realistic cases, stacking's benefits become even more pronounced.

The second essay (Chapter 3) expands the first essay by introducing an analytical model designed to investigate the dynamic utilization of batteries over their operational lifespan. Specifically, the models capture two distinct types of battery performance degradation: *energy capacity degradation* and *energy efficiency degradation*. As a battery undergoes these

forms of degradation, its operation should be adjusted accordingly. An ideal policy must balance immediate revenues, achieved through intensive battery usage, against future opportunities that arise from more economical usage later on. Due to the complexities involved in modeling these trade-offs, a significant portion of existing research relies on naive heuristics. Common examples include amortizing battery replacement costs or even disregarding usage costs entirely, without conducting a systematic profitability analysis. This essay develops an analytical framework for studying the optimal dynamic policy that accounts for both capacity and efficiency degradation. To highlight the significance of capturing efficiency degradation, I compare two settings: in the first model, I assume capacity degradation only, while the second model allows for the presence of efficiency degradation. I demonstrate a structural and systematic difference in optimal behavior over time. For instance, under capacity degradation only, battery utilization under the optimal policy increases monotonically over time. In contrast, when efficiency degradation is present, optimal utilization may decline over the battery's lifetime, highlighting when and why commonly used heuristics can lead to severe suboptimality. Given the popularity of heuristics and the absence of theoretical or systematic evaluations of their performance, I investigate when and where heuristic policies exhibit small or large suboptimality. I show that, while a well-calibrated heuristic is optimal under certain scenario, its performance can be disappointing in more realistic settings. I analytically derive its worst-case performance under a finite-horizon, capacity-degradation-only model (90.25% of optimal revenue) and numerically show diminished performance under an infinite-horizon model that also includes efficiency degradation. Also, this work shows that simple policies can still perform effectively; for example, in an undiscounted setting, a fixed-revenue policy is optimal. I derive managerial implications by examining how different battery types and operating environments influence utilization and cumulative revenue. I further show that a battery experiencing both capacity and efficiency degradation always operates at a strictly lower utilization than one facing only capacity degradation, regardless of parameterization. In addition, I extend our models to incorporate multiple energy prices and alternative forms of degradation functions, finding that the overall insights remain robust.

The third essay (Chapter 4) explores the benefits of diversifying battery portfolios. With rapid technological advancements and the growing availability of batteries, including those retired from electric vehicles, operators have the opportunity to invest in hybrid energy storage systems, which combine different battery chemistry, sizes, efficiencies, etc. Unlike prior justifications for hybrid systems, which rely on budget constraints, differentiated physical capabilities, environmental effects, C-rate effects, or peak capacity, I show that profit improvements can arise purely from intrinsic differences in degradation convexity across batteries. I formally identify and characterize the *protection effect* as a distinct economic mechanism

underlying the value of hybrid battery portfolios. Under this mechanism, the "more convex" battery is assigned a workload which maximizes its energy revenue (or minimizes its degradation and energy loss), and the remaining work is handled by the "less convex" battery, which is more flexible with respect to its workload pattern. In particular, the "more convex" battery benefits from adopting an increasing workload over time and from evening out its cycle sizes between large and small workloads, whereas the "less convex" battery absorbs less favorable workload profiles—including decreasing patterns and uneven cycle sizes—to maximize overall portfolio performance. I quantify the economic value of the protection effect using an all-cost measure (defined as the sum of battery acquisition costs and the lost revenue due to degradation during charging and discharging) relative to a benchmark setting with efficiency degradation. Using parameters calibrated from data, this essay numerically explores a broad parameter space to assess the benefits of hybrid storage systems relative to homogeneous portfolios. I numerically evaluate cost savings under three settings: stationary deterministic workload, nonstationary deterministic workload, and stationary stochastic workload. Cost savings are below 4% under stationary deterministic workloads, but increase up to 3%–9% under nonstationary or stochastic workloads with realistic battery and market specifications. These results provide clear managerial guidance on when hybrid battery portfolios deliver the greatest value.

Collectively, these three essays contribute to our understanding of how to better manage these expensive yet valuable battery resources, with potential implications for increasing their use on the grid and enabling more renewable energy on the grid.

CHAPTER 2

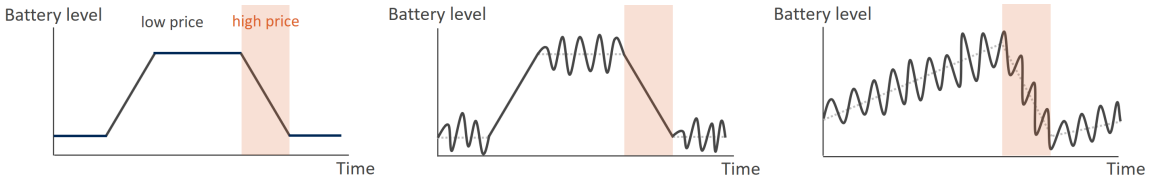
Cost-Saving Synergy: Energy Stacking in Battery Energy Storage Systems

2.1 Introduction

With uncertainty in both supply and demand for electricity, energy storage has been treated as an extremely desirable addition to the electrical grid. In reality, however, the actual volume of energy storage remains modest, mostly because of its high cost. Two elements have been gradually changing this situation: increased use of renewable energy resources and, while still very high, decreasing prices of batteries.

Renewable energy resources such as solar, wind, and hydropower are promising alternatives for a cleaner and more sustainable energy system. To accelerate investment in renewable energy sources, different forms of policies have been studied such as subsidies [102, 103, 9, 94], net metering/feed-in tariff [8, 67, 180], non-ownership business models [2], and various other mechanisms [3]. However, the increased use of renewable energy resources further increases existing challenges to electrical grids due to their intermittency — they produce electricity only when the sun shines or the wind blows. One challenge is short-term swings in energy supply, which make matching supply with demand more challenging and threaten grid reliability. Another challenge is various forms of misalignment between demand and supply, e.g., depressed energy prices during the peak hours of renewable availability (lots of wind power), which diminishes economic incentives for continued investment in renewable energy generation.[1] Clearly, energy storage can help address some of these issues by allowing electricity produced at one time to be stored for later use. As a result, energy storage has been described as a key ingredient needed to continue the trend of grid integration of renewable energy [93]. Though many forms of energy storage exist (e.g., pumped hydro, flywheels, thermal), battery energy storage systems (BESS) have been identified as one of

[1]Energy prices can become negative due to very high energy supply [215]. Intermittency can also drive up the price of electricity in the presence of forward contracts for energy [147].



(a) (b) (c)

Figure 2.1: Different strategies to use a battery — (a): arbitrage alone; (b): arbitrage with frequency regulation during the otherwise idle periods (time-exclusive stacking); and (c): combined arbitrage and regulation throughout the day (simultaneous stacking).

the most promising forms of storage due to their high efficiency, fast ramp rate (they can quickly change the charging/discharging rate), and decreasing costs due to research and development within the electric vehicle (EV) market.

Despite their promise, in 2024 BESS remain expensive and mostly unprofitable for standalone services. For instance, [110] states that batteries performing energy arbitrage alone (buying during low-price periods, selling during high-price periods, and remaining idle otherwise; Figure 2.1a) stand to make \$14–\$142 per kW-year for service provided, against a levelized cost of \$55–\$322 per kW-year. Similar claims of unprofitability of batteries are stated in [79] and [49].

The key cost component of using batteries is capital costs — not only are batteries expensive to buy, but they have limited lifespans due to capacity degradation. This capacity degradation has been studied extensively in the engineering literature, both in laboratory settings [51, 204] and using real-world evidence [57], showing that battery degradation is mostly due to how a battery is used. The key factor is the intensity and patterns of charging/discharging.[2] Interestingly, for a single service, capacity degradation costs are often high compared to the revenue gained from the corresponding service.

Given the potential benefits BESS have for the electrical grid and challenges due to the non-profitability of most standalone services, there has been growing interest in increasing profitability of batteries by providing two or more services with a single battery, which is labeled as energy stacking. However, the term "stacking" has been used in at least two ways, **time-exclusive** stacking and **simultaneous** stacking. Figure 2.1b illustrates time-exclusive stacking, where a battery provides two completely different services in different periods of time: a BESS that already provides the previously mentioned energy arbitrage service now also provides frequency regulation (a grid-stabilizing service that requires rapid battery charging/discharging) during times when the battery would otherwise be idle. Simultaneous

[2]A smaller (often negligible) amount of capacity degradation comes from aging (regardless of usage patterns).

stacking, illustrated in Figure 2.1c, occurs when the battery provides two or more services simultaneously, which significantly changes the economics of operating batteries.

Stacking has been referred to in many white papers and identified by industry reports as a key lever in achieving better profitability [110, 65]. Grid-scale battery projects like the Escondido energy storage project in California or the Hornsdale Power Reserve in Australia, the world's largest lithium-ion BESS projects, are reported to stack multiple services ([79, 160]). Companies such as Fluence and E3 have advertised their capabilities of boosting the profitability of a battery by simultaneously stacking services ([64, 49]).

Interestingly, despite the broad use of the term "stacking," most white papers and research articles studying the stacking of battery services provide limited or oversimplified explanations of the sources of stacking's benefits. Perhaps the most common simplification of stacking's benefits occurs when papers ignore the fact that battery costs raise with utilization, thereby assuming that increased revenue associated with providing two services, instead of one, leads to increased profitability, as well. A canonical example of this sort of reasoning is the influential *Lazard's Levelized Cost of Storage Analysis* annual industry report, which relies on the assumption of a fixed 10-year battery lifetime regardless of usage to conclude that stacking can enable batteries to reach profitability [110]. This sort of reasoning is common — many, if not most, of the papers that consider stacking treat battery costs as independent of usage patterns, as detailed in our Literature Review section. Clearly, such reasoning may break down under a more accurate accounting of battery costs. For instance, time-exclusive stacking may still be economically infeasible if the two services being combined are individually unprofitable, due to degradation costs exceeding the revenues from the services. In such a case, moving from one service (e.g. arbitrage alone in Figure 2.1a) to time-exclusive stacking (Figure 2.1b) can actually make battery operations *more unprofitable* — we have replaced the idle period with a period where costs exceed revenues.[3]

Given the societal importance of being able to profitably add storage to the electric grid coupled with the fact that even the most fundamental questions regarding the benefits of stacking battery services remain unanswered in the literature, it is unsurprising that [141] lists stacking as an area with some of the most important unanswered research questions related to the electric power industry for the operations management (OM) academy. In this work, we seek to make progress on these important questions using analytical modeling to establish general lessons about why and when stacking works, focusing on standard battery operations and using state-of-the-art models of usage-based battery degradation.

[3] [133] raises a similar issue — even if a BESS is technically capable of providing multiple services, the additional cycling of the battery (charging and discharging) may degrade the battery and shorten its lifetime and economic viability.

2.1.1 Results and Contributions

We consider stacking day-ahead (forward) arbitrage and frequency regulation, two of the most commonly provided services by large-scale battery deployments [54]. The periods of time when these services are offered may partially (or completely) overlap. We focus on a profit-maximizing decision-maker (battery farm owner) balancing the quantity of grid services provided and, therefore, the revenue obtained, with degradation costs that are a key factor hampering profitability. We assume the decision-maker is a price-taker, reflecting the reality that almost all batteries participate in markets as price-takers, primarily relying on historical prices (Appendix A.1.3). The degradation is described in a manner consistent with engineering literature. To the best of our knowledge, this is the first to use analytical modeling to systematically characterize the benefits of stacking and establish general lessons in this area.

In this essay, we make the following contributions:

- Driver of benefit. When arbitrage and regulation are provided simultaneously (see Figure 2.1c), we often observe a superlinear profit improvement in comparison to providing standalone services: $\Pi^*_{stk} > \Pi^*_{arb} + \Pi^*_{reg}$ where Π^*_i represents the optimal profit under the operation of arbitrage alone ($i = arb$), frequency regulation alone ($i = reg$), or stacking ($i = stk$). The driver is cost-saving synergy, where the cost of performing joint services (stacking) often becomes smaller than the sum of individual costs if we had performed each service separately. Even in cases where each standalone service is unprofitable, stacking may result in positive profits.

- Synergistic behavior. We show that the provision of one service creates incentives to use more of (or at least neutrally supports) the other service. We show that (1) the optimal quantity of one service is monotone increasing in both service prices, (2) stacking always increases the optimal quantity of services, compared to standalone operations, and (3) it is always optimal to mix two services.

- Benefit of simultaneous stacking. We analyze the benefit of simultaneous stacking under various grid/market conditions (e.g., prices paid for offering these services). We also provide a theoretical upper bound on stacking's profitability, showing that it can approximately double the profit of the best standalone service.

- Our base model is intended to be simple enough to describe key interactions and sources of benefits of simultaneous stacking. We investigate several generalizations of our base model, such as inefficient batteries (energy loss) and correlated service prices.

We not only show that the main lessons continue to hold but, in several realistic cases, the lessons are expanded (stacking's benefit becomes stronger). For example, with inefficient batteries, stacking can expand battery deployment on the grid because inefficient batteries can still be profitably used via stacking, which would not be possible with standalone operations.[4]

2.2 Literature Review

2.2.1 Energy Storage Research in Operations Management[5]

The OM literature on energy has grown in multiple directions, with recent review papers identifying several subareas (e.g. [141]). Most analytical works study the use of batteries for standalone services, describing optimal policies [86, 41], the value of storage [200, 131], and optimal storage capacity [198]. Other papers integrate renewable generation with storage, studying optimal bidding [101, 119], optimal dispatch [216], capacity investment [161], optimal location of energy storage [199], the effect of constraints on integrating storage [216], and the optimal mix of generation assets [73]. Recent interest in EVs and smart cities explores infrastructure investment [121, 15], vehicle charging schedules [201, 33], dynamic pricing for charging [191, 41], and challenges and opportunities in this domain [162, 70].

However, almost all of the above OM papers do not consider battery degradation, except for a handful of papers such as [86], [23], and [213]. Yet, these papers focus on standalone services and do not consider simultaneous stacking.

2.2.2 Stacking

Recently, stacking has been considered as a promising approach to improving the economics of batteries. Among the papers that consider energy stacking, a very significant portion of them study time-exclusive stacking (Figure 2.1b). Most of the vehicle-to-grid literature focuses on time-exclusive stacking, where the batteries in electric vehicles provide one of the grid services (e.g., frequency regulation or energy arbitrage) during their idle time (when cars are parked) and earn additional revenue [99, 213, 109]. However, these papers do not consider the case when multiple services are provided simultaneously, which is our focus.

An increasing number of papers study simultaneous stacking by considering multiple services that can be performed at the same time (Figure 2.1c). Some of these papers focus

[4]This was actually one of the key questions that a technology provider (within the energy sector) expressed an interest in during our conversations with them.

[5]See Appendix A.1.4 for a comparison of traditional inventory theory and battery economics.

only on revenue and continue to ignore any costs of provided services or assume constant costs regardless of how the battery is used (e.g., [47]), which may lead to significantly suboptimal policies.

Some numerical studies such as [144] consider simultaneous stacking and non-linear costs to show that stacking can increase profitability (by yielding revenue increases greater than cost increases). A few numerical papers also indicate some forms of synergies when combining multiple services. The two most relevant to our study are [36] and [174]. [36] considers arbitrage and regulation, developing a dynamic program to optimize battery dispatch across different time scales. The paper numerically shows how deviating from frequency regulation requests can profit from real-time price spikes, with a 1.75 – 80% revenue improvement from stacking compared to standalone frequency regulation. [174] numerically illustrates potential "superlinear" profit gains (the profits under stacking can be higher than the sum of profits from individual services) from stacking peak-shaving and regulation services, where the provision of regulation services incentivizes increased peak-shaving service. However, both papers rely on scenario-based numerical evaluations, limiting generalizability and insight into conditions that maximize stacking benefits (we establish general lessons on when and why stacking works using analytic modeling). Further, neither of these papers focuses on degradation (degradation is a key driver of our results).

In summary, the literature has largely overlooked the mechanism by which stacking improves battery economics. The studies that model battery usage costs (i.e., the effect of increased utilization on degradation costs) have all been numerical, demonstrating profitability increases without systematically exploring why and when stacking works. Our work expands the numerical insights and contributes to the literature by analytically identifying the key drivers of benefits. Specifically, we show how simultaneous stacking can lead to cost savings through two synergies — degradation cost saving and replenishment cost saving. We derive the upper bound on stacking performance versus its strongest standalone competitor and show that stacking can often achieve superlinear profit improvement with extensive comparative statics.

2.3 The Preliminaries

We start with the characteristics of the key services that we consider in our model, followed by the characterization of degradation costs of batteries.

2.3.1 Key Services: Arbitrage and Frequency Regulation

Grid operators such as independent system operators (ISO) and regional transmission organizations (RTO) administer a region's electricity markets. Their task is matching supply with demand and guaranteeing the reliability/safety of the grid systems. Matching supply and demand takes place on an hourly basis as well as in shorter timeframes of minutes and seconds and is done by deciding which resources (with different costs and different response times) need to be activated at any time. In the short and medium term, energy storage and particularly batteries (BESS) are exceptionally capable of playing a role in matching supply and demand, as they provide the capability of bidirectional energy injection/withdrawal with quick response times.

In this work, we seek to build a parsimonious model of the day-to-day benefits and costs of stacking services for a large-scale battery operator, and we choose to focus on two key services of arbitrage and frequency regulation. They, along with peak shaving,[6] are by a considerable margin (as measured by MWh of service provided) the top three services provided by large-scale battery deployments, and they are also among the most frequently combined pairs of services [54].

Arbitrage is buying energy at a low price and selling it at a high price. With the price of energy dramatically varying throughout the day, this is a natural service for batteries to provide. Grid-scale BESS has long been proposed as a key element of a properly functioning grid, including the use of batteries for arbitrage.

Frequency regulation (or *regulation* hereafter) is a stabilizing service maintaining the grid's frequency within a tight tolerance by providing short-term energy injection/withdrawal in response to a regulation signal constructed by ISO/RTOs. Specifically, the ISO/RTO provides a signal changing between -1 and +1, usually every 2 – 4 seconds. A battery or other market participant commits (ahead of time) to a certain regulation capacity and, in response to the signal, the energy flow from battery to the grid becomes $signal \times capacity$. The battery is paid for each unit of committed capacity for each hour and receives an additional credit (performance payment) based on the actual amount of work (measured as the sum of the total amount of charging and the total amount of discharging requested for a given time period) as well as its performance score, based on how accurately the battery followed the signal.

In this work, we consider day-ahead (forward) energy and regulation markets where energy/regulation prices are cleared on an hourly basis. Appendix A.1.3 explains details of the

[6] Peak shaving may be used by customers to avoid charges or by system operators to defer the need to build new generation capacity. Since we focus on day-to-day battery operations, we do not model peak shaving, which only requires a battery to operate for a handful of peak demand days throughout the year.

market clearing mechanics (e.g., bidding and commitment processes) and market structures for both arbitrage and regulation. As illustrated in Figure 2.1c, a battery can provide arbitrage and regulation simultaneously by pre-specifying an arbitrage charge/discharge rate (or base rate) and then adjusting above and below that base rate based on the regulation signal from the grid.[7]

2.3.2 Battery Degradation Cost

The biggest cost of using batteries is the cost of batteries themselves. Upon use, all batteries suffer from degradation, which is an irreversible chemical process, eventually reaching a point where certain operations cannot be provided. Lithium-ion batteries are the dominant form of technology and, for these batteries, the three most critical factors affecting degradation are temperature, charging/discharging rate (C-rate), and depth-of-discharge (DOD); see [204]. We restrict our focus to DOD since the other two factors have a minor impact in our setting.[8]

The key factor in degradation is the proportion of the battery's capacity used in a cycle, which corresponds to the cycle's DOD. Every time a battery is discharged and then recharged back to the original level, the DOD u ($0 \leq u \leq E$) is defined as the amount of energy discharged (MWh), where E is the maximum amount of energy that can be stored in the battery. It is well known that DOD has a significant and nonlinear (convex) impact on degradation: larger DODs incur much faster degradation per unit of discharged energy.

In this work, we model a battery operator who chooses to maintain a constant battery capacity by paying a replenishment cost to replace battery capacity lost due to usage-based degradation.[9] The energy capacity E, maintained over time, is treated as a limiting physical constraint in all the models we present, such as (2.8) in Section 4.3. We begin by considering how to account for a full cycle. A battery operated at its full capacity ($u = E$) has a certain lifetime, N, which denotes the expected number of cycles the battery can provide before it is completely degraded. Therefore, the cost of a full cycle can be defined as the cost of the battery divided by its lifetime N. We can then expand this logic to account for the

[7] For example, with the regulation capacity of 1MW and an arbitrage discharging rate of 2MW, the battery needs to be discharged at the rate of 3MW when the regulation signal has the value of +1, while it is discharged at the slower rate of 1MW with the signal value of -1.

[8] With advancements in battery management and cooling systems, the impact of temperature and C-rate can be minimized, especially for the large-scale stationary batteries considered in this work. See Appendix A.1.1.1 for details.

[9] Typically, batteries are operated by large-scale operators, who often maintain a specific capacity level ([130, 163]). They augment the decreased capacity through adding new batteries to ensure the deliverability of a certain level/quality of services. In a scenario where a battery operator chooses to maintain a constant battery capacity and battery capacity degradation is the key form of degradation experienced by the battery, the objective function that we consider can be directly interpreted as reflecting an actual cash flow. This approach is standard in the literature for accounting for battery degradation costs (e.g., [204]).

degradation cost of a cycle of any size u ($0 \leq u \leq E$). Based on commonly reported values in empirical papers and battery specifications (see Table A.1 in Appendix A.1.1), the cost of a single cycle of DOD u is quadratic in DOD and can be characterized by the function $\Phi(u) : [0, E] \to \mathbb{R}$:

$$\Phi(u) = \underbrace{(c_0^b E)}_{\substack{\text{The cost of} \\ \text{a full cycle}}} \cdot (\frac{u}{E})^2 = \frac{c_0^b}{E} \cdot u^2, \tag{2.1}$$

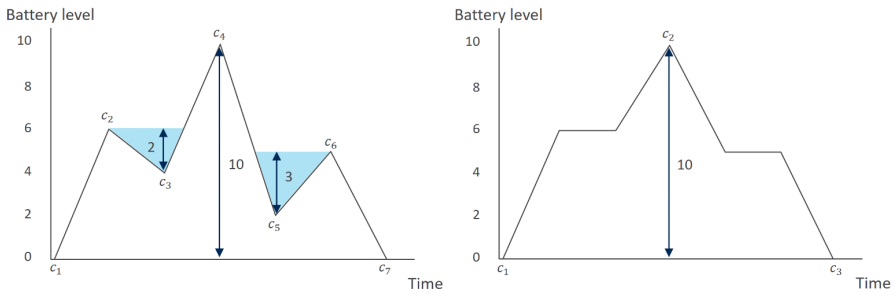
where c_0^b is the degradation coefficient of a battery representing the degradation cost incurred by a full cycle of a battery with a single-unit capacity (see Appendix A.1.1.2 for details). This model can be generalized; in Appendix A.4, we report the sensitivity of our results to this degradation assumption by considering other coefficients and other functional forms.

Rainflow-Counting Algorithm: Degradation cost is generally modeled as the sum of degradation costs for each discharge/charge cycle. However, when cycles of a battery are uneven or overlapping, characterizing the degradation cost can be non-obvious. In the energy literature, empirical papers have established a gold-standard approach to quantifying degradation cost called the 'rainflow-counting' algorithm, which is inspired by streams of rainwater flowing down a hill [204]. The algorithm processes the state of charge (SOC) profile to identify cycles of various DODs that were experienced by the battery.[10] The principle of rainflow counting is to first account for the degradation caused by smaller cycles, which are then removed from the SOC profile. By successively removing the smaller cycles, the algorithm eventually captures the degradation caused by the main cycles. If $U = \{u_i\}$ is the set of cycles identified by rainflow counting, then the battery degradation cost is defined as $\frac{c_0^b}{E} \sum_{u_i \in U} u_i^2$, based on (2.1).

Example 2.1. *Consider the SOC profile in Figure 2.2a. The rainflow-counting algorithm first captures the two smaller cycles ($u_1 = 2, u_2 = 3$), which collect rain above the SOC profile. After removing the two cycles (Figure 2.2b), we identify the main cycle ($u_3 = 10$). The total degradation is the sum of costs corresponding to two small cycles: $c^b(2)^2 + c^b(3)^2$, plus the cost of the big cycle $c^b(10)^2$.*

Since battery cost is a key factor in BESS profitability and is reflected through battery degradation, the above degradation cost model is central to our overall modeling approach.

[10] SOC is the level of charge of a battery relative to its capacity (0% = empty; 100% = full). For details on the rainflow-counting algorithm, see Appendix A.1.1.



(a) (b)

Figure 2.2: A simple illustration of rainflow-counting algorithm (Example B.44)

2.4 Model

Our model focuses on a profit-maximizing decision-maker (battery farm owner) operating a battery throughout a day, balancing the quantity of grid services provided and, therefore, the revenue obtained, with the degradation costs. We model arbitrage and regulation opportunities using a cycle of one day with one peak. We assume that a day consists of T (short) base periods. We explain base periods later in this section, after Assumption 2.2.

For **arbitrage**, we assume two prices throughout the day: high price $\bar{p}$ and low price $\underline{p}$ with a stylized rectangular structure for the energy price. Since we have the flexibility of choosing when our cycle starts, we assume:

Assumption 2.1 (Price profile)**.**

- *The horizon of T base periods consists of T_L base periods with low price $\underline{p}$ followed by T_H base periods with high price $\bar{p}$. That is, energy price $p(t)$ satisfies*

$$p(t) = \begin{cases} \underline{p}, & \text{if } t \in [0, T_L) \\ \bar{p}, & \text{if } t \in [T_L, T), \end{cases} \tag{2.2}$$

  where $T = T_L + T_H$. We assume $T_H \leq T_L$.

- *We define the* **arbitrage price** *as the gap between the two prices: $p^a := \bar{p} - \underline{p} > 0$.*

- *The* **regulation price** *$p^r > 0$, representing the expected payment for providing 1MW of regulation capacity for one base period, is assumed to be constant throughout the day.*[11]

[11] In the base model, a single regulation price is used by incorporating capacity and performance payments (see Appendix A.1.3 for details). In the extensions, we explore various forms of the regulation price, including correlated prices (in Section 2.6.1) and quantity-dependent regulation prices (in Section 2.6.3).

For the arbitrage price, this setting reflects typical day-ahead forward market environments in which the lowest/highest prices last at least an hour each (day-ahead prices are settled on an hourly basis) and where they stay at a fairly constant level for a few hours.[12] We interpret service prices as the expected values learned from historical data: $p^a = \mathbb{E}[p^a]$ and $p^r = \mathbb{E}[p^r]$, reflecting the fact that almost all large-scale batteries are self-scheduling (they bid/commit service quantities and accept any cleared market prices);[13] see Appendix A.1.3.2 for empirical evidence supporting the self-scheduling assumption. Assuming the price profile is representative of typical grid/market conditions, we assume that the optimal operation of the day will be repeated across multiple days, so we require that the battery's initial and ending SOC of a day should match.[14]

For **regulation**, we consider an ISO sending a signal that changes between -1 and 1 through time, instructing the battery to charge (when the value is negative) and discharge (when the value is positive). The battery commits to a certain capacity r, which implies responding to the ISO's signal in $[-1, 1]$ with a corresponding portion of the committed capacity. Reflecting the realities of "fast regulation" signals provided by ISO/RTOs like Pennsylvania-New Jersey-Maryland Interconnection (PJM) and ISO New England (ISO-NE), we further model the ISO as committing to an energy-neutral signal, where the total charges and discharges balance each other out within a specific period of time (in the case of PJM, 30 minutes).[15] While regulation signals are fairly unpredictable and change frequently (every few seconds), to analytically model the battery degradation cost, we introduce a stylized +1/-1 regulation signal as follows:

Assumption 2.2 (Energy-neutral signal)**.** *We assume that the regulation signal alternates between +1 and -1, and stays at a given level for one time unit.*

Note that we define time units (base periods) in terms of the energy neutrality guarantees: energy neutrality must be achieved within 2 time units in our model. For analytical simplicity, we express T_L, T_H and T using the normalized time units and further assume that

[12] Empirically, periods of peak prices are shorter than periods of low prices and the timing of peak price periods are fairly predictable (see Appendix A.4.1), which drives the predictability assumption on the peak with $T_H \leq T_L$.

[13] This framework has been frequently used in the literature (either relying on perfect foresight assumption or using expected service prices calibrated to historical price data) to study the benefits of battery storage in day-ahead markets (e.g., [47, 99, 206]). Furthermore, a numerical study shows that the overall lessons of this work continue to hold and can even expand (i.e., the relative benefit of stacking versus standalone services becomes stronger) when we allow participation in real-time markets to respond to uncertainty, such as real-time price spikes.

[14] More complex price profiles are treated in the numerical results in Appendix A.4.2, in which we numerically consider hourly prices (and hourly decision variables accordingly).

[15] PJM has switched to conditional energy neutrality since 2017. See Appendix A.1.2 for details.

T_L and T_H are even integers and $T \geq 6$.[16] For instance, energy neutrality within 30 minutes implies that the time unit equals 15 minutes and a day-long horizon with a 2-hour peak period has $T_H = 8, T_L = 88$ and $T = 96$.

The following proposition shows that this +1/-1 signal maximizes battery degradation costs among a broad class of regulation signals. All proofs are in the appendix (Appendices B.2 and B.3).

Proposition 2.1. *Among all frequency regulation signals that guarantee energy neutrality within two time units, the signal alternating +1 and -1 every one time unit generates the largest battery degradation cost.*

The +1/-1 signal enables us to analytically establish key properties of optimal battery operations, including the magnitudes and patterns of stacking and standalone services. Later, we consider other regulation signal patterns in Section 2.6.3 (we find that stacking provides somewhat reduced benefits when trinary signals are introduced), and Appendix A.4 provides a numerical evaluation of stacking's performance with realistic regulation signals.

Based on the price profile (Assumption 2.1), we express our optimization as a two-period model, charging the battery at a constant arbitrage rate and providing a constant regulation rate throughout the low-price period, and discharging the battery at a constant arbitrage rate and providing a constant regulation rate during the high-price period. Thus, the daily **revenue** is

$$-\underline{p}a_L T_L + \bar{p}a_H T_H + p^r r_L T_L + p^r r_H T_H, \tag{2.3}$$

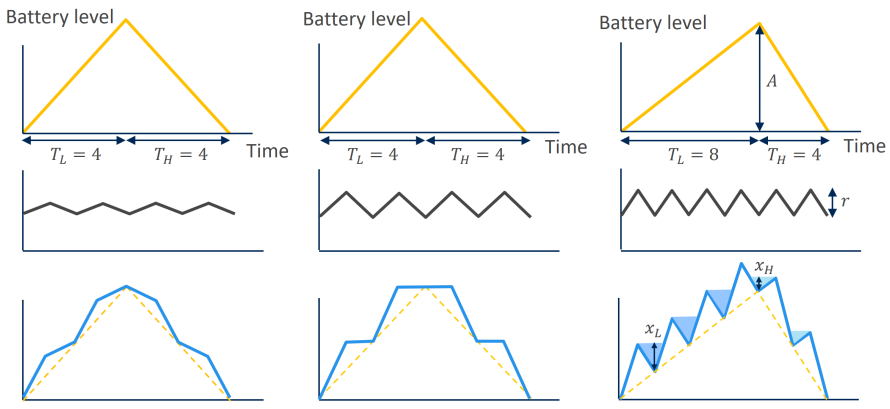
where $\underline{p}, \bar{p}, p^r, T_L$, and T_H are assumed to be exogenously given, while a_L, a_H, r_L, and r_H are decision variables (measured in MW):

- a_L and a_H are the arbitrage charging and discharging rates during low-price and high-price periods, respectively, and
- r_L and r_H are the regulation capacity sold to the grid in the low-price and high-price periods, respectively.

We will also use, when convenient, the total amount of arbitrage (regulation) instead of arbitrage (regulation) charging and discharging rates:

- A is the total amount of arbitrage, that is, the total amount of energy charged during the low-price period and discharged during the high-price period. Given energy-neutral

[16] All key findings of the chapter also hold for the $T = 4$ case, but we assume $T \geq 6$ to simplify the presentation of results such as Theorem 2.2 and Corollary A.6.



(a) $a > r$ (b) $a = r$ (c) $x_L > x_H > 0$

Figure 2.3: SOC profiles of arbitrage (top), regulation (middle), and stacking (bottom), where the stacking profiles are established by superimposing the arbitrage and regulation profiles.

regulation, our requirement that the initial and final SOC match, and a lossless battery (we later extend the model to incorporate energy loss in Section 2.6.2), the arbitrage amounts match between the high- and low-price periods: $A = a_L \cdot T_L = a_H \cdot T_H$.

- R is the total regulation capacity provided throughout the day: $R = r_L \cdot T_L + r_H \cdot T_H$.

2.4.1 Cost of Degradation

With these preliminaries in place, we can state the degradation costs when offering only arbitrage, only regulation, and stacked services. Figure 2.3 illustrates some potential SOC profiles of arbitrage (top), regulation (middle), and stacking (bottom).

Arbitrage Only: As there is one cycle having DOD of A, the degradation cost is $\frac{c_0^b}{E} A^2$.

Regulation Only: When providing regulation alone, we have only one regulation capacity bid throughout the day, so $r_L = r_H = r$. With $T/2$ cycles, each having DOD of r, the degradation cost is $\frac{c_0^b}{E} r^2 (T/2)$.

Stacked Services: When we stack arbitrage and regulation, depending on the relative magnitudes of arbitrage rates a_L and a_H and regulation rates r_L and r_H, we may observe different SOC patterns and degradation costs. Figure 2.3a and 2.3b show the phenomenon of *free regulation*: a battery providing some amount of arbitrage A (at degradation cost $\frac{c_0^b}{E} A^2$) may be able to add some amount of regulation without increase in the degradation cost.

To formalize this concept, let $x_i := (r_i - a_i)^+$, for $i = L, H$, be the excess regulation over the arbitrage rate, where $z^+ := \max(z, 0)$.

Observation 2.1. *(a) When $x_L = x_H = 0$ (Figure 2.3a and 2.3b), regulation is free. (b) Figure 2.3b illustrates the maximum free regulation – any additional regulation will increase the degradation cost over the cost of providing arbitrage alone.*

Note that adding regulation up to the corresponding arbitrage level ($r_i \leq a_i$) is cost-free, as $a_i - r_i$ and $a_i + r_i$ have the same sign. Intuitively, the battery charges during the low-price period and then discharges during the high-price period, since high arbitrage rates completely offset all the fluctuations from regulation. Since the SOC profile remains monotonic before and after the peak and the regulation signal is energy-neutral, the rainflow-counting algorithm extracts a single cycle of size A (regulation does not increase degradation). This finding is robust — consistent with the rainflow-counting algorithm, other cycle-detecting algorithms (e.g., [144]) identify a single cycle.

Figure 2.3c shows a non-monotonic SOC profile when $x_L > x_H > 0$, where the battery switches between charging and discharging, creating many smaller cycles. Although regulation is no longer free, we later show in Proposition 2.2 that stacking can still reduce costs by decreasing the size of these smaller cycles compared to performing regulation alone. During the first T_L periods, we alternate between charging at rate $r_L + a_L$ for one time unit and discharging at rate $r_L - a_L = x_L$ for one unit, so the rainflow-counting algorithm will extract $\frac{T_L}{2} - 1$ small cycles of depth x_L. Similarly, during the following T_H periods, the rainflow-counting algorithm will extract $\frac{T_H}{2} - 1$ small cycles of depth x_H. One additional small cycle of depth $\min(x_L, x_H)$ occurs at the transition between the two periods. After removing the smaller cycles, the remaining large cycle has a depth of $A + \max(x_L, x_H)$. Thus, the degradation cost can be stated as a function of arbitrage amount A and excess regulation rates x_L and x_H:

$$Deg(A, x_L, x_H) = \frac{c_0^b}{E}[A^2 + 2A\max(x_L, x_H) + \frac{T_L}{2}x_L^2 + \frac{T_H}{2}x_H^2]. \tag{2.4}$$

2.4.2 Formulation

We can now state our base optimization formulation:

$$\max_{A, r_L, r_H} \quad \Pi = p^a A + p^r r_L T_L + p^r r_H T_H - \tfrac{c_0^b}{E}[A^2 + 2A \cdot \max(x_L, x_H) + \tfrac{T_L}{2}x_L^2 + \tfrac{T_H}{2}x_H^2] \tag{2.5}$$

$$\text{s.t.} \quad a_i = A/T_i \text{ for } i = L, H \tag{2.6}$$

$$x_i = (r_i - a_i)^+ \text{ for } i = L, H \tag{2.7}$$

$$A \leq E \tag{2.8}$$

$$A, r_i \geq 0 \text{ for } i = L, H. \tag{2.9}$$

The energy capacity constraint (2.8) caps the maximum amount of arbitrage the battery can provide.[17] As confirmed in our numerical experiments in Appendix A.4, the quadratic (convex) degradation costs imply that it is usually optimal to operate using less than the full battery capacity under typical grid/market conditions. This outcome is intuitive: using half of a battery's capacity instead of the full capacity to provide service on a given day reduces the revenue for that day by 50% but reduces degradation costs by 75%, which can often be a good tradeoff for a very expensive battery. This differs from linear costs considered in most of the operations literature, where we would not install capacity that would remain unused. Still, for completeness, we study the effect of binding constraints. In Section 2.6, we extend the model in several ways, including the battery's limited power capacity for arbitrage and regulation.

2.5 Properties

In this section, we characterize the source of benefits (cost-saving synergy) of stacking. Section 2.5.1 illustrates that stacking delivers increased battery profitability and synergistic behaviors compared to providing standalone services. To establish clear benchmarks, we first characterize the optimal policies when the battery offers only one type of service.

Regulation Only: With regulation being the only service ($A = 0$), $r_L = r_H = r$ and the objective function (2.5) becomes $\max_r \{p^r \cdot r \cdot T - \frac{c_0^b}{E} \cdot r^2 \cdot T/2\}$. Thus, the optimal amount of frequency regulation is $r^*_{reg} = \frac{p^r}{c_0^b} E$. The corresponding profit is

$$\Pi^*_{reg} = \frac{(p^r)^2 T}{2c_0^b} E. \tag{2.10}$$

Arbitrage Only: For arbitrage only ($r_L = r_H = 0$), the objective function (2.5) becomes $\max_A \ \{p^a A - \frac{c_0^b}{E} A^2\}$. Thus, the optimal amount of standalone arbitrage is $A^*_{arb} = \min(\frac{p^a E}{2c_0^b}, E)$. The corresponding profit is

$$\Pi^*_{arb} = \begin{cases} \frac{(p^a)^2}{4c_0^b} E, & \text{if } p^a \le 2c_0^b, \\ (p^a - c_0^b) E, & \text{otherwise.} \end{cases} \tag{2.11}$$

For both services, note that the optimal service quantity and corresponding profit increase

[17] The energy constraint can take an alternative form such as $A + \max(x_L, x_H) \le E$ to reflect that excess regulation can expand the SOC range of a battery. To keep the exposition as simple as possible, we choose to model the constraint as $A \le E$, but the overall lessons remain consistent with either formulation. We consider a more sophisticated energy capacity constraint (which still leads to consistent results) in the numerical experiments in Appendix A.4.

linearly in energy capacity E.[18]

2.5.1 Stacking

When arbitrage and frequency regulation are stacked (offered simultaneously), the battery degradation cost for stacking could be either smaller or bigger than the sum of costs of individually providing the two services:

Proposition 2.2 (**Cost-saving**). *Jointly offering arbitrage A and regulation (r_L, r_H), compared to separately performing these same amounts of arbitrage and regulation, results in the following cost-saving*:

$$\begin{aligned} \textit{Cost-saving} &= Deg(A,0,0) + Deg(0,r_L,r_H) - Deg(A,x_L,x_H) \\ &= \begin{cases} \frac{c_0^b}{E} \cdot [\frac{T_L}{2} r_L^2 + \frac{T_H}{2} r_H^2], & \text{if } x_L = x_H = 0, \\ \frac{c_0^b}{E} \cdot [A(\frac{a_i}{2} - x_i) + \frac{T_j}{2} r_j^2], & \text{if } x_i > x_j = 0, \\ \frac{c_0^b}{E} \cdot A \cdot [\frac{a_i + a_j}{2} + x_j - x_i], & \text{if } x_i \geq x_j > 0. \end{cases} \end{aligned}$$

While there could be cost increases with highly imbalanced excess regulation values (e.g., x_L very large and x_H very small), positive cost-saving, or cost-saving synergy, takes place when the excess regulation values are close enough (e.g., $x_L \approx x_H$) or the excess regulation values are not too large (e.g., $x_L \leq \frac{a_L}{2}$ and $x_H \leq \frac{a_H}{2}$). Below, we prove that at optimality we must have $x_L^* = x_H^*$.

Lemma 2.1 (**Equal excess regulation**). *For fixed arbitrage quantity A, $x_L^* = x_H^* = (\frac{p^r E}{c_0^b} - \frac{2A}{T})^+$.*[19]

Lemma 2.1 shows how the two regulation rates are related under simultaneous stacking. If $x_L \neq x_H$, then we can always rebalance the excess regulation rates to be equal, keeping the same revenue (the total amount of regulation remains the same) while decreasing degradation costs. At optimality, a positive cost saving is guaranteed from Proposition 2.2 whenever $A^* > 0$. Having expressed the optimal excess regulation x^* as a function of arbitrage quantity A, it is straightforward to find the optimal A^*. The following theorem establishes the optimal stacking decisions and demonstrates synergy between arbitrage and regulation.

[18] This result is intuitive: Consider a scenario where we buy multiple homogeneous battery modules (or battery storage systems) with the same characteristics (e.g., degradation coefficient c_0^b). If a battery module with a unit capacity maximizes profit by providing A amount of arbitrage, the exact same amount should be provided by other unit-capacity modules as well (i.e., the same policy should be replicated when the size of the battery increases).

[19] We drop subscript stk for stacking's optimal actions/profits if no confusion arises in doing so.

Theorem 2.1 (**Optimal stacking**). *(a) The optimal arbitrage quantity weakly increases in both the price of arbitrage p^a and the price of regulation p^r, (b) The optimal regulation quantity weakly increases in both the price of arbitrage p^a and the price of regulation p^r, and (c) The battery uses free regulation only ($x^* = 0$) when the price of regulation is low compared to the price of arbitrage ($p^r \leq \frac{p^a}{T-2}$) and compared to the per-unit price of the battery ($p^r \leq \frac{2c_0^b}{T}$); it otherwise uses positive excess regulation ($x^* > 0$). The optimal stacking actions and profit are as follows*:

Var.	Cases	
	$p^r \leq \min(\frac{p^a}{T-2}, \frac{2c_0^b}{T})$	$p^r \geq \min(\frac{p^a}{T-2}, \frac{2c_0^b}{T})$
A^*	$\min(\frac{(p^a+2p^r)E}{2c_0^b}, E)$	$\min(\frac{p^aTE}{2c_0^b(T-2)}, E)$
r_L^*	$\frac{A^*}{T_L}$	$\frac{p^rE}{c_0^b} - \frac{T_L-T_H}{T_LT}A^*$
r_H^*	$\frac{A^*}{T_H}$	$\frac{p^rE}{c_0^b} + \frac{T_L-T_H}{T_HT}A^*$
R^*	$2A^*$	$\frac{p^rTE}{c_0^b}$
x^*	0	$\frac{p^rE}{c_0^b} - \frac{2A^*}{T}$
Π^*	$(p^a + 2p^r)A^* - \frac{c_0^b}{E}(A^*)^2$	$p^aA^* + \frac{TE}{2c_0^b}(p^r)^2 - \frac{(T-2)c_0^b}{TE}(A^*)^2$

Table 2.1: Optimal stacking.

Theorem 2.1 allows us to evaluate the effect of problem parameters on optimal stacking. As expected, both arbitrage and regulation increase as c_0^b decreases.[20] While one might expect that the amount of regulation service provided is more sensitive to battery price than the amount of arbitrage provided due to its frequent cycling of the battery, this is in fact not always the case: For sufficiently high battery prices ($c_0^b > \min(\frac{p^aT}{2(T-2)}, \frac{p^rT}{2})$), the battery price scales the optimal quantities of both services by the same factor, which results in the same optimal ratio.

Observation 2.2. *The ratio of the optimal regulation amount R^* and the optimal arbitrage amount A^* is*:

$$\frac{R^*}{A^*} = \max\left(2, \frac{2p^r}{\min(\frac{p^a}{T-2}, \frac{2c_0^b}{T})}\right).$$

Observation 2.2 implies that we always provide at least twice as much regulation as arbitrage in a given day (i.e., $\frac{R^*}{A^*} \geq 2$), even if the regulation price p^r is extremely low.

[20]Recall that c_0^b represents the degradation cost for a full cycle of a unit-capacity battery and is proportional to the battery price. We use battery price and degradation coefficient interchangeably if no confusion arises in doing so.

This is because there is no added degradation cost for providing free regulation, so we take advantage of it regardless of p^r.[21]

Synergistic behavior. To better understand the synergy between the two services, let $f(A, R, p^a, p^r, -c_0^b)$ be the unconstrained profit of delivering A total amount of arbitrage and R total amount of regulation across a given day when the parameter set is given as $(p^a, p^r, -c_0^b)$.

Proposition 2.3 (Supermodularity). *(a) $f(A, R, p^a, p^r, -c_0^b)$ is supermodular in $(A, R, p^a, p^r, -c_0^b)$. (b) $\Pi^* = \max_{A,R} f(A, R, p^a, p^r, -c_0^b)$ is supermodular in $(p^a, p^r, -c_0^b)$. (c) (A^*, R^*) increases in $(p^a, p^r, -c_0^b)$.*

Proposition 2.3 implies the complementarity between arbitrage and frequency regulation under simultaneous stacking, which leads to synergistic behaviors. We first compare the optimal amounts of services provided with stacking (Theorem 2.1) versus what would be optimal if we provided one of the services, regulation only or arbitrage only.

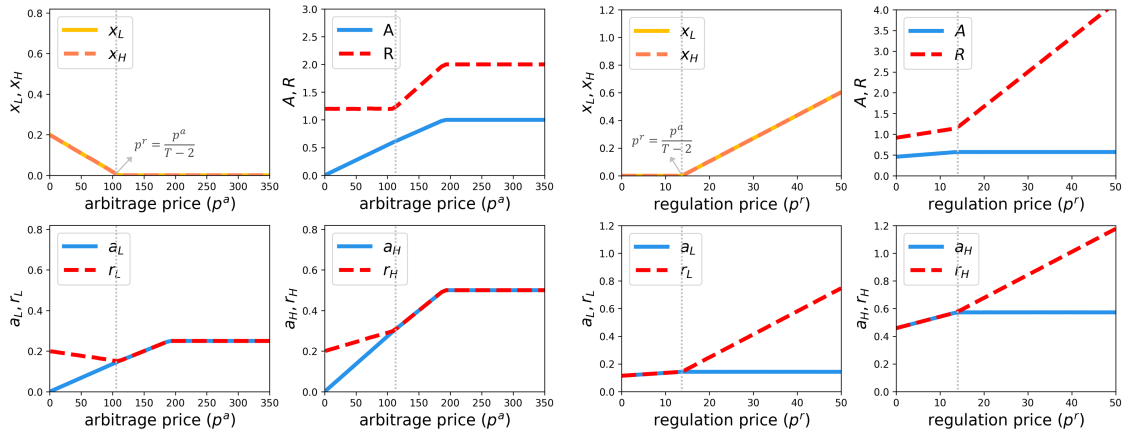
Observation 2.3 (Increased utilization). *(a) Stacking always strictly increases the amount of arbitrage compared to arbitrage-alone operation ($A^*_{stk} > A^*_{arb}$), except when high arbitrage prices cause both to use the full energy capacity of the battery ($p^a \geq 2c_0^b$). (b) For a sufficiently low price of regulation ($p^r < \min(\frac{p^a}{T-2}, \frac{2c_0^b}{T})$), it is optimal to only use free regulation ($x_L^* = x_H^* = 0$), and the optimal arbitrage and regulation amounts are both strictly monotone increasing in p^a and p^r as long as prices are sufficiently low so that the battery does not use its full energy capacity ($p^a + 2p^r < 2c_0^b$). The total regulation capacity provided throughout the day is also strictly increased compared to regulation-alone operation ($R^*_{stk} > R^*_{reg}$). (c) For a sufficiently high price of regulation ($p^r \geq \min(\frac{p^a}{T-2}, \frac{2c_0^b}{T})$), $R^*_{stk} = R^*_{reg}$, and A^*_{stk} (R^*_{stk}) is independent of p^r (p^a).*

Observation 2.3 highlights the increased utilization under simultaneous stacking — the provision of one service supports other services — that cannot be achieved with time-exclusive stacking (no cost-saving synergy). It also implies that we always provide a positive arbitrage amount under stacking for any $p^a > 0$.

Observation 2.4. *At least a small amount of arbitrage is always beneficial, since the sum of increased revenue and cost saving for regulation is larger than the increased cost for arbitrage.*

Figure 2.4 illustrates the optimal values of decision variables A, R, a_i, r_i and x_i as we vary the exogenous parameters of arbitrage price p^a and regulation price p^r. With the price

[21] Note that frequency regulation is provided both during the arbitrage charge and discharge periods, which explains why twice as much regulation is provided as arbitrage when providing free regulation only.



(a) p^a effect (b) p^r effect

Figure 2.4: Comparative statics: optimal stacking actions in Theorem 2.1 ($T = 24,\ T_H = 8,\ c_0^b = 100,\ E = 1$).

of arbitrage p^a increasing, we have two types of behavior: For lower values of p^a, excess regulation decreases while arbitrage rates increase.[22] To see this, we decompose the profit function (2.5) as:

$$\Pi = p^a A + \underbrace{2p^r A}_{Rev_f} + \underbrace{p^r T x}_{Rev_x} - \frac{c_0^b}{E}[A^2 + 2Ax + \frac{T}{2}x^2], \tag{2.12}$$

where the second term (Rev_f) denotes the regulation revenue from providing free regulation alone (larger A allows for more free regulation), and the third term (Rev_x) is the additional regulation revenue from maintaining excess regulation $x = x_L = x_H$. The product term $2Ax$ in the degradation function implies that maintaining positive excess regulation becomes more burdensome as A^* increases. Therefore, with a sufficiently high arbitrage price p^a (which induces a sufficiently large A^*), excess regulation disappears; that is, we "prioritize" arbitrage and only offer the maximum free regulation, $r_i^* = a_i^*$. Since in this regime, the regulation and arbitrage rates are fixed to match one another, increasing p^a or p^r causes both the optimal regulation and arbitrage amounts to increase.

Benefit of stacking: We now quantify the benefits of stacking and investigate when the synergy is maximized/minimized. Recall that (2.10) and (2.11) provide optimal profits when a single service is offered, while Theorem 2.1 establishes the profit for optimal stacking. This allows us to characterize the benefits of stacking versus providing standalone services. It is

[22] For this region ($x^* > 0$), more (less) regulation is provided in the high-price (low-price) period as p^a increases.

clear, from Proposition 2.2, that optimal stacking saves on degradation costs (compared to providing the same amount of arbitrage and regulation as standalone services) and chooses to provide more arbitrage and regulation than would optimally be provided if they were performed as standalone services (Observation 2.3). It turns out that optimal stacking achieves a superlinear increase in profit compared to optimally performing standalone services.

Proposition 2.4 (**Superlinear gain).** *Stacking achieves superlinear profit improvement: the optimal profit of stacking is strictly larger than the sum of the optimal profits from the individual services,* $\Pi^*_{stk} - [\Pi^*_{arb} + \Pi^*_{reg}] > 0$*, where*

$$
\begin{aligned}
&\Pi^*_{stk} - [\Pi^*_{arb} + \Pi^*_{reg}] \\
&= \begin{cases}
\frac{p^r[2p^a - p^r(T-2)]E}{2c_0^b}, & \text{if } p^r \le \frac{p^a}{T-2},\ \frac{p^a+2p^r}{2} < c_0^b, \\
\frac{(p^a)^2 E}{2c_0^b(T-2)}, & \text{if } p^r \ge \frac{p^a}{T-2},\ \frac{p^a T}{2(T-2)} < c_0^b, \\
(p^a + 2p^r)E - c_0^b E - (\frac{(p^a)^2 E}{4c_0^b} + \frac{(p^r)^2 TE}{2c_0^b}), & \text{if } p^r \le \frac{p^a}{T-2},\ \frac{p^a}{2} \le c_0^b \le \frac{p^a+2p^r}{2}, \\
p^a E - \frac{(p^a)^2 E}{4c_0^b} - \frac{T-2}{T} c_0^b E, & \text{if } p^r \ge \frac{p^a}{T-2},\ \frac{p^a}{2} \le c_0^b \le \frac{p^a T}{2(T-2)}, \\
\frac{p^r E}{2c_0^b}(4c_0^b - p^r T), & \text{if } p^r \le \frac{p^a}{T-2},\ \frac{p^a}{2} \ge c_0^b, \text{ and} \\
\frac{2}{T} c_0^b E, & \text{if } p^r \ge \frac{p^a}{T-2},\ \frac{p^a}{2} \ge c_0^b.
\end{cases}
\end{aligned}
$$

We note that the complementarity between two services (e.g., Propositions 2.2 – 2.4) rely on simultaneous provision of services and interaction between superimposed battery profiles and thus cannot be applied to time-exclusive stacking where revenue and cost are additive.

Theorem 2.2 (**Upper bound on stacking performance).**

$$
S := \frac{\Pi^*_{stk}}{\max(\Pi^*_{arb}, \Pi^*_{reg})} \le \frac{2T-2}{T-2}.
$$

The upper bound on S *is tight, and* $S = \frac{2T-2}{T-2}$ *when* $\frac{p^a}{p^r} = \sqrt{2T}$ *and* c_0^b *is sufficiently large such that* $A^*_{stk} < E$*.*

From now on, when we refer to stacking's performance, we specifically mean the relative performance (ratio) of stacking compared to the best standalone service, as measured by S. The closed-form expression of S can be straightforwardly derived by combining Theorem 2.1 and Eqs. (2.10) – (2.11). Figure 2.5 (blue curve) illustrates the behavior of S when c_0^b is sufficiently large (energy capacity is not binding for any strategy) over different service price ratios $\frac{p^a}{p^r}$: S is unimodal in $\frac{p^a}{p^r}$ — it increases from 1 up to a maximum value of $S = \frac{2T-2}{T-2}$ for $\frac{p^a}{p^r} \le \sqrt{2T}$, and then decreases back down to 1 for $\frac{p^a}{p^r} \ge \sqrt{2T}$. Theorem 2.2 provides a

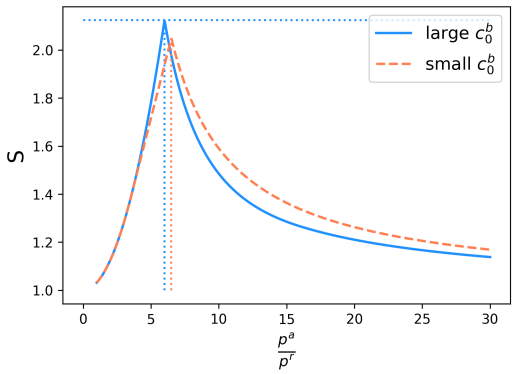


Figure 2.5: $S = \frac{\Pi^*_{stk}}{\max(\Pi^*_{arb}, \Pi^*_{reg})}$ over different service price ratios $\frac{p^a}{p^r}$ ($T = 18$).

theoretical upper bound on stacking's profitability, showing that it can approximately double the profit of the best standalone service ($\max S \approx 2$) when T is sufficiently large.

While Theorem 2.2 implies that the maximum possible S ratio is achieved when energy capacity is not binding (see Figure 2.5, blue-colored curve), stacking's relative performance can be improved for a given p^a and p^r with a small c_0^b (and binding energy capacity). For instance, when $\frac{p^a}{p^r} \geq 6.5$ in Figure 2.5, the orange-colored curve outperforms the blue-colored curve. This can occur when arbitrage-only is the most profitable standalone service, and a binding energy constraint impacts its profitability more strongly than it impacts the profitability of the stacking strategy.

2.6 Generalizations/Extensions

In this section, we investigate several generalizations and extensions to our base model. These include (1) correlated service prices, (2) round-trip energy efficiency, (3) non-uniform regulation signals, and (4) limited battery power capacity. In Section 2.6.5 we summarize the key differences in the results for the considered generalizations and extensions compared to the base model and illustrate how the main lessons remain largely unchanged.

2.6.1 Correlated Prices

In some ISOs, prices of grid services tend to be positively correlated due to the fact that the same power source may provide multiple services. In this section, we show that the benefits of stacking still exist and may become more powerful when we extend our model to include correlated prices. Under the rectangular (off-/on-peak) price assumption, we assume that

regulation prices for the low- and high-price time periods can be stated as follows:

$$\bar{p}^r = p_0^r + k \cdot \bar{p}, \tag{2.13}$$

$$\underline{p}^r = p_0^r + k \cdot \underline{p}. \tag{2.14}$$

Here, $p_0^r > 0$ is the base regulation price and $k \geq 0$ is the slope ($k = 0$ corresponds to the base model). Appendix A.3.1 provides the full characterization of the optimal stacking strategy (Theorem A.1) and the upper bound on stacking's performance (Theorem A.2). Here, we mainly focus on the key properties and see how they are influenced by the correlated prices.

Synergistic behavior. Interestingly, Observation 2.3 (the optimal arbitrage and regulation amounts are strictly monotonically increasing in p^a and p^r) can be expanded under correlated prices: increasing k (which leads to an increase in the average regulation price $p^r := \frac{T_L \underline{p}^r + T_H \bar{p}^r}{T}$) causes both the optimal arbitrage and regulation amounts to increase as long as $x_L^* = x_H^*$ ($k \leq \frac{1}{T_H - 1}$) and energy capacity is non-binding. As one might expect, highly unequal regulation prices $\bar{p}^r \gg \underline{p}^r$ can cause the model to deviate from the base model's optimal decision to select $x_L^* = x_H^*$ and therefore always achieve positive cost-saving synergy (see Proposition 2.2). For sufficiently large values of $\bar{p}^r - \underline{p}^r = kp^a$, we can observe $x_H^* > x_L^* > 0$ and eventually negative cost-saving synergy (when $kp^a > 2c_0^b/T_H$).

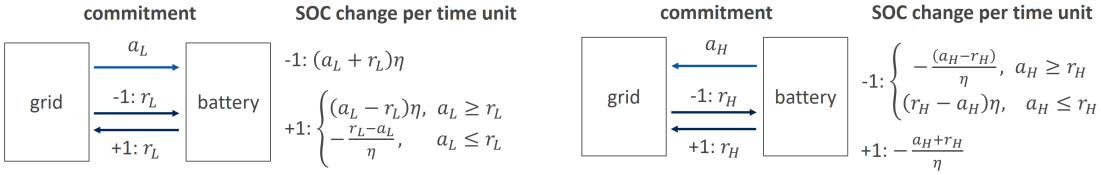
Certain properties can be restricted under binding energy capacity. For instance, when $k \leq \frac{1}{T_H - 1}$, the positive cost-saving synergy no longer holds if the arbitrage price is high enough compared to the per-unit price of the battery ($p^a \geq \frac{2c_0^b}{kT_H}$). This phenomenon does not occur in the base model, where positive cost savings are consistently achieved.

Benefit of stacking. Similar to Theorem 2.2, Theorem A.2 states that when energy capacity is not binding, the relative performance of stacking, $S = \frac{\Pi_{stk}^*}{\max(\Pi_{arb}^*, \Pi_{reg}^*)}$, is unimodal in $\bar{p}$ when $k \leq \frac{1}{\sqrt{2T_H}}$. When $k \geq \frac{1}{\sqrt{2T_H}}$, on the other hand, S is monotonically decreasing in $\bar{p}$ and $S = 1$ for $k \geq 1$. Furthermore, the maximum attainable relative performance for fixed k is unimodal in k, and the grand maximum ratio across all k converges to 2 as $T_L, T_H \to \infty$ (Corollaries A.2 and A.3). Numerically, the relative performance of stacking against the best standalone service can improve under correlated prices. For example, when $T = 24, T_H = 2$ with 1-hour energy neutrality, $k = 0.3125$ (the maximizer of S from Corollary A.2), and $\underline{p}^r = 15$, then $\max S = 2.375 > 2.09 = \frac{2T-2}{T-2}$, a sizable increase in the maximum attainable profit ratio compared to the uncorrelated setting. Interestingly, both PJM and ISO-NE have $k \in [0.1, 0.4]$ (see Appendix A.3.1 for numerical evidence related to k), which implies that realistic values of k are in the range where the benefit of stacking compared to standalone services may be particularly large.

2.6.2 Operations with Energy Loss: Round-Trip Energy Efficiency (η^2)

Until now, we have assumed perfect round-trip efficiency. In practice, there exists some inevitable energy loss when charging or discharging a battery due to friction and heat generation. In this section, we consider an imperfect battery with energy losses and show that stacking can be even more beneficial than under the previously considered perfect efficiency case. In fact, there exists another type of synergy, **energy replenishment cost saving**, due to stacking, which plays a powerful role and reinforces the benefits of cost-saving synergy.

Let $\eta^2 \in [0,1]$ denote the round-trip efficiency.[23] Then, decreasing the battery storage level by one unit delivers η units of energy to the grid, while increasing the storage level by one unit requires η^{-1} units of energy to be withdrawn from the grid. This requires differentiating between the amount of energy exchanged on the grid and battery SOC changes. As before, let $a_i, r_i, i = L, H$ be the arbitrage and regulation capacity that a battery commits to provide to the grid. Figure 2.6 illustrates the corresponding SOC changes with the +1/-1 regulation signal.



(a) low-price period (b) high-price period

Figure 2.6: Stacking's energy flow with round-trip efficiency $\eta^2 \in [0,1]$.

Arbitrage Only: The energy loss forces us to buy more energy in the low-price period ($\frac{A}{\eta^2} = a_L T_L$) while selling less energy in high-price period ($A = a_H T_H$). Thus, the objective function becomes:

$$\max_{A} \quad \bar{p}A - \underline{p}\frac{A}{\eta^2} - \frac{c_0^b}{E}(\frac{A}{\eta})^2 \tag{2.15}$$

$$\text{s.t.} \quad \frac{A}{\eta} \leq E. \tag{2.16}$$

The energy constraint (2.16) states that a battery selling A energy in the high-price period must store at least A/η energy in the battery. By redefining $\underline{p}' := \frac{\underline{p}}{\eta^2}, c_0^{b'} := \frac{c_0^b}{\eta}, E' := \eta E, p^{a'} := \bar{p} - \underline{p}'$, (2.15) – (2.16) can be restated as an arbitrage problem

[23] We assume the charging efficiency (η_c) and discharging efficiency (η_d) are the same ($\eta_c = \eta_d = \eta$) based on commonly reported values in empirical papers and battery specifications (e.g., [31]).

with perfect efficiency. When $p^{a'} > 0$, we obtain $A^*_\eta = \min(\frac{p^{a'}}{2c_0^{b'}}E', E')$ and $\Pi^*_{arb} = \begin{cases} \frac{(p^{a'})^2}{4c_0^{b'}}E', & \text{if } p^{a'} \le 2c_0^{b'} \\ (p^{a'} - c_0^{b'})E', & \text{otherwise} \end{cases}$. Otherwise, $A^*_\eta = 0$, as earning a positive profit is impossible due to battery inefficiency.[24]

Stacking: Frequency regulation requires an exact amount of committed energy r_i for $i = L, H$ to be withdrawn from the grid (-1 signal) or injected to the grid (+1 signal). With energy loss, the asymmetry in energy flow results in a net energy deficit of $r_i(\frac{1}{\eta} - \eta)$ every two time units when regulation is provided alone. Thus, additional energy needs to be replenished to the battery to ensure the deliverability of regulation service [58]. Combining the information from Figure 2.6 we can define D to be the absolute SOC increase during the low-price period, which must match the absolute SOC decrease during the high-price period:

$$D = \begin{cases} \frac{T_L}{2}[a_L(\frac{1}{\eta} + \eta) - r_L(\frac{1}{\eta} - \eta)], & \text{if } r_L \ge a_L \\ T_L a_L \eta, & \text{if } r_L < a_L, \end{cases} \tag{2.17}$$

$$= \begin{cases} \frac{T_H}{2}[a_H(\frac{1}{\eta} + \eta) + r_H(\frac{1}{\eta} - \eta)], & \text{if } r_H \ge a_H \\ \frac{T_H a_H}{\eta}, & \text{if } r_H < a_H. \end{cases} \tag{2.18}$$

We define the excess regulation values (in terms of DOD changes from the battery's perspective) as $x_L = \frac{(r_L - a_L)^+}{\eta}, x_H = (r_H - a_H)^+\eta$. Then, with energy loss, the objective of stacking becomes:

$$\max_{a_L, a_H, r_L, r_H} \quad \bar{p}a_H T_H - \underline{p}a_L T_L + p^r r_L T_L + p^r r_H T_H$$
$$-\tfrac{c_0^b}{E}(D^2 + 2D\max(x_L, x_H) + \tfrac{T_L}{2}x_L^2 + \tfrac{T_H}{2}x_H^2). \tag{2.19}$$

When $\eta = 1$, the objective function reduces to the base model ($D = a_L T_L = a_H T_H$). For simpler exposition, throughout Section 2.6.2, we follow the arbitrage-only model by modeling the energy constraint as $A/\eta \le E$, since selling A arbitrage to the grid will always require at least A/η energy to be charged to the battery and later discharged (the impact of binding energy capacity is illustrated in Appendix A.3.2). In Appendix A.4, we instead model the energy constraint as $D \le E$ and numerically check the sensitivity of our results.

Regulation Only: With regulation being the only service, we assume all additional energy for regulation is replenished in the low-price period without reselling energy to the grid in

[24]Note that with energy losses $\eta < 1$, the actual prices $(\bar{p}, \underline{p})$ matter, while previously for $\eta = 1$, the difference between prices, $p^a = \bar{p} - \underline{p}$, solely determined the profit of the arbitrage-only strategy.

the high-price period ($a_H = 0$).

Expanded Synergy and Improved Stopping Threshold. We leave the analysis of the optimal structure to Appendix A.3.2. We now mainly focus on *benefits of stacking* and expanded synergistic behavior.

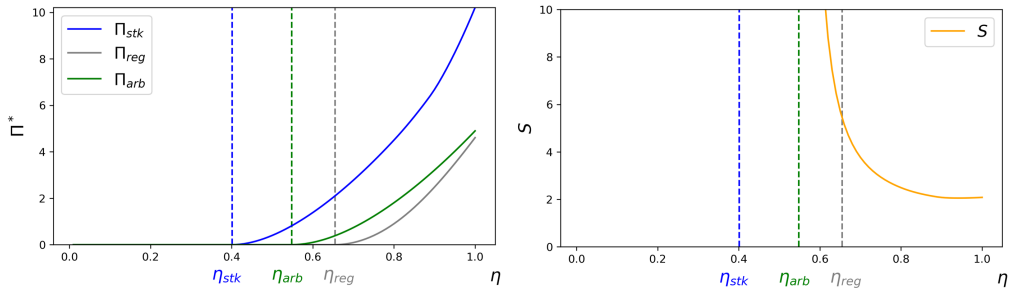
We examine one highly relevant effect of stacking: stacking broadens the battery utilization/deployment rate on the grid. In particular, low-efficiency batteries that would be uneconomical for standalone services due to negative profits can sometimes still achieve positive profits under stacking. To demonstrate this, we compare the minimum round-trip efficiencies that result in positive profits. Note that the profit is monotonic in η and there exists a threshold below which a positive profit is impossible due to inefficient batteries losing too much energy. Let $\eta_i,\ i \in \{arb, reg, stk\}$ be the efficiency stopping threshold for each operation such that $\Pi_i^* = 0$ for every $\eta < \eta_i$ and $\Pi_i^* > 0$ for every $\eta > \eta_i$. The following theorem states that stacking improves the stopping threshold.

Theorem 2.3 (**Improved stopping threshold**).
(a) $\eta_{arb} = \sqrt{\frac{\underline{p}}{\bar{p}}}$, $\eta_{reg} = \sqrt{\frac{(\underline{p}-p^r)^+}{\underline{p}+p^r}}$, *and* $\eta_{stk} = \sqrt{\frac{(\underline{p}-p^r)^+}{\bar{p}+p^r}}$.
(b) $\eta_{stk} \leq \min(\eta_{arb}, \eta_{reg})$.[25]
(c) $S = \frac{\Pi^*_{stk}}{\max(\Pi^*_{arb}, \Pi^*_{reg})} \to \infty$ *for* $\eta \downarrow \min(\eta_{arb}, \eta_{reg})$ *when* $\underline{p} > p^r$.

Theorem 2.3 highlights that stacking can expand battery deployment on the grid, since less efficient batteries can still be profitably used. Figure 2.7 illustrates stacking's enhanced profitability with an inefficient battery. Note that stacking more than doubles the profit of the best standalone service across all profitable efficiencies ($S > 2$ for every $\eta \in [\eta_{stk}, 1]$) and also significantly improves the stopping threshold (in Figure 2.7a, $\eta_{arb} = 0.548, \eta_{reg} = 0.655$, and $\eta_{stk} = 0.401$).

Beyond degradation cost savings, improved profitability can be explained by stacking's superiority in reducing energy loss. Analogous to the fact that cost-saving synergy reduces degradation costs due to the reduced size of smaller cycles compared to the cycle size of regulation alone, for inefficient batteries we have energy-saving synergy, which decreases net energy losses (and, therefore, decreases energy replenishment costs). For instance, (2.17)–(2.18) highlight that the SOC change in the low- or high-price period is not impacted as long as only free regulation is being used; this means that free regulation adds no extra energy losses compared to arbitrage alone. The following

[25]The inequality is strict for $p^r < \underline{p}$. When $p^r > \underline{p}$, the equality holds, and both regulation-only and stacking always make a positive profit regardless of η (no black region in Figure 2.8). Even with $\eta = 0$, a battery can provide regulation by adjusting energy consumption rates (energy is withdrawn unidirectionally from the grid, similar to demand response).



(a) Profit of each service (Π_i^*)

(b) Higher S ratios

Figure 2.7: Stacking performance with energy loss ($T = 16, T_H = 4, \bar{p} = 100, \underline{p} = 30, p^r = 12, c_0^b = 160$).

observation summarizes stacking's additional energy-saving benefits when dealing with an inefficient battery ($\eta < 1$).[26]

Observation 2.5 (Energy replenishment cost-saving). *Stacking reduces the round-trip energy loss (or, equivalently, the energy replenishment cost required for service deliverability) compared to providing the same quantity of individual services alone.*

By plotting optimal stacked battery operations for differing values of p^a/p^r and η, Figure 2.8 helps capture the extent to which stacking is beneficial for inefficient batteries. Stacking nearly always improves over standalone service when η is large — Figure 2.8's red region, corresponding to regulation-only service, only occurs for very small p^a/p^r values. Further, stacking can make a battery profitable even for very small η as long as p^a/p^r is sufficiently large (see the green region of Figure 2.8). Consistent with the base model, stacking shows the broadest synergistic properties (e.g. A^* strictly increasing in p^r) when free regulation only is optimal (the green region of Figure 2.8). While this only occurs for large p^a/p^r ratios in the perfect efficiency case, free regulation only may be optimal for a much wider range of p^a/p^r values for less efficient batteries. Other synergy properties are similarly expanded for inefficient batteries (see Corollary A.4 and Figure A.3).

2.6.3 Non-Uniform Regulation Signal

In the main model, we assumed a +1/-1 signal with strict energy neutrality. In reality, the signal does not need to follow this exact pattern. For example, ISO-NE's ENT (energy neutral trinary) signal consists of three discrete values (+1, 0, -1), where batteries are idle for

[26] As mentioned in the Introduction, executives from a major energy equipment supplier wanted to evaluate this.

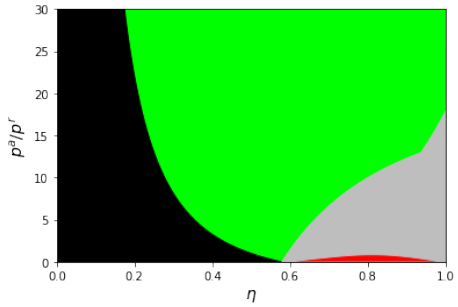


Figure 2.8: Illustration of optimal stacking for inefficient batteries when $p^r < \underline{p}$: green (free regulation; $a_H^* > 0$, $x_L^* = x_H^* = 0$), black (no battery use), red (regulation only; $a_H^* = 0$), and gray (excess regulation; $a_H^* > 0$, $x_L^* > 0$ and/or $x_H^* > 0$). Parameters: $T_L = 16$, $T_H = 4, \underline{p} = 20$, $p^r = 10$, and $c_0^b = 160$, with η and p^a varied.

signal value 0, while charging/discharging at their maximum regulation capacity for -1 and +1, respectively. Also, PJM's regD (dynamic) or ISO-NE's ENC (energy neutral continuous) signals have continuous values fluctuating between +1 and -1, reducing degradation from the setting used in the base model. In this section, we modify our initial assumption by introducing the dispatch-to-contract ratio and investigate the impact of this relaxation on our key findings.

Trinary Signal as a Proxy: We introduce here a trinary signal (+1, 0, -1) as a proxy for a non-uniform regulation signal. Let a constant α ($0 < \alpha < 1$) represent the dispatch-to-contract ratio, which is the fraction of time the signal takes value -1 or 1.[27] Specifically, we assume the following regulation signal sequence: +1, 0, -1, 0, +1, 0, -1, 0, $\cdots$, with the time spent in each segment of $\alpha, 1-\alpha, \alpha, 1-\alpha, \cdots$. When $\alpha = 1$, the trinary signal is equivalent to the +1/-1 signal from the base model. Predictably, a small α implies smaller degradation costs. For batteries, degradation costs vary with the amount of regulation service needed, e.g., 10% of the time ($\alpha = 0.1$) versus 100% ($\alpha = 1$), due to different depths of discharge (DOD).

In general, regulation prices could be related to the typical portion of time that the regulation signal is active (non-zero). Thus, we assume the regulation price $p^r(\alpha)$ to be an increasing function of α. While $p^r(\alpha)$ can take various functional forms, in Appendix A.3.3 we present comparative statics under two cases: (1) $p^r(\alpha) = c_1$ and (2) $p^r(\alpha) = c_2 \cdot \alpha$, where c_1 and c_2 are some positive constants. For simplicity, we will omit the dependency on α and use p^r when no confusion arises.

[27] [99] introduced the dispatch-to-contract ratio of regulation to represent the actual energy provided over the contract period (as a result of being called by ISO/RTOs) divided by the contracted capacity. This is equivalent to the average absolute value of the regulation signal.

With the trinary signal, our base model is easily modified: x_L and x_H are now multiplied by α as $x_i = \alpha(r_i - a_i)^+$ for $i = L, H$, capturing the fact that the small cycles due to regulation are shorter than in the base model. Appendix A.3.3 presents the optimal stacking strategy (Theorem A.5) and the upper bound on stacking's performance relative to standalone services (Corollary A.6).

Synergistic behavior. Synergistic behavior such as strict complementarity (obtained when using the maximum free regulation only) is still present for sufficiently large α. However, it requires a stronger condition than in the base model ($\alpha = 1$) under both constant and linear regulation price assumptions. This is because, for a constant regulation price, regulation becomes very attractive with a small α, making it generally optimal to use excess regulation instead of free regulation only. This remains true even with a linear regulation price, as the reduction in degradation from regulation (due to a small α) outweighs the decrease in regulation revenue.[28]

Benefit of stacking. When energy capacity is not binding, similar to the results for the base model, S is unimodal in $\frac{p^a}{p^r}$ (Corollary A.6); $\max S = \frac{2T+2\alpha^2-4\alpha-2(1-\alpha)\sqrt{2T}}{T-2}$ is achieved at $\frac{p^a}{p^r} = \frac{\sqrt{2T}}{\alpha}$, and $\max S$ is increasing in α. Since $\alpha = 1$ in the base model, the non-uniform signal decreases the maximum benefit. However, with sufficiently large T, the decrease is small ($\max S \approx 2$).[29] In Appendix A.3.3, Theorem A.6 states that $S \leq \frac{2T-2}{T-2}$, implying that binding energy capacity never improves the grand maximum of the S ratio. Interestingly, a binding energy capacity can enhance the relative advantage of stacking over standalone services for certain α. Such a scenario arises when $A^*_{stk} < A^*_{arb} = E$ and $\Pi^*_{arb} > \Pi^*_{reg}$ — the limited capacity restricts standalone arbitrage (which outperforms standalone regulation), whereas stacking remains unaffected due to its ability to balance the quantities of the two services (see Figure A.4 and Observation A.3 in Appendix A.3.3).

2.6.4 Power Capacity is Binding

Another key physical constraint of a battery is its power capacity (the maximum rate at which it can charge/discharge). In Appendix A.4 we present numerical evaluations using recent grid/market conditions to show that batteries maximizing profits would rarely be expected to use their full power or energy. Still, for the sake of completeness, we study binding constraints in this extension.[30]

[28] When regulation prices decrease faster than a linear function (e.g., $p^r = c_3 \cdot \alpha^2$), then synergistic behavior can expand beyond that of the base model.

[29] For $T = 96$ (representing a day with energy neutrality achieved within 30-minute intervals) and $\alpha \geq 0.6$ (as empirically observed in PJM), $\max S \geq 1.90$. As $T \to \infty$, $\max S \to 2$, regardless of α.

[30] Proposition A.2 in Appendix A.3.4 shows the equivalence of the optimal structure.

Effect of Bounded Power. In the low-price period, the maximum power used is $a_L + r_L$, which is the battery charge rate with a (-1) regulation signal. Similarly, the maximum power in the high-price period is $a_H + r_H$, the discharge rate with a (+1) signal. When enforcing a battery's limited power capacity, the optimization problem becomes:

$$\max_{A, r_L, r_H \geq 0} \quad \Pi = p^a A + p^r r_L T_L + p^r r_H T_H - \frac{c_0^b}{E}[A^2 + 2A \cdot \max(x_L, x_H) + \frac{T_L}{2} x_L^2 + \frac{T_H}{2} x_H^2] \tag{2.20}$$

$$\text{s.t.} \quad a_i = A/T_i \text{ for } i = L, H \tag{2.21}$$

$$x_i = (r_i - a_i)^+ \text{ for } i = L, H \tag{2.22}$$

$$r_i + a_i \leq P \text{ for } i = L, H \tag{2.23}$$

$$A \leq E. \tag{2.24}$$

Binding power capacity P may force the battery to choose between offering less arbitrage or less regulation.[31] Now, optimal excess regulation may no longer be equal:

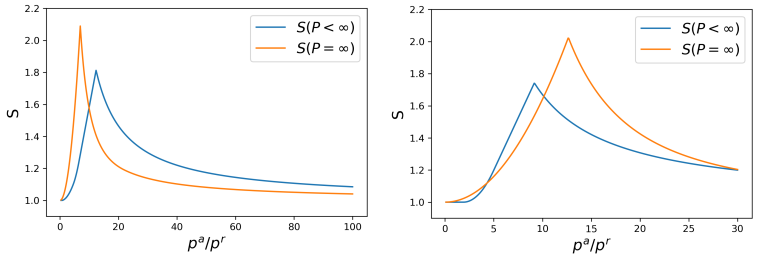
Lemma 2.2 (Excess regulation: Bounded power). *$r_L^* + a_L^* \leq r_H^* + a_H^*$ and $x_L^* \geq x_H^*$.*

A high arbitrage discharge rate a_H may drive high power usage ($a_H + r_H$) in the high-price period. Without a power constraint, we always prefer equal excess (Lemma 2.1); however, if the power capacity limits the amount of regulation provided in the high-price period, then Lemma 2.2 suggests choosing $x_L^* > x_H^*$ to take advantage of the remaining power in the low-price period. See Propositions A.1 – A.2 and Figures A.7 – A.8 in Appendix A.3.4 for details of the optimal structure.

Synergistic behavior. Though most key properties of the base model hold when power P is sufficiently large but still binding (e.g., $A_{stk}^* > A_{arb}^*$ and $R_{stk}^* > R_{reg}^*$; see Table A.7 for details), it is worthwhile to mention some consequences of the constraint. When power is binding in the high- or low-price period, there is a trade-off between the amount of arbitrage and regulation. For example, limited power might prevent the battery from using the maximum free regulation.

Benefit of stacking. According to Proposition 2.2, negative cost-saving synergy may occur when excess regulation values are highly imbalanced: $x_L^* \gg x_H^*$. As detailed in Proposition A.1 and Figure A.6, negative cost-saving synergy can occur with sufficiently large regulation price p^r and sufficiently small power P. Though some synergy properties may be weakened under binding power constraints, below we show that stacking may continue to bring significant benefits in these scenarios.

[31] We assume a single power capacity for charging/discharging following the typical large-scale battery specifications reported by the U.S. Energy Information Administration [55]. Many batteries are inherently designed to have the same charging/discharging capacity for safety/reliability (e.g., Tesla's Powerwall).



(a) narrow peak (small $\frac{T_H}{T}$) (b) tight energy neutrality

Figure 2.9: Stacking's performance with power binding ($P < \infty$) versus power not binding ($P = \infty$).
(a): $P/E = 0.25$ (blue), $c_0^b = 100$, $\frac{T_H}{T} = \frac{1}{24}$, (b): $P/E = 0.15$ (blue), $c_0^b = 100$, $\frac{T_H}{T} = \frac{1}{8}$.

Impact of Power Capacity on Benefits of Stacking. Recall from Theorem 2.2 that at its upper bound, stacking can roughly double the profit of the best standalone service in the base model setting. In this section, we show that the same upper bound of $\frac{2T-2}{T-2}$ is a tight upper bound on stacking performance with limited power capacity.

Theorem 2.4 (Upper bound on stacking's performance: Bounded power). $S \leq \frac{2T-2}{T-2}$.

The theorem implies that the maximum value of S under the power binding setting does not improve over the maximum in the non-binding setting. Interestingly, however, this does not necessarily mean stacking's benefits always decrease with a tighter constraint.

Figure 2.9 illustrates two circumstances in which $S(P = \infty) < S(P < \infty)$. In each of these cases, power limits the more profitable standalone service, while stacking allows adding the alternative service. The blue peak in (a) corresponds to a case when the arbitrage price is very attractive, but the revenue potential of arbitrage-alone is limited due to the short length of the high-price period and the power constraint. In such a case, adding extra regulation during the low-price period (when power is not binding) yields significant improvements over the single-service alternatives; such a relative improvement is not possible once the power constraint is removed. The blue peak in (b) is based on a symmetric logic (for the case when regulation is more profitable). Interestingly, even in the limiting case as $P \to 0$, stacking can maintain a relative benefit over the best single service as long as $p^a \geq 2p^r$ (see Proposition A.1 in Appendix A.3.4).

2.6.5 Summary of the Generalizations and Extensions

Table 2.2 summarizes key properties under the considered generalizations/extensions; for simplicity, we compare cases when energy capacity is non-binding (when c_0^b is sufficiently

Properties	Base model	Correlated prices	Inefficiency	Trinary signal	$P < \infty$
A^* increases in p^r	$p^a \geq (T-2)p^r$	expanded	expanded	reduced	reduced
R^* increases in p^a	$p^a \geq (T-2)p^r$	expanded	expanded	reduced	reduced
$A^*_{stk} > A^*_{arb}$	always	same*	same*	same†	same‡
$R^*_{stk} > R^*_{reg}$	$p^a > (T-2)p^r$	expanded	expanded	reduced	same‡
$A^* > 0$	always	same*	same*	same†	same‡
$x^*_L = x^*_H$	always	same*	same*	same	same‡
$\frac{R^*}{A^*}$ indpt. of c^b_0	always	same	same	same	dependent
$\frac{R^*}{A^*} \geq 2$	always	same	same*	same	same‡
$\max S$ (large T_L, T_H)	2	2	∞	2	2
Cost-saving synergy	always	same*	same*	same†	same‡
Superlinear profit	always	same*	same	reduced	reduced

Table 2.2: Key properties under the generalizations considered when c^b_0 is sufficiently large.

*: sufficiently small $k > 0$; *: sufficiently large $\eta < 1$; †: sufficiently large $\alpha < 1$;
‡: sufficiently large P, at least one of which is still binding at optimality.

large). The key messages are three-fold. First, the structural properties of the base model, such as maintaining equal excess regulation ($x^*_L = x^*_H$), largely hold. Second, synergistic behaviors under simultaneous stacking, e.g., supermodularity (Proposition 2.3) and increased utilization (Observation 2.3), are still present except when providing one service alone is optimal (e.g., when α is sufficiently low). In fact, the synergy can be expanded and increased with either (1) correlated prices or (2) round-trip energy loss. Third, the benefits of stacking (compared to standalone services) identified in Theorems 2.1–2.2 remain the same or even improve (e.g., with inefficient batteries). Some properties only hold within certain parameter ranges, detailed in Table A.8.

We perform an extensive numerical study in Appendix A.4 to confirm that our analytical insights continue to hold with real-world price and regulation signal datasets and more sophisticated optimization models. We also demonstrate how battery operators may benefit from this work by exploring when the benefits of stacking are likely to be higher by addressing two questions: (1) "Which ISO markets offer the greatest benefits for battery operators adopting stacking?" and (2) "Which types of batteries derive the greatest benefit from stacking in a given grid/market environment?" We find that (i) benefits of stacking tend to be greater in ISO markets that are favorable to arbitrage and less favorable to regulation services (e.g., a smaller $\frac{p^r}{p^a}$ ratio or weak energy neutrality guarantees), and (ii) second-hand batteries (many EV batteries will retire and become available after being repurposed), due to their reduced cycle counts and lower round-trip efficiency, benefit the most from stacking's cost savings and thus should prioritize implementing stacking.

2.7 Closing Remarks

Energy stacking is one of the most important open research questions related to the electric power industry for the OM academy. Our research fills an important gap in the literature by providing insights into the mechanism by which stacking improves profitability. This work reveals that there often exists a cost-saving synergy where the degradation cost of joint services becomes smaller than the sum of individual costs if we had performed each service alone. We illustrate how cost savings induce synergies and show that these key properties remain quite consistent (and can even be expanded) under more realistic model extensions.

This work opens several avenues for future research. First, our model could be extended to incorporate a broader set of services, such as peak shaving, which has a different revenue mechanism than arbitrage. Second, exploring the impact of alternative battery ownership models, such as the servicization model [138], could be valuable. Lastly, we believe that future research could apply our model to electricity market design, especially considering the recent adjustments made to market rules in the United States (e.g., FERC Order No. 755), as more batteries are expected to increasingly leverage stacking.

CHAPTER 3

Dynamic Valuation of A Battery Under Performance Degradation

3.1 Introduction

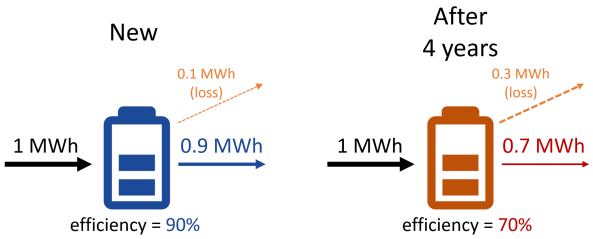
The modern electrical grid is facing unprecedented challenges amid a rapidly evolving energy landscape. Two of the most pressing issues are the growing nonstationarity or fluctuations in electricity supply and demand, and the surging electricity consumption.

Fluctuations in supply and demand have always existed, but the increasing reliance on variable renewable energy sources has made them more volatile and less predictable, complicating efforts to maintain grid stability. At the same time, the rapid growth of energy-intensive technologies—especially AI/ML and cryptocurrencies—is significantly amplifying electricity demand. By 2026, the combined electricity consumption of these technologies is projected to reach 300 TWh, surpassing the total domestic electricity usage of countries like the Netherlands, Sweden, and Japan ([182]).

Grid-scale battery energy storage systems (BESS) are batteries on the electric grid that store energy and then supply it back to the grid at a more beneficial time, such as during nighttime when solar power is unavailable or during lulls in the wind when wind turbines cannot produce power. Among many storage options (e.g., hydropower storage, thermal storage), BESS are considered to be a pivotal technology in establishing cleaner and more sustainable energy systems due to batteries' fast responsiveness and flexibility. BESS support power system reliability (e.g., via real-time supply/demand match) and facilitate the seamless integration of renewable energy sources (e.g., by mitigating variability from solar and wind generation). The growing importance of BESS is recognized in major policy roadmaps, including The Long-Term Strategy of the United States and the International Energy Agency's Net Zero Emissions by 2050 Scenario, both of which anticipate substantial expansion in battery deployment.



(a) Energy capacity degradation



(b) Energy efficiency degradation

Figure 3.1: Two types of battery performance degradation: (a) Energy capacity degradation—a reduction in the maximum amount of energy a battery can store; and (b) Energy efficiency degradation—a decrease in the amount of retrievable energy per unit of energy charged.

However, batteries have a finite lifespan and require periodic replacement. The problem of how to optimally use a battery with a finite lifespan relates to other streams of literature, such as the machine replacement problem and Hotelling's rule, which addresses the extraction of non-renewable resources by reflecting their scarcity and ensuring economically optimal use over time; however, the lessons from these streams of work are not directly transferable to the battery control problem due to its unique dynamics. Specifically, batteries suffer from two main types of performance degradation. The first is energy capacity degradation, which refers to a reduction in the maximum amount of energy that a battery can hold over time, as shown in Figure 3.1a.[1]

The second type is energy efficiency degradation. When a battery is charged and discharged, a portion of the energy is lost and released as heat. Round-trip energy efficiency measures the percentage of energy injected into a battery that can be retrieved later (with the remainder being lost). As the battery keeps operating, its energy efficiency diminishes over time, resulting in less retrievable energy per unit of energy charged, as illustrated in

[1]In the case of electric vehicles (EVs), for example, energy capacity determines the vehicle's range (the maximum distance the vehicle can travel before recharging the battery). Due to permanent decrease in capacity (and corresponding reduction in range), EV batteries typically require replacement once the capacity degrades to 80% of the nominal value ([217]).

Figure 3.1b. This also implies that when a battery is committed to providing a service—such as delivering a certain amount of energy at a given time—more energy must be stored over time, typically by purchasing from the grid, to offset increased losses and ensure service deliverability. For many battery applications, efficiency degradation may significantly affect the profitability of the battery.

This work is primarily motivated by the observation that both academic literature and industry practices face fundamental challenges in accurately quantifying the operational costs of batteries. Notably, most existing research does not optimize battery usage over its lifetime. Surprisingly, a majority of papers on the value of battery storage and optimal battery control in operations research and management science either overlook battery degradation altogether or treat it in an oversimplified manner (see Table 3.1 in the Literature Review section). Among the studies that do account for degradation, most focus solely on capacity degradation only and adopt a static framework. Cost-amortization, which is arguably the most widely adopted approach for quantifying battery usage costs in the battery literature and industry practice, assumes battery characteristics remain unchanged.[2] However, the approach is inherently static, failing to capture the gradual performance deterioration over the battery life.

Secondly, until recently, even when some form of capacity degradation was considered, efficiency degradation has been largely ignored in both battery research and industry practice. In the operations literature, efficiency is almost always assumed to be constant over time (see Table 3.1). However, several experimental and empirical papers have reported a non-trivial amount of energy efficiency degradation (e.g., [115] report a 7.5% decrease in efficiency within the first 160 cycles). Some recent studies, such as [52], have reported the deployment of batteries with very low energy efficiency (e.g., 30 – 70%) in electrical grids. This raises concerns about the economic feasibility of battery applications, particularly when a service's profit margins are slim. In fact, for many battery applications, energy efficiency degradation may be more critical than capacity degradation as we illustrate later.

Recognizing these gaps, our research investigates how capacity and efficiency degradation influence optimal battery control decisions. Below, we summarize our key research questions (RQs) and corresponding contributions:

- **RQ1: Optimal Dynamic Policy.** We analytically characterize the optimal con-

[2]Cost-amortization assumes periodic replacements of batteries within a specified time frame, such as every 11 years, as indicated in [110]. Cost-amortization has gained popularity due to its intuitive nature and simplicity in incorporating it into optimization models as a cost/penalty term. Examples include assuming fixed costs per day ($/day), fixed costs per energy throughput ($/MWh), or fixed costs per cycle for a given depth-of-discharge (DOD). The cost values are typically based either on shelf lives (e.g., manufacturers' warranty) or cycle counts (e.g., cycle-DOD graphs).

trol policy, recognizing that our usage will impact battery degradation. To highlight the significance of capturing efficiency degradation, we compare two settings: in the first model, we assume capacity degradation only, while the second model allows for the presence of efficiency degradation. We demonstrate a structural and systematic difference in optimal behavior over time. For instance, under capacity degradation only, battery utilization under the optimal policy increases monotonically over time. In contrast, when efficiency degradation is present, optimal utilization may decline over the battery's lifetime, highlighting when and why commonly used heuristics can lead to severe suboptimality. We provide an economic interpretation by analytically quantifying the opposing forces of discounting and degradation.

- **RQ2: Systematic Performance Evaluation of Commonly Used Heuristics.** Given the popularity of heuristics and the absence of theoretical or systematic evaluations of their performance, we investigate when and where heuristic policies exhibit small or large suboptimality. We show that existing heuristics indeed become near-optimal under certain circumstances (e.g., no discounting or infinite horizon). However, in general, we show that a fixed depth-of-discharge (DOD) policy is 90.25%-optimal measured in cumulative revenue. As [111] highlights the extremely thin margins in most battery applications as of 2025, even this level of suboptimality can have a significant impact on battery profitability. In the presence of efficiency degradation, these heuristics may result in much more severe profit losses.

- **RQ3: Sensitivity Analysis for Managerial Implications.** We derive managerial implications by examining how different battery types and operating environments influence utilization and cumulative revenue. We further show that a battery experiencing both capacity and efficiency degradation always operates at a strictly lower utilization than one facing only capacity degradation, regardless of parameterization. In addition, we extend our models to incorporate multiple energy prices and alternative forms of degradation functions. We find that while the overall insights remain robust, certain properties require more nuanced analysis. For instance, when considering different forms of degradation functions, we examine how the DOD-elasticity of the degradation function—the extent to which the degradation rate responds to changes in the DOD level—affects the distribution of revenue over time.

3.2 Background and Setting

We first provide some background on battery operations. Section 3.2.1 introduces energy arbitrage, the battery application we consider in this work; Section 3.2.2 explains battery performance degradation including the functional form of degradation and the relationship between capacity and efficiency degradation; Section 3.2.3 illustrates commonly used heuristics in the literature/practice.

3.2.1 Battery Application: (Day-Ahead) Energy Arbitrage

In electric markets, batteries can earn arbitrage revenues by being charged when wholesale prices are low and discharged when prices are high. While providing arbitrage, batteries support grid sustainability by shifting energy from periods of low to high value. Arbitrage also helps smooth energy prices throughout the day, thereby enhancing the economic viability of integrating additional renewable energy capacity.

In this study, we examine a day-ahead (forward) energy market where energy prices are set and settled on an hourly basis. Assuming representative energy market conditions, we consider two prices: high price $\bar{p}$ and low price $\underline{p}$, which will be repeated across multiple days.[3]

We now explain how a battery performs energy arbitrage. Let $x \in (0, 1]$ denote one-way energy efficiency of the battery. Discharging the battery by one unit delivers (sells) x units of energy to the electric grid. Charging the battery by one unit requires $1/x$ units of energy to be withdrawn (bought) from the grid. Thus, the effective profit from providing x units of arbitrage service (measured by the amount of energy sold) can be expressed as:

$$p^a(x) := \bar{p}x - \frac{\underline{p}}{x}. \tag{3.1}$$

We refer to the lower bound $\underline{x} := \sqrt{\frac{\underline{p}}{\bar{p}}}$ as a shut-off efficiency, since operating the battery leads to negative margin for any $0 \le x < \underline{x}$.

3.2.2 Battery Performance Degradation

Battery degradation refers to the physical deterioration of a battery over time. The impact of battery degradation is multifaceted: it limits the amount of energy that can be stored in the battery due to capacity degradation and reduces the arbitrage margin $\bar{p}x - \frac{\underline{p}}{x}$ due to

[3]We interpret these energy prices as expected values derived from historical data: $\bar{p} = \mathbb{E}[\bar{p}]$ and $\underline{p} = \mathbb{E}[\underline{p}]$. We later relax this assumption in Section 3.5.2, allowing for multiple price pairs $(\bar{p}_i, \underline{p}_i)$ for $i \in [N]$.

efficiency degradation.

There are many factors affecting degradation rates. High temperatures, high charge rates, and deep discharges are well-known accelerating factors. In this work, we mainly focus on depth-of-discharge as a key driver of battery performance degradation, since modern battery management systems can control the effects of temperature and charge rate.[4]

To capture gradual degradation of battery performance over time, we adopt a fluid approximation of the degradation process. This is appropriate because each charge/discharge cycle contributes only a small fraction to overall degradation, making a continuous model suitable for long-term analysis. This justification is formally stated in Appendix B.2.1.

The depth of discharge (DOD) for a given time t, denoted by $u(t) \in [0, 1]$, is defined as the ratio of the amount of energy discharged, $D(t)$ (in MWh), to the battery's current[5] (i.e., remaining) energy capacity, $E(t)$ (in MWh):

$$u(t) := \frac{D(t)}{E(t)}. \tag{3.2}$$

Here, $E(t)$ represents the maximum energy the battery can store at time t, which declines over time due to capacity degradation.

It is well-known that DOD has a significant and nonlinear (convex) effect on battery degradation, with higher DOD levels accelerating degradation per unit of discharged energy. The cost of a single cycle of DOD u can be characterized by the (quadratic) degradation cost function $\Phi(u) : [0, 1] \to \mathbb{R}$ ([205]):

$$\Phi(u) = ku^2, \tag{3.3}$$

for some degradation coefficient $k > 0$ (see Appendix B.1.2 for details). This quadratic form follows standard models in the engineering literature and captures the nonlinear, convex relationship between DOD and degradation observed in experimental studies.

Following broad empirical and experimental evidence (e.g., [204, 158]), we model the

[4]For stationary battery applications (e.g., energy arbitrage), advanced battery management and HVAC (heating, ventilation, and air conditioning) systems allow control of temperature and charge rate, making their impact on degradation minor ([107, 181]).

[5]Nominal capacity, $E(0)$, is sometimes used to define DOD as $u(t) = \frac{D(t)}{E(0)}$, particularly in cost amortization. However, this definition can be misleading, as it does not account for capacity degradation over time (e.g., discharging an amount $D(t)$ may become infeasible as the battery's capacity decreases). See Appendix B.1 for details.

battery's capacity over time using the following degradation dynamic:[6]

$$\dot{E}(t) = -E(t)\Phi(u(t)). \tag{3.4}$$

The two types of degradation—capacity degradation and energy efficiency degradation—are closely related, often occurring simultaneously due to underlying physical and chemical processes such as increased internal resistance (see [154]). While the relative rates of degradation can vary by battery chemistry, design, manufacturer, and usage patterns, empirical and experimental studies consistently report a strong correlation between the two ([164, 37]). Appendix B.1.4 provides experimental/empirical evidence on the linear relationship between capacity and efficiency degradation. Following the empirical evidence, we model a linear relationship between $\Delta E := E(0) - E(t)$ (capacity loss) and $\Delta x := x(0) - x(t)$ (one-way efficiency loss):

$$\Delta x = \alpha_1 \cdot \Delta E,$$

where $E(0)$ and $x(0)$ represent nominal capacity and efficiency, respectively, and $\alpha_1 \geq 0$ is a constant that can be fitted using experimental or empirical data. This is equivalent to:

$$x(t) = \alpha_0 + \alpha_1 \cdot E(t), \tag{3.5}$$

for $\alpha_0 := x(0) - \alpha_1 E(0)$ ($\alpha_0 \in \mathbb{R}$).

3.2.3 Commonly-Used Heuristics

Cost Amortization. A battery operator needs to balance the revenues of battery utilization with the costs of usage-based battery degradation. Arguably, the most common way to factor in degradation is called "cost amortization." This approach is supported by the practices of large-scale battery operators, who maintain a specific capacity level by augmenting the decreased capacity with new batteries to ensure consistent service delivery and quality ([25, 130, 163]). We describe two heuristics below.

Heuristic I: Fixed-A policy. One simplest approach to account for degradation is to assume a fixed cost ($/year), often under the assumption of a predetermined usage pattern. For instance, [110] assumes in its Levelized Cost of Storage Analysis that the battery (100MW/200MWh) discharges 180MWh (one cycle per day), operating 350 days per year. Similar assumptions appear in many white papers evaluating the economics of BESS (e.g.,

[6] A discrete counterpart is given by $E_{i+1} - E_i = -\Delta t \cdot E_i \cdot k u_i^2$, where E_i and u_i denote the battery energy capacity and DOD at time index i, respectively, and Δt is the time interval between cycles.

[63, 49]). The cost is typically based on the battery's shelf life (often 20 to 30 years) or the terms of the manufacturer's warranty. Such assumptions are also commonly used in the machine replacement literature (e.g., [185]), where machines deteriorate under a fixed production schedule (e.g., a constant number of units produced per day).

Under such assumption, a battery-operating policy yields a constant throughput, i.e., the amount of arbitrage quantity A (defined as the energy amount sold at the high price) is fixed. Throughout this work, we refer to such a policy (that considers only batteries' shelf life or that is based on \$/year) as a "fixed-A policy" or "fixed throughput policy."

Heuristic II: Fixed-DOD policy. Another common cost-amortizing approach factors in the effect of the usage level on degradation. This is mainly motivated by the experimental/empirical observations that batteries are replaced much earlier than their shelf lives ([130, 69]). Most common approaches assume a fixed cost per energy throughput (\$/MWh), which is popularly used in the literature due to its simplicity (e.g., [174]).

A more refined approach models a fixed cost per DOD-cycle (\$/DOD-cycle), capturing the nonlinear and convex impact of DOD on degradation, as described in Equation (B.3) in Appendix B.1. Specifically, from our two-price setting ($\bar{p}$ and $\underline{p}$) in Section 3.2.1 and the quadratic degradation in (3.4), the optimal fixed-DOD level $\bar{u}$ can be determined as follows:

$$\bar{u} := \arg\max_{u\in[0,1]} [p^a \cdot u - c^b u^2]E,$$

where $p^a = \bar{p}x - \frac{p}{x} > 0$ is the arbitrage margin and c^b (\$/MWh) is the battery price coefficient (it is a function of the battery's characteristics such as cycle counts and chemical composition; see Appendix B.1.2 for details). The penalty term $c^b E u^2$ reflects that battery degradation—representing the battery replacement cost—is proportional to the battery price coefficient and the battery size, and increases quadratically with DOD. This fixed-DOD policy yields

$$\bar{u} = \min(\frac{p^a}{2c^b}, 1).^7 \tag{3.6}$$

Throughout this work, we refer to such a policy as a "fixed-DOD policy."[8] Alternatively, rather than relying on cost amortization, one can construct a fixed-DOD policy by explicitly accounting for gradual battery deterioration, which we will discuss later.

Remark on cost amortization. Clearly, cost amortization simplifies optimization by avoiding the need to model gradual performance deterioration; the resulting models and policies are static, treating battery characteristics as fixed (e.g., no efficiency degradation).[9]

[8]Under a fixed-DOD policy, a constant portion of capacity is used, while the total battery capacity decreases; that is, the arbitrage quantity A decreases monotonically over time.

[9]In practice, technological restrictions are often imposed. For example, some battery manufacturers limit

Field	Study	Optimal Operations			Degradation-Awareness			
		Usage	Maintenance	Analytic	Capacity (Quantity)	Efficiency (Quality)	Maintenance Cost	Dynamic Model
OR/MS	[116, 124]	×	✓	×	×	×	✓	✓
	[185]	×	✓	✓	✓	×	×	✓
	[189, 179, 46, 45]	✓	✓	✓	×	×	✓	✓
White papers	[63, 49, 110]	✓	×	×	✓	×	×	×
Enginr.	[52, 164, 12, 115]	×	×	×	✓	✓	×	✓
	[174, 192]	✓	×	×	✓	×	×	×
	[71, 203, 34]	✓	×	×	✓	×	×	✓ (DP)
	[4, 122, 35]	✓	×	×	✓	✓	×	✓
	[72, 37, 193]	✓	×	×	✓	✓	×	✓
OR/MS	[101, 200, 198, 161, 215, 131, 41, 216, 117, 201, 93, 199, 33]	✓	×	✓	×	×	×	×
	[121, 15]	✓	×	✓	✓	×	×	×
	[213]	✓	×	✓	✓	×	×	×
	[17]	✓	×	✓	✓	×	×	×
	[23]	✓	×	×	✓	×	×	×
	This study	✓	×	✓	✓	✓	×	✓ (DP)

Table 3.1: Related literature: Modeling battery performance degradation.

Table 3.1 in the Literature Review lists studies that adopt either a fixed annual cost or a fixed-DOD policy. Later, we will evaluate these heuristics against the optimal policy.

3.3 Literature Review

This work contributes to the optimal battery control literature by highlighting the importance of capturing both capacity and efficiency degradation for the economic viability of battery energy storage systems (BESS). To our knowledge, it is the first to analytically examine the dynamic, optimal use of batteries when both forms of degradation are present. Table 3.1 provides a comprehensive, though not exhaustive, overview of related studies. Section 3.3.1 reviews degradation-aware research from the machine maintenance and re-

operation to specific state-of-charge (SOC) ranges (e.g., 5% to 95%) to mitigate extreme degradation from deep cycling. In these cases, it is natural to define energy capacity in terms of "usable energy" E rather than the technical maximum, enabling our results to generalize accordingly.

placement literature as well as the non-renewable resource extraction (commonly referred to as Hotelling's rule) literature in operations research and management science (OR/MS), while Section 3.3.2 covers relevant studies on battery energy storage in both OR/MS and engineering fields.

3.3.1 Degradation-Aware Models in OR/MS: Machine Replacement and Non-Renewable Resource Extraction

Machine maintenance and replacement problems have been extensively studied for decades, with initial works dating back to the 1940s ([183]). Since then, the literature has expanded in numerous directions, including: one-unit vs. multi-unit systems; deterministic vs. stochastic deterioration; finite vs. infinite horizons; discrete vs. continuous time; binary-state (fully functional or failed) vs. multi-state deterioration; and complete vs. incomplete information. For comprehensive overviews, see survey papers by [190, 194]. In parallel, Hotelling's rule has been extensively studied to examine the optimal extraction of non-renewable natural resources, emphasizing how scarcity considerations shape intertemporal allocation ([75, 43]). Our work is most closely related to three substreams of this research: (1) condition-based production, (2) multi-state deterioration, and (3) optimal control theory. We elaborate on each below.

Condition-based Production and Maintenance. Early studies in the machine maintenance literature focused on optimizing maintenance policies under exogenous (constant or time-varying) production or usage rates. Integrated models that jointly optimize production and maintenance decisions have only recently gained attention.

[189] examine the value of dynamically adjusting production based on condition monitoring—to balance deterioration, maintenance costs, and production revenue. Several follow-up studies (e.g., [46, 179, 45]) build on this framework.

However, all of these works assume binary health states, where the machine operates perfectly until the deterioration level exceeds a failure threshold. In such settings, degradation influences only maintenance costs—not production quantity or quality—as long as the system remains functional. Such degradation dynamics significantly differ from the battery performance degradation considered in this work, where the quantity and quality of the service provided by the battery, and thus its economics, continuously evolve as two distinct types of degradation (capacity and efficiency) progress.

Multi-State Deterioration. Some studies, particularly in engineering, model machines as undergoing gradual, multi-state deterioration—transitioning through several health levels from new to failed (e.g., [116, 176, 124]). These models typically assume Markov processes,

with transitions from higher to lower performance states. While the framework is flexible and broadly applicable, most findings in this stream rely on numerical analysis. In contrast, we focus specifically on battery systems and provide analytical insights into optimal operations under two distinct performance degradation models: capacity and efficiency loss.

Optimal Control Theory

To study optimal battery operation over its lifetime, we employ optimal control theory. [171] outlines six canonical model types in optimal control theory, classified by the structure of the objective function and state equations. Our unified model—which accounts for both capacity and efficiency degradation—belongs to a category[10] for which few general results have been established, aside from the insight that the optimal policy may take values either at the boundary or in the interior. We will establish the structural properties of the optimal policy for our model.

In the OR/MS literature, several studies apply optimal control theory to machine replacement and maintenance problems. [185] is among the earliest to solve a generalized machine replacement problem using Pontryagin's Maximum Principle, determining both the (typically bang-bang) maintenance policy and the optimal sale date of a machine. Subsequent studies extended this framework (e.g., [13, 91]). However, these works assume exogenous production rates and do not capture the performance degradation characteristic of batteries, where both capacity and efficiency degrade simultaneously.

Hotelling's model employes optimal control theory to study the optimal extraction rate of a non-renewable resource. Hotelling's rule predicts that the price of a non-renewable resource will increase over time at a rate equal to the discount rate to ensure efficient or optimal extraction. Many variants of the problem have been considered, such as increasing extraction costs as the resource becomes more scarce (e.g., see [75, 113]). Also, the degradation dynamics of the batteries—stemming from both capacity and efficiency losses—make the lessons from these models nontransferable to battery control (we later derive implications that differ from Hotelling's model).

3.3.2 Optimal Control of (Battery) Energy Storage

Studies in OR/MS. The OR/MS literature has shown rapidly growing interest in the optimal control of energy storage and sustainable operations in the energy sector (see review papers such as [141]). A wide range of studies explores the optimal control of energy storage across various applications. These include integration with renewable energy sources (e.g.,

[10]The objective function takes the form $c(x)q(u)$, and the state equation is $(ax + d)b(u) + e(x)$, where x and u denote the state and control variables, respectively (see Table 3.3 of [171]).

[73, 101, 161, 216, 199, 92]), battery use in electric vehicles (EVs) (e.g., [41, 162, 70, 201, 33]), and grid services (e.g., [200, 131, 117, 11]). Notably, most of these studies abstract away battery performance degradation when deriving analytical insights or characterizing optimal policies.

A few studies do consider battery capacity degradation. For example, [121] and [15] model EV battery charging and swapping systems where accounting for battery lifespan is essential for economic analysis. However, these models assume a fixed annual cost ($/year), and do not account for how usage patterns influence degradation.

A small subset of papers—such as [86], [23], [213], and [17]—do incorporate usage-based capacity degradation (e.g., cost per depth-of-discharge cycle). Still, these studies exclusively focus on capacity degradation and do not consider efficiency degradation, which is a central and distinguishing feature of our work.

Degradation-Aware Numerical Studies in Engineering.

Empirical/experimental study. Historically, research has focused on capacity degradation (e.g., [204]), largely due to its impact on EV range and the battery design improvements driven by EV applications. Recently, a growing number of studies have stressed the economic importance of efficiency degradation (e.g., [52, 164, 12, 115]). These works consistently report that as capacity declines, efficiency also deteriorates, highlighting the need to incorporate both degradation types in operational decision-making. However, while these studies provide valuable insights into degradation patterns and the relationship between capacity and efficiency loss, they do not address how to optimize operations to maximize economic or environmental outcomes. Additionally, empirical findings from experimental studies and industry reports on battery performance degradation show how a battery's charge-discharge curve (i.e., voltage-capacity curve) shifts with usage, providing insight into the deterioration of key performance metrics—most notably, capacity and efficiency (e.g., [204, 164, 12, 115]; see Appendix B.1 for further details).

Dynamic Valuation of Energy Storage. A few studies propose dynamic valuation frameworks incorporating battery degradation ([71, 34]). For example, [203] introduces a dynamic evaluation approach considering capacity degradation and concludes that second-life batteries—repurposed from EVs—can be more cost-effective for grid services than new batteries. However, the paper does not account for efficiency degradation (constant efficiency is assumed).

Some papers go further by modeling both capacity and efficiency degradation, especially in the context of second-life batteries. [4] conduct a sensitivity analysis using a fixed depth-of-discharge (DOD) policy (75%)[11] to assess how efficiency loss affects cumulative energy output

[11]The DOD level is fixed and not optimized in their model.

(kWh) and life-cycle greenhouse gas emissions. They find that battery efficiency degradation may limit environmental benefits—a concern also noted in [122]. Similarly, [37] simulate two dispatch strategies—one assuming fixed round-trip efficiency and the other accounting for diminishing efficiency—and find that accounting for efficiency loss leads to less frequent use, reduced operating costs, and extended system lifespan. Several numerical studies account for both capacity and efficiency degradation, including depth-of-discharge (DOD)-specific effects, highlighting that battery degradation is a critical factor in determining profitability ([72, 193]).

However, these studies are primarily simulation-based, relying on specific scenarios without generalizing their findings. They do not characterize optimal control policies or explore the value of dynamic decision-making relative to static approaches—gaps that this essay aims to address.

In summary, we contribute to the battery operations literature by emphasizing the critical importance of capturing both capacity and efficiency degradation in optimizing lifelong battery economics. We introduce two models—starting with capacity-degradation-only, and later incorporating efficiency degradation—to highlight systematic differences in optimal policies. Additionally, by applying optimal control theory to battery systems, we analytically characterize the structure of optimal control policies, and evaluate the benefits of dynamic policies compared to the heuristics commonly used in practice.

3.4 Optimal Control Problem

3.4.1 Capacity-Degradation-Only

We first consider a case where the battery experiences capacity degradation without any efficiency loss. We use a fluid approximation to formulate a continuous-time problem, taking advantage of the fact that a battery typically operates over many days (usually over several years), with each day contributing only a small fraction of the total revenue and degradation. See Appendix B.2.1 for a formal description, which translates the discrete-time formulation into the continuous-time model.

We operate a battery over a horizon T, with the aim of maximizing the cumulative discounted arbitrage revenue. Following the description of a day-ahead energy market in Section 3.2.1, we assume a fixed energy price pair $(\underline{p}, \bar{p})$ with $\bar{p} > \underline{p}$.[12]

Let $E(t)$ denote the battery's current energy capacity, and let $u(t) \in [0, 1]$ represent the depth-of-discharge (DOD) at time t. Let $x \in (0, 1]$ denote the one-way efficiency. which

[12]We relax this to a multiple-price setting in Section 3.5.2.

remains constant regardless of battery utilization. Under this setup, discharging an amount $E(t)u(t)$ of energy from the battery effectively results in selling $E(t)u(t)x$ units at the high price $\bar{p}$, and $\frac{E(t)u(t)}{x}$ units of energy must be purchased at the low price $\underline{p}$. The resulting arbitrage margin is:

$$\bar{p} \cdot E(t)u(t)x - \underline{p} \cdot \frac{E(t)u(t)}{x} = p^a E(t)u(t),$$

where $p^a := \bar{p}x - \underline{p}/x > 0$ denotes the effective profit per unit of discharge, as defined in (3.1). We use $\delta \geq 0$ to denote a discount factor. Then a optimization problem can be stated as follows:

$$\begin{aligned} \max_{u(t)\in[0,1], 0\leq t\leq T} \int_0^T e^{-\delta t} p^a E(t)u(t)dt \\ \text{s.t. } \dot{E}(t) = -E(t)\Phi(u(t)) \\ \Phi(u(t)) := ku(t)^2, \end{aligned} \tag{3.7}$$

where $r(t) := e^{-\delta t} p^a E(t)u(t)$ and $\dot{E}(t)$ are the discounted immediate revenue rate and the (quadratic) capacity degradation dynamics, respectively, at time t. The multiplicative degradation dynamics is based on empirical/experimental evidence ([204, 158]). Both revenue $r(t)$ and degradation $\Phi(u(t))$ are increasing in $u(t)$, which implies that aggressive use of a battery (larger $u(t)$) generates more revenue but also incurs more degradation. Thus, an ideal policy should strike a balance between immediate revenue, obtained by exploiting/front-loading the battery, and future opportunities, achieved by delaying its use until later.

For simplicity, we will assume $E(0) = 1$.[13] We now examine the optimal DOD policy over time under the capacity-degradation-only model.

Theorem 3.1 (**Capacity-degradation-only: Finite horizon**). *For capacity-degradation-only under a finite horizon T, it is optimal to use the battery at full DOD either if the discount factor is high ($\delta \geq k$) or if the time horizon is short ($\delta < k,\ T \leq \frac{\log(\frac{2k}{k-\delta})}{k+\delta}$). Otherwise, there exists a threshold time*

$$0 < t_A := T - \frac{\log(\frac{2k}{k-\delta})}{k+\delta} < T,$$

such that the battery's capacity is used partially before t_A ($u^*(t) < 1$ for all $0 \leq t < t_A$) and at full capacity afterwards. We define the shadow price of energy capacity by $p(t)$, and its current-value form by $p(t)e^{\delta t}$. Let $A^*(t)$ denote the optimal amount of energy sold to the grid. The resulting dynamics over the time horizon are as follows:

[13] Assuming a unit energy capacity is without loss of generality, since increasing or decreasing the number of (homogeneous) battery cells, modules, or racks would involve the exact same operations.

Var.	Cases		
	$k > \delta, T > \frac{\log(\frac{2k}{k-\delta})}{k+\delta}$		$k \leq \delta$ or $k > \delta,\ T \leq \frac{\log(\frac{2k}{k-\delta})}{k+\delta}$
	Discounted ($\delta > 0$)	Undiscounted ($\delta = 0$)	
$u^*(t)$	$\begin{cases} \left[\frac{k\left(e^{2\delta(t_A-t)}-1\right)+\delta}{\delta e^{2\delta(t_A-t)}}\right]^{-\frac{1}{2}}, & 0 \leq t \leq t_A, \\ 1, & t_A \leq t \leq T. \end{cases}$	$\begin{cases} [1+2k(t_A-t)]^{-\frac{1}{2}}, & 0 \leq t \leq t_A, \\ 1, & t_A \leq t \leq T. \end{cases}$	1
$p(t)e^{\delta t}$	$\begin{cases} \frac{p^a}{2k}\left[\frac{k\left(e^{2\delta(t_A-t)}-1\right)+\delta}{\delta e^{2\delta(t_A-t)}}\right]^{\frac{1}{2}}, & 0 \leq t \leq t_A, \\ \frac{p^a}{k+\delta}(1-e^{-(k+\delta)(T-t)}), & t_A \leq t \leq T. \end{cases}$	$\begin{cases} \frac{p^a}{2k}[1+2k(t_A-t)]^{\frac{1}{2}}, & 0 \leq t \leq t_A, \\ \frac{p^a}{k}(1-e^{-k(T-t)}), & t_A \leq t \leq T. \end{cases}$	$\frac{p^a}{k+\delta}(1-e^{-(k+\delta)(T-t)})$
$A^*(t)$	$\begin{cases} e^{\delta(t_A-t)}\sqrt{\frac{\delta}{k(e^{2\delta t_A}-1)+\delta}}, & 0 \leq t \leq t_A, \\ e^{-k(t-t_A)}\sqrt{\frac{\delta}{k(e^{2\delta t_A}-1)+\delta}}, & t_A \leq t \leq T. \end{cases}$	$\begin{cases} \frac{1}{\sqrt{2kt_A+1}}, & 0 \leq t \leq t_A, \\ \frac{e^{-k(t-t_A)}}{\sqrt{2kt_A+1}}, & t_A \leq t \leq T. \end{cases}$	e^{-kt}

Table 3.2: Capacity-degradation-only (Finite horizon).

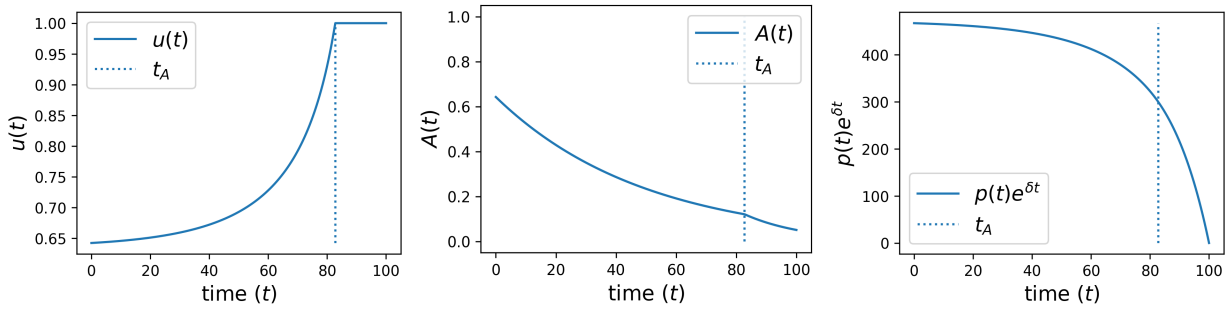
All of the proofs of the main results are in Appendix B.2. Theorem B.1 in Appendix B.2.1 presents a detailed version of Theorem 3.1, including the evolution of energy capacity $E^*(t)$ and the cumulative revenue.

Observation 3.1. *From Theorem 3.1, the following results hold:*

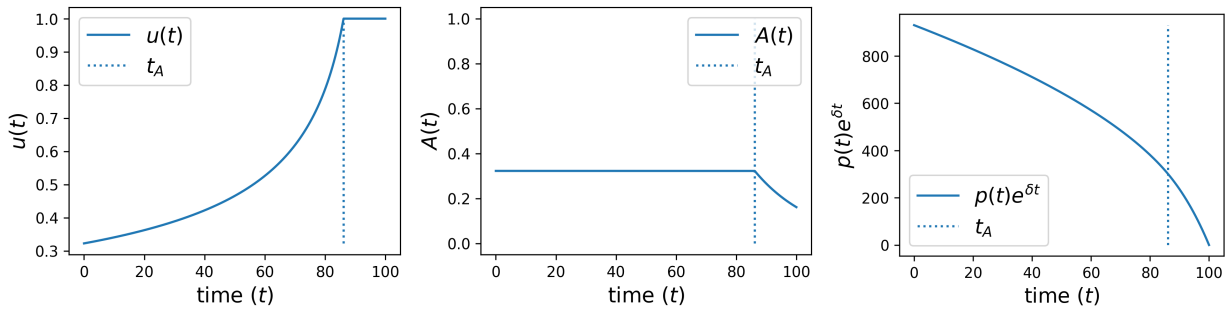
- *Optimal DOD $u^*(t)$ is strictly monotone increasing for $t \in [0, t_A)$,*
- *The shadow price of energy capacity $p(t)$, as well as that shadow price normalized by the time discounting, $p(t)e^{\delta t}$, are strictly monotone decreasing across the full horizon, and*
- *Under time discounting ($\delta > 0$), the optimal amount of energy to sell to the grid, $A^*(t)$, is strictly monotone decreasing across the full horizon. Under the undiscounted model $A^*(t)$ is a constant for $t \in [0, t_A]$ and then strictly monotone decreasing for $t > t_A$.*

Note that the optimal DOD policy has monotone increasing utilization regardless of δ (e.g., even with heavy discounting, we gradually increase DOD over time until reaching full DOD). Later in Section 3.4.2, we will see that this is, in general, not true in the presence of efficiency degradation.

Recall from Section 3.2.3 that one common heuristic from the literature assumes a battery provides a fixed amount of arbitrage through time (i.e., fixed-A policy). Theorem 3.1 establishes that this heuristic matches the optimal behavior under no time discounting ($\delta = 0$). In fact, Theorem B.6 in Appendix B.3.1.2 establishes that this behavior continues to hold for other strictly convex power degradation functions. The logic behind this behavior is



(a) Discounted



(b) Undiscounted

Figure 3.2: Illustration of Observation 3.1. (a) Discounted: $\delta = 0.02$ ($t_A = 82.75$); (b) Undiscounted: $\delta = 0$ ($t_A = 86.13$). Other parameters: $\bar{p} = 40$, $\underline{p} = 10$, $k = 0.05$, $x_0 = 1$, $T = 100$.

subtle—the undiscounted problem implies that both the immediate revenue function $r(t)$ and the state equation $\dot{E}(t)$ are time-independent (such a system is called autonomous). The reasoning is as follows.

Suppose we wish to provide a total arbitrage quantity $\bar{A}$ over a time interval $[t_1, t_2]$ under an arbitrary strictly convex degradation function $\Phi(u)$. Compared to evenly distributing arbitrage work over time (i.e., $A(t) = \bar{A}/(t_2 - t_1)$), shifting some arbitrage work later reduces early degradation but increases degradation later to accommodate the total work. This higher utilization in the later periods offsets the initially reduced degradation rate, ultimately leading to a faster overall growth in capacity loss over time.[14] By analyzing these opposing effects, we show that it is degradation-minimizing to keep the adjusted arbitrage intensity

$$A(t) \cdot [1 - \frac{1}{\epsilon(u(t))}],$$

constant over the interval $t \in [t_1, t_2]$, when the energy capacity is not binding (i.e., $u(t) < 1$; see Lemma B.8 in Appendix B.3.1.2). Here, $\epsilon(u) := \frac{\frac{d\Phi(u)}{\Phi(u)}}{\frac{du}{u}}$ denotes the DOD-elasticity of degradation, which measures the percentage change in the degradation rate relative to the percentage change in DOD. The DOD-elasticity plays a central role in determining how to allocate revenue and/or arbitrage quantity across time periods. Notably, only power functions of the form $\Phi(u) := k \cdot u^\beta$ with $\beta \geq 1$ exhibit constant elasticity, making it optimal to evenly spread arbitrage across time periods, i.e., $A(t) = \bar{A}/(t_2 - t_1)$.[15] Since this result is derived for a general setting with an arbitrary total arbitrage quantity $\bar{A}$, it must also hold for the optimal total quantity $\bar{A}^*$. The effect no longer holds under time discounting ($\delta > 0$), as the battery front-loads service and sees strictly decreasing revenues through time.

Recall from Section 3.2.3 that another common heuristic from the literature takes a fixed-DOD through time (i.e., fixed-DOD policy). While Theorem 3.1 establishes that this behavior is not optimal under a fixed horizon—except in the extreme case where the maximum DOD is used throughout the entire horizon—it is optimal under the infinite horizon. In this case, the battery's value depends solely on its remaining (current) capacity and is independent of time t. In other words, the current-value shadow price $p(t)e^{\delta t}$ (which measures the marginal value of capacity measured at time t) becomes constant, with the end-of-horizon effect vanishing.

Corollary 3.1 (**Capacity-degradation-only: Infinite horizon**). *With $T \to \infty$, discount*

[14] Shifting work earlier and reducing later-period work produces a similar net effect, increasing total degradation.

[15] Theorem B.6 in Appendix B.3.1.2 considers other degradation functions to show how DOD-elasticity determines the arbitrage rate over time in an unconstrained, undiscounted setting.

$\delta > 0$, and capacity-degradation-only, a fixed-DOD policy is optimal:

$$u^*(t) = \min(\sqrt{\delta/k}, 1), \text{ and}$$
$$p(t)e^{\delta t} = \begin{cases} \frac{p^a}{k+\delta} & \text{if } k \le \delta, \text{ and} \\ \frac{p^a}{2\sqrt{k\delta}} & \text{if } k > \delta. \end{cases}$$

Theorem 3.1 and Corollary 3.1 provide theoretical justifications for the simple heuristics that have been used in the literature/practice under some special cases of the capacity-degradation-only model: a fixed-A policy is optimal for an undiscounted problem, while a fixed-DOD policy is optimal for a discounted, infinite-horizon problem.

A natural follow-up question is whether these heuristics remain effective in general capacity-degradation-only models, including scenarios with discounting and finite horizons, which we explore below. Another question is whether these heuristics still continue to work well under efficiency degradation, a question we will address in Section 3.4.2 (a short answer is no).

Heuristics. Although the fixed-DOD and fixed-A policies are commonly used to account for battery degradation, the lack of theoretical or systematic evaluation raises concerns about their effectiveness. In this subsection, we explore various battery operating environments to investigate when and where the fixed-DOD heuristic exhibits small or large suboptimalities, assuming the battery experiences capacity degradation only. Appendix B.4.1 considers the fixed-A policy.

Fixed-DOD. Corollary 3.1 states that a fixed-DOD policy is optimal under the special case of the infinite horizon. Here, we evaluate the performance of the fixed-DOD policy under a finite horizon.

Given a fixed-DOD level (i.e., $u(t) = u$ for $0 \le t \le T$), the system dynamic of (B.5) implies

$$E(t) = e^{-ku^2 t}.$$

Based on (B.5), the best DOD level u can be selected as the constant maximizing the revenue over the full horizon:

$$R_{cum}^{DOD} := \max_{0 \le u \le 1} \bar{R}(u) = \frac{p^a u}{ku^2 + \delta}[1 - e^{-T(ku^2+\delta)}], \tag{3.8}$$

where $\bar{R}(u)$ is the full-horizon discounted revenue associated with a fixed-DOD level u and quadratic capacity degradation. Let $\bar{u}$ be the optimal fixed-DOD level, aka, $\bar{u} :=$

$\arg\max_{0\le u\le 1} \bar{R}(u)$. Compared with the fixed-DOD policy in (3.6), which relies on cost amortization, $\bar{u}$ explicitly accounts for the battery's gradual deterioration and thus maximizes cumulative revenue among fixed-DOD policies. We can show that the maximum revenue is achieved at a unique maximizer.

Lemma 3.1. *$\bar{R}(u)$ in (3.8) has a unique maximizer $0 < \bar{u} \le 1$, which uses the full DOD ($\bar{u} = 1$) if the discount factor is high ($\delta \ge k$) or if the time horizon is short ($\delta < k,\ e^{-T(k+\delta)}[2Tk(k+\delta) + (k-\delta)] \ge (k-\delta)$), and a smaller DOD otherwise.*

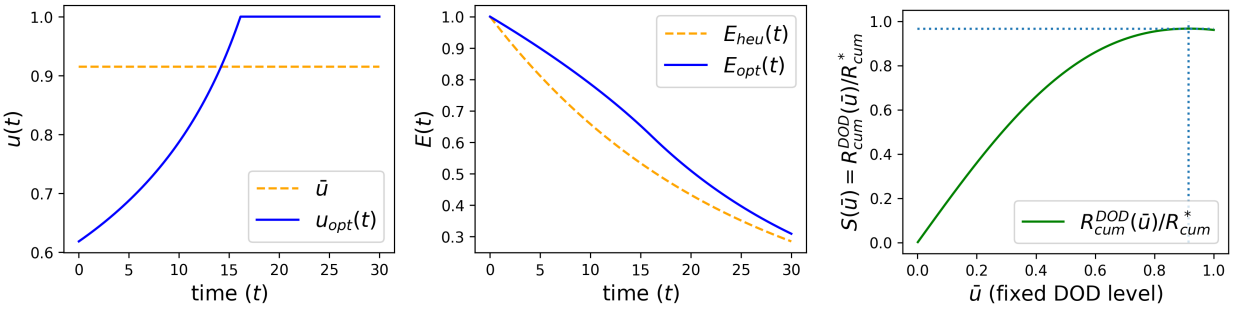
In general, $\bar{u}$ and the corresponding cumulative revenue $r(\bar{u})$ do not have closed-form expressions, but $\bar{u}$ can easily be found numerically. Since $u^*(t)$ is strictly increasing in t up to the full capacity (when $\delta < k$ and $T > \frac{\log(\frac{2k}{k-\delta})}{k+\delta}$, as shown in Theorem 3.1), $\bar{u}$ is typically set higher than $u^*(0)$ (the initial DOD at time $t = 0$) and lower than the full capacity. This implies that the fixed-DOD policy may lead to overuse of the battery in the early periods and underuse in the later periods, relative to the optimal dynamic policy, as illustrated in Figure 3.3. The initial overuse has a lingering impact on energy capacity, resulting in lower $E(t)$ over long horizons (throughout the entire period in Figure 3.3(a) and up to $t = 85$ in Figure 3.3).

A key question, then, is how much additional revenue can be obtained through a dynamic policy—specifically, by using the battery more conservatively in the initial periods and more aggressively in the later periods, compared to operating it at a fixed-DOD level. To answer this, let $S(\delta) := \frac{R^{DOD}_{cum}}{R^{*}_{cum}}$ be the ratio between the cumulative discounted revenues from the fixed-DOD heuristic at optimal level $\bar{u}$ and optimal dynamic policy, respectively. While S also depends on parameters such as p^a, T, and k, we focus here on the effect of the discount factor $\delta > 0$, holding the other parameters fixed. We show that S is monotonically decreasing in δ—the heuristic performs worse relative to optimal as we discount less.

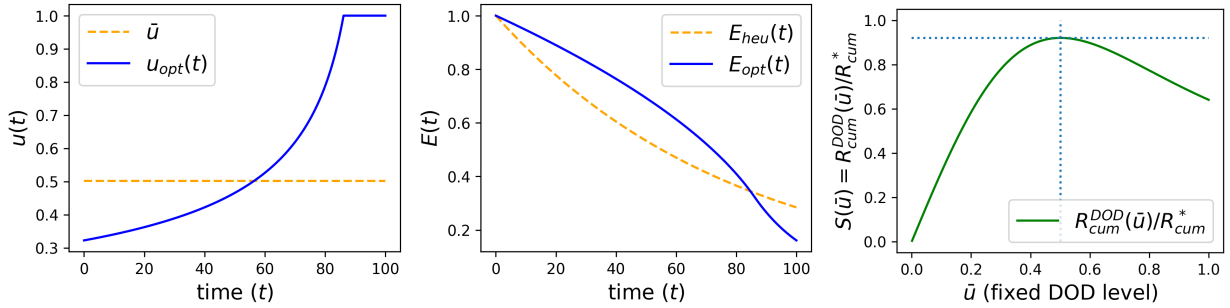
Lemma 3.2. *Under capacity-degradation-only, $S(\delta)$ is monotone increasing in δ for fixed $p^a,\ k$, and T.*

Lemma 3.2 captures the intuition that the fixed-DOD heuristic can match the optimal strategy under highly discounted scenarios where it is optimal to operate the battery at full DOD for the whole horizon, while it performs much worse under less discounted settings where more intricate management of the battery capacity is needed. Lemma 3.2 implies that the lower bound on S (the worst case of the heuristic) can be inferred from the no discounting case ($\delta = 0$). Using this fact, the following corollary shows that the optimal fixed-DOD policy can achieve at least 90.25% of the optimal cumulative revenue.

Corollary 3.2 (**Performance lower bound**). *Under capacity-degradation-only with quadratic degradation, the optimal fixed-DOD heuristic is 90.25%-optimal.*



(a) Short horizon



(b) Long horizon

Figure 3.3: Comparison of the fixed-DOD heuristic and the optimal policy. (a) $T = 30$ ($\bar{u} = 0.91$); (b) $T = 100$ ($\bar{u} = 0.50$). Other parameters: $\bar{p} = 40$, $\underline{p} = 10$, $k = 0.05$, $x_0 = 1$, $\delta = 0$.

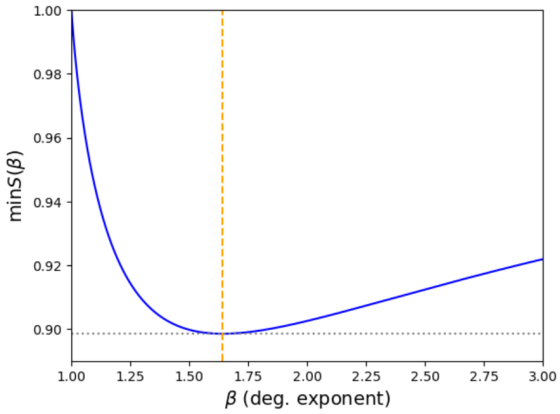


Figure 3.4: Performance of the fixed-DOD heuristic: Illustration of the worst-case performance across a range of power function exponents $\beta \geq 1$ (Corollary B.2). $\min S(\beta) \approx 0.898$ is achieved at $\beta \approx 1.64$ (dashed line).

In the proof of Corollary 3.2, we express $S = \frac{R^{DOD}_{cum}}{R^{*}_{cum}}$, the ratio between the cumulative undiscounted revenues from the fixed-DOD policy and the optimal policy, as a function of T. We then show that $S(T)$ is monotone decreasing and approaches its infimum (where 90.25% optimality is achieved) as T increases to infinity. Intuitively, when the horizon T is short—analogous to the case of heavy discounting—the battery tends to be operated more aggressively from the start (i.e., $u^*(0)$ is already high), leading to smaller additional benefits from dynamic adjustments in later periods (see Figure 3.3(a)). Conversely, when the horizon T is long, the battery tends to be operated more conservatively, starting with a lower $u^*(0)$, which allows for greater additional benefits from dynamic adjustments (see Figure 3.3(b)). In the numerical section, we provide a detailed comparison of the performance of this heuristic against dynamic approaches.

Although a worst-case ratio of 90.25% may appear high, this optimality gap analysis is based on cumulative revenues. According to [111], most battery applications remain unprofitable or barely profitable as of 2025, and the missed revenue could have a significant impact on battery economics.

The overall lessons in this section are robust to the choice of the degradation function, as demonstrated by a sensitivity analysis in Appendix B.3.1. By considering any convex power function with order $\beta > 1$, the key lessons in Section 3.4.1—such as the monotonicity of $u^*(t)$ in capacity-degradation-only models and the optimality of simple heuristics in special cases—remain valid. Corollary B.2 extends Corollary 3.2 to a general power function of order $\beta > 1$ for the undiscounted problem. Figure 3.4 illustrates the undiscounted worst-case performance of the fixed DOD policy across a range of exponents $\beta \in [1, 3]$. Below, we state some key observations for different degradation functions.

Observation 3.2 (**Undiscounted worst-case performance for** $\beta > 1$)**.** *The worst-case performance for the undiscounted problem, denoted by* $\min S(\beta)$*, is unimodal in* β*, with the minimum S ratio of 89.8% achieved at* $\beta \approx 1.64$*. It remains stable across a range of* β*, e.g.,* $\min S(\beta) \leq 92\%$ *for* $\beta \in [1.2, 2.8]$ *and gradually increases to 1 as* $\beta \to 1$ (*linear degradation*) *or* $\beta \to \infty$*.*

Observation 3.2 captures the fact that a dynamic policy is unnecessary with linear degradation ($\beta = 1$), as a fixed (full) DOD heuristic can be optimal due to both revenue and capacity deterioration rates being linear in DOD.

For very large values of β, the strong convexity ensures that any model can operate at nearly full capacity (DOD=1) with negligible degradation.[16] Consequently, all models converge to the same revenue corresponding to 100%, and the benefit of dynamic adjustment diminishes (e.g., with $\beta = 30$, $\min S(\beta) \approx 99\%$).

These two extreme cases are evidently unrealistic. In contrast, nonlinear degradation ($1 < \beta < \infty$) requires dynamic adjustments through gradually increasing utilization over time. Additionally, the optimal fixed-DOD policy achieves nearly 90% of the optimality (measured in terms of cumulative revenues) across a range of exponents β.

3.4.2 Unified Model (In the Presence of Efficiency Degradation)

Most, if not all, papers in the OM literature assume that the battery has constant efficiency, as detailed in Section 3.3. Since the actual profit margin for unit arbitrage can vary significantly depending on the battery's life stage (or the degree of performance degradation), the cost associated with these mismatches in battery management policies (or the cost of not modeling efficiency degradation) may also be significant.

To tackle this issue, we establish a unified model assuming both capacity and efficiency experience degradation. Following the experimental/empirical evidence illustrated in Section 3.2.2, we assume a linear relationship between capacity and efficiency degradation $x(t) = \alpha_0 + \alpha_1 E(t)$ for $\alpha_1 \geq 0$. With one-way efficiency $x(t)$, the effective profit of arbitrage is $p^a(x(t)) = \bar{p}x(t) - \frac{p}{x(t)}$. Our unified optimization problem that captures both capacity and

[16] The cumulative revenue R^*_{cum} converges to the revenue under full DOD with no degradation as $\beta \to \infty$.

efficiency degradation as follows:

$$\begin{aligned} \max_{u(t)\in[0,1],0\le t\le T} \int_0^T e^{-\delta t}\big(\bar{p}x(t) - \frac{\underline{p}}{x(t)}\big)E(t)u(t)dt \\ \text{s.t. } \dot{E}(t) = -E(t)\Phi(u(t)) \\ \Phi(u(t)) = ku(t)^2 \\ x(t) = \alpha_0 + \alpha_1 E(t). \end{aligned} \tag{3.9}$$

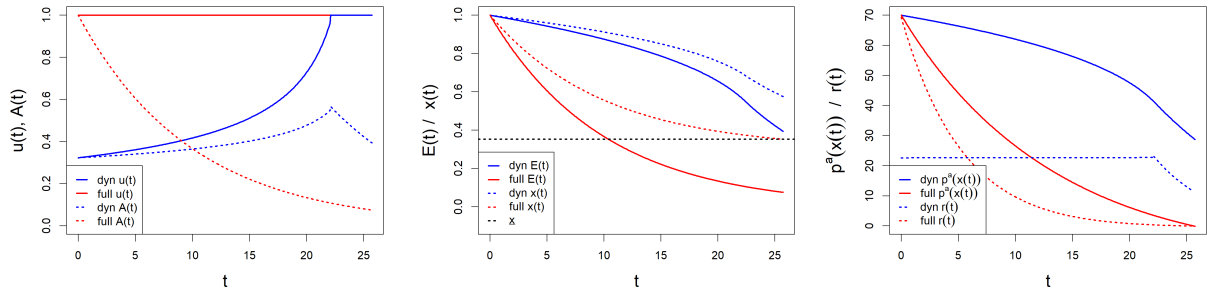
Without loss of generality, we assume $E(0) = 1$ and $\alpha_0 + \alpha_1 \le 1$, which encodes the battery's initial efficiency as $x(0) = \alpha_0 + \alpha_1 \le 1$. Recall from (3.1) that we stop operating the battery when the profit margin is $p^a(x(t)) \le 0$, or equivalently, when $x(t) \le \underline{x} := \sqrt{\frac{\underline{p}}{\bar{p}}}$, where $\underline{x}$ denotes the **shut-off efficiency**. Also, note that $\alpha_1 = 0$ denotes the capacity-degradation-only model in Section 3.4.1.

Motivating Example: Why Dynamic DOD Adjustments Matter. To illustrate how critical it is to account for efficiency degradation and to highlight the importance of dynamically adjusting the depth-of-discharge (DOD) policy, define a "short time horizon" to be a time horizon T^s such that operating the battery at full DOD throughout (i.e., $u(t) = 1, 0 \le t \le T^s$) does not cause $p^a(x(t))$ to fall below 0 for any t. Assuming a zero salvage value (i.e., remaining capacity at the end is worthless), it may seem desirable to operate at maximum DOD in such a scenario. This yields the following question:

Q. Assuming a zero salvage value and a "short time horizon," is it always optimal to operate a battery at maximum DOD throughout the horizon, or are there cases where it is better to intentionally preserve some remaining capacity at the end—by operating the battery more conservatively—even though the remaining capacity provides no salvage value?

Interestingly, operating at maximum DOD throughout the horizon can be **severely sub-optimal**. For instance, under realistic market parameters, the ratio $S = \frac{R^{DOD}_{cum}}{R^*_{cum}}$, which compares cumulative revenue under the full DOD policy to that under the optimal policy, is approximately 62%.[17] Figure 3.5 compares how the full DOD and optimal policies affect the arbitrage quantity $A(t)$, as well as the evolution of capacity $E(t)$, efficiency $x(t)$, effective profit $p^a(t)$, and revenue rate $r(t)$. While operating at a strictly lower DOD up to $t = 22$, the optimal policy generates higher revenue rate as early as $t = 6$ and continues to outperform the full DOD policy thereafter, since the effective profit margin remains higher. Although the optimal policy leaves strictly positive efficiency, effective profit, and more capacity at the

[17] In fact, the ratio $S = \frac{R^{DOD}_{cum}}{R^*_{cum}}$ can become arbitrarily small as $\frac{\bar{p}}{\underline{p}} \to \infty$. For example, when $\underline{p} = 1, k = 0.1$, and $\delta = 0$, the ratio S decreases monotonically with increasing $\bar{p}$; although the decrease is slow, S is not bounded by any positive number.



(a) $u(t)$ and $A(t)$ (b) $E(t)$ and $x(t)$ (c) $p^a(t)$ and $r(t)$

Figure 3.5: Motivating example: Comparison of the full DOD and optimal policies. Under the optimal policy, $x^*(T) = 0.57 > 0.35 = \underline{x}, E^*(T) = 0.39 > 0.07 = \underline{E} := \frac{\underline{x}-\alpha_0}{\alpha_1}$, and the revenue ratio is $S = \frac{R^{DOD}_{cum}}{R^*_{cum}} = 0.62$. The following parameters are used: $\alpha_1 = 0.7, \alpha_0 = 0.3, k = 0.1, \bar{p} = 80, \underline{p} = 10$, $\delta = 0$, and $T^s = 25.70$.

end, it achieves a greater cumulative arbitrage quantity with much higher effective profit.

Optimal Dynamic Policy. We now provide a description of the general structure of the optimal policy, considering both capacity and efficiency degradation. In general, no closed-form solution exists for optimization model (3.9). However, we can still prove structural properties of the optimal policy under the unified degradation model.

We first examine the unconstrained solution, in which the battery's capacity is partially used (i.e., for all t such that $u^*(t) < 1$). Managing the battery to optimize discounted revenue over the horizon must balance: discounting versus capacity degradation and efficiency degradation. We can formalize this tradeoff to characterize the battery's optimal usage:

Theorem 3.2 (**Unified: Unconstrained solution**).
When the battery capacity is not constrained ($u^*(t) < 1$),

- *The optimal DOD* $u^*(t)$ *satisfies:*

$$\frac{[u^*(t)]'}{u^*(t)} = \underbrace{\frac{-E'(t)}{E(t)}}_{\substack{=k[u^*(t)]^2 \\ \textit{(capacity degradation)}}} + \underbrace{\frac{-[p^a(t)]'}{p^a(t)}}_{\substack{=k[u^*(t)]^2 \cdot h(x(t)) \\ \textit{(efficiency degradation)}}} + \underbrace{\frac{[e^{-\delta t}]'}{e^{-\delta t}}}_{\substack{=-\delta \\ \textit{(time discounting)}}}$$

$$= k[u^*(t)]^2\Big(1 + h(x)\Big) - \delta, \ \textit{for} \tag{3.10}$$

$$h(x) := \frac{(x-\alpha_0)(\bar{p} + \underline{p}/x^2)}{\bar{p}x - \underline{p}/x}.$$

- *The discounted revenue rate* $r(t) := e^{-\delta t} p^a(t) E(t) u^*(t)$ *satisfies:*

$$r(t) = r(0) e^{-2\delta t}.$$

Theorem 3.2 highlights a fundamental structural difference in the optimal policy when efficiency degradation is present, compared to the capacity-degradation-only case. The optimal DOD pattern must account for efficiency loss and thus becomes more nuanced. As we will see, a battery subject to both capacity and efficiency degradation can exhibit non-monotonic operating patterns. This non-monotonicity arises from the trade-off between time discounting, which favors front-loading battery usage, and the effects of capacity and efficiency degradation, which encourage conserving battery life. When time discounting is negligible ($\delta \to 0$), shifting "work" to later periods can reduce degradation without incurring significant loss from discounting. Thus, it becomes desirable to extend the operating period during which the battery runs at high efficiency levels by starting with a low DOD level and gradually increasing it as the horizon approaches. This is reflected in (3.10), where the optimal control $u^*(t)$ increases over time. However, unlike the capacity-degradation-only case—where Theorem 3.1 shows that the optimal DOD increases monotonically regardless of time discounting—the presence of efficiency degradation, represented by $h(x)$, can result in a period of decreasing utilization.

The term $h(x)$ may converge to a near-zero value when $\alpha_0 > \underline{x}$, where the battery operates at nearly constant efficiency, or approach infinity when $\alpha_0 < \underline{x}$, where the battery reaches the shut-off efficiency such that $p^a(t) = 0$. In the latter case, even a small increment in usage can have a substantial percentage-wise impact on the profit margin.

Theorem 3.2 also characterizes the optimal revenue rate (i.e., how much money is extracted) from the battery, highlighting the role of the discount rate δ in distributing revenue over time. To highlight the difference from the capacity-degradation-only case, let us examine two special cases.

When $\delta = 0$ (no discounting), the revenue rate $r(t)$ remains constant whenever $u^*(t) < 1$. This policy differs from that in the capacity-degradation-only case. Recall from Theorem 3.1 that, under capacity-degradation-only and no discounting, a fixed-A policy is optimal. In the presence of efficiency degradation, however, the profit margin from each unit of arbitrage declines over time, causing a fixed-A policy to generate gradually lower revenue. Instead, the optimal policy is to maintain a constant revenue stream by monotonically increasing $u^*(t)$ (and $A^*(t)$) over time.

Next, we examine another special case of the infinite horizon ($T \to \infty$) and $\delta > 0$, in which

a closed-form solution can be derived as a function of the battery's efficiency $x(t)$.[18] In this case, the system always converges to either the shut-off efficiency $\underline{x}$ or the efficiency intercept term α_0. Moreover, since the battery's value depends solely on its remaining efficiency and capacity, and not explicitly on time t, the optimal DOD $u^*(t)$ and current-value shadow price $\tilde{p}(t) := p(t)e^{\delta t}$ (which measures the marginal value of capacity and/or efficiency measured at time t) can be expressed solely in terms of one-way efficiency, denoted by $u^*(x)$ and $\tilde{p}(x)$, respectively.

Theorem 3.3 (**Unified: Infinite horizon**). *If $T \to \infty$, then the optimal DOD and the corresponding current-value shadow price can be expressed solely as functions of the one-way efficiency $x \in [\max(\underline{x}, \alpha_0), \alpha_0 + \alpha_1]$, as follows:*

$$
\begin{aligned}
u(x) &= \frac{\sqrt{c + g(x)}}{2k \cdot (x - \alpha_0) \cdot (\bar{p}x - \underline{p}/x)}, \\
\tilde{p}(x) &= \frac{(x - \alpha_0)(\bar{p}x - \underline{p}/x)^2}{\sqrt{c + g(x)}}, \quad \textit{for} \\
g(x) &= \frac{2\delta k}{3} \cdot \left(\bar{p}^2 x^3 (3x - 4\alpha_0) - 12\bar{p}\underline{p}x(x - 2\alpha_0) + 12\underline{p}^2(\log x + \alpha_0/x) \right) \textit{ and} \\
c &= \begin{cases} -g(\underline{x}), & \textit{if } \underline{x} \geq \alpha_0, \\ -g(\alpha_0), & \textit{if } \underline{x} < \alpha_0. \end{cases}
\end{aligned}
$$

Moreover, $u^*(x)$ exhibits one of five patterns as a function of x: monotone increasing, monotone decreasing, up-down, down-up, or down-up-down.

We will later show that while introducing a finite horizon T adds complexity to the problem, the set of optimal policy patterns is limited to just three of these patterns.

We further show that the specific pattern that emerges depends on the energy prices $\bar{p}$ and $\underline{p}$, as well as the efficiency intercept term α_0.

Theorem 3.4. *The optimal battery trajectory $u^*(t)$ under the infinite horizon follows the following patterns:*

- *Monotone increasing if $\alpha_0 \geq \sqrt{9/8} \cdot \underline{x}$,*
- *Monotone decreasing if $\alpha_0 \leq \min\{\underline{x}, \frac{4\bar{p}\underline{p}}{\bar{p}^2 + 4\bar{p}\underline{p} - \underline{p}^2}\}$,*
- *One of the following five patterns—monotone increasing, monotone decreasing, down-up, up-down, or up-down-up—if $\min\{\underline{x}, \frac{4\bar{p}\underline{p}}{\bar{p}^2 + 4\bar{p}\underline{p} - \underline{p}^2}\} < \alpha_0 < \sqrt{9/8} \cdot \underline{x}$.*

[18] The infinite horizon, undiscounted case ($\delta = 0$) yields infinite revenue, which is unrealistic.

Theorem 3.4 implies that in batteries that remain sufficiently efficient even after heavy utilization (i.e., $\alpha_0 \geq \sqrt{9/8} \cdot \underline{x}$) the effect of battery utilization on the margin decreases over time ($h(x)$ is an increasing function), encouraging an increasing utilization pattern over the lifetime of the battery. Meanwhile, in batteries that become sufficiently inefficient after heavy utilization (i.e., $\alpha_0 \leq \min\{\underline{x}, \frac{4\bar{p}\underline{p}}{\bar{p}^2+4\bar{p}\underline{p}-\underline{p}^2}\}$) the effect of battery utilization on the margin increases over time ($h(x)$ is a decreasing function), encouraging a decreasing utilization pattern over the lifetime of the battery. More complex utilization patterns can emerge for batteries that fall between these two extremes, as documented in Appendix B.2.2 and Theorem 3.4; however, this range for α_0 may be narrow under realistic parameter values (e.g., with $\bar{p} = 40$ and $\underline{p} = 10$, $\min\{\underline{x}, \frac{4\bar{p}\underline{p}}{\bar{p}^2+4\bar{p}\underline{p}-\underline{p}^2}\} = 0.5$ and $\sqrt{9/8} \cdot \underline{x} = 0.53$).

We now examine how different battery types (e.g., relative magnitudes of capacity and efficiency degradation, degradation coefficients) and operating environment (e.g., energy prices, discount factors) affect utilization and cumulative revenue. Based on Theorem 3.3, we conduct a sensitivity analysis of the optimal DOD and the current-value shadow price for a given x (denoted by $\frac{\partial u^*(x)}{\partial y}$ and $\frac{\partial \tilde{p}(x)}{\partial y}$), as well as of the cumulative revenue, with respect to different parameters $y \in \{\alpha_0, \bar{p}, \underline{p}, k, \delta\}$. For the degradation intercept α_0, we vary its value while keeping $\alpha_0 + \alpha_1$ fixed, thereby maintaining the same initial battery efficiency $x_0 = \alpha_0 + \alpha_1$. This allows us to compare how different combinations of (α_0, α_1) affect battery utilization.

Corollary 3.3 (**Sensitivity analysis**). *Under the unified degradation model with $T \to \infty$, the optimal DOD $u^*(x)$, the current-value shadow price $\tilde{p}(x)$, and the cumulative revenue R^*_{cum} exhibit the following patterns:*

1. ***(Utilization)*** *$u^*(x)$ is higher for batteries with weaker efficiency degradation (large α_0), longer life cycles (small k), heavier time discounting (large δ), and higher energy price differentials (large $\bar{p} - \underline{p}$).*

2. ***(Current-value shadow price)*** *$\tilde{p}(x)$ is higher for batteries with stronger efficiency degradation, longer life cycles, lighter time discounting, and higher energy price differentials.*

3. ***(Cumulative revenue)*** *R^*_{cum} is higher for batteries with weaker efficiency degradation, longer life cycles, lighter time discounting, and higher energy price differentials.*

Given the same fixed initial efficiency $\alpha_0 + \alpha_1$, both the optimal DOD and the cumulative revenue increase as the battery experiences less efficiency degradation (i.e., as α_0 increases and α_1 decreases). In contrast, for any fixed efficiency level x, the current-value shadow price decreases with α_0, since a higher α_0 implies a smaller energy capacity (the battery reaches

Var.	Cases		
y	$\frac{\partial u^*(x)}{\partial y}$	$\frac{\partial \tilde{p}(x)}{\partial y}$	$\frac{\partial R^*_{cum}}{\partial y}$
α_0	$\uparrow$	$\downarrow$	$\uparrow$
$\bar{p}$	$\uparrow$	$\uparrow$	$\uparrow$
$\underline{p}$	$\downarrow$	$\downarrow$	$\downarrow$
k	$\downarrow$	$\downarrow$	$\downarrow$
δ	$\uparrow$	$\downarrow$	$\downarrow$

Table 3.3: Sensitivity analysis (Corollary 3.3). For the degradation intercept α_0, we vary its value while keeping $\alpha_0 + \alpha_1$ fixed, thereby maintaining the same initial battery efficiency ($x_0 = \alpha_0 + \alpha_1$).

efficiency level x at a lower energy capacity). Obviously, unlike in the capacity-degradation-only model, the energy prices $\bar{p}$ and $\underline{p}$ affect the optimal DOD level once the battery is subject to efficiency degradation.

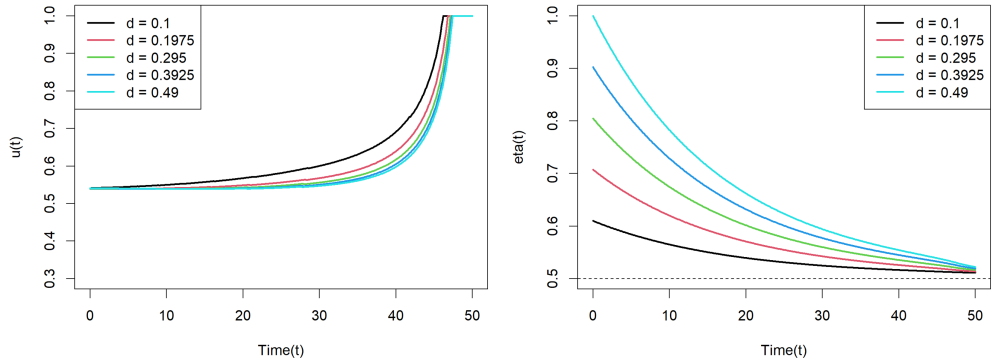
We further illustrate the effect of efficiency degradation on battery utilization by comparing it with a battery that experiences no efficiency degradation.

Corollary 3.4 (**Reduced utilization**). *Let Battery 1 ($\alpha_1 = 0$) experience only capacity degradation, and let Battery 2 ($\alpha_1 > 0$) experience both capacity and efficiency degradation. Let $u^*_{\alpha_1=0}(t)$ and $u^*_{\alpha_1>0}(t)$ denote the optimal DOD at time t for Batteries 1 and 2, respectively. Then, their optimal DODs satisfy:*

1. *If $\delta < k$, then $u^*_{\alpha_1=0}(t) > u^*_{\alpha_1>0}(t)$ for all t,*
2. *If $\delta \geq k$, then $u^*_{\alpha_1=0}(t) \geq u^*_{\alpha_1>0}(t)$ for all t. The strict inequality $u^*_{\alpha_1=0}(t) > u^*_{\alpha_1>0}(t)$ for all t may still hold, when $\underline{x} < \alpha_0$ and δ is not sufficiently large.*

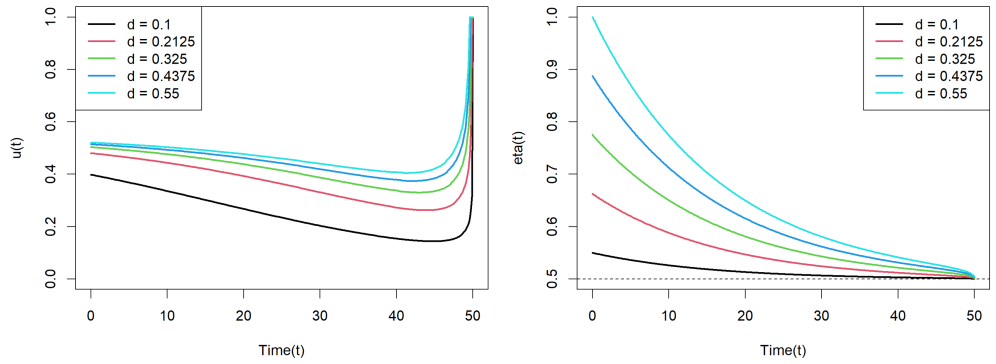
Importantly, Corollary 3.4 holds broadly: regardless of Battery 2's efficiency—whether higher or lower, or whether it experiences mild or severe efficiency degradation—it always operates at a lower DOD than Battery 1.

Under low discounting ($\delta < k$), Battery 1 will always operate at a strictly higher DOD then Battery 2 at any time t, regardless of how these two batteries are parameterized. Figure 3.6a illustrates this result: $u^*_{\alpha_1>0}$ (black) consistently remains strictly below $u^*_{\alpha_1=0}$ (blue) for all $x_2 \in (\alpha_0, 1]$, despite Battery 2 having a higher efficiency than Battery 1 (i.e., $x_1(t) < x_2(t)$ for all t). Under high discounting ($\delta \geq k$), Battery 1 operates with 100% DOD at all times (Corollary 3.1). Nevertheless, the strict inequality $u^*_{\alpha_1=0}(t) > u^*_{\alpha_1>0}(t)$ may still hold. For instance, when $\underline{x} < \alpha_0$ and δ is not sufficiently large, the strict inequality holds for any t. Figure 3.6b confirms this by showing that $u^*_{\alpha_1>0}$ (black) remains strictly below 100% across all x.



(a) $\delta < k$

$(\sqrt{\delta/k} = u^*_{\alpha_1=0}(t) > u^*_{\alpha_1>0}(t),\ \forall t)$



(b) $\delta \geq k$

$(1 = u^*_{\alpha_1=0}(t) > u^*_{\alpha_1>0}(t),\ \forall t)$

Figure 3.6: Strictly reduced utilization in the presence of efficiency degradation (Corollary 3.4). Battery 1's efficiency x_1 is fixed at 0.875. For Battery 2, its efficiency $x_2(t)$ evolves as follows: (a) $x_2(t) \in [0.9, 1]$ (i.e., $x_2(t) > x_1$ for all t) with $\alpha_1 = 0.1$ and $\alpha_0 = 0.9$; (b): $x_2(t) \in [0.87, 1]$ with $\alpha_1 = 0.2$ and $\alpha_0 = 0.8$. Other parameters are: $\bar{p} = 40, \underline{p} = 30, k = 1$, with $\delta = 0.6$ for (a) and $\delta = 2$ for (b).

Lastly, we now turn to the discounted problem with a finite horizon T. We first note that we always use full DOD when t is sufficiently close to T, regardless of the relationship between capacity and efficiency degradation, due to end-of-horizon effects. This excludes two infinite-horizon patterns, leaving three possible patterns, as summarized below.

Theorem 3.5 (**Unified: Finite horizon**). *Under the unified model with a finite horizon T, the optimal control satisfies the following:*

- *There exists $0 \leq \hat{t} < T$ such that $u^*(t) = 1$ for all $t \in [\hat{t}, T]$,*
- *The optimal DOD $u^*(t)$ is either monotone increasing, down-up, or up-down-up in t.*

Analogous to Theorem 3.4, we can characterize the patterns of the optimal battery trajectory under a finite horizon T. Noting that the battery is always operated at full capacity when t is sufficiently close to the end of the horizon T, we obtain the following patterns:

Theorem 3.6. *The optimal battery trajectory $u^*(t)$ for $t \in [0, T]$ follows the following patterns:*

- *Monotone increasing if $\alpha_0 \geq \sqrt{9/8} \cdot \underline{x}$,*
- *Either monotone increasing or down-up if $\alpha_0 \leq \frac{4\bar{p}\underline{p}}{\bar{p}^2 + 4\bar{p}\underline{p} - \underline{p}^2}$,*
- *Either monotone increasing, down-up, or up-down-up if $\frac{4\bar{p}\underline{p}}{\bar{p}^2 + 4\bar{p}\underline{p} - \underline{p}^2} < \alpha_0 < \sqrt{9/8} \cdot \underline{x}$.*

We note that the overall results in this section extend to more general degradation functions of the form $\Phi(u) = ku^\beta$ with $\beta > 1$, as shown in Appendix B.3.1. The parameter β represents the DOD-elasticity of degradation and refers to the degree to which the degradation rate $\Phi(u)$ responds to a change in a DOD level; see Section 3.5.1 for detailed analysis. Theorem 3.5 and Theorem 3.6 continue to hold under this generalized setting, as illustrated in Theorem B.4. Theorem B.3 generalizes Theorem 3.2, showing how both the discount rate δ and the degradation elasticity β influence the optimal distribution of revenue over time. In particular, the ratio

$$\frac{r(t)}{r(0)} = e^{-\delta t \cdot \frac{\beta}{\beta - 1}},$$

shows that as the degradation elasticity β increases (i.e., as the battery's degradation rate becomes more sensitive to changes in DOD), the rate of revenue decline slows down.

3.5 Generalization/Extension

We consider several generalizations of the main models (both the capacity-degradation-only and unified models), including (1) alternative degradation functions and (2) an N-price setting. Before proceeding, we summarize the key findings across these models in Table 2.2.

In the following sections, we examine generalizations of the main models and demonstrate how the key findings remain robust, with some modifications.

3.5.1 Alternative Degradation Functions

Power functions: $\Phi(u) = ku^\beta, \beta > 1$. As noted in Appendix B.1.2, one of the most common approaches for modeling the nonlinear, convex impact of DOD on degradation is through power functions. In the main model, we assume a quadratic degradation function ($\beta = 2$). In fact, the overall structural lessons/insights on the optimal policy do not depend on the quadratic function and can be generalized to any power function with the exponent of $\beta > 1$.

To understand this robustness of the results, we can define the DOD-elasticity of degradation as $\epsilon(u)$:

$$\epsilon(u) := \frac{\frac{d\Phi(u)}{\Phi(u)}}{\frac{du}{u}} = \frac{\Phi'(u)u}{\Phi(u)}.$$

$\epsilon(u)$ refers to the degree to which the degradation rate $\Phi(u)$ responds to a change in a DOD level. Then we can use the fact that $\Phi(\cdot)$ has constant elasticity β if and only if $\Phi(\cdot)$ is a power function of the form $\Phi(u) = ku^\beta$ for some constant $k > 0$. Thus, with any power function, the constant elasticity implies that when DOD level rises by 1%, the degradation rate rises by β%. Appendix B.3.1 presents detailed analyses of degradation in the form of power functions in both the capacity-degradation-only and the unified models.

While the structural properties remain unchanged, the DOD-elasticity β plays a key role in interpreting the results and implementing battery dispatch. For instance, the way we distribute unconstrained revenue over time under the unified model can be described as follows:

Theorem 3.7 (Unified: Unconstrained revenue rate). *When $u^*(t) < 1$, the discounted revenue rate $r(t) := e^{-\delta t} p^a(t) E(t) u(t)$ satisfies:*

$$r(t) = r(0) e^{-\delta t \cdot \frac{\beta}{\beta - 1}}.$$

For a fixed β, a larger δ implies faster decline of $r(t)$. Conversely, for a fixed δ, as β increases (i.e., as the degradation rate becomes more sensitive to changes in DOD), the effective decay factor $\frac{\beta}{\beta-1}$ decreases toward 1, so $r(t)$ decays more slowly over time.

General Convex Functions. Although power functions are the most common choice for modeling, the model can be further extended to incorporate alternative convex and increasing degradation functions (i.e., $\Phi'(u), \Phi''(u) > 0$ for any $u \in [0, 1]$), such as exponential functions. This extension is beyond the main scope of our analysis, but we briefly highlight several points below.

Several key insights continue to hold (see Appendix B.3.1.1), although some properties are modified under a general degradation function. As an example, we discuss below how the DOD-elasticity of the degradation function affects the optimal policy for the unconstrained, undiscounted problems. Interestingly, we can show that, at optimality, the DOD-elasticity fully determines how the pattern of the immediate revenue functions behaves for the unconstrained, undiscounted models.

Theorem 3.8 (**Elasticity**). *For the unconstrained, undiscounted unified model with a convex increasing degradation function $\Phi(u)$, the optimal revenue rate $r^*(t)$ satisfies the following:*

- *A constant revenue policy is optimal ($r^*(t) = c$ for some c) if and only if the DOD-elasticity of degradation is constant for any $u < 1$ (i.e., $\Phi(u)$ is a power function),*
- *$r^*(t)$ is decreasing if and only if the DOD-elasticity of degradation is increasing in u,*
- *$r^*(t)$ is increasing if and only if the DOD-elasticity of degradation is decreasing in u.*

Theorem 3.8 shows that the "constant revenue" phenomenon for the undiscounted problems happens if and only if DOD-elasticity of degradation is constant at $\beta > 1$ (convex)—when DOD level rises by 1%, the degradation rate rises by β%. Intuitively, if the DOD-elasticity of degradation is increasing in u, the battery should be operated more conservatively, in terms of the revenue generated, over time. Conversely, if the DOD-elasticity of degradation is decreasing in u, the battery should be operated more aggressively, in terms of the revenue generated, over time.

3.5.2 Multiple Prices

In the main model, we consider a single arbitrage price (with fixed $\bar{p}$ and $\underline{p}$). Our model can be extended to incorporate multiple prices, which are realized according to some probability distribution. Specifically, we generalize the high energy price to take N possible values, $P(t) \in \bar{p}_1, \ldots, \bar{p}_N$, where each price $\bar{p}_i$ occurs with probability p_i for all $i \in [N] := 1, \ldots, N$,

and, without loss of generality, satisfies $\bar{p}_1 \leq \bar{p}_2 \leq \cdots \leq \bar{p}_N$.[19] Under this setup, let $(u_1(t), \cdots, u_N(t))$ denote the DOD allocation at time t associated with the high price vector $(\bar{p}_1, \cdots, \bar{p}_N)$. Under this setup, Appendix B.3.2 shows that the main insights from the single-price setting continue to hold for both the capacity-degradation and unified models. We summarize the key results below.

Capacity-Degradation-Only. Under capacity degradation only, Theorem B.8 shows that the optimal DOD for each price pair, $u_i^*(t)$, increases monotonically in t for all $i \in [N]$, with $u_i^*(t) \leq u_j^*(t)$ for all $i < j$. Consistent with Section 3.4.1, we highlight two special cases. First, when $\delta = 0$, the optimal expected arbitrage quantity $A^*(t) := \sum_{i=1}^N p_i u_i^*(t) E(t)$ remains constant as long as capacity is non-binding (see Corollary B.4), confirming that the constant-throughput policy widely used in practice and literature can be optimal. Second, as $T \to \infty$, the optimal DOD sequence becomes time-invariant (see Corollary B.5). Moreover, when capacity is non-binding for all p_i^a (i.e., $u_N^*(t) < 1$), the N-price dynamics coincide with those of the base model,[20] implying that the 90.25% optimality of the fixed-DOD heuristic continues to hold.

Unified Degradation With a unified degradation model, Theorem B.9 show that when $\delta = 0$, $u_i^*(t)$ is monotone increasing in t for all $i \in [N]$, and the expected arbitrage revenue rate $r(t) := \sum_{i=1}^N p_i p_i^a(x(t)) u_i^*(t) E(t)$, remains constant as long as the battery's capacity is not binding (i.e. ,$u_N^*(t) < 1$). With a general discounted setting, Theorem B.10 shows that a battery subject to both capacity and efficiency degradation may exhibit non-monotonic patterns due to the trade-off between time discounting and degradation effects, and characterize the expected revenue rate $r(t)$ in a closed-form.

3.5.3 Summary of Generalization

With these generalizations, our model has been extended to more realistic settings, either by incorporating alternative degradation functions or multiple prices. As summarized in Table 2.2, our findings remain robust to the assumptions used in Sections 3.4.1–3.4.2. In the following section, we proceed further by conducting numerical experiments on realistic scenarios, using parameters calibrated from historical and operational data to highlight these generalizations.

[19]The result trivially holds for $\{(\bar{p}_1, \underline{p}_1), \cdots, (\bar{p}_N, \underline{p}_N)\}$ (with p_i being the probability of $(\bar{p}_i, \underline{p}_i)$ to be the energy price pair) as long as $\bar{p}_i x - \frac{p_i}{x} \leq \bar{p}_j x - \frac{p_j}{x}$ holds for any $i < j$ and $x \in (0, 1]$.

[20]There exists p^a such that $\sum_{i=1}^N p_i (p_i^a)^2 = (p^a)^2$, yielding identical degradation dynamics and revenue rates.

Type	Notation	Parameter	Value	Unit	Sources
Grid/market condition	p_i^e	energy hourly price ($i = 1, \cdots, 24$)	historical values	\$/MWh	[137, 84]
	δ	discount factor	$[0, 0.25]$	-	[111]
	T	project length	$[10, 1000]$	-	[130, 163]
Battery specification	β	degradation exponent	$[1, 3]$	-	[51, 17]
	k	degradation coefficient	$(0, 0.1]$	-	[51]
	E_0	Nominal energy capacity	1	MWh	-
	x_0	Nominal one-way efficiency	$[0.90, 0.95]$	-	[52, 56]
	α_0	intercept of capacity-efficiency degradation	$[-1, 1]$	-	[77], [52], [32], [129], [127]
	α_1	slope of capacity-efficiency degradation	$[0, 1]$	-	

Table 3.4: Summary of the model parameters used in Section 3.6.

3.6 Numerical Study

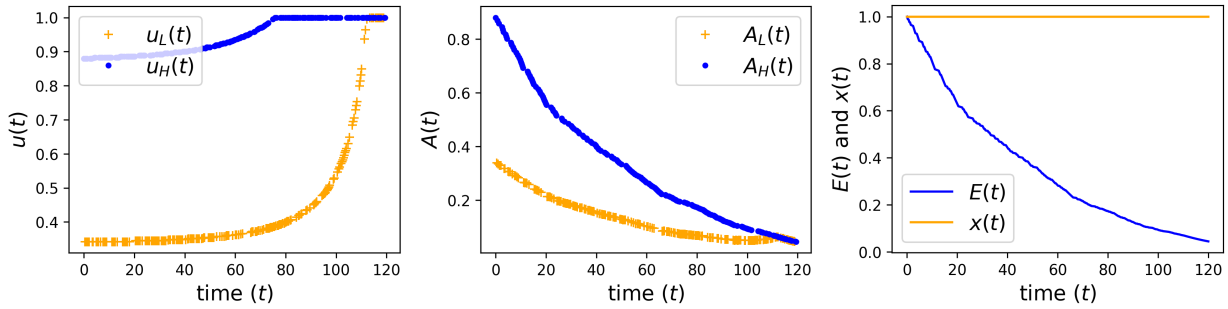
In this section, we numerically examine the sensitivity of our results to key modeling assumptions and evaluate the benefits of dynamically adjusting battery utilization while accounting for both capacity and efficiency degradation under various plausible scenarios. Our goal is to quantify the realistically achievable advantages of the optimal dynamic policy given current grid conditions and battery specifications.

3.6.1 Calibration of Model Parameters with Data

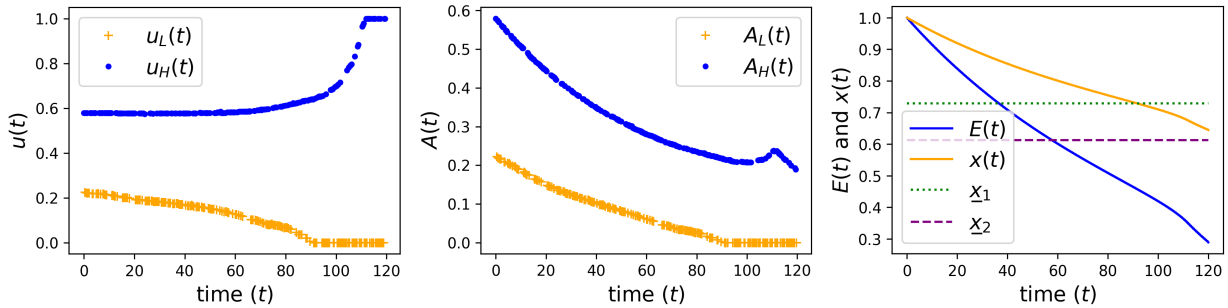
To calibrate our models, we use real-world historical and operational data from multiple independent system operators (ISOs) and battery operators across the United States. For grid and market conditions, we primarily rely on the New York ISO (NYISO) and ISO-New England (ISO-NE) day-ahead energy price datasets, covering the period from January 1, 2024, to September 30, 2025. We consider a lithium-ion battery energy storage system (BESS) with a nominal energy capacity of $E_0 = 1$ MWh and a nominal one-way efficiency x_0 of 92%. Table A.9 summarizes all model parameters and data sources employed in our numerical study.

3.6.2 Effect of Grid/Market Environments

Multiple Price Effects. To identify representative daily patterns in the day-ahead energy price, we use historical hourly price data. Each day is represented as a 24-dimensional vector of hourly prices. For each day, we extract the minimum and maximum prices as the low-



(a) Capacity-degradation-only



(b) Unified degradation

Figure 3.7: Optimal system dynamics under multiple prices (Theorems B.8 and B.10): (a) capacity degradation only ($\alpha_1 = 0$), and (b) unified degradation ($\alpha_1 = 0.4$). Other parameters: $\underline{p}_1 = 42,\ \bar{p}_1 = 79,\ \underline{p}_2 = 57,\ \bar{p}_2 = 152,\ p_1 = 0.62, \delta = 0.02, k = 0.05, T = 120$.

and high-price pairs for arbitrage.[21] We then apply K-means clustering with $K = 2$ clusters to identify the two most frequent price patterns. Based on the cluster centers, we extract the expected $(\underline{p}_i, \bar{p}_i)$ for $i = 1, 2$, along with their corresponding probabilities p_i. We assume perfect foresight of prices (i.e., the battery operator can react optimally to either low- or high-price realizations), which is a common modeling assumption for estimating arbitrage profits [146, 207, 159].

Figure 3.7 illustrates the dispatch policy under (a) capacity-degradation-only and (b) unified degradation for a given price realization path consisting of two price pairs. Figure 3.7(a) shows that, under capacity degradation only, the optimal battery utilization $u_i^*(t)$ increases monotonically over time for all price pairs $i \in [N]$ (consistent with Theorem B.8). In contrast, Figure 3.7(b) shows that when the battery undergoes both capacity and efficiency degradation, it must be operated more conservatively than under capacity degradation alone. Battery utilization in this case may decline over time and exhibit non-monotonic behavior.

[21] Some markets may have multiple price peaks per day. In such cases, the procedure described above can be applied separately for each peak.

Unlike the capacity-degradation-only scenario, where the battery responds to all price pairs throughout the horizon, a battery subject to unified degradation may initially react to all price pairs but gradually focus on high price opportunities as its efficiency deteriorates. Specifically, when $\underline{x}_2 < x(t) < \underline{x}_1$ for $90 < t \leq T$, the battery can generate a positive revenue only with p_2^a, not p_1^a.

This implies that batteries with lower efficiency—such as those that have been in operation for an extended period or repurposed batteries following their original use (e.g., from electric vehicles)—may have limited applications.[22] As the battery's performance dynamically degrades over time, it may be optimal to adapt its operational role—starting with frequent arbitrage when the efficiency is high and gradually transitioning to a peaking application as efficiency deteriorates.

3.6.3 How Costly Ignoring Efficiency Degradation Can Be?

Lastly, we examine how costly it can be to ignore efficiency degradation in realistic settings. This question is particularly relevant because most operations management studies, white papers, and even battery operators often overlook efficiency degradation, as discussed in the Introduction and Literature Review. To quantify this effect, we compare the lifelong revenues generated under three benchmark models (fixed-A, fixed-DOD, and capacity-degradation-only) with those under the unified model, assuming that the underlying battery mechanism experiences both types of degradation. To capture the effect of different market conditions and price distributions, we use price datasets from NYISO and ISO-NE. Furthermore, to account for differences in battery specifications, we vary the relative magnitudes of degradation by changing the slope parameter $\alpha_1 \in \{0.1, 0.2, 0.3, 0.4\}$ while keeping $\alpha_0 + \alpha_1$ fixed at the nominal efficiency level x_0. Finally, we explore alternative degradation functions with the exponent $\beta \in \{1.5, 2.0, 2.5\}$.

Key findings from Table 3.5 are as follows. First, ignoring efficiency degradation can be costly, as reflected in the revenue losses across all benchmark models. The magnitude of missed opportunities increases with α_1, as the battery experiences more severe efficiency loss relative to capacity loss. Interestingly, the sharp decrease in the revenue ratio (e.g., from 95.2% to 29.4% for Cap.-deg.-only as α_1 increases from 0.1 to 0.4 under the ISO-NE case) highlights that missed opportunities are highly sensitive to the characterization of the true efficiency degradation mechanism, potentially leading to substantial losses. Moreover, dynamic adjustments based solely on capacity degradation do not necessarily outperform the commonly used heuristics (fixed-A and fixed-DOD policies).

[22] A canonical example is serving as peaker plants—that is, batteries operated only occasionally to supply power during periods of high demand or extreme price spikes.

(a) NYISO

$\alpha_1^\dagger$	β	Lifelong Revenue Ratio		
		Fixed-A	Fixed-DOD	Cap.-deg.-only
0.1	1.5	94.6%	65.3%	96.1%
	2.0	97.4%	69.1%	98.0%
	2.5	97.9%	72.9%	98.4%
0.2	1.5	90.4%	59.8%	85.3%
	2.0	92.5%	62.4%	88.6%
	2.5	93.9%	65.7%	91.1%
0.3	1.5	77.1%	54.8%	67.1%
	2.0	81.6%	58.0%	71.9%
	2.5	83.6%	61.6%	74.3%
0.4	1.5	63.7%	53.6%	46.2%
	2.0	67.3%	56.9%	49.1%
	2.5	70.2%	60.3%	52.4%

(b) ISO-NE

α_1	β	Lifelong Revenue Ratio		
		Fixed-A	Fixed-DOD	Cap.-deg.-only
0.1	1.5	91.7%	92.5%	92.0%
	2.0	95.3%	95.9%	95.2%
	2.5	96.9%	97.5%	96.8%
0.2	1.5	83.5%	85.4%	77.2%
	2.0	89.6%	90.9%	81.8%
	2.5	90.5%	95.3%	86.5%
0.3	1.5	73.6%	85.1%	52.8%
	2.0	76.1%	88.0%	56.3%
	2.5	79.5%	91.7%	60.5%
0.4	1.5	52.7%	79.5%	26.3%
	2.0	57.7%	83.0%	29.4%
	2.5	63.2%	86.8%	36.7%

Table 3.5: Comparison of lifelong revenue ratios under different benchmark models and parameter settings. (a) $\underline{p}_1 = 54, \bar{p}_1 = 79, \underline{p}_2 = 63, \bar{p}_2 = 151, p_1 = 0.63$, (b) $\underline{p}_1 = 58, \bar{p}_1 = 82, \underline{p}_2 = 61, \bar{p}_2 = 124, p_1 = 0.71$. Other parameters used: $T = 120,\ k = 0.07,\ \delta = 0.01$.

Second, the magnitude of missed opportunities varies across markets, depending on factors such as low and high prices and the frequency distribution of prices. During the observation period, NYISO tends to exhibit higher price spreads (with higher chances of spikes from $p_2 = 0.37$ under NYISO versus $p_2 = 0.29$ under ISO-NE) than ISO-NE, which places greater emphasis on capturing efficiency losses for profitability.

Third, Table 3.5 provides practical insights for battery operators, including which types of batteries are more or less sensitive to efficiency degradation. Batteries with a smaller β (i.e., a less convex degradation function) tend to be used more aggressively, accelerating efficiency loss in the early periods and potentially causing long-lasting effects on the remaining lifetime, ultimately lowering lifelong revenue. Moreover, because the evaluations are based on realistic parameter calibrations, batteries subject to greater efficiency degradation (i.e., with a larger α_1) require careful consideration of efficiency loss in operational planning.

3.7 Conclusion

This research examines how capacity and efficiency degradations impact battery control decisions throughout the battery's lifetime. Using an optimal control framework, we analytically characterize the optimal control policy, recognizing that usage affects battery performance degradation. Comparing two models—one with capacity degradation only and the other with the presence of efficiency degradation—we reveal a systematic difference. Under capacity-degradation-only, the optimal utilization increases monotonically over time, regardless of energy prices or discounting. In contrast, when efficiency degradation is present, optimal utilization tends to be substantially lower (even when the average efficiency remains higher than that of a battery without efficiency degradation) and may decrease or exhibit non-monotonic patterns (e.g., an "up–down–up" trajectory over a finite horizon), underscoring the limitations of commonly used heuristic approaches.

Given the widespread use of heuristics without rigorous evaluation in the existing literature, we contribute by examining suboptimality and quantifying the optimality gap. While some approaches achieve near-optimal performance under specific conditions, a fixed depth-of-discharge (DOD) policy is generally only 90.25%-optimal. This indicates substantial suboptimality, especially considering that most battery applications operate on thin profit margins as of 2025. Furthermore, in the presence of efficiency degradation, these heuristics may overlook even greater losses. As demonstrated in the motivating example in Section 3.4.2, fully depleting the battery can be severely suboptimal, underscoring the importance of dynamically adjusting DOD levels to enhance battery economics.

Lastly, we take several additional steps to make our work more applicable to battery

operators. We generalize our models by incorporating alternative forms of degradation and multiple energy prices. Using numerical experiments calibrated with realistic market parameters and battery specifications, we illustrate the consequences of model misspecifications, specifically highlighting the costs of ignoring efficiency degradation.

CHAPTER 4

Choice of Battery Portfolios and Benefits of Heterogeneity

4.1 Introduction and Literature Review

A battery energy storage system (BESS) enables more flexible and efficient use of generation resources and helps maintain grid stability. BESSs are hierarchically organized: individual cells are grouped into modules, modules are assembled into packs (or racks), and multiple packs are integrated to form a complete energy storage system. Operationally, battery management systems (BMSs) monitor and control each pack separately, making the pack the smallest dispatchable unit, while cells within a pack are typically of the same type to ensure safe operation and reliable balancing. Due to their structure, BESSs can be deployed at different scales, which allows capacity to be chosen with high granularity.[1]

Traditionally, grid-scale energy storage deployments have relied on a single, homogeneous pack (Figure 4.1(a)). In such settings, all cells have the same chemistry and performance characteristics, so the entire system behaves uniformly. However, advances in battery technology and the growing availability of storage resources (e.g., the influx of second-life EV batteries; see [68]) are creating new opportunities to combine multiple packs (potentially with different chemistry or performance characteristics) within a single energy storage system (see [22] for details).

This shift raises an important question: should packs be combined to have as similar characteristics as possible, forming a homogeneous portfolio, or are there advantages to constructing heterogeneous portfolios—hereafter referred to as hybrid portfolios (Figure 4.1(b))—that leverage packs with different performance and degradation characteristics?

[1]For example, Tesla has introduced a range of energy storage technologies, including electric vehicle (EV) batteries (e.g., Models S has a 85 kWh pack composed of 16 modules, each containing hundreds of Panasonic 18650 cells [60]) and stationary storage products such as the Powerwall (13.5 kWh) for residential applications, the Powerpack (roughly 200 kWh Powerpack 2) for commercial and industrial use, and the Megapack (roughly 4 MWh) for utility-scale projects [184].

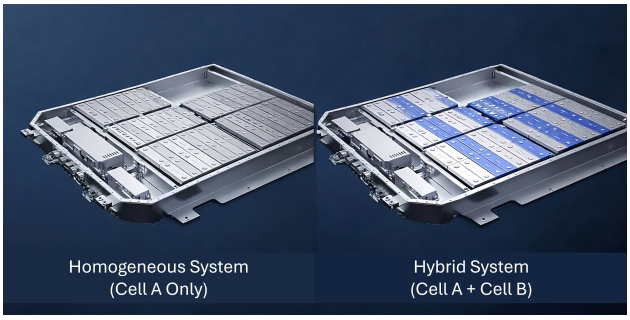


Figure 4.1: Illustration of a battery energy storage system: (a) homogeneous system, composed of identical packs (and cells), and (b) hybrid system, composed of two different pack types (Cell A and Cell B). Reproduced from [22].

In this essay, we study a battery system committed to providing a specific energy or service quantity profile. This implies an exogenously determined workload profile, which specifies when and how much the battery should charge or discharge. This modeling choice is motivated by the institutional design of renewable-plus-storage projects operating under long-term Power Purchase Agreements (PPAs), which have become increasingly prevalent in the United States and globally [10, 78]. In such contracts, while ownership of both assets (renewable and battery storage) remains with the project developer, operational control of the battery is often contractually delegated to the off-taker (e.g., a utility). Under solar-plus-storage PPAs, the contracts typically require batteries to charge when solar generation is high and discharge later to shift energy to higher-value periods [140, 211]. Daily variations in renewable output (driven by stochastic weather patterns) introduce variability in the battery workload from day to day. Thus, the battery owner does not optimize the battery system's aggregate load (e.g., in response to market prices), but retains flexibility to optimize the allocation of load across packs. This means that a hybrid portfolio may distribute workload when needed (e.g., to reduce operating costs) while still meeting externally imposed service requirements. In Section 4.2.1, we later expand this motivation of an exogenous service profile with the example of a solar-plus-storage PPA (the most common hybrid), explaining the details of the required service rate $d(t)$.

Hybrid battery portfolios, which typically combine multiple energy storage technologies with complementary characteristics (e.g., lithium-ion batteries paired with supercapacitors, flow batteries, or lead–acid batteries), have attracted growing attention as a cost-effective alternative to homogeneous storage systems. Recent studies have investigated the mechanisms by which hybrid battery portfolios can outperform homogeneous alternatives. Several distinct rationales for employing hybrid systems have been proposed across different research streams.

The budget effect arises when upfront capital constraints prevent investment in a single high-performance battery. In such cases, the operator combines a smaller, efficient battery with a cheaper, less efficient alternative, allowing the system to meet demand while respecting budget constraints [62, 1, 6, 98]. Notably, all the mechanisms discussed in this essay exist without any budget constraints enforced.

Another line of work focuses on combining technologies with differentiated physical capabilities, such as resources with significantly different power-to-energy ratios [48, 112, 38, 66]. Hybrid systems can allocate high-power, short-duration services (such as frequency regulation or peak shaving) to power-oriented resources and energy-intensive, long-duration services (such as load shifting) to energy-oriented resources, thereby reducing overall system costs compared to homogeneous systems [104, 143]. These benefits are particularly pronounced in applications with space or weight constraints. For example, in electric vehicles, supercapacitors are often combined with batteries: supercapacitors' high power density supports rapid acceleration and regenerative braking, while lithium-ion batteries provide energy for longer trips [5, 29, 139, 218]. If a single battery were required to handle both high-power and high-energy demands (e.g., rapid EV acceleration versus long-distance travel), it would need to be oversized for either power or energy, leading to excessive cost, mass, or volume. Hybridization allows the system to reduce overall capacity requirements, mass, and size, thereby lowering costs while meeting both types of applications [39, 212]. Our work differs from this stream of work as we only model energy-intensive tasks (load shifting for renewable integration), and we further show our effects even in completely undifferentiated workloads.

The environmental effect arises when environmental factors, such as temperature, make some batteries more costly to operate. For example, supercapacitors can function over a wide temperature range (from -40°C to +70°C), whereas batteries are more sensitive to extreme conditions [202, 178]. Among batteries, NMC cells generally retain 70–80% of their rated power at -20°C, while LFP cells maintain only 50–60%. Combining resources with different temperature sensitivities can help maintain higher overall efficiency and reduce costs [218, 100]. In our setting, we do not explicitly consider such factors, as we consider a BESS that is managed by a battery management system (BMS) with advanced cooling systems that mitigate environmental impacts [107, 181], and all mechanisms discussed in this essay exist independently of such factors.

Another stream of work focuses on the C-rate effect, which is closely linked to thermal effects. The C-rate measures how quickly energy flows in a cell, and higher C-rates are known to accelerate battery degradation, particularly by generating high temperatures [123, 90, 204]. In nonstationary applications, such as urban EV driving, the storage system experiences sudden current changes and rapid power fluctuations due to frequent acceler-

ation and deceleration. By combining batteries with supercapacitors—which can handle rapid power fluctuations with negligible degradation—hybrid systems can relieve batteries from high-C-rate tasks, thereby reducing battery wear and extending the system's effective lifespan [212, 175, 88, 188, 114, 44, 18]. In our stationary setting, the C-rate effect is limited because again the BMS and cooling systems can control battery temperature to have minimal impact on degradation [107, 181]. Instead, we focus on degradation caused by daily cycles rather than second-to-second fluctuations. We also account for operating costs due to efficiency degradation—a reduction in the ratio of retrievable energy per unit of energy charged. Efficiency degradation can significantly impact battery profitability and constitutes a key component of our model.

The peaker effect arises when service requirements exhibit rare but extreme workloads. Even in the absence of upfront budget constraints, it may be inefficient to size a single high-performance battery (i.e., an expensive-to-procure, cheap-to-operate battery) to cover both typical and extreme demand levels. Instead, the efficient battery is sized to meet normal operating conditions, while a less efficient battery (i.e., a cheaper-to-procure, expensive-to-operate battery) provides additional capacity during infrequent peak events [16, 210, 195]. This logic is analogous to conventional peaker plants: fossil-fueled (gas or oil) power plants that are used to meet rare peak events (e.g., hot summer afternoons when air conditioners run heavily), supplementing cleaner baseload plants [61, 7]. In this essay, the mechanism we propose exists even under deterministic workloads with no variability and is therefore fundamentally different from the peaker effect. Moreover, our mechanism under stochastic workloads provides benefits by combining batteries with differing operational flexibility driven by degradation characteristics, not merely differences in costs. To illustrate this point, note that the battery with higher efficiency will always be selected to serve the baseload under a traditional peaker effect, while the battery serving the baseload in our setting may be either more or less efficient, depending on its degradation convexity (Observation 4.1).

This essay highlights that different battery technologies have fundamentally different degradation dynamics, which generate distinct intertemporal preferences for how work is allocated over time. We model degradation costs as functions of depth of discharge (DOD), where the impact of DOD varies by battery type to reflect differences in cell chemistry. As we will show, some cell chemistries are significantly more sensitive to how work is distributed over time than others. Unlike the literature above, we explicitly account for both the loss of energy capacity and efficiency degradation.

We develop a unified framework that jointly optimizes investment decisions (capacity sizing) and operational decisions (allocation of work across batteries) for hybrid battery portfolios. Our model maximizes total profit, capturing both capital cost and energy rev-

enue. Using optimal control theory, we model batteries' gradual performance degradation. Specifically, we account for the simultaneous reduction in energy capacity (the maximum energy a battery can store) and round-trip efficiency (the fraction of energy retrievable per unit charged). Our framework provides new insights into the design and operation of hybrid storage systems that cannot be captured by existing models with simplified degradation assumptions.

Our contributions are threefold.

1. **Theoretical Identification of the "Protection Effect":** We formally identify the protection effect as a distinct economic mechanism underlying the value of hybrid battery portfolios. Using stylized models, we analytically show that while the operating cost of a battery with linear degradation is invariant to the temporal allocation of service, batteries with strictly convex degradation incur lower costs when operated along specific trajectories, typically favoring increasing discharge over time and evenly sized cycles. This asymmetry allows "less convex" batteries to protect "more convex" batteries by absorbing unfavorable service patterns—such as decreasing or highly variable discharge requirements—while jointly meeting the exogenous workload. As a result, the "more convex" batteries can operate closer to their revenue-maximizing (or energy-loss-minimizing) trajectories, by avoiding workloads that cause excessive degradation. Unlike the existing mechanisms discussed in the literature, the protection effect arises even in the absence of capital constraints, extreme demand spikes, or workloads requiring different physical capabilities. Instead, it is driven by differences in battery degradation characteristics across battery types and by the structure of the required service profile, and the strategy for allocating service across these batteries may become an important determinant of total system profit.

2. **Numerically Quantifying Cost Savings from the Protection Effect:** We numerically quantify the economic value of the protection effect across a range of workload environments using an all-cost measure to benchmark the economic value of hybrid battery portfolios. Specifically, we use the AllCost measure, defined as the sum of battery acquisition costs and the lost revenue due to efficiency degradation while delivering energy, relative to a benchmark setting without efficiency losses. Using parameters calibrated from real-world battery and market data, we numerically evaluate cost savings under three settings: stationary deterministic workload, nonstationary deterministic workload, and stationary stochastic workload. Cost savings from heterogeneity (compared to homogeneous batteries) are below 4% under stationary deterministic workloads, but increase up to 3%–9% under nonstationary or stochastic workloads

with realistic battery and market specifications. These results provide clear managerial guidance on when hybrid battery portfolios deliver the greatest value and on the magnitude of achievable cost savings.

3. **Analytically Establishing the Potential Cost Saving:** To formally illustrate why a hybrid battery portfolio provides greater benefits under stochastic workloads than under deterministic workloads, we consider a stylized model with two assumptions: (1) no efficiency degradation and (2) continuous battery replacement to offset capacity loss due to degradation. We redefine an all-cost measure to capture the potential cost savings from hybrid battery portfolios, defined as the sum of battery acquisition costs, replacement costs, and energy losses compared to the most efficient battery. We show that as the convexity parameter of the more convex battery approaches infinity, an even service allocation becomes optimal. We also analytically derive the cost savings of a hybrid battery portfolio for a given demand profile.

4.2 Preliminaries for the Model

4.2.1 Renewable-plus-Storage with PPA

The global addition of renewable energy (e.g., solar and wind) has driven the deployment of grid-scale battery storage to manage variability and ensure reliable electricity supply. Solar-plus-storage systems are especially prominent: more than 60% of newly contracted renewable capacity (MW) in the U.S. involve solar, and over half of the annual solar capacity added to the grid comes paired with storage [10, 28]. By storing excess renewable generation during periods of abundant supply (and therefore low energy prices) and discharging during peak demand, these systems enhance grid stability and allow more efficient use of generation resources.

Renewable projects are frequently launched under long-term Power Purchase Agreements (PPAs), which are contracts between a project developer (e.g., a renewable energy company) and an off-taker (typically a utility) that secure the sale of generated electricity. By guaranteeing a buyer over a long horizon (typically 15–25 years [28]), PPAs reduce revenue risk for the project developer, lower the cost of capital, and facilitate project financing relative to merchant (market-based) settings [78]. For example, the Green River Energy Center in Utah combines 400 MW of solar generation with 1,600 MWh of battery storage under a PPA between PacifiCorp (utility) and rPlus Energies (renewable energy company), representing one of the largest solar-plus-storage facilities in the U.S. Such contracts are becoming increasingly common worldwide due to their financial and operational benefits. PPA contracts

accounted for over 50% of the total annual solar and wind capacity added to the grid between 2019 and 2024 [10, 28].

Many PPAs for renewable-plus-storage restrict battery charging to the co-located renewable generator, explicitly prohibiting grid charging (see e.g., [50, 14]), which guarantees that all discharged energy is from renewable plants. For example, PacifiCorp, the largest grid operator in the western United States, has this as a standard part of its PPA with collocated batteries [140]. In addition, some agreements grant the utility full operational control over the battery, determining the timing, magnitude, and targets of dispatch within contractual limits (e.g., Entergy, a Fortune 500 energy company and one of the largest U.S. utilities, [59]; PacifiCorp [140]; East Bay Community Energy [50]; and Ava Community Energy [14]). These contractual provisions ensure predictable service delivery but limit the flexibility of the project owner.

As a result, many renewable-plus-storage projects face an effectively exogenous workload on their batteries, with the utility determining when and how much energy is not immediately used and must therefore be charged to or discharged from the storage system. Under solar-plus-storage PPAs, utilities often set the workload to charge during periods of high solar generation and discharge later (intertemporal energy shifting with storage) [140, 211]. Daily variations in renewable output—driven by stochastic weather patterns—introduce day-to-day variability into the workload.

This PPA setup motivates our modeling framework, in which battery operators allocate workload across multiple cell types within a BESS to meet service commitments while maximizing cumulative profits, accounting for energy revenues as well as battery investment costs. Our model captures both operational decisions (how each day's workload is distributed among multiple heterogeneous batteries) and investment decisions (initial sizing of battery capacities), providing a realistic representation of hybrid battery operation under PPA constraints.

4.2.2 Battery Performance Degradation

Battery degradation refers to the physical deterioration of a battery over time and manifests primarily through two performance losses: capacity fade and efficiency loss. Among the many factors influencing degradation (e.g., temperature and charge rates), we focus on depth of discharge (DOD) as a primary driver.

The depth of discharge at time t, denoted by $u(t) \in [0, 1]$, is defined as the ratio of discharged energy to the battery's current (remaining) energy capacity. The degradation cost associated with a discharge cycle of depth u is modeled by the convex polynomial

function [205]

$$\Phi(u) = ku^{\beta}, \tag{4.1}$$

where $k > 0$ is a degradation coefficient and $\beta \geq 1$ governs the convexity of the degradation function. This specification is standard in the engineering literature and captures empirically observed behavior: degradation increases with DOD, with a battery-specific exponent β that depends on the battery chemistry.

To model gradual degradation over time, we adopt a fluid approximation of the degradation process. Consistent with empirical and experimental evidence [204, 158], we model the evolution of battery capacity according to

$$\dot{E}(t) = -E(t)\,\Phi(u(t)). \tag{4.2}$$

Moreover, following the empirical literature [77, 32, 129], we assume a linear relationship between one-way efficiency $x(t)$ and remaining capacity $E(t)$:

$$x(t) = \alpha_0 + \alpha_1 \cdot \frac{E(t)}{C},$$

where α_0 and α_1 are constants, and $C = E(0)$ denotes the battery's initial capacity (yielding initial efficiency $x(0) = \alpha_0 + \alpha_1 \leq 1$). For simplicity, we also define $\lambda := \frac{\alpha_1}{C}$, so

$$x(t) = \alpha_0 + \lambda E(t). \tag{4.3}$$

4.3 Model

Consider a (hybrid) battery storage system that is committed to providing an exogenously determined service rate over some time horizon.

Our model incorporates stochastic workload with two possible realizations (high and low), occurring according to some probability distribution. Specifically, let $d_L(t)$ and $d_H(t)$ ($d_L(t) \leq d_H(t)$ for all t) denote the low and high realizations of the service requirement at time t (that is, the total amount of energy produced by the renewable resource at time t, which must be charged by the BESS as it is produced and later discharged to the grid). Let $p_L(t)$ and $p_H(t)$ be the corresponding probabilities that the workload at time t will be low or high, respectively, with $p_L(t) + p_H(t) = 1$ for all t.

If we define our horizon as the discrete set of times $t \in \{0, \cdots, T-1\}$, then at time t the battery is required to charge an amount $d_L(t)$ with probability $p_L(t)$ and $d_H(t)$ with

probability $p_H(t)$. Accordingly, the battery is expected to perform a cycle of size $d_L(t)x(t)$ with probability $p_L(t)$ and of size $d_H(t)x(t)$ with probability $p_H(t)$, where $x(t)$ denotes the battery's one-way efficiency. We then consider a continuous-time approximation in which $d_L(t), d_H(t), p_L(t)$, and $p_H(t)$ vary continuously over horizon $t \in [0, T]$. We may consider several special cases of the stochastic model:

- Stationary stochastic workload: $d_L(t)$, $d_H(t)$, $p_L(t)$, and $p_H(t)$ are constant over time.
- Non-stationary deterministic workload: $p_H(t) = 1$ for all t, while $d_H(t)$ is non-constant.
- Stationary deterministic workload: $p_H(t) = 1$ and $d_H(t)$ is constant for all t.

The system consists of two battery cell types, indexed by $i \in \{1, 2\}$. Let $R_{i,L}(t)$ and $R_{i,H}(t)$ represent the service rates (in kW) supplied by battery type i under the low and high workload realizations, respectively, at time t. These rates must satisfy the workload requirements:

$$\begin{aligned} R_{1,L}(t) + R_{2,L}(t) &= d_L(t) \quad \forall t \in [0, T] \quad \text{and} \\ R_{1,H}(t) + R_{2,H}(t) &= d_H(t) \quad \forall t \in [0, T]. \end{aligned}$$

Let $E_i(t)$ and $x_i(t)$ denote the energy capacity and one-way efficiency of battery type i at time t, respectively. We assume the linear relationship described in (4.3):

$$x_i(t) = \alpha_{0,i} + \alpha_{1,i} \frac{E_i(t)}{C_i},$$

given the initial capacity $E_i(0) = C_i$.

Again, for intuition, in discrete-time with periods $t = 0, 1, \cdots, T-1$, battery type i charges an amount $R_{i,j}(t)$ from solar generation under scenario $j \in \{L, H\}$. Given a one-way efficiency $x_i(t)$, charging $R_{i,j}(t)$ increases the battery's energy by $R_{i,j}(t)x_i(t)$, and fully discharging this energy delivers $R_{i,j}(t)x_i^2(t)$ units of usable energy. The corresponding energy revenue is therefore

$$c^e \cdot R_{i,j}(t)x_i^2(t),$$

where c^e is the exogenous energy price, modeled for simplicity to be constant across time.

Using the continuous-time approximation, we treat $R_{i,j}(t)$ as an instantaneous charge rate under scenario $j \in \{L, H\}$ over the horizon $[0, T]$, and we model the rate of degradation incurred by the battery at time t based on the depth of discharge experienced under each scenario $j \in \{L, H\}$:

$$u_{i,j}(t) := \frac{R_{i,j}(t)x_i(t)}{E_i(t)},$$

as well as the probabilities $p_j(t)$ of each scenario and the degradation dynamics (4.1)–(4.2).

4.3.1 Optimal Control Problem (Profit Maximization)

We first formulate the optimization problem of maximizing the total profit for a hybrid battery system, which takes into account investment and energy replenishment costs. This introduces a natural trade-off: larger batteries increase upfront investment cost, but their higher capacity allows the system to suffer less battery degradation and maintain higher efficiency, increasing energy revenues. The optimal solution balances these opposing effects to determine the best combination of battery capacities and service allocations.

The decision variables are the initial capacities C_i and the service rate profiles $R_{i,L}(\cdot), R_{i,H}(\cdot)$ for $i \in \{1,2\}$. The optimization is subject to satisfying the workload (required service) constraints. $R_{i,j}(t)$ denotes the amount of solar generation allocated to battery type $i \in \{1,2\}$ under generation scenario $j \in \{L,H\}$ at time t. If battery type i has one-way efficiency x_i, then $R_{i,j}(t)x_i$ units are effectively stored in the battery, and $R_{i,j}(t)x_i^2$ units are ultimately delivered after charging and discharging losses. Since depth of discharge is determined by the energy cycled through the battery cell, the degradation term depends on $R_{i,j}(t)x_i$. Using (4.1)–(4.3), we formulate the problem as:

$$
\begin{aligned}
\max_{C_i, R_{i,L}(\cdot), R_{i,H}(\cdot), \forall i} \quad & \sum_{i=1}^{2} \Big(\mathbb{E}[r_i^{\text{energy}}(C_i)] - C^{\text{invest}}(C_i) \Big), && (4.4)\\
\text{s.t.} \quad C^{\text{invest}}(C_i) &= c_i^b \cdot C_i, \quad \forall i \in \{1,2\},\\
\mathbb{E}[r_i^{\text{energy}}(C_i)] &= c^e \int_0^T \Big[p_L(t) R_{i,L}(t) x_i^2(t) + p_H(t) R_{i,H}(t) x_i^2(t) \Big] dt, \quad \forall i \in \{1,2\},\\
\dot{E}_i(t) &= -E_i(t) \Big[p_L(t) \Phi_i\Big(\frac{R_{i,L}(t)x_i(t)}{E_i(t)}\Big) + p_H(t) \Phi_i\Big(\frac{R_{i,H}(t)x_i(t)}{E_i(t)}\Big) \Big],\\
& \qquad \forall i \in \{1,2\},\ \forall t \in [0,T],\\
x_i(t) &= \alpha_{0,i} + \alpha_{1,i} \frac{E_i(t)}{C_i}, \quad \forall i \in \{1,2\},\ \forall t \in [0,T],\\
d_L(t) &= R_{1,L}(t) + R_{2,L}(t), \quad \forall t \in [0,T],\\
d_H(t) &= R_{1,H}(t) + R_{2,H}(t), \quad \forall t \in [0,T],\\
E_i(t) &\geq \max\{R_{i,L}(t), R_{i,H}(t)\} x_i(t), \quad \forall i \in \{1,2\},\ \forall t \in [0,T],\\
R_{i,L}(t), R_{i,H}(t) &\geq 0, \quad \forall i \in \{1,2\},\ \forall t \in [0,T],\\
E_i(0) &= C_i, \quad \forall i \in \{1,2\},\\
C_i &\geq 0, \quad \forall i \in \{1,2\}.
\end{aligned}
$$

Here, $\Phi_i(u) = k_i u^{\beta_i}$ denotes the degradation function of battery type i, with constant $k_i > 0$ and exponent $\beta_i \geq 1$, and c_i^b represents the per-unit capacity investment cost of battery type i. We assume no salvage value at the end of the horizon, so the operator balances the initial capacity investments C_1 and C_2 against the incremental energy revenues obtained over time.

We define Π^*_{hybrid} as the optimal objective value of (4.4). The optimal profit for a homogeneous system using only battery 1, Π^*_{homo1}, can be obtained by re-solving (4.4) with the additional constraint $C_2 = 0$. Similarly, Π^*_{homo2} is obtained by re-solving with $C_1 = 0$.

4.3.2 Dynamic Program for Numerical Exploration

We now present a dynamic programming (DP) framework for numerical experiments. We discretize time t and the state space $(E_1(t), E_2(t))$.

State variables. At time τ, the system state is given by $(E_1(\tau), E_2(\tau))$, where $E_i(\tau)$ denotes the remaining energy capacity of battery type $i \in \{1, 2\}$.

Decision variables. At each time τ, the decision variables are the service allocations $(R_{1,L}(\tau), R_{1,H}(\tau))$. The allocations to battery 2 are then determined by feasibility:

$$R_{2,j}(\tau) = d_j(\tau) - R_{1,j}(\tau), \quad j \in \{L, H\}.$$

State transition. For analytical simplicity, we now proceed with $\alpha_{0,i} = 0$, which is consistent with empirical observations for common Li-ion battery types [52, 129, 32]. With this, we have closed-form expressions for the key terms. Let $\text{NewCap}_i(e_i, r_i)$ denote the updated energy capacity of battery type i at time $\tau + \delta$ (after one time step of length δ), given its current energy capacity $E_i(\tau) = e_i$ and allocated service rate r_i over the entire time range $[\tau, \tau + \delta]$. Then for $t \in [\tau, \tau + \delta]$, using $\lambda_i := \frac{\alpha_{1,i}}{C_i}$, we have

$$\begin{aligned} E_i'(t) &= -E_i(t) \cdot k_i \cdot \left(\frac{r_i x_i(t)}{E_i(t)}\right)^{\beta_i} \\ &= -E_i(t) \cdot k_i \cdot \left(\frac{r_i \lambda_i E_i(t)}{E_i(t)}\right)^{\beta_i} \\ &= -k_i r_i^{\beta_i} \lambda_i^{\beta_i} E_i(t). \end{aligned}$$

This is a standard ordinary differential equation with solution:

$$E_i(t) = e_i e^{-k_i (r_i \lambda_i)^{\beta_i} \cdot (t - \tau)}.$$

Thus, we have:

$$\text{NewCap}_i(e_i, r_i) = e_i e^{-\delta k_i (r_i \lambda_i)^{\beta_i}}. \tag{4.5}$$

Stage reward. We also define $\text{Energy}_i(e_i, r_i)$ as the energy revenue generated by battery type i over the interval $[\tau, \tau + \delta]$, given current energy capacity e_i and service rate r_i:

$$\begin{aligned}\text{Energy}_i(e_i, r_i) &= \int_{\tau}^{\tau+\delta} c^e r_i \lambda_i^2 E_i(t)^2 dt \\ &= \frac{c^e e_i^2 \lambda_i^{2-\beta_i} r_i^{1-\beta_i}}{2k_i} \left(1 - e^{-2\delta k_i (r_i \lambda_i)^{\beta_i}}\right).\end{aligned} \tag{4.6}$$

Feasible action set. Using (4.5)–(4.6), we define the value function $V(e_1, e_2, \tau)$ as the expected maximum cumulative energy revenues from time τ onward, given battery states e_1 and e_2. Since the service allocations must satisfy $R_{1,L}(\tau) + R_{2,L}(\tau) = d_L(\tau)$ and $R_{1,H}(\tau) + R_{2,H}(\tau) = d_H(\tau)$ at every τ, the decision variables reduce to $R_{1,L}(\tau)$ and $R_{1,H}(\tau)$. We define the feasible action set as

$$\mathcal{A}(\tau) := \left\{ (R_{1,L}, R_{1,H}) : \begin{array}{l} \max\left\{0, d_L(\tau) - \frac{1}{\lambda_2}\right\} \le R_{1,L} \le \min\left\{\frac{1}{\lambda_1}, d_L(\tau)\right\}, \\ \max\left\{0, d_H(\tau) - \frac{1}{\lambda_2}\right\} \le R_{1,H} \le \min\left\{\frac{1}{\lambda_1}, d_H(\tau)\right\} \end{array} \right\}. \tag{4.7}$$

The feasible set $\mathcal{A}(\tau)$ is induced by the DOD constraints $R_{i,j} x_i(e_i) \le e_i$ (which simplify to $R_{i,j} \le 1/\lambda_i$ under $x_i(e_i) = \lambda_i e_i$), for each battery type i and state $j \in \{L, H\}$, which is then combined with the workload conditions $R_{1,j} + R_{2,j} = d_j(\tau)$.

Bellman equation. For each τ and each grid point (e_1, e_2), the dynamic program solves:

$$\begin{aligned} & V(e_1, e_2, \tau) \\ := & \max_{(R_{1,L}, R_{1,H}) \in \mathcal{A}(\tau)} \Big[p_L(\tau) \Big(\text{Energy}_1(e_1, R_{1,L}) + \text{Energy}_2(e_2, d_L(\tau) - R_{1,L}) \\ & \qquad + V(\text{NewCap}_1(e_1, R_{1,L}), \text{NewCap}_2(e_2, d_L(\tau) - R_{1,L}), \tau + \delta) \Big) \\ & \quad + p_H(\tau) \Big(\text{Energy}_1(e_1, R_{1,H}) + \text{Energy}_2(e_2, d_H(\tau) - R_{1,H}) \\ & \qquad + V(\text{NewCap}_1(e_1, R_{1,H}), \text{NewCap}_2(e_2, d_H(\tau) - R_{1,H}), \tau + \delta) \Big) \Big]. \end{aligned} \tag{4.8}$$

Terminal condition. The terminal condition reflects the zero salvage value at the end of

the horizon:

$$V(e_1, e_2, T) = 0, \quad \forall e_1 \in [0, C_1],\ \forall e_2 \in [0, C_2]. \tag{4.9}$$

To jointly optimize investment decisions (initial capacities C_1 and C_2) and operational decisions (work allocation across batteries), we proceed as follows.

1. **Operational optimization for fixed capacities.** For a candidate capacity pair (C_1, C_2), we solve the dynamic program described above to determine the optimal operational policy. With continuous state variables E_1 and E_2, we apply bilinear interpolation as follows:

   - For each state (e_1, e_2) and time τ, we partition the feasible ranges of $R_{1,L}$ and $R_{1,H}$ into subintervals such that, within each subinterval, the resulting next state under the relevant scenario (L or H) remains in the same grid square of the (E_1, E_2) state grid.
   - We then evaluate the objective over all such subintervals, using bilinear interpolation over the four neighboring value-to-go values within each subinterval, and select the action that yields the highest value.

   This approximates the maximum expected energy revenues given the chosen capacities.

2. **Capacity optimization.** We repeat the above procedure over a grid of candidate capacity pairs to identify the optimal initial capacities (C_1^*, C_2^*) that achieve the highest total expected profits (accounting for both revenues and investment costs).

4.3.3 Numerical Experiments

We now proceed with numerical experiments to understand how workloads are distributed under optimal solutions and to quantify the magnitude of the benefits conferred by hybrid portfolios over homogeneous portfolios. To examine the impact of workload profile structure, we consider three workload profiles: (1) stationary deterministic, (2) stationary stochastic, and (3) non-stationary deterministic.

It is challenging to obtain meaningful relative comparisons between profit measures, as profits under a required workload can be positive, negative, or near-zero, so we instead define an all-cost measure that is more appropriate for benchmarking the economic value of hybrid

portfolios. For any system $s \in \{\text{hybrid}, \text{homo1}, \text{homo2}\}$, define

$$\begin{aligned}\text{AllCost}_s &:= C_s^{\text{invest}} + \left(R^{\text{benchmark}} - R_s\right) \\ &= R^{\text{benchmark}} - \Pi_s,\end{aligned}$$

where C_s^{invest} is the total investment cost of system s, R_s is the realized operating revenue of system s, and $R^{\text{benchmark}}$ is a benchmark revenue level representing the revenue that could be obtained under an idealized benchmark battery. For the benchmark revenue level $R^{\text{benchmark}}$, we assume that all generation is processed by a battery whose efficiency is fixed at the highest initial efficiency among the available battery types without experiencing efficiency degradation:

$$\begin{aligned}R^{\text{benchmark}} &:= c^e \int_0^T \left[p_L(t)d_L(t) + p_H(t)d_H(t)\right](x_0^{\max})^2 dt, \text{ for} \\ x_0^{\max} &:= \max\{x_1(0), x_2(0)\}.\end{aligned}$$

Hence, $R^{\text{benchmark}} - R_s$ is interpreted as the lost revenue due to not being able to convert the exogenous solar generation into delivered energy as efficiently as the benchmark battery. Using this definition, we measure the economic benefit of hybridization through the all-cost saving:

$$S^C := 1 - \frac{\text{AllCost}_{\text{hybrid}}}{\min(\text{AllCost}_{\text{homo1}}, \text{AllCost}_{\text{homo2}})} \geq 0.$$

We calibrate our model parameters, such as battery specifications (e.g., degradation costs) and workload profiles, using real-world datasets.

Battery Characteristics Data. Following [204], we use polynomial degradation functions to model battery degradation. We calibrate the per-unit capacity investment cost of battery, c_i^b based on market reports [111, 65]. The degradation coefficient, k_i, and the slope of capacity-efficiency degradation, $\alpha_{1,i}$, are calibrated based on lab experiments such as accelerated degradation tests, and we set $\alpha_{0,i} = 0$, in line with the literature [52, 32, 129, 127]. Most importantly, considering the combination of battery chemistry and manufacturer summarized in Table 4.1, we use a range of $\beta_i \in [1, 3.5]$ for all $i \in \{1, 2\}$.

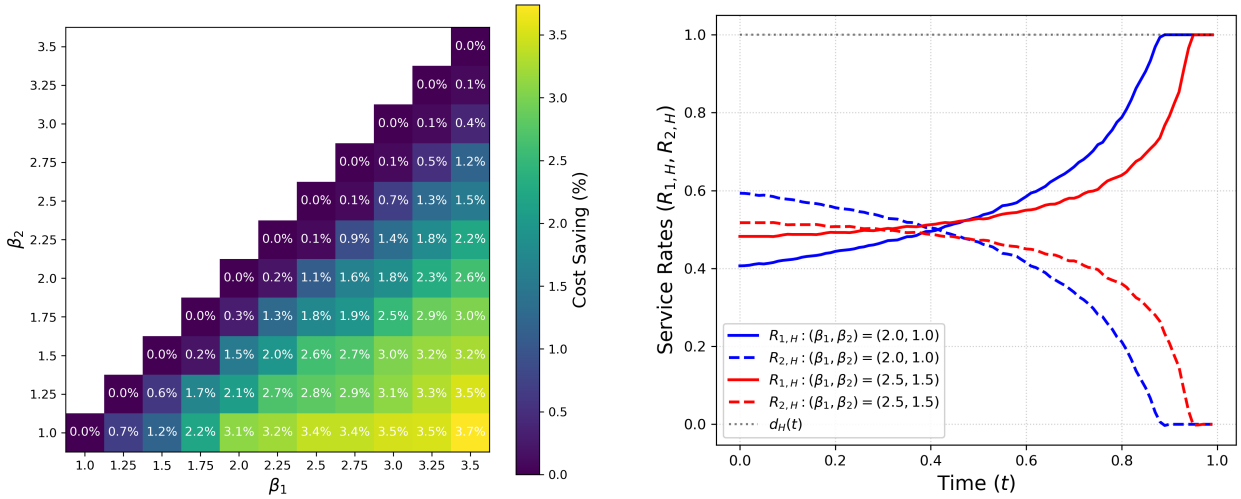
CAISO Dataset. To derive a realistic workload profile, we use data from the California Independent System Operator (CAISO). Specifically, we use net demand data (defined as system load minus renewable generation) as well as solar generation data, both reported at 5-minute intervals [26]. We use these data to calibrate the stationary stochastic workload profile, which we describe in detail later.

Reference	β	Battery type	Manufacturer
[157]	2.3	LiFePO4 (16000mAh)	Power Tech Systems
[157]	1.9	LiFePO4	Power Tech Systems
[24]	2.1	Li-ion	Saft Batteries
[156]	2.0	Li-ion	Saft Batteries
[145]	1.5	LiFePO4 (ANR26650M1 cell)	A123 Systems
[85]	3.3	LiFePO4 (pouch cell)	A123 Systems
[214]	1.7	Li/MoS2	Not reported
[170]	1.1	Li-ion	U.S. Battery Mfg Co.
[142]	1.2	Lead-acid	U.S. Battery Mfg Co.
[76]	2.9	Li-ion	Not reported
[120]	2.8	Li-ion (NMC)	EIG Electrical Systems
[120]	3.2	Li-ion (NMC)	Not reported

Table 4.1: Degradation functions in the industry and literature

Below, we present the results.

1. Stationary Deterministic Workload



(a) Cost-saving measures (S^C)

(b) Optimal service allocation

Figure 4.2: Stationary deterministic workload: $d_H(t) = 1, p_H(t) = 1$ for all t.

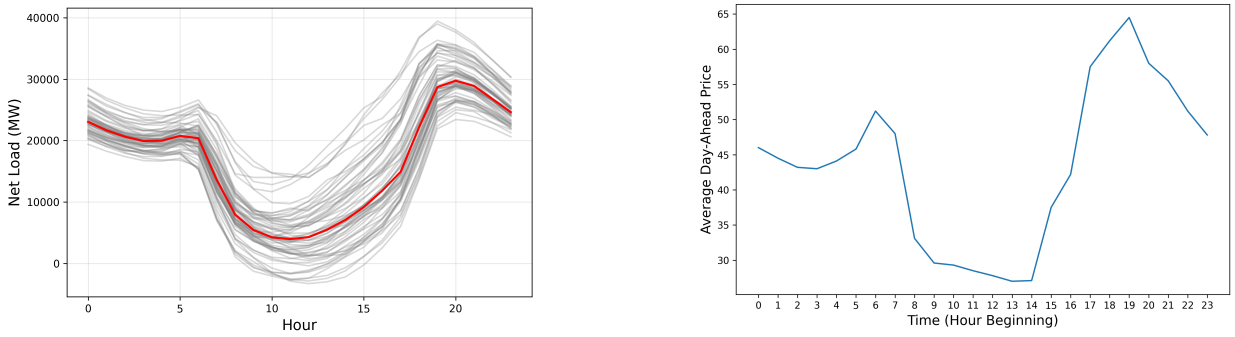
We first consider a stationary deterministic workload, i.e., $d_H(t) = 1$ and $p_H(t) = 1$ for all $t \in [0, T]$. The experimental setup selects parameters from the calibrated values in Section 4.3.3 such that each homogeneous battery system has the same costs (as measured by the AllCost metric) for the full workload. In this way, both homogeneous systems incur equal profits (and equal AllCost measures) when delivering the full workload.

Figure 4.2a illustrates the cost-saving measure, S^C, across various combinations of degradation exponents for the two batteries, (β_1, β_2), where $1 \leq \beta_2 \leq \beta_1 \leq 3.5$. We observe a consistent pattern: as the gap $\beta_1 - \beta_2$ increases, the cost savings also tend to increase. Thus, the largest improvement occurs at $(\beta_1, \beta_2) = (3.5, 1)$, yielding an 3.7% reduction in total cost.

Figure 4.2b illustrates the optimal dynamic service allocation under two exponent combinations: $(\beta_1, \beta_2) = (2, 1)$ and $(\beta_1, \beta_2) = (2.5, 1.5)$. The case $(\beta_1, \beta_2) = (2, 1)$ exhibits an increasing service rate for the battery with quadratic degradation. A similar pattern arises in other combinations, such as $(\beta_1, \beta_2) = (2.5, 1.5)$, where the battery with the higher exponent β has an increasing service rate, while the battery with the lower exponent β shows a decreasing service rate, indicating that batteries with different degradation functions have different service allocations through time. Later, we formally establish the protection effect (in Theorem 4.1) and explain why such dynamics arise. Overall, cost improvements under a stationary deterministic workload profile are below 4%. In the following section, we show that the impact of the protection effect can be substantially larger under alternative workload profiles.

2. Stationary Stochastic Workload

Next, we consider a stationary stochastic workload profile, where the exact magnitude of the required service rate is uncertain, capturing the inherent day-to-day variability in grid operations.



(a) (b)

Figure 4.3: Illustration of the CAISO duck curve: (a) net load and (b) average hourly price [27].

This setting is empirically motivated by historical *net load* data (system demand minus renewable generation) in regions with high solar penetration, such as California. In these regions, the grid exhibits systematic oversupply during peak solar hours, a pattern commonly

referred to as the "duck curve." Substantial midday solar generation lowers net load, and during these hours wholesale electricity prices collapse (see Figure 4.3b, where prices between 9 a.m. and 2 p.m. are lowest).

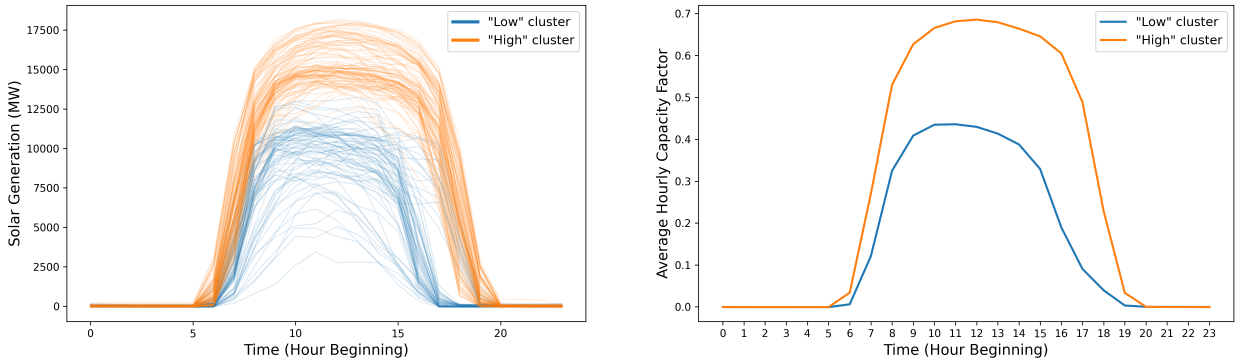
As discussed in Section 4.2.1, under solar-plus-storage PPAs, utilities often use batteries to shift energy to higher-value periods. In particular, batteries are charged during periods of high solar generation and discharged later during periods of higher net load and prices, with charging typically restricted to the co-located renewable generator [140, 211, 50, 14]. In this setting, daily variations in renewable output—driven by stochastic weather patterns—introduce variability into the battery workload.

Consequently, we model a stochastic workload. To simplify the experimental setting, we focus on a stationary stochastic workload in which $d_L(t) = d_L, d_H(t) = d_H, p_L(t) = p_L$, and $p_H(t) = p_H$ for some constants d_L, d_H, p_L, and p_H.

Calibration. We employ historical CAISO solar generation data to identify clusters of "High" and "Low" solar-output days and to calibrate the corresponding probability distribution. Using the k-means clustering algorithm, we first cluster days into "High" and "Low" days based on aggregate daily solar generation. Figure 4.4a illustrates daily solar generation by cluster.

Next, we identify representative "High" and "Low" charge requirements. We calibrate these requirements by measuring how much battery capacity is typically charged during the periods of lowest energy prices (due to peak solar generation). To do so, we compute hourly solar capacity factors, defined as the ratio of actual energy produced to nameplate solar capacity. As the end of 2024, CAISO's installed solar nameplate capacity was approximately 22,500 MW [30]. Using cluster-specific hourly solar generation data (Figure 4.4a), we derive cluster-wise average hourly capacity factors, which are summarized in Figure 4.4b.

Summing capacity factors over the daily period with the lowest energy prices (e.g., 9 a.m.–3 p.m.), translates into the amount of solar energy that might be charged under a typical solar-plus-storage PPA, expressed relative to nameplate solar capacity. Over the 9 a.m.–3 p.m. window, the summed capacity factors are 3.6 for the average high-generation cluster and 2.3 for the average low-generation cluster. A typical solar-plus-storage project has a storage capacity equal to four times the nameplate solar capacity. Examples include largest solar-plus-storage projects such as Blythe/McCoy/Arlington (812 MW solar, 3,248 MWh storage), Edwards & Sanborn (821 MW solar, 3,280 MWh storage), Nova Power (680 MW solar, 2,720 MWh storage), and Bisha (500 MW solar, 2000 MWh storage) [172]. Under a typical storage capacity, all energy produced between 9 a.m. and 3 p.m. can be stored along the average trajectory for either cluster, confirming that real-world examples of solar-plus-storage PPAs match our modeling setup where batteries must be sized to store all produced

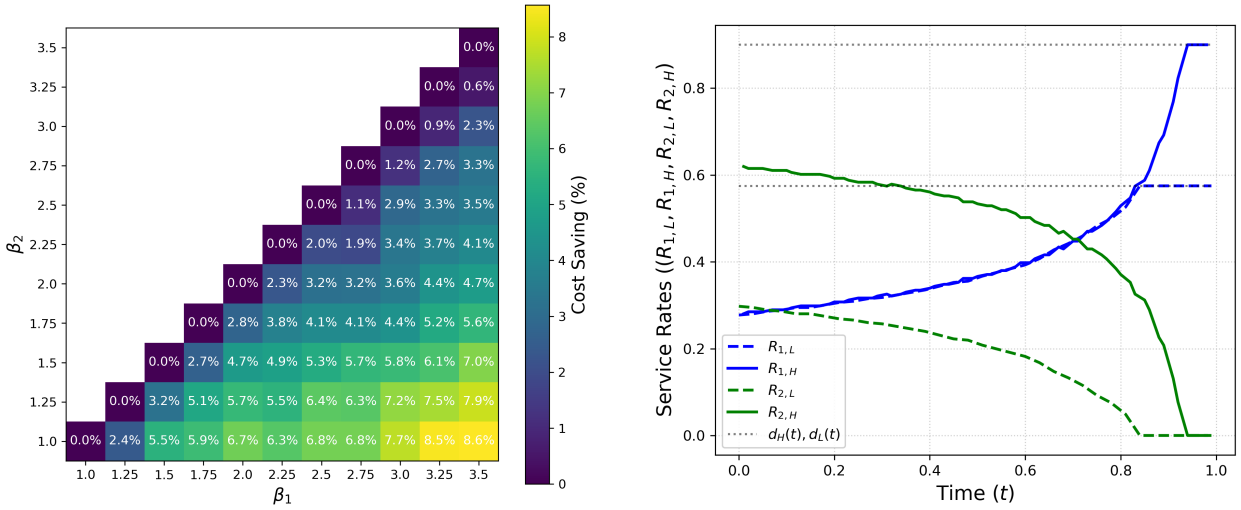


(a) (b)

Figure 4.4: Illustration of "High" and "Low" days: (a) daily solar generation and (b) average hourly capacity factors.

solar energy, even on sunny days.

Charging between 9 a.m. and 3 p.m. implies workload requirements (expressed as a fraction of a typical battery nameplate capacity) of $d_L = 0.575$ and $d_H = 0.9$, with corresponding probabilities $p_L = 0.37$ and $p_H = 0.63$. Consistent with the stationary deterministic workload setting, the experimental setup selects parameters from the calibrated values such that both homogeneous battery systems have equal profits (and equal AllCost measures).



(a) Cost-saving measures (b) Optimal service allocation ($\beta_1 = 2, \beta_2 = 1$)

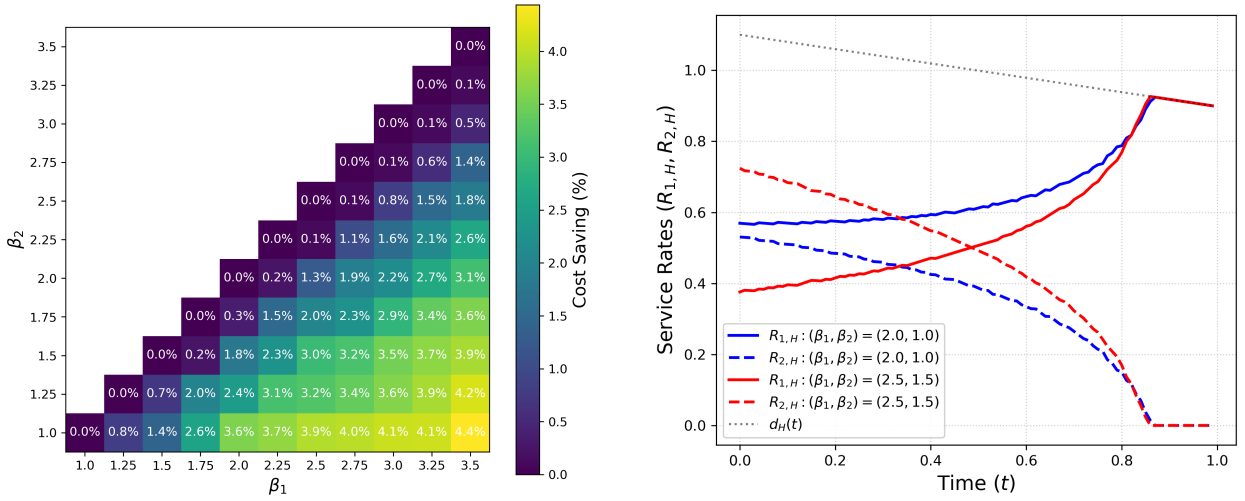
Figure 4.5: Stationary stochastic workload.

Figure 4.5a illustrates the cost savings across various degradation exponents under the stationary stochastic workload profile. The cost savings can be substantially larger than in

the deterministic-workload case, with typical reductions ranging from 3–9%. Figure 4.5b illustrates the optimal dynamic service allocation for $(\beta_1, \beta_2) = (2, 1)$. We observe a pattern consistent with the constant workload case (Figure 4.2b): the battery with the higher exponent ("more convex" battery) exhibits an increasing service rate (regardless of whether the workload is high or low), whereas the battery with the lower exponent ("less convex" battery) exhibits a decreasing service rate. Moreover, the "more convex" battery is utilized at similar levels under both high- and low-workload profiles. These structural patterns are driven by the protection effect, which we explain in Section 4.4. Finally, unlike in the peaker effect, the battery serving the base workload ($d_L(t)$ in this setting) may be either more or less efficient, as we formalize later in Observation 4.1.

3. Non-Stationary Deterministic Workload

Finally, we consider non-stationary deterministic workloads. Specifically, we examine profiles that exhibit monotonic decreasing trends over the operating horizon. This scenario captures settings where the available energy for storage declines over time. In solar-plus-storage systems, the charging obligation is exogenously determined by solar generation. Since solar PV panels experience annual degradation of approximately 0.5–1%, the amount of energy available for storage naturally declines. Over a typical 10–20 year operating horizon (or PPA contract duration), this implies an approximately 10–20% decline in generation. We capture such workload profiles using $d_H(t) = 1.1 - 0.2t$ and $p_H(t) = 1$ for all $t \in [0, 1]$.



(a) Cost-saving measures

(b) Optimal service allocation

Figure 4.6: Non-stationary deterministic workload: $d_H(t) = 1.1 - 0.2t$.

Figure 4.6a shows the cost savings under the decreasing workload profile. Note that the decreasing workload profile yields higher cost reductions than the stationary deterministic

case. With battery exponents ranging between 1 and 3.5, cost reductions reach up to 4.5% under the decreasing workload profile, slightly increased compared to under a stationary deterministic workload profile. The reason why the magnitude of benefits from a hybrid battery portfolio is greater under a decreasing workload profile will become clearer in the following section, where we formally state the protection effect and illustrate that more convex batteries prefer increasing workload profiles, while less convex batteries have similar costs regardless of the profile. Figure 4.6b illustrates the optimal dynamic service allocation under two exponent combinations, $(\beta_1, \beta_2) = (2, 1)$ and $(\beta_1, \beta_2) = (2.5, 1.5)$. The results again confirm the protection effect: the battery with the higher exponent β exhibits an increasing service rate.

4.4 The Protection Effect

Recall from the numerical experiments in Section 4.3.3 (see Figures 4.2b, 4.5b, and 4.6b) that optimal hybrid portfolios often allocate increasing workloads to the "more convex" battery, while completing the remaining work with the "less convex" battery. Further, in the stochastic setting (see Figure 4.5b) they allocate an even workload to the "more convex" battery and the rest to the "less convex" battery. We jointly refer to this behavior as the protection effect, where the "more convex" battery is assigned a workload that minimizes its degradation, and the remaining work is handled by the "less convex" battery, which is more flexible with respect to its workload pattern. We first explain the increasing-over-time aspect using a deterministic model (Section 4.4.1) and then explain the even-cycle-size aspect with an example (Section 4.4.2) and with a stylized model (Section 4.4.3).

4.4.1 Deterministic Setting: Characterizing Preferred Workload Trajectories

In this section, we formally establish the existence of the protection effect and explain how it increases revenues. To do so, it is useful to understand how a battery operator would optimally distribute its workload across time if it sought to maximize energy revenues but only had W total workload to allocate. Specifically, we will show that, depending on the shape of the degradation function, a battery may prefer different service-rate profiles over the horizon $[0, T]$, which we refer to as "preferred trajectories" of battery usage to maximize energy revenues (or minimize energy losses from degradation).

Consider a deterministic energy revenue maximization problem for a single battery with initial capacity C, which cannot perform more than total workload W (in kWh) over the

horizon $[0, T]$. Since the problem is deterministic, for notational simplicity, we denote the selected service rate at time t by $R(t)$. In this setting, the battery does not need to follow any exogenous service profile, as long as the workload limit is respected:

$$\int_0^T R(t)dt \leq W.$$

We optimize how to allocate work over time, i.e., choosing $R(t)$ for all $t \in [0, T]$, to maximize the total energy revenues. With the setup, we show that: (1) a battery with linear degradation is indifferent to how the service rate is allocated over time; and (2) a battery with strictly convex polynomial degradation favors an increasing service rate $R(t)$ over time.

To gain intuition about the operation of the system, we propose a simplified model that does not enforce a DOD constraint. Formally, the energy revenue maximization problem is given by:

$$\begin{aligned}
\max_{R(\cdot)} \quad & c^e \int_0^T R(t)(\alpha_0 + \lambda E(t))^2 \, dt \\
\text{s.t.} \quad & E(0) = C, \\
& \dot{E}(t) = -E(t)\Phi\left(\frac{R(t)(\alpha_0 + \lambda E(t))}{E(t)}\right), \quad \forall t \in [0, T], \\
& S(0) = 0, \\
& \dot{S}(t) = R(t), \quad \forall t \in [0, T], \\
& S(T) \leq W, \\
& R(t) \geq 0, \quad \forall t \in [0, T].
\end{aligned} \tag{4.10}$$

Here $S(t)$ tracks cumulative work done and $E(t)$ tracks remaining capacity. The terminal condition $S(T) \leq W$ implies that the battery cannot perform more than W total workload.

Theorem 4.1 (**Energy-Revenue-Maximizing Service Profile**). *For a homogeneous battery with maximum total workload W and initial capacity C that is sufficiently large to serve the total workload, the service-rate profile $R(t)$ that maximizes the energy revenue satisfies:*

- *Linear degradation ($\beta = 1$): Any $R(t)$ that performs W total work across the horizon will have the same total energy revenue.*
- *Strictly convex degradation ($\beta > 1$): The optimal trajectory $R(t)$ is increasing in time.*

Theorem 4.1 implies that a battery with linear degradation can play a complementary role in a hybrid portfolio, as its energy revenue is a function of the total work across the horizon but independent of the timing of that work. That is, the revenue remains the same for any usage profile $R(t)$ satisfying $\int_0^T R(t)dt = W$. This flexibility allows it to support batteries

with other degradation functions, which may favor a strictly increasing service rate over $[0, T]$ due to the curvature of their degradation function, thereby enabling a more efficient overall operation. Recall from Figure 4.2b under the stationary deterministic workload that the "more convex" battery follows an increasing service pattern, while the "less convex" battery provides the remaining workload. This occurs because the more convex battery chooses a configuration that maximizes its own revenue, and assigning the remaining work to the less convex battery does not significantly decrease its revenue (or incurs zero revenue loss in the case of linear degradation).

This illustrates the protection effect: the linear battery allows the convex battery to follow its preferred revenue-maximizing profile, thereby increasing overall portfolio profits. Importantly, the effect does not arise simply because a cheaper battery protects a more expensive one; rather, it is driven by the shapes of the batteries' degradation functions.

4.4.2 Stochastic Setting: Even Workload Allocation under Unbalanced Workloads

Next, we explain why the magnitude of benefits from a hybrid battery portfolio is significantly greater under a stochastic workload than under a stationary deterministic workload. Consider two stationary workload profiles:

1. **Scenario 1: Deterministic profile.** The battery performs w work in each period.
2. **Scenario 2: Stochastic profile.** Each period has its workload drawn independently and identically at random from the set $\{0.5w, 1.5w\}$ with equal probability.

The total work over the horizon is approximately equal in both scenarios, $w \cdot T$. Consequently, for a battery with linear degradation, the cumulative degradation is similar between the two scenarios. However, for batteries with strictly convex degradation ($\beta > 1$), Scenario 2 induces greater cumulative degradation than Scenario 1. For example, under quadratic degradation, the degradation incurred by performing $0.5w$ work in one period and $1.5w$ work in the next is roughly 25% higher than the degradation incurred by performing w work in both periods ($0.5 \cdot 0.5^2 + 0.5 \cdot 1.5^2 = 1.25$), and under cubic degradation, it increases by roughly 75% ($0.5 \cdot 0.5^3 + 0.5 \cdot 1.5^3 = 1.75$).

Consider Scenario 2 when the linear and quadratic battery both have identical expected profit Π (or equivalently, $\text{AllCost}_{\text{homo1}} = \text{AllCost}_{\text{homo2}}$) when serving the stochastic workload across the full horizon. We might expect considerable improvements in the profit by dividing the workload between the two batteries. In particular, if we allocated $0.5w$ work to the quadratic battery each period and the remaining work to the linear battery, we expect the

linear battery to produce roughly $\Pi/2$ profit over the horizon (it is doing half of the full workload) but we might expect the quadratic battery to produce considerably more than $\Pi/2$ profit over the horizon (it now experiences considerably less degradation per unit of work performed). The optimal workload split between the more and less convex battery in Figure 4.5b indeed demonstrates a similar optimal workload distribution between the two batteries under a stochastic workload.

4.4.3 Static Analytical Model for Stochastic Setting

To formally illustrate why a hybrid battery portfolio provides more benefit under a stochastic workload than under a deterministic workload, we consider a stylized analytical model that enables us to study the benefits of stochastic workloads above and beyond the preferred workload trajectories across time discussed in Section 4.4.1. To do so, we propose a model with two key departures from the model in Section 4.3: (1) there is no efficiency degradation, so each battery's capacity is fixed at x_i across the horizon, and (2) the battery operator continuously purchases new batteries to offset the capacity lost due to capacity degradation, meaning battery capacity E_i equals the initial capacity C_i across the full horizon. Since the batteries' capacities and efficiencies do not change over time under these simplifying assumptions, optimal workload allocations $R_{i,L}$ and $R_{i,H}$ remain fixed across the horizon, considerably simplifying the analysis.

We consider two batteries with polynomial degradation—battery 1 has strictly convex degradation ($\beta_1 > 1$), while battery 2 has linear degradation ($\beta_2 = 1$). We face a stationary stochastic workload with d_j work for $j \in \{L, H\}$, with $d_H > d_L$. Let n_j for $j \in \{L, H\}$ denote the expected number of periods with each type of work across the horizon ($n_L + n_H = T$), with $n_L, n_H > 0$, meaning $p_L := \frac{n_L}{n_L+n_H}$ and $p_H := \frac{n_H}{n_L+n_H}$. The objective consists of three terms. The first is the **investment cost** for cell type $i \in \{1, 2\}$:

$$C_i^{\text{invest}} = c_i^b \cdot C_i.$$

Next is the **revenue** for cell type $i \in \{1, 2\}$:

$$\begin{aligned} R_i^{\text{energy}} &= c^e \sum_{j \in \{L,H\}} n_j \cdot R_{i,j} x_i^2 \\ &= \underbrace{c^e x_i^2}_{:= r_i^{energy}} \cdot \underbrace{\sum_{j \in \{L,H\}} n_j \cdot R_{i,j}}_{:= TotalWork_i}, \end{aligned}$$

where r_i^{energy} denotes the per-unit energy revenue for battery type i, given its round-trip

efficiency x_i^2 and the unit energy price c^e.

The third component is the **battery replacement degradation cost** for cell type $i \in \{1, 2\}$, where the battery lifetime is L_i full (100% DOD) cycles:

$$\begin{aligned} C_i^{\text{deg}} &= \frac{c_i^b \cdot C_i}{L_i} \cdot \sum_{j \in \{L,H\}} n_j \cdot (\frac{R_{i,j} x_i}{C_i})^{\beta_i} \\ &= \underbrace{\frac{c_i^b \cdot x_i^{\beta_i}}{L_i}}_{:= c_i^{deg}} \cdot C_i^{1-\beta_i} \cdot \sum_{j \in \{L,H\}} n_j \cdot (R_{i,j})^{\beta_i}. \end{aligned}$$

For each $j \in \{L, H\}$, the depth of discharge (DOD) of battery type i is given by $\frac{R_{i,j} x_i}{C_i}$. Factoring out efficiency and battery capacity, we define c_i^{deg} as the per-unit degradation coefficient for battery type i.

The full profit-maximizing optimization model can then be stated as:

$$\begin{aligned} \max_{C_i, R_{i,j}} \quad & \left(\sum_{i=1}^{2} r_i^{energy} \sum_{j \in \{L,H\}} n_j \cdot R_{i,j} \right) - \left(\sum_{i=1}^{2} c_i^b C_i \right) - \left(\sum_{i=1}^{2} c_i^{deg} C_i^{1-\beta_i} \sum_{j \in \{L,H\}} n_j (R_{i,j})^{\beta_i} \right) \\ \text{s.t.} \quad & \sum_{i=1}^{2} R_{i,j} = d_j, \quad \forall j \in \{L, H\}, \\ & R_{i,j}, C_i \geq 0, \quad \forall i \in \{1, 2\}, \ j \in \{L, H\}. \end{aligned} \tag{4.11}$$

To have a more parsimonious model, we do not impose DOD constraints. Modeling DOD constraints in this stylized setting is left for future work.

Lemma 4.1 (Unconstrained Capacity)**.** *Any optimal solution* $(R_{1,L}^*, R_{1,H}^*)$ *to* (4.11) *satisfies:*

$$R_{1,L}^* = \min\{d_L, R_{1,H}^*\}.$$

We now establish structural properties for the case where the two homogeneous batteries yield the same profit.

Theorem 4.2. *If the optimal solutions to* (4.11) *for the two homogeneous batteries yield the*

same profit ($\Pi^*_{homo1} = \Pi^*_{homo2}$)*, then*

$$
\begin{aligned}
R^*_{1,L} =& d_L < R^*_{1,H} < d_H, \quad \textit{for} \\
R^*_{1,H} =& \left[\frac{n_L d_L^{\beta_1}}{\left(\frac{n_L d_L + n_H d_H}{(n_L d_L^{\beta_1} + n_H d_H^{\beta_1})^{1/\beta_1}}\right)^{\frac{\beta_1}{\beta_1 - 1}} - n_H} \right]^{1/\beta_1}, \ \textit{and} \\
AllCost_{hybrid} =& \frac{\beta_1}{\beta_1 - 1} c_1^b \left[\frac{(\beta_1 - 1) c_1^{deg} [n_L d_L^{\beta_1} + n_H (R^*_{1,H})^{\beta_1}]}{c_1^b} \right]^{1/\beta_1} \\
& + c_2^{deg} n_H (d_H - R^*_{1,H}) \\
& + c^e \Big[\max(x_1, x_2)^2 (n_L d_L + n_H d_H) - x_1^2 [n_L d_L + n_H R^*_{1,H}] \\
& - x_2^2 [n_H (d_H - R^*_{1,H})] \Big].
\end{aligned}
$$

Theorem 4.2 implies that whenever $\Pi_{\text{homo1}} = \Pi_{\text{homo2}}$, the more convex battery (i.e., battery type 1) serves all work in the low-demand periods, regardless of whether it is more or less efficient than the linear battery. Below, we will show that the protection effect can boost profits regardless of whether the more convex battery is more or less efficient (Corollary 4.2).

Motivated by our numerical evidence from Section 4.3 of particularly large benefits of heterogeneous portfolios as β_1 grows large, we now consider a special case where $\beta_1 \to \infty$, which allows us to derive clean managerial insights.

Corollary 4.1 (Even Work Allocation: $\beta_1 \to \infty$)**.** *As $\beta_1 \to \infty$, the optimal solution $(R^*_{1,L}, R^*_{1,H})$ from Theorem 4.2 satisfies $R^*_{1,H} \to R^*_{1,L} = d_L$.*

This corollary implies that as battery type 1 has an increasingly convex degradation function, the optimal policy evens out workloads for that battery across different workload scenarios, allocating similar (and eventually identical) usage levels in both low- and high-workload periods. This structural property aligns with the policy explored in Section 4.4.2 and the numerical evidence in Figure 4.5b.

Next, we compute the all-cost saving measure as $\beta_1 \to \infty$. In this limit, $R^*_{1,H} = R^*_{1,L} = d_L$, and the capacity of battery type 1 under the hybrid portfolio, C^*_1, becomes:

$$
\lim_{\beta_1 \to \infty} C^*_1 = \lim_{\beta_1 \to \infty} d_L \cdot \left[\frac{(\beta_1 - 1) c_1^{deg} (n_L + n_H)}{c_1^b} \right]^{1/\beta_1} = d_L.
$$

Corollary 4.2 (All-Cost Saving: $\beta_1 \to \infty$)**.** *If the optimal solutions to* (4.11) *for the two homogeneous batteries yield the same profit* ($\Pi^*_{homo1} = \Pi^*_{homo2}$)*, then as $\beta_1 \to \infty$, S^C converges*

to:

$$S^C \to \bar{S}^C := \begin{cases} \frac{n_L d_L (d_H - d_L)}{d_H (n_L d_L + n_H d_H)}, & x_1 \geq x_2, \\ \frac{n_L d_L (d_H - d_L)}{d_H (n_L d_L + n_H d_H)} \left(1 - \frac{c^e (x_2^2 - x_1^2)}{c_2^{deg}}\right), & x_1 \leq x_2. \end{cases}$$

Corollary 4.2 implies that the benefit of a hybrid portfolio increases when the more convex battery is more efficient and the less convex battery is less efficient. Intuitively, the protection effect is strongest when the battery assigned to base (or low) workloads can operate efficiently, while the battery assigned to high workloads is relatively inefficient. This is consistent with the traditional peaker effect; however, our results show that the more convex battery need not be more efficient—it can be either more or less efficient than the less convex battery. Further, note that

$$\frac{n_L d_L (d_H - d_L)}{d_H (n_L d_L + n_H d_H)} = \underbrace{\frac{n_L d_L}{n_L d_L + n_H d_H}}_{\text{low-work share}} \cdot \underbrace{(1 - \frac{d_L}{d_H})}_{\text{workload gap}}.$$

As in the peaker effect, the potential benefit of the protection effect is greatest when there are rare but very large spikes in workload ($n_H \ll n_L$ and $d_H \gg d_L$), simultaneously yielding a large "low-work share" and a large "workload gap."

Observation 4.1. *Unlike in the peaker effect, where the baseload is served by the more efficient resource, in our setting the battery assigned to the baseload may be either more or less efficient. Instead, the allocation is driven by the convexity of the degradation function (Theorem 4.2). The protection effect can boost profits regardless of whether the battery serving the baseload is more or less efficient (Corollary 4.2).*

This is also consistent with the service allocation patterns observed in Figure 4.5b, where the low workload is primarily served by the more convex battery, regardless of whether it is more or less efficient. Also, Observation 4.1 does not rely on the equal-profit condition, which is only used for deriving the cost-saving measure in Corollary 4.2.

4.5 Future Directions and Concluding Remarks

In this work, we examine the economic viability of hybrid battery portfolios and identify an economic mechanism that we term the *protection effect*. Using stylized models, we show that while a battery with linear degradation is invariant to the temporal allocation of service, batteries with strictly convex degradation benefit from specific service trajectories,

typically favoring increasing workloads over time and evenly sized cycles. This asymmetry allows less convex batteries to protect more convex batteries by absorbing unfavorable service patterns—such as decreasing or uneven workloads—while jointly meeting exogenous workload requirements. As a result, more convex batteries can operate closer to their revenue-maximizing (or energy-loss-minimizing) trajectories by avoiding excessively degrading workloads. Unlike prior justifications for hybrid systems, which rely on budget constraints, differentiated physical capabilities, environmental effects, C-rate effects, or peak capacity, we show that cost savings can arise purely from intrinsic differences in degradation convexity across batteries. By formulating a joint optimization framework for investment and operational decisions, we demonstrate how one battery (e.g., with a lower degradation exponent) can effectively "protect" another by absorbing unfavorable workload patterns, thereby boosting total portfolio profitability.

Our analysis further reveals that the value of the protection effect is highly sensitive to the profile of the exogenous service requirement. Cost improvements are below 4% under a stationary deterministic workload, but can become larger under stochastic or non-stationary profiles. The "more convex" battery's service rate increases over time and evens out across different stochastic workload levels. To formally explain this, we use a stylized model to show that as the convexity parameter of the more convex battery approaches infinity, an even service allocation becomes optimal. We also analytically characterize the resulting benefits of a hybrid battery portfolio for a given demand profile.

Taken together, these findings offer actionable insights for battery operators and system planners. They suggest that strategically pairing heterogeneous assets—such as combining units with differing levels of degradation convexity—can provide a cost-effective means of managing specific load profiles in wholesale grid environments.

Several avenues remain for future research. First, our stylized models in Sections 4.4.1–4.4.3 can be extended to accommodate more general setups. For instance, DOD constraints can be incorporated into these models. While we do not include DOD constraints in these models to maintain parsimony, incorporating them would allow for a more realistic representation of battery operations. Section 4.4.3 can be also extended to consider a broader set of battery pairings, e.g. cases where both batteries have strictly convex degradation functions (i.e., $\beta_1, \beta_2 > 1$).

Second, our analysis of the potential magnitude of the protection effect—that is, how large cost savings can be under different operational and grid conditions—in Section 4.4.3 could be extended in several directions. For example, Corollary 4.2 could be generalized to incorporate general $\beta_1, \beta_2 > 1$. Consistent with the previous point, incorporating DOD constraints and allowing for general combinations of degradation convexity would further

refine our cost comparison analysis.

Third, the framework could be extended to incorporate a broader range of degradation functions. For example, investigating exponential degradation models—another widely adopted class in the literature alongside the polynomial models considered in this essay [204]—would help confirm if the protection effect remains robust across different mathematical representations of battery degradation.

APPENDIX A

Proofs in Chapter 2

A.1 Justifications of Key Assumptions

A.1.1 Degradation Cost

Almost all batteries (e.g., lithium-ion) suffer a degradation process, and thus, should be replaced after some amount of time/work. Considering that more than 90% of the newly installed large-scale batteries in 2024 are lithium-ion batteries and the fact that lithium-ion batteries are predicted to remain dominant for the near future ([54, 126]), this study provides general lessons on energy stacking with BESS.

A.1.1.1 Key Stress Factors

The process of degradation depends on numerous factors, which have been extensively studied in the engineering literature. The three critical factors are temperature, charging/discharging rate (C-rate), and depth-of-discharge (DOD) [123, 90, 204].

Two of these factors are highly interrelated and controllable: temperature and C-rate. The temperature at which the battery operates significantly impacts degradation and also influences batteries' safety [155]. Though C-rate has been well documented to also increase degradation, [107] and [181] report in cell-level experimental studies that C-rates showed only a minor impact on degradation when the cell temperature is well controlled, implying that C-rate indirectly accelerates degradation by increasing cell temperature due to Ohmic (resistive) heating. With the design of battery management systems (BMS) and the development of thermal/cooling systems (e.g., liquid-based coolants), the impact of temperature and therefore C-rates can be minimized, especially for stationary batteries that we consider in this work.[1] Given our domain of application (large-scale battery deployments, which typically deploy BMSs), we restrict our focus to DOD, which we describe next.

[1]Controlling temperature and the effect of C-rate is less straightforward for mobile batteries used in electric vehicles (EVs), though active cooling systems are also used in most EVs.

A.1.1.2 Degradation Function

Several engineering papers have experimentally tested the effect of DOD on degradation, most often by relating the expected number of cycles N_i that a battery can provide before it is completely degraded if operated at DOD level δ_i ($0 \leq \delta_i \leq 1$). This is called the Wöhler curve or the SN curve showing the relationship between the stress level (S) and the number of cycles (N); see [167] and [51] for two representative studies of this form. Though many functional forms for this relationship have been explored, the most commonly adopted form assumes

$$N_i = \left(\frac{1}{z\delta_i}\right)^{\beta}, \tag{A.1}$$

where $z > 0$ and $\beta > 1$ are constants that do not depend on the DOD. Rewriting (B.2), the cost of a single cycle of DOD δ_i can be characterized by the degradation cost function $\Phi(\delta_i) : [0, 1] \to \mathbb{R}$ ([205]):

$$\Phi(\delta_i) = \underbrace{c_{cell} \cdot E}_{battery\ price} \cdot \frac{1}{N_i} = c_{cell} \cdot E \cdot (z\delta_i)^{\beta}. \tag{A.2}$$

For notational simplicity, we define DOD level $u_i = \delta_i \cdot E$ as the actual energy charged/discharged in a cycle (MWh). Accordingly, we redefine the degradation cost function $\Phi(u_i) : [0, E] \to \mathbb{R}$:

$$\Phi(u_i) = c_{cell} \cdot E \cdot z^{\beta} \cdot (\frac{u_i}{E})^{\beta} \tag{A.3}$$

$$= \frac{c_{cell} \cdot E \cdot z^{\beta}}{E^{\beta}} \cdot u_i^{\beta} = \frac{c_0^b}{E^{\beta-1}} \cdot u_i^{\beta}, \tag{A.4}$$

where

- $c_0^b := c_{cell} \cdot z^{\beta}$ is the battery degradation coefficient and represents the cost of operating a battery with capacity $E = 1$ MWh for a single full cycle at DOD $u = 1$ MWh,
- z (unitless) is the longevity coefficient from the Wöhler curve,
- β (unitless) is the degradation growth exponent from the Wöhler curve,
- c_{cell} (\$/MWh) is the battery cell price per unit of energy capacity, and
- E (MWh) is the battery capacity.

Note that z and $\beta > 1$ are E-invariant properties of the battery that depend on the battery's

manufacturer and chemistry (e.g., lithium iron phosphate), and can be fitted based on lab experiments (e.g., accelerated degradation test).

In this essay, we assume $\beta = 2$ based on the evaluations of several empirical papers [156, 105, 108, 208, 204]. This particular degradation model is also called the quadratic model [204]. In practice, $\beta > 2$ and $1 < \beta < 2$ were also reported depending on the combination of a battery's chemistry and manufacturer; see Table A.1. In Appendix A.4, we numerically evaluate the sensitivity of our results to the quadratic degradation assumption used in the main analysis by comparing different exponents $\beta \in [1.5, 2.5]$.

Reference	β	Battery type	Manufacturer
[157]	2.3	LiFePO4 (16000mAh)	Power Tech Systems
[157]	1.9	LiFePO4	Power Tech Systems
[24]	2.1	Li-ion	Saft Batteries
[156]	2.0	Li-ion	Saft Batteries
[145]	1.5	LiFePO4 (ANR26650M1 cell)	A123 Systems
[214]	1.7	Li/MoS2	-

Table A.1: Degradation functions in the industry and literature

Another degradation model introduced in the literature is an exponential model as follows:

$$\Phi(u_i) = c_1^b u_i \exp(c_2^b u_i),$$

where $c_i^b, i = 1, 2$ again depend on a battery's characteristics [123, 204]. We performed numerical experiments with a class of exponential models. While the value of the degradation function influences the profits, the structural results hold unchanged.

Our model is intended to describe the mechanism behind simultaneous stacking and to show how stacking balances potentially increased utilization (and corresponding degradation costs) and revenues. There are several additional cost factors that we do not consider such as fixed costs for financing, personnel, land, electrical equipment (e.g., transformers, battery management system), and HVAC (heating, ventilation, and air conditioning) that are incurred every time period. [53] provides overall capital cost estimates including these factors.

A.1.1.3 Rainflow-Counting Algorithm

Definition A.1 shows the rainflow-counting algorithm [165, 205]:

Definition A.1. *Let $C = (c_1, c_2, ..., c_{|C|})$ denote the state of charge of the battery across time, with the c_i values capturing all local minima and maxima.*

Algorithm: Rainflow-counting algorithm

Input: *Battery SOC profile* C

Output: *A set of full cycles* $U = \{u_i\}$ *and half cycles* $\tilde{U} = \{\tilde{u}_i\}$

1 $U = \emptyset$

2 **while** $|C| \geq 4$ **do**

3 *Calculate* $\Delta c_1 = |c_1 - c_2|, \cdots, \Delta c_i = |c_i - c_{i+1}|, \cdots, \Delta c_{|C|-1} = |c_{|C|-1} - c_{|C|}|$.

4 **if** there exists some $2 \leq i \leq |C| - 2$ such that $\Delta c_{i-1} \geq \Delta c_i$ and $\Delta c_{i+1} \geq \Delta c_i$ **then**

5 $C := (c_1, \cdots, c_{i-1}, c_{i+2}, \cdots, c_{|C|})$, *and* $U := U \cup \{\Delta c_i\}$.

6 **else**

7 *Go to line 8*

8 $\tilde{U} = \{|c_1 - c_2|, \cdots, |c_{|C|-1} - c_{|C|}|\}$.

The battery degradation cost of C *is defined as* $\frac{c_0^b}{E} \sum_{u_i \in U} u_i^2 + \frac{c_0^b}{2E} \sum_{\tilde{u}_i \in \tilde{U}} \tilde{u}_i^2$ *based on eq.* (2.1) *with* $\beta = 2$.

A.1.2 Energy Neutrality of Regulation Signals

Many ISO/RTOs have introduced an energy-neutrality commitment for their regulation signals. However, the level of guarantee may differ across types of signals and across ISOs. For example, PJM initially introduced strict energy neutrality for the regD signal within 15 minutes. Since, at times, this strict-neutrality of the regD signal dispatched a measurable amount of energy in an undesirable direction, PJM switched to conditional energy neutrality within 30 minutes in 2017.[2] Also, different ISOs use different signals for regulation: ISO-NE uses continuous and trinary signals, while PJM uses its regD and regA signals. More than 80% of PJM's regD and ISO-NE's continuous signals restored their initial SOC within 30 minutes, whereas it takes on average more than an hour for ISO-NE's energy-neutral trinary signal to restore a battery's initial SOC 80% of the time. In our work, we adjust our definition of time periods T_L, T_H, and T to model different levels of energy-neutrality of regulation signals. Appendix A.4.1 illustrates regulation signals and the corresponding net energy change.

[2]Prior to 2017, [148] biased the regA signal to overcorrect the regD signal to achieve energy neutrality. Since 2017, however, regA and regD signals work together so that energy neutrality is only supported for regD resources when there are available regA resources with extra capacity (conditional energy neutrality).

A.1.3 Market Clearing Mechanics and Market Structure

In this work, we consider day-ahead (forward) energy and regulation markets. In this section, we provide details on bidding and commitment decisions.

A.1.3.1 Scheduling/Bidding/Market Clearing Process

In most ISO/RTOs in the US, energy markets consist of two markets: (1) a day-ahead market and (2) a real-time market. Frequency regulation is procured by the ISO/RTO through an ancillary services market, which consists of either two markets (e.g., NYISO) or a single real-time market (e.g., PJM). Below we briefly explain bidding and market clearing processes and discuss commitment/settlement rules based on PJM's Manual 11 (Energy & Ancillary Services Market Operations), Manual 12 (Balancing Operations), and Manual 28 (Operating Agreement Accounting), but other ISO/RTOs share very similar processes ([151, 152, 153, 134, 136]).

Battery participation models: ISO/RTOs match supply with demand by choosing the least expensive resource available (aka "economic dispatch"). ISO/RTOs do this by allowing market participants (e.g., batteries) to either (1) self-schedule (aka, batteries bid/commit service quantities and accept any cleared market prices; also called the "must-run" mode), or (2) bid a curve (aka, pooled-scheduled or ISO-scheduled mode), specifying a list of price ($/MW or $/MWh) and quantity (MW or MWh) pairs over multiple segments (e.g., 10 segments in CAISO/PJM).[3]

(1) In the day-ahead market (forward market), service prices are cleared on an hourly basis. Bidding and market clearing processes happen a day before the operating day, and ISOs post the market clearing results. The resources cleared in the market commit to following the day-ahead schedule and have no ability to react to uncertainty, except for additionally participating in real-time markets to respond to real-time price spikes and/or purposely deviating from the schedule/signal requested by the grid and incurring the associate penalties, e.g., [36].

(2) The real-time (energy and ancillary) market is a spot market where prices are cleared every 5 minutes. Bidding for the real-time market starts after the day-ahead results are posted, and bids can be updated up to an hour prior to the operating hour (65 minutes prior in PJM, 75 minutes prior in NYISO).

For regulation, resource owners must provide hourly capability (above and below regulation basepoint, MW). The battery is paid for each unit of committed capacity for each hour (regulation capability credit) and receives an additional credit (regulation performance

[3]FERC 841 ensures that a battery can bid curves as both a seller and a buyer.

credit) based on the actual amount of work. Oftentimes, the mileage (measured as the sum of the total amount of charging and the total amount of discharging requested for a given time period) or their derivatives are used to measure the amount of work requested of a resource following the regulation signal.

A resource-specific performance score is then calculated based on how accurately the battery followed the signal. For instance, PJM calculates a resource's performance score by combining accuracy (the correlation between the signal and the unit's response), delay, and precision (instantaneous error between the signal and the unit's response). This performance score works as a multiplier to determine the unit's performance credit. Batteries generally perform well; e.g., in 2022, 77% of batteries (which follow the regD signal) had average performance scores within the 0.91 – 1.00 range, compared with 25% of slower-responding regA resources ([125]).

A.1.3.2 Market-Related Assumptions in the Essay

In this work, we consider day-ahead markets and do not consider real-time markets. This assumption is largely motivated by a desire to retain a parsimonious model for a battery operator, coupled with the fact that the literature provides mixed messages about the importance of real-time arbitrage for a battery's overall profitability (e.g., [106, 118]).

Though we opt to defer focus on stacking in the real-time energy market to future work, we note that preliminary numerical experiments (results not shown) suggest that the key lessons continue to hold (i.e., the inclusion of the real-time markets does not lead to different lessons from what we establish with day-ahead markets), and the benefits of stacking versus standalone services can actually be expanded in this setting compared to what we report in this work with the day-ahead market alone. For instance, we can obtain higher S ratios, which means that simultaneous stacking may become more attractive relative to standalone services when the battery can participate in both day-ahead and real-time energy markets. This is because, under recent grid/market conditions, regulation is significantly more profitable for batteries than arbitrage, and including real-time arbitrage improves the profitability of stacking (which provides both services) versus its strongest competitor (regulation-only).

In both energy and regulation markets, we assume that the battery is self-scheduling (the battery bids/commits service quantities and accepts any cleared market prices) based on empirical evidence. According to [125], 96.5% (98.7%) of all regulation MW clearing PJM's regD regulation market had an effective price of \$0.00 in 2022 (2021) from MWs with zero offers plus self-scheduled MWs. Similarly, ISO-NE's 2023 regulation offer dataset ([83]) showed that almost all batteries make zero-price offers, which again confirms that they are

effectively self-scheduling.[4]

A.1.4 Additional Literature Review

A.1.4.1 Inventory Theory versus Economics of Batteries

Storage of energy in batteries brings parallels to inventory management, as buying batteries could be treated as capacity management and storing energy as inventory management. The conventional inventory problem focuses on physical storage and typically considers three types of costs: a purchase cost, a holding cost, and a shortage/penalty cost [168]. This framework has been extended in multiple dimensions including stochastic settings (e.g., [96]), interdependent multi-echelon systems (e.g., [40]), and capacitated settings (e.g., [95]).

In the operations management (OM) literature, one of the key elements related to storage is the tradeoffs between the cost of holding inventory and the cost of ordering frequency or running out of inventory. In battery settings, holding costs are almost negligible.[5] Instead, batteries lose some fraction of energy during charging/discharging, which incurs an additional cost to compensate for the loss (energy replenishment cost). Loss of energy bears a resemblance to yield models in OM such as [209]. However, yield models generally apply to a production process, not to a storage process, and the results cannot be translated to losses connected with the injection and discharge of energy.

Furthermore, the most significant cost driver for batteries is degradation (batteries become practically useless after some volume of "use"), which is a key element of our model. Degradation is, however, somewhat complicated. It is based on netted flows in opposite directions and has a nonlinear relationship with the amount a battery is charged or discharged,[6] which is challenging to capture in an inventory model. While convex holding cost can be incorporated into inventory models, it does not seem possible to apply these techniques to the change of inventory level (which is analogous to the battery charge/discharge amount). Clearly multiple of these path-dependent complexities in the cost function are not present in the inventory literature, yet they are central to the profitability of battery operations. The only OM papers that bear some partial methodological or structural similarity are the ones explicitly analyzing energy markets with storage such as [169].

[4]Regulation prices are mainly determined by other resources such as natural power plants. [125] reported that 67.1% of regulation was settled by natural gas and hydro resources, while 24.6% was settled by batteries. These empirical evidences show that battery operators in day-ahead markets bid based on expected values (historical prices).

[5]The concept corresponding to holding cost would be batteries' *self-discharge* or *leakage*, a phenomenon in which the stored energy is reduced without any connection to external circuits. Lithium-ion batteries are known to lose 2–7% of their stored energy per month [87, 128].

[6]Interestingly, as we describe in Section 2.3.2, some literature in the engineering area focuses on evaluation and estimation of these nonlinearities.

Uncertainty plays a key role in classical inventory models such as the newsvendor model. In the newsvendor model, uncertainty in the demand realization incurs the key costs of the model through overage and underage costs, and the optimal order level is selected to balance these two costs. The ordering decision interacts critically with the demand uncertainty, because if we over-order then we must salvage the extra items (or incur holding costs in multi-period models), while if we under-order then we cannot meet all our demand. Our optimal objective value is critically linked to the amount of uncertainty we have – we will have much higher expected cost with additional uncertainty in the demand.

In our battery stacking application there are two main sources of uncertainty: 1) uncertainty around the specific realization of the regulation signal that we will face, and 2) uncertainty around the prices for the arbitrage and regulation service that we will receive as price-takers in the day-ahead market. The first source of uncertainty (regulation signal uncertainty) is much less critical than demand uncertainty in a typical inventory model. Under demand uncertainty, we may under-order and not be able to meet the actual demand, incurring large costs due to unfulfilled demand. While penalties for not following the regulation signal also exist for the frequency regulation service, it is quite uncommon for a battery to be unable to provide the requested regulation due to the energy neutrality of the regulation signal. We can see evidence of this in the near-perfect performance scores that batteries obtain when providing the regulation service (see Appendix A.1.3.1 for details). Since batteries are generally able to follow the regulation signal closely regardless of the signal realization, the key impact of regulation signal uncertainty would be to add some day-to-day variability in the degradation of a battery, an effect that would balance out over time (days with higher-than-expected degradation balance days with lower-than-expected degradation). A similar story exists for our second source of uncertainty (price uncertainty). While our decision-maker is a price-taker in the day-ahead market and faces uncertainty in the daily price of arbitrage and regulation, these uncertainties are expected to balance out over time (days with higher-than-expected prices balance days with lower-than-expected prices). Unlike a newsvendor model where the expected cost objective function grows as demand uncertainty grows, we would not necessarily expect our expected profit to differ under low-uncertainty versus high-uncertainty scenarios for our prices and regulation signal realizations.

In short, standard inventory models do not capture critical aspects of battery systems. In this work, we capture the key aspects of batteries in our modeling (see Section 2.3.2 and Appendix A.1.1), and they drive many of our findings in this work.

A.2 Proofs of Statements (Main)

Proof of Proposition 2.1

Let $\underline{c}$ be the minimum SOC experienced by the battery while providing regulation. By energy neutrality, each incidence of SOC $\underline{c}$ will be followed by another incidence of SOC $\underline{c}$ within two time units. Consider a sequence c_i of the local minima and maxima of the battery SOC, for $i = 1, ..., K$. Consequently, the sign of $(c_{i+1} - c_i)$ alternates and $c_1 = c_K = \underline{c}$. Let the u_i's be the sizes of cycles identified by the rainflow-counting algorithm. It is easy to argue that $\sum_{i=1}^{K-1} |c_i - c_{i+1}| = 2 \sum_i u_i$.[7]

If we are providing r units of frequency regulation, energy neutrality in two periods implies that the maximum SOC $\bar{c}$ satisfies $\bar{c} \leq \underline{c} + r$, and therefore that all cycles returned by the rainflow-counting algorithm cannot exceed size r. This bound on the cycle size in turn yields a bound on the total degradation cost, as the total absolute SOC change cannot exceed Tr when providing r units of regulation for T time periods:

$$\begin{aligned} Deg &= \frac{c_0^b}{E} \sum_i u_i^2 \leq \frac{c_0^b}{E} r \sum_i u_i = \frac{c_0^b r}{2E} \left(\sum_{i=1}^{K-1} |c_i - c_{i+1}| \right) \\ &\leq \frac{c_0^b r^2 T}{2E}. \end{aligned}$$

The signal alternating +1 and -1 every one time unit yields $T/2$ cycles of size r, meaning it achieves the maximum possible degradation cost of $\frac{c_0^b r^2 T}{2E}$. □

Proof of Proposition 2.2 (Cost-saving)

Proposition 2.2 follows trivially from degradation function (2.4). □

Proof of Lemma 2.1 (Equal excess regulation)

Assume that A is chosen. At optimum we clearly have $r_L \geq a_L$ and $r_H \geq a_H$, so maximizing (2.5) is equivalent to maximizing

$$(p^a + 2p^r)A + p^r x_L T_L + p^r x_H T_H - \frac{c_0^b}{E}[A^2 + 2A \cdot \max(x_L, x_H) + \frac{T_L}{2} x_L^2 + \frac{T_H}{2} x_H^2].$$

[7] While Definition A.1 allows for half cycles and full cycles to be returned by the rainflow-counting algorithm, for simplicity, we assume here that only full cycles are returned. The argument can trivially be extended to the case with both full and half cycles.

At the optimal point, if x_L and x_H are not identical, (due to the symmetry of the expression) let $x_L < x_H$. Then $\partial\Pi/\partial x_L = T_L(p^r - \frac{c_0^b}{E}x_L) = 0$ and $\partial\Pi/\partial x_H = T_H(p^r - \frac{c_0^b}{E}(\frac{2A}{T_H} + x_H)) = 0$. This immediately implies a contradiction, $x_L \geq x_H$. Thus, at optimality we must have $x = x_L = x_H$.

Expressing (2.5) with x gives

$$(p^a + 2p^r)A + p^r xT - \frac{c_0^b}{E}[A^2 + 2Ax + \frac{T}{2}x^2],$$

and the first-order condition becomes $x = \frac{p^r E}{c_0^b} - \frac{2A}{T}$. Since x must be non-negative at the optimal point, we conclude that $x_L^* = x_H^* = (\frac{p^r E}{c_0^b} - \frac{2A}{T})^+$. □

Proof of Theorem 2.1 (Optimal stacking)

From Lemma 2.1, we have expressed optimal excess regulation x^* as a function of arbitrage quantity A, yielding profit function

$$\Pi(A) = \begin{cases} p^a A + \frac{(p^r)^2 TE}{2c_0^b} - \frac{c_0^b(T-2)}{TE}A^2, & \text{if } A < \frac{Tp^r E}{2c_0^b}, \text{ and} \\ (p^a + 2p^r)A - \frac{c_0^b}{E}A^2, & \text{otherwise.} \end{cases}$$

When $T > 2$, $\partial\Pi/\partial A$ is continuous, piecewise linear, and decreasing, with a single change of slope when $A = \frac{Tp^r E}{2c_0^b}$.

We first optimize A_{FOC}^*, the optimal arbitrage when ignoring the energy constraint. If $A < \frac{p^r TE}{2c_0^b}$, then $\partial\Pi/\partial A = p^a - \frac{2c_0^b(T-2)A}{TE}$. We conclude that the profit will be maximized at some $A < \frac{p^r TE}{2c_0^b}$ if and only if $p^a < (T-2)p^r$, in which case $A_{FOC}^* = \frac{p^a TE}{2c_0^b(T-2)}$. Otherwise, $\frac{\partial\Pi}{\partial A} = p^a + 2p^r - 2\frac{c_0^b}{E}A$, so $A_{FOC}^* = \frac{(p^a+2p^r)E}{2c_0^b}$. Since $\frac{\partial\Pi}{\partial A}$ is decreasing, we conclude that $A^* = \min(A_{FOC}^*, E)$. The corresponding r_L^*, r_H^*, x^*, and Π_{stk}^* follow immediately from Lemma 2.1.

□

Figure A.1 summarizes the structure of the optimal stacking as service prices change.

Proof of Proposition 2.3 (Supermodularity)

We defined $f(A, R, p^a, p^r, -c_0^b)$ to be the optimal profit of delivering A total amount of arbitrage and R total amount of regulation across a given day when the price/degradation

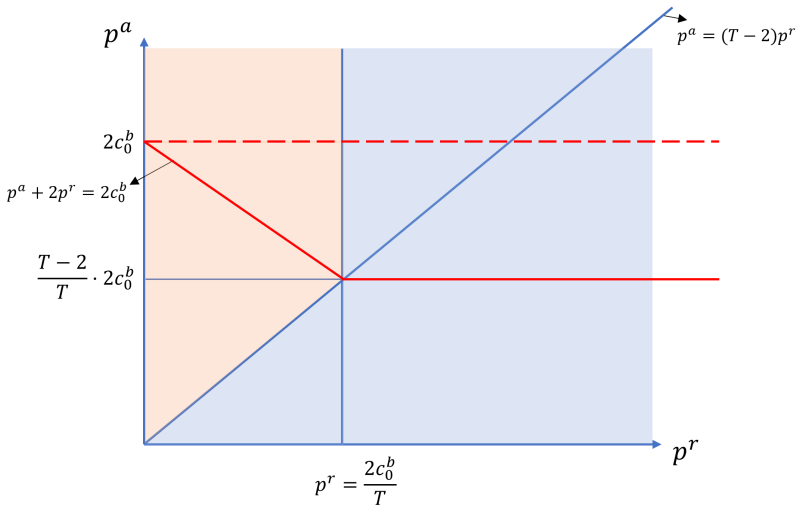


Figure A.1: Illustration of Theorem 2.1 – The shaded region denotes the optimal excess regulation: $x^* = 0$ (orange) and $x^* > 0$ (blue). Energy capacity is binding on the red line and above for stacking (solid) and standalone arbitrage (dashed).

parameter set is given as $(p^a, p^r, -c_0^b)$:

$$
\begin{aligned}
f(A, R, p^a, p^r, -c_0^b) = \max_{r_L, r_H, x_L, x_H} \; & p^a A + p^r R - \frac{c_0^b}{E}[A^2 + 2A\max(x_L, x_H) + \frac{T_L}{2}x_L^2 + \frac{T_H}{2}x_H^2] \\
s.t.\ & a_i = \frac{A}{T_i},\ i = L, H \\
& R = r_L T_L + r_H T_H \\
& x_i = (r_i - a_i)^+,\ i = L, H \\
& A \le E, \\
& A, r_L, r_H \ge 0.
\end{aligned}
$$

By Lemma 2.1, $x_L^* = x_H^* = \frac{(R-2A)^+}{T}$, and we have

$$
f(A, R, p^a, p^r, -c_0^b) = \begin{cases} p^a A + p^r R - \frac{c_0^b}{E}A^2, & \text{if } R \le 2A, \text{ and} \\ p^a A + p^r R - \frac{c_0^b}{E}[A^2 \cdot \frac{T-2}{T} + \frac{R^2}{2T}], & \text{if } R > 2A. \end{cases}
$$

We first note that f is defined over a lattice since (1) $R, p^a, p^r, c_0^b \in [0, \infty)$, and $A \in [0, E]$ are lattices and (2) the direct product of lattices is a lattice. We then show the supermodularity of f by showing that the function has increasing differences on each pair of variables using [186], Theorem 3.2.

For all variable pairs except $(x_i, x_j) = (R, -c_0^b)$ and $(A, -c_0^b)$, f is twice differentiable in x_i, x_j with $\frac{\partial^2 f}{\partial x_i \partial x_j} \geq 0$ everywhere, establishing increasing differences. We now establish increasing differences for $(A, -c_0^b)$ and $(R, -c_0^b)$.

First, we show increasing differences in $(A, -c_0^b)$. Consider $A' \geq A$ and $-c_0^{b'} \geq -c_0^b$. Further, we assume $A' \geq R/2$ and $A \leq R/2$ (if not, second derivative arguments establish increasing differences). Writing $\frac{R}{2} = A + \delta_1,\ A' = A + \delta_2$ for some $\delta_2 \geq \delta_1 \geq 0$ leads to

$$\begin{aligned}
&f(A', -c_0^{b'}) + f(A, -c_0^b) - f(A', -c_0^b) - f(A, -c_0^{b'}) \\
=&(c_0^b - c_0^{b'})[(A')^2 - A^2 \cdot \frac{T-2}{T} - \frac{R^2}{2T}] \\
=&(c_0^b - c_0^{b'})[\delta_2(2A + \delta_2) - \frac{2}{T}\delta_1(2A + \delta_1)] \geq 0,
\end{aligned}$$

so we have increasing differences in $(A, -c_0^b)$.

Second, we show increasing differences in $(R, -c_0^b)$. Consider $R' \geq R$ and $-c_0^{b'} \geq -c_0^b$. Further, we assume $R' \geq 2A$ and $R \leq 2A$ (if not, second derivative arguments establish increasing differences). Then

$$f(R', -c_0^{b'}) + f(R, -c_0^b) - f(R', -c_0^b) - f(R, -c_0^{b'}) = \frac{(c_0^b - c_0^{b'})}{2T}[(R')^2 - (2A)^2] \geq 0,$$

so we have increasing differences in $(R, -c_0^b)$.

Next, we show that $\Pi^*(p^a, p^r, -c_0^b) = \max_{A,R} f(A, R, p^a, p^r, -c_0^b)$ is supermodular in $(p^a, p^r, -c_0^b)$. Since the supermodularity is preserved under the maximization operator from Theorem 2.7.6 of [187], the result immediately follows.

Lastly, we show the complementarity between decision variables and parameters, i.e., (A^*, R^*) increases in $(p^a, p^r, -c_0^b)$. From Theorem 2.8.1 of [187], the result immediately follows. □

Proof of Proposition 2.4 (Superlinear gain)

For completeness, we first present the closed-form expression of $\Pi^*_{stk} - [\Pi^*_{arb} + \Pi^*_{reg}]$:

$$\begin{aligned}
&\Pi^*_{stk} - [\Pi^*_{arb} + \Pi^*_{reg}] \\
&= \begin{cases}
\frac{p^r[2p^a - p^r(T-2)]E}{2c_0^b}, & \text{if } p^r \le \frac{p^a}{T-2},\ \frac{p^a+2p^r}{2} < c_0^b \\
\frac{(p^a)^2E}{2c_0^b(T-2)}, & \text{if } p^r \ge \frac{p^a}{T-2},\ \frac{p^aT}{2(T-2)} < c_0^b \\
(p^a+2p^r)E - c_0^bE - (\frac{(p^a)^2E}{4c_0^b} + \frac{(p^r)^2TE}{2c_0^b}), & \text{if } p^r \le \frac{p^a}{T-2},\ \frac{p^a}{2} \le c_0^b \le \frac{p^a+2p^r}{2} \\
p^aE - \frac{(p^a)^2E}{4c_0^b} - \frac{T-2}{T}c_0^bE, & \text{if } p^r \ge \frac{p^a}{T-2},\ \frac{p^a}{2} \le c_0^b \le \frac{p^aT}{2(T-2)} \\
\frac{p^rE}{2c_0^b}(4c_0^b - p^rT), & \text{if } p^r \le \frac{p^a}{T-2},\ \frac{p^a}{2} \ge c_0^b, \text{ and} \\
\frac{2}{T}c_0^bE, & \text{if } p^r \ge \frac{p^a}{T-2},\ \frac{p^a}{2} \ge c_0^b.
\end{cases}
\end{aligned}$$

Next, we will prove the superlinear gain result, $\Pi^*_{stk} - [\Pi^*_{arb} + \Pi^*_{reg}] > 0$. When $p^r \le \min(\frac{p^a}{T-2}, \frac{2c_0^b}{T})$, we can lower-bound stacking's profit with $\tilde{\Pi}^{(1)}_{stk}$, which we define to be the profit of stacking when it uses arbitrage amount A^*_{arb} and the maximum free regulation ($R = 2A^*_{arb}$). Then

$$\begin{aligned}
\Pi^*_{stk} - [\Pi^*_{arb} + \Pi^*_{reg}] &\ge \tilde{\Pi}^{(1)}_{stk} - [\Pi^*_{arb} + \Pi^*_{reg}] \\
&= \begin{cases}
\frac{p^r[2p^a - p^rT]E}{2c_0^b} \ge \frac{(p^r)^2(T-4)E}{2c_0^b} > 0, & \text{if } \frac{p^a}{2} < c_0^b, \text{ and} \\
\frac{p^rE}{2c_0^b}[4c_0^b - p^rT] > 0, & \text{if } \frac{p^a}{2} \ge c_0^b.
\end{cases}
\end{aligned}$$

When $p^r \ge \min(\frac{p^a}{T-2}, \frac{2c_0^b}{T})$, we can lower-bound stacking's profit with $\Pi^{(2)}_{stk}$, which we define to be the profit of stacking when it uses arbitrage amount A^*_{arb} and regulation amount $R^*_{reg} = \frac{p^rTE}{c_0^b}$, distributed between the low- and high-price regions to ensure equal excess regulation amounts. Then

$$\begin{aligned}
\Pi^*_{stk} - [\Pi^*_{arb} + \Pi^*_{reg}] &\ge \tilde{\Pi}^{(2)}_{stk} - [\Pi^*_{arb} + \Pi^*_{reg}] \\
&= \frac{2c_0^b}{TE}(A^*_{arb})^2 > 0.
\end{aligned}$$

□

Proof of Theorem 2.2 (Upper bound on stacking performance)

We first consider the case when energy capacity is not binding at optimality for arbitrage-only or stacking. Then:

(a) The ratio of stacking profit to arbitrage profit, $\frac{\Pi^*_{stk}}{\Pi^*_{arb}}$, is monotonically increasing in $\frac{p^r}{p^a}$:

$$\frac{\Pi^*_{stk}}{\Pi^*_{arb}} = \begin{cases} \frac{T}{T-2} + 2T(\frac{p^r}{p^a})^2, & \text{if } p^a \le (T-2)p^r, \text{ and} \\ (1+2\frac{p^r}{p^a})^2, & \text{if } p^a \ge (T-2)p^r. \end{cases} \tag{A.5}$$

(b) The ratio of stacking profit to frequency-regulation profit, $\frac{\Pi^*_{stk}}{\Pi^*_{reg}}$, is monotonically increasing in $\frac{p^a}{p^r}$:

$$\frac{\Pi^*_{stk}}{\Pi^*_{reg}} = \begin{cases} 1 + \frac{1}{2(T-2)}(\frac{p^a}{p^r})^2, & \text{if } p^a \le (T-2)p^r, \text{ and} \\ \frac{1}{2T}(\frac{p^a}{p^r}+2)^2, & \text{if } p^a \ge (T-2)p^r. \end{cases} \tag{A.6}$$

The two ratios are equal when $\Pi^*_{arb} = \Pi^*_{reg}$, or $p^a = \sqrt{2T}p^r$. Since $T \ge 6$, then $\sqrt{2T}p^r \le (T-2)p^r$, and the maximum S value of $S = \frac{2T-2}{T-2}$ follows by evaluating (A.5) and (A.6) at $p^a = \sqrt{2T}p^r$.

We now proceed to show that $\frac{2T-2}{T-2}$ is the upper bound for energy-binding cases. When energy capacity is binding for stacking but not for standalone arbitrage or when $\Pi^*_{reg} > \Pi^*_{arb}$, the S ratio is upper-bounded by the S ratio under no energy constraint, meaning $S \le \frac{2T-2}{T-2}$. As a result, the remainder of this proof will focus on the case when $\Pi^*_{arb} > \Pi^*_{reg}$ ($p^aE - c_0^bE > \frac{(p^r)^2TE}{2c_0^b}$) and when standalone arbitrage is energy-constrained ($p^a \ge 2c_0^b$). Then Theorem 2.1 states that

$$\Pi^*_{stk} = \begin{cases} \frac{(p^r)^2TE}{2c_0^b} + p^aE - c_0^b(1-\frac{2}{T})E, & \text{if } p^r > \frac{2c_0^b}{T}, \text{ and} \\ (p^a+2p^r)E - c_0^bE, & \text{otherwise.} \end{cases}$$

If $p^r \le \frac{2c_0^b}{T}$, then

$$\begin{aligned} \frac{\Pi^*_{stk}}{\Pi^*_{arb}} = \frac{(p^a+2p^r)E - c_0^bE}{p^aE - c_0^bE} &\le \frac{p^aE + \frac{4c_0^bE}{T} - c_0^bE}{p^aE - c_0^bE} \\ &\le \frac{1}{1-\frac{c_0^b}{p^a}} \ (\because T \ge 4) \\ &\le 2 \ (\because p^a \ge 2c_0^b). \end{aligned}$$

If $p^r > \frac{2c_0^b}{T}$, then

$$\begin{aligned}\frac{\Pi^*_{stk}}{\Pi^*_{arb}} &= \frac{\frac{(p^r)^2TE}{2c_0^b} + p^aE - c_0^b(1-\frac{2}{T})E}{p^aE - c_0^bE} \\ &< \frac{2(p^aE - c_0^bE) + \frac{2c_0^b}{T}E}{p^aE - c_0^bE} = 2 + \frac{\frac{2c_0^b}{T}}{p^a - c_0^b} \ (\because \Pi^*_{reg} < \Pi^*_{arb}) \\ &\leq 2 + \frac{2}{T} \ (\because p^a \geq 2c_0^b) \\ &< 2 + \frac{2}{T-2} = \frac{2T-2}{T-2}.\end{aligned}$$

□

Proof of Theorem 2.3 (Improved stopping threshold)

We derive the stopping threshold for each operation and then we can easily compare the stopping thresholds between stacking and standalone services and complete the proof.

First, we derive the stopping threshold for standalone arbitrage. Recall that providing arbitrage with efficiency η is equivalent to providing arbitrage with perfect efficiency, low-period price $\underline{p}' = \frac{\underline{p}}{\eta^2}$, and degradation coefficient $c_0^{b'} = \frac{c_0^b}{\eta^2}$. As derived at the beginning of Section 2.5, it is optimal to provide arbitrage as long as $\bar{p} > \underline{p}'$, or, equivalently, whenever $\eta \in (\eta_{arb}, 1]$, where $\eta_{arb} = \sqrt{\frac{\underline{p}}{\bar{p}}}$ is the stopping threshold for standalone arbitrage.

Next, consider stacking arbitrage and regulation. At optimality, we must have $r_L \geq a_L$ and $r_H \geq a_H$. Defining $A = T_H a_H$ to be the amount of arbitrage sold to the grid in the high-price period and $X = T_L(r_L - a_L) + T_H(r_H - a_H)$ to be the amount of excess regulation sold to the grid, the energy balance equations (2.17)-(2.18) imply $T_L a_L = \frac{A}{\eta^2} + \frac{X}{2}(\frac{1}{\eta^2} - 1)$ (the amount of arbitrage energy we must buy in the low-price period $T_L a_L$ is a linear function of A and X). Then we have $\Pi_{stk} = \tilde{p}^a A + \tilde{p}^x X - Deg(D, x_L, x_H)$, for constants $\tilde{p}^a = \bar{p} - \frac{\underline{p}}{\eta^2} + p^r(1 + \frac{1}{\eta^2})$ and $\tilde{p}^x = \frac{p^r}{2}(\frac{1}{\eta^2} + 1) - \frac{\underline{p}}{2}(\frac{1}{\eta^2} - 1)$.

For stacking with sufficiently small A, $X = O(\epsilon)$, we have degradation of order $O(\epsilon^2)$. Therefore, we will always provide at least a bit of service if either $\tilde{p}^a > 0$ or $\tilde{p}^x > 0$. When $\underline{p} \leq p^r$, then $\tilde{p}^a, \tilde{p}^x > 0$, so we always provide service regardless of η. Otherwise, $\tilde{p}^a > 0$ is equivalent to $\eta > \eta_{stk} := \sqrt{\frac{(\underline{p} - p^r)^+}{\bar{p} + p^r}}$ and $p^x > 0$ is equivalent to $\eta > \eta_{reg} := \sqrt{\frac{(\underline{p} - p^r)^+}{\underline{p} + p^r}}$. Since $\eta_{stk} \leq \eta_{reg}$, we provide stacked service whenever $\eta > \eta_{stk}$.

For regulation-only service, we require $A = 0$. Therefore, similar reasoning shows that we provide service if $\eta > \eta_{reg}$.

Proof of Lemma 2.2 (Excess regulation: Bounded power)

We prove the statement by contradiction, in all cases showing that an adjustment to the regulation bids can result in an increased profit while still respecting the power and energy constraints. Suppose $x_H^* > x_L^*$. Then $r_H^* > 0$ and $a_L^* + r_L^* < a_H^* + r_H^*$, meaning there's excess power capacity in the low-price period, so it is feasible to decrease r_H^* by some sufficiently small $\epsilon > 0$ and to increase r_L^* by $\epsilon T_H/T_L$. The net changes in regulation revenues between the low- and high-price periods cancel out, while the adjustment reduces degradation costs by $\frac{c_0^b}{E}(2A^* + T_H(x_H^* - x_L^*))\epsilon + O(\epsilon^2) > 0$, a contradiction to optimality.

Similarly, if $r_L^* + a_L^* > r_H^* + a_H^*$, then $r_L^* - a_L^* > r_H^* - a_H^*$ and, thus, $x_L^* > x_H^*$ or $x_L^* = x_H^* = 0$. If $x_L^* > x_H^*$, then for sufficiently small $\epsilon > 0$ it is feasible to increase r_H^* by ϵ and to decrease r_L^* by $\epsilon T_H/T_L$, yielding identical revenue but reducing degradation costs by $\frac{c_0^b}{E} T_H(2A^*/T_L + x_L^* - x_H^*)\epsilon + O(\epsilon^2) > 0$. If $x_L^* = x_H^* = 0$, then it is feasible to increase r_H^* by some small $\epsilon > 0$, increasing profit by $p^r T_H \epsilon + O(\epsilon^2) > 0$. Thus, both cases yield a contradiction to optimality. □

Proof of Theorem 2.4 (Upper bound on stacking's performance: Bounded power)

We first state the optimal single-service solutions:

$$r_{reg}^* = \begin{cases} \frac{p^r E}{c_0^b}, & \text{if } P > \frac{p^r E}{c_0^b}, \text{ and} \\ P, & \text{otherwise,} \end{cases}$$

$$\Pi_{reg}^* = \begin{cases} \frac{(p^r)^2 TE}{2c_0^b}, & \text{if } P > \frac{p^r E}{c_0^b}, \text{ and} \\ p^r PT - \frac{c_0^b T P^2}{2E}, & \text{otherwise,} \end{cases}$$

$$A_{arb}^* = \begin{cases} \frac{p^a E}{2c_0^b}, & \text{if } p^a < 2\frac{c_0^b}{E} \cdot \min(PT_H, E), \text{ and} \\ \min(PT_H, E), & \textit{otherwise,} \end{cases}$$

$$\Pi_{arb}^* = \begin{cases} \frac{(p^a)^2 E}{4c_0^b}, & \text{if } p^a < 2\frac{c_0^b}{E} \cdot \min(PT_H, E), \text{ and} \\ p^a \cdot \min(PT_H, E) - \frac{c_0^b}{E}[\min(PT_H, E)]^2, & \text{otherwise.} \end{cases}$$

We next introduce and prove two technical lemmas (Lemma A.1 and Lemma A.2). Then we prove the main result.

Lemma A.1. *If* $P \leq \frac{p^r E}{c_0^b}$, *then* $\Pi_{stk}^* \leq \Pi_{arb}^* + \Pi_{reg}^*$.

We first show that power is binding in both time periods for stacking when $P \leq \frac{p^r E}{c_0^b}$

(regulation-only is power binding). Suppose power is not binding in the low-price period at the optimality under $P \leq \frac{p^r E}{c_0^b}$. Since $x_L^* \geq x_H^*$ (Lemma 2.2), we can increase the objective (2.5) by increasing r_L as follows:

$$\frac{\partial \Pi}{\partial r_L} = \begin{cases} p^r T_L - \frac{c_0^b}{E}[2A^* + T_L(r_L^* - a_L^*)] = T_L[p^r - \frac{c_0^b}{E}[r_L^* + a_L^*]], & \text{if } r_L^* \geq a_L^*, \text{ and} \\ p^r T_L, & \text{if } r_L^* < a_L^*. \end{cases}$$

The marginal profit change is always positive as $r_L^* + a_L^* < P$ and $P \leq \frac{p^r E}{c_0^b}$, which is a contradiction.

Since power is binding in both time periods, stacking can be expressed as a single-variable optimization problem — given arbitrage amount A we have $r_i = P - \frac{A}{T_i}$ and $x_i = (P - \frac{2A}{T_i})^+$ for $i = L, H$. Define $\Pi_{stk}(A) = (p^a - 2p^r)A + p^r PT - Deg(A, x_L, x_H)$ to be the profit of stacking with A fixed, define $\Pi_{reg}^* = p^r PT - \frac{c_0^b T P^2}{2E}$ to be the optimal profit of regulation-only, and define $\Pi_{arb}(A) = p^a A - \frac{c_0^b}{E} A^2$ to be the profit of arbitrage-only with A fixed. Then we have

$$\begin{aligned} \Pi_{arb}(A) + \Pi_{reg}^* - \Pi_{stk}(A) &= 2p^r A - \frac{c_0^b T P^2}{2E} + \frac{c_0^b}{E}[2Ax_L + \frac{T_L}{2}x_L^2 + \frac{T_H}{2}x_H^2] \\ &\geq \frac{c_0^b}{E}[2AP - \frac{TP^2}{2} + 2Ax_L + \frac{T_L}{2}x_L^2 + \frac{T_H}{2}x_H^2], \end{aligned}$$

where the inequality is from $p^r \geq P\frac{c_0^b}{E}$. Let $f(A) = 2AP - \frac{TP^2}{2} + 2Ax_L + \frac{T_L}{2}x_L^2 + \frac{T_H}{2}x_H^2$.

$$f'(A) = \begin{cases} 2P, & \text{if } A > \frac{PT_L}{2} \ (x_L = x_H = 0), \\ 2P - \frac{4A}{T_L}, & \text{if } \frac{PT_H}{2} \leq A \leq \frac{PT_L}{2} \ (x_L > x_H = 0), \text{ and} \\ 4A(\frac{1}{T_H} - \frac{1}{T_L}), & \text{if } A < \frac{PT_H}{2} \ (x_H > 0), \end{cases}$$

so $f(A)$ is increasing in A from an initial value of 0 at $A = 0$. Defining A^* to be the profit-maximizing arbitrage amount under stacking, $\Pi_{stk}^* = \Pi_{stk}^*(A^*) \leq \Pi_{reg}^* + \Pi_{arb}^*(A^*) \leq \Pi_{reg}^* + \Pi_{arb}^*$. □

Lemma A.2. *If* $P > \frac{p^r E}{c_0^b}$ *and* $p^a \geq 2\frac{c_0^b}{E} \cdot \min(PT_H, E)$, *then* $\frac{\Pi_{stk}^*}{\max(\Pi_{arb}^*, \Pi_{reg}^*)} \leq \frac{2T-2}{T-2}$.

Proof. From $P > \frac{p^r E}{c_0^b}$, we know that frequency regulation-only is not power binding at optimality. Therefore, when $\Pi_{reg}^* \geq \Pi_{arb}^*$, the result that $\frac{\Pi_{stk}^*}{\max(\Pi_{arb}^*, \Pi_{reg}^*)} \leq \frac{2T-2}{T-2}$ follows from Theorem 2.2. The remainder of this proof will focus on the case when $\Pi_{arb}^* > \Pi_{reg}^*$. We consider the two subcases of (1) $PT_H \leq E$ and (2) $E \leq PT_H$.

(1) $PT_H \leq E$: In this case, $\Pi_{reg}^* = \frac{(p^r)^2 TE}{2c_0^b}$ and $\Pi_{arb}^* = p^a(PT_H) - \frac{c_0^b}{E}(PT_H)^2$. First, we establish that stacking is power-binding in the high-price period. From Observation 2.3,

unconstrained stacking has a strictly larger A^* (and therefore strictly higher power use in both time periods) than unconstrained arbitrage-only. Since arbitrage-only is power-binding when $p^a \geq 2\frac{c_0^b}{E}PT_H$, stacking must be as well.

Next, we establish that $x_H^* = 0$. Suppose not ($x_H^* > 0$). Given high-price period power use $2a_H^* + x_H^* = P$, $A^* < \frac{PT_H}{2}$. Then consider increasing A by some small $\epsilon > 0$ and decreasing r_L by $\frac{\epsilon}{T_L}$ and r_H by $\frac{\epsilon}{T_H}$, which does not affect the power usage in either time period. This implies a $\frac{2\epsilon}{T_L}$ decrease in x_L and a $\frac{2\epsilon}{T_H}$ decrease in x_H. Then the marginal profit change becomes

$$\begin{aligned}
[p^a - 2p^r - 2\frac{c_0^b}{E}(A(1-\frac{2}{T_L}) - x_H)]\epsilon + O(\epsilon^2) &> \frac{c_0^b}{E}\epsilon[2PT_H - 2A(1-\frac{2}{T_L}+\frac{2}{T_H})] + O(\epsilon^2) \\
&> \frac{c_0^b}{E}\epsilon PT_H[2-(1-\frac{2}{T_L}+\frac{2}{T_H})] + O(\epsilon^2) \\
&= \frac{c_0^b}{E}\epsilon PT_H[1+\frac{2}{T_L}-\frac{2}{T_H}] + O(\epsilon^2),
\end{aligned}$$

where the first inequality is from $\frac{p^r E}{c_0^b} < P < \frac{p^a E}{2c_0^b T_H}$ and the second inequality is from $A^* < \frac{PT_H}{2}$. This is positive for sufficiently small $\epsilon > 0$, a contradiction of optimality.

Next, we establish that if $x_L^* = x_H^* = 0$, then $\Pi_{stk}^* \leq 2\Pi_{arb}^*$:

$$\begin{aligned}
\Pi_{stk}^* &= p^a A^* + p^r r_L^* T_L + p^r r_H^* T_H - \frac{c_0^b}{E}(A^*)^2 \\
&\leq p^a A^* - \frac{c_0^b}{E}(A^*)^2 + 2p^r A^* \ (\because r_i^* \leq \frac{A^*}{T_i}, i = L, H) \\
&\leq p^a(PT_H) - \frac{c_0^b}{E}(PT_H)^2 + 2p^r(PT_H) \ (\because p^a \geq 2\frac{c_0^b}{E}PT_H \geq 2\frac{c_0^b}{E}A^*) \\
&< \Pi_{arb}^* + 2\frac{c_0^b}{E}P^2T_H \leq \Pi_{arb}^* + \frac{c_0^b}{E}(PT_H)^2 \leq 2\Pi_{arb}^*.
\end{aligned}$$

Last, we establish that if $x_L^* > x_H^* = 0$, then $\Pi_{stk}^* \leq \Pi_{arb}^* + \Pi_{reg}^*$. We first note that power is not binding in the low-price period for stacking when $P > \frac{p^r E}{c_0^b}$. Suppose this is not true ($x_L^* + \frac{2A^*}{T_L} = P$). Then we can increase the profit by decreasing r_L (and x_L) by a unit as the marginal profit change is $-p^r T_L - \frac{c_0^b}{E}[-2A - T_L x_L] = T_L[\frac{c_0^b}{E}P - p^r] > 0$. Thus, the power constraint in the low-period is always inactive ($r_L + a_L < P$). For given A, the optimal x_L can be found by taking the first-order condition in terms of x_L and setting it equal to zero, which leads to $x_L^*(A) = \frac{p^r E}{c_0^b} - \frac{2A}{T_L}$ and $r_L^*(A) = \frac{p^r E}{c_0^b} - \frac{A}{T_L}$. Thus, the $x_L^* > 0$ region only

happens when $p^r > \frac{2c_0^b A^*}{T_L E}$. Noting that $r_H^* = P - a_H^*$ when $x_H^* = 0$, then

$$\begin{aligned}\Pi_{stk}^* &= \Pi_{reg}^* + p^a A^* - \frac{c_0^b}{E}(A^*)^2 + \frac{2c_0^b}{T_L E}(A^*)^2 + p^r(PT_H - 2A^* - \frac{p^r E}{2c_0^b}T_H) \\ &< \Pi_{reg}^* + (p^a + \frac{2c_0^b PT_H}{T_L E})A^* - \frac{c_0^b}{E}(1 + \frac{2T}{T_L^2})(A^*)^2,\end{aligned}$$

where the strict inequality comes from the fact that $p^r(PT_H - 2A^* - \frac{p^r E}{2c_0^b}T_H)$ is strictly decreasing in p^r (since $x_H^* = 0$ implies $A^* \geq \frac{PT_H}{2}$), so we obtain an upper bound by plugging in $p^r = \frac{2c_0^b A^*}{T_L E}$. All that remains is to prove that $(p^a + \frac{2c_0^b PT_H}{T_L E})(A^*) - (1 + \frac{2T}{T_L})(A^*)^2 \leq \Pi_{arb}^*$. Using $p^a \geq 2\frac{c_0^b}{E}PT_H$, the first-order condition of $f(A) = (p^a + \frac{2c_0^b PT_H}{T_L E})A - (1 + \frac{2T}{T_L})A^2$ implies that $f(A)$ is maximized at $B = \min(PT_H, \bar{B})$ for some $\bar{B} \geq \frac{PT_H(T_L^2 + T_L)}{T_L^2 + 2T} \geq \frac{PT_H}{2}$. This leads to

$$\begin{aligned}\Pi_{stk}^* &< \Pi_{reg}^* + (p^a + \frac{2c_0^b PT_H}{T_L E})B - \frac{c_0^b}{E}(1 + \frac{2T}{T_L^2})B^2 \\ &\leq \Pi_{reg}^* + \Pi_{arb}^* + \frac{2c_0^b PT_H}{T_L E}B - \frac{c_0^b}{E}\frac{2T}{T_L^2}B^2.\end{aligned}$$

Since $\frac{2c_0^b PT_H}{T_L E}B - \frac{c_0^b}{E}\frac{2T}{T_L^2}B^2$ is decreasing in B for $B \geq \frac{PT_H}{2}$ and is negative when evaluated at lower bounds $B = PT_H$ and $B = \frac{PT_H(T_L^2 + T_L)}{T_L^2 + 2T}$, we conclude that $\Pi_{stk}^* < \Pi_{reg}^* + \Pi_{arb}^*$.

(2) $E \leq PT_H$: In this case, standalone arbitrage is energy constrained. Let $\tilde{\Pi}_{stk}^*$ be the optimal stacking profit under $P = \infty$. Then $\frac{\Pi_{stk}^*}{\Pi_{arb}^*} \leq \frac{\tilde{\Pi}_{stk}^*}{\Pi_{arb}^*} \leq \frac{2T-2}{T-2}$, where the second inequality is immediate from the proof of Theorem 2.2.

□

Lastly, we prove the main result.

When $p^r \geq \frac{c_0^b}{E}P$ or $p^r < \frac{c_0^b}{E}P, p^a \geq 2\frac{c_0^b}{E} \cdot \min(PT_H, E)$, then Lemmas A.1 and A.2 combined imply that $\frac{\Pi_{stk}^*}{\max(\Pi_{arb}^*, \Pi_{reg}^*)} \leq \frac{2T-2}{T-2}$. When $p^r < \frac{c_0^b}{E}P$ and $p^a < 2\frac{c_0^b}{E} \cdot \min(PT_H, E)$, then arbitrage-only and regulation-only are not power/energy constrained at optimality, so $\frac{\Pi_{stk}^*}{\max(\Pi_{arb}^*, \Pi_{reg}^*)} \leq \frac{2T-2}{T-2}$ immediately follows from Theorem 2.2. □

A.3 Generalizations/Extensions and Proofs

A.3.1 Extension 1: Correlated Prices

A.3.1.1 Empirical Evidence

Many ISO/RTOs publish their operational datasets (e.g., market-clearing results). From two different ISOs (PJM and ISO-NE), we obtained three types of data for period July 2020 - June 2021: (1) day-ahead hourly energy prices, (2) 5-min based regulation prices (the sum of capacity price (\$/MWh) + performance price (\$/MW) $\times$ mileage (ΔMW)), and (3) regulation signal. We calibrate the model parameters from the data as follows: Daily peak prices $\bar{p}$ are obtained by computing the 2-hour period with the highest average price each day. Daily off-peak prices $\underline{p}$ are an average of the remaining 22 hours. The 5-min based regulation prices are averaged on an hourly basis since both ISOs make capacity commitments on an hourly basis and at least an hour ahead of time. Daily $\bar{p}^r$ and $\underline{p}^r$ are obtained using the same 2-hour and 22-hour periods identified in each day when computing $\bar{p}$ and $\underline{p}$. This gives 365 data points (1 year) for $(\underline{p}, \underline{p}^r)$ and $(\bar{p}, \bar{p}^r)$. Then the base regulation price p_0^r and the linear coefficient k are fitted via linear regression. For ISO-NE we have $k = 0.23$ and $p_0^r = 10.99$, and for PJM we have $k = 0.29$ and $p_0^r = 12.65$.

A.3.1.2 Optimal Stacking: Correlated Prices

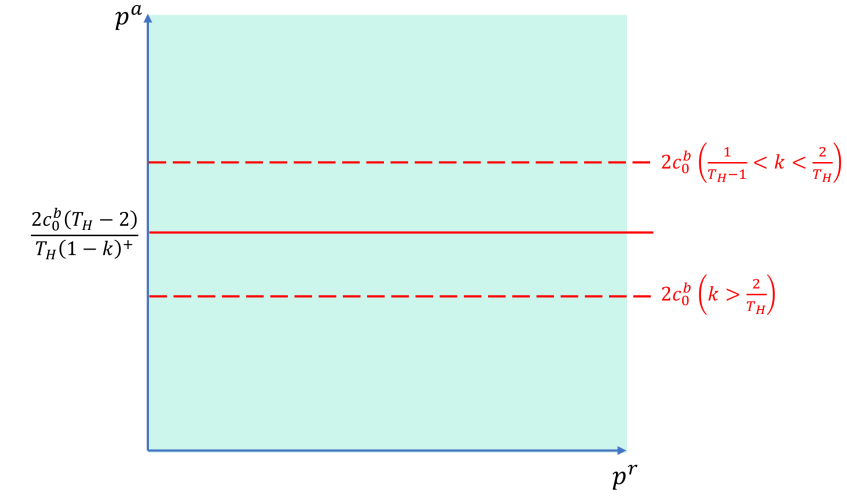
Optimal structure. Unlike the uncorrelated setting, we might expect maintaining unequal excess regulation ($x_H^* > x_L^*$) to be optimal when k is sufficiently large (such that regulation during the high-price period is attractive enough). The following theorem states the optimal actions and the corresponding profit.

Theorem A.1 (Correlated prices)**.** *With correlated prices, the optimal arbitrage and regulation quantities and profit are as follows:*

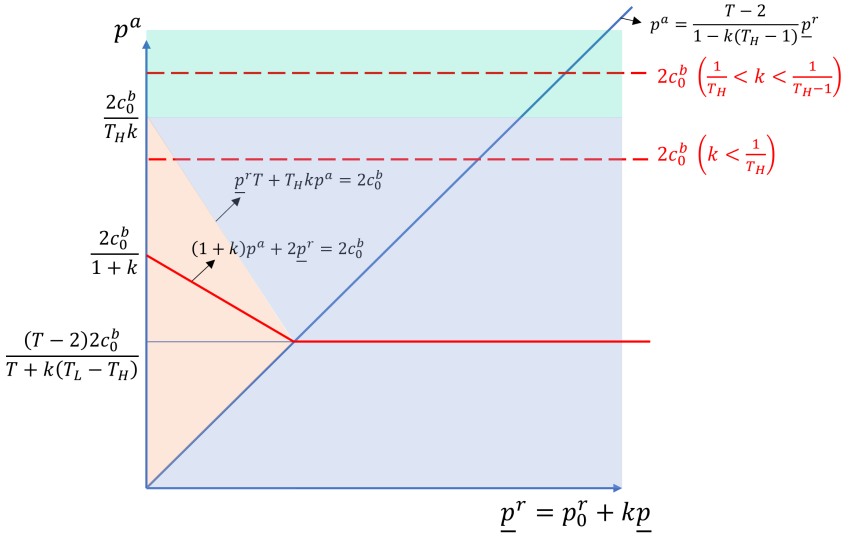
Var.	Cases		
	$x_H^* > x_L^* > 0$	$x_H^* = x_L^* = 0$	$x_H^* = x_L^* > 0$
cond.	$k > \frac{1}{T_H - 1}$ or $p^a > \frac{2c_0^b}{kT_H}$	$p^r \le \min(\frac{1+\frac{k(T_L - T_H)}{T}}{T-2} p^a, \frac{2c_0^b}{T})$	otherwise
A^*	$\min(\frac{T_H p^a (1-k)^+}{2c_0^b (T_H - 2)} E, E)$	$\min(\frac{(1+\frac{k(T_L - T_H)}{T}) p^a + 2p^r}{2c_0^b} E, E)$	$\min(\frac{p^a [T + k(T_L - T_H)]}{2c_0^b (T-2)} E, E)$
R^*	$\frac{p^r T E}{c_0^b}$	$2A^*$	$\frac{p^r T E}{c_0^b}$

Table A.2: Optimal stacking (correlated prices).

where $p^r := \frac{T_L \underline{p}^r + T_H \bar{p}^r}{T}$ *is defined to be the average regulation price throughout the day.*



(a) $k > \frac{1}{T_H-1}$



(b) $k \leq \frac{1}{T_H-1}$

Figure A.2: Illustration of Theorem A.1 – The shaded region denotes the optimal excess regulation: $x_H^* > x_L^* > 0$ (green), $x_H^* = x_L^* = 0$ (orange), and $x_H^* = x_L^* > 0$ (blue). Energy capacity is binding on the red line and above for stacking (solid) and standalone arbitrage (dashed).

Figure A.2 summarizes the structure of the optimal stacking.

Proof. First, we establish that $x_H^* \geq x_L^*$. If this were not the case ($x_L^* > x_H^*$), then we could decrease r_L^* by some sufficiently small $\epsilon > 0$ and increase r_H^* by $\frac{T_L \epsilon}{T_H}$, yielding a profit change of at least $((\bar{p}^r - \underline{p}^r)T_L + \frac{c_0^b}{E}(2A + T_L(x_L^* - x_H^*))\epsilon + O(\epsilon^2)$. This achieves a profit improvement for sufficiently small $\epsilon > 0$, a contradiction of optimality.

Let $x_H - x_L := \delta \geq 0$. Then we can rewrite the objective function as

$$\Pi = (\bar{p} - \underline{p})A + \underline{p}^r(x_L + a_L)T_L + \bar{p}^r(x_L + \delta + a_H)T_H - \frac{c_0^b}{E}[A^2 + 2A(x_L + \delta) + \frac{T_L}{2}x_L^2 + \frac{T_H}{2}(x_L + \delta)^2].$$

For fixed A and x_L the first-order conditions indicate an optimal δ value of

$$\delta^*(A, x_L) = (\frac{\bar{p}^r E}{c_0^b} - \frac{2A}{T_H} - x_L)^+,$$

which can be used to derive the optimal profit for fixed A and x_L.

Next, we derive the optimal x_L value given fixed A. When $A \geq \frac{\bar{p}^r T_H E}{2c_0^b}$, then $\delta^* = 0$ regardless of the value of x_L. The first-order condition immediately yields $x_L^* = \frac{(\underline{p}^r T_L + \bar{p}^r T_H - 2\frac{c_0^b}{E}A)^+}{\frac{c_0^b}{E}T}$. Otherwise, $\delta^* > 0$ for $x_L < \frac{\bar{p}^r E}{c_0^b} - \frac{2A}{T_H}$ and $\delta^* = 0$ otherwise. In this case, $\Pi(A, x_L)$ is a strictly concave function of x_L with a continuous, piecewise linear, decreasing derivative that takes value

$$\Pi'(A, \frac{\bar{p}^r E}{c_0^b} - \frac{2A}{T_H}) = \frac{2c_0^b A T_L}{T_H E} - kp^a T_L.$$

We conclude that $\delta^* > 0$ whenever $\Pi'(A, \frac{\bar{p}^r E}{c_0^b} - \frac{2A}{T_H}) < 0$ ($A < \frac{kp^a T_H E}{2c_0^b}$), in which case $x_L^* = \frac{\underline{p}^r E}{c_0^b}$. Otherwise, $\delta^* = 0$, in which case $x_L^* = \frac{\underline{p}^r T_L + \bar{p}^r T_H - 2\frac{c_0^b}{E}A}{\frac{c_0^b}{E}T}$.

Taken together, these results yield the optimal profit for fixed A. $\Pi(A)$ is a strictly concave function with a continuous, piecewise linear, decreasing derivative that takes values

$$\Pi'(\frac{kp^a T_H E}{2c_0^b}) = p^a(1 - k(T_H - 1)) \text{ and}$$
$$\Pi'(\frac{\bar{p}^r T_H + \underline{p}^r T_L E}{2c_0^b}) = p^a - (T_H - 1)\bar{p}^r - (T_L - 1)\underline{p}^r.$$

Then the optimal solution satisfies the following:

- $A^* < \frac{kp^a T_H E}{2c_0^b}$ whenever $\Pi'(\frac{kp^a T_H E}{2c_0^b}) < 0$ (equivalently, $k > \frac{1}{T_H - 1}$) or $E < \frac{kp^a T_H E}{2c_0^b}$,

- $A^* \geq \frac{\bar{p}^r T_H + \underline{p}^r T_L E}{2c_0^b}$ whenever $\Pi'(\frac{\bar{p}^r T_H + \underline{p}^r T_L E}{2c_0^b}) \geq 0$ and $E \geq \frac{(\bar{p}^r T_H + \underline{p}^r T_L)E}{2c_0^b}$, and
- $\frac{kp^a T_H E}{2c_0^b} \leq A^* < \frac{(\bar{p}^r T_H + \underline{p}^r T_L)E}{2c_0^b}$ otherwise.

The optimal A^* values follow immediately from the first-order conditions of the various regions of $\Pi(A)$ and the energy constraint E.

□

Synergistic behavior. Following Theorem A.1, let $p^r := \frac{T_L \underline{p}^r + T_H \bar{p}^r}{T}$ denote the weighted average of the regulation prices. Consistent with Observation 2.3, A^* (R^*) increases in p^r (p^a) whenever $x_H^* = x_L^* = 0$ (free regulation-only region). However, the threshold for how high the arbitrage price needs to be to trigger this free regulation-only region is relaxed whenever $k > 0, T_L > T_H$ compared to the base model.

Observation A.1. *The criterion for the free regulation-only region is relaxed whenever $k > 0, T_L > T_H$ compared to the base model.*

The synergistic behavior is further expanded under correlated prices: for fixed p^a, A^* increases in k (or $\bar{p}^r - \underline{p}^r$; the gap between the regulation prices) whenever $x_H^* = x_L^*$. That is, as long as the gap $\bar{p}^r - \underline{p}^r$ is not too high ($k \leq \frac{1}{T_H - 1},\ p^a \leq \frac{2c_0^b}{kT_H}$), the additional margin from the higher regulation price as k is increased leads to a higher arbitrage quantity, which is used to maximize the cost saving benefit from equal excess regulation. When $\bar{p}^r - \underline{p}^r$ is high enough, we opt to maintain unequal excess $x_H^* > x_L^* > 0$, which reduces cost-savings (see Proposition 2.2) and causes A^* to no longer increase in k for fixed p^a.

We now establish whether other key properties from the base model hold under correlated prices:

Corollary A.1. *With the correlated prices, the following hold for stacking:*

- $x_H^* = x_L^*$ *when* $k \leq \frac{1}{T_H - 1}$ *and* $p^a \leq \frac{2c_0^b}{kT_H}$,
- $A_{stk}^* > A_{arb}^*$ *when* $k < \frac{2}{T_H}$ *and* $p^a < 2c_0^b$,
- $\frac{R^*}{A^*} \geq 2$,
- $R_{stk}^* > R_{reg}^*$ *when* $p^a[1 + k(\frac{T_L - T_H}{T})] > (T-2)p^r,\ \frac{2c_0^b}{T} > p^r$,
- *Positive cost-saving synergy when* $k < \frac{5T_L + T_H}{(4T_H - 3)T_L + T_H}$ *and* $p^a < \frac{(T_H + 5T_L)c_0^b}{2T_L T_H k}$.

Proof. (i) The first property can be immediately checked from Theorem A.1.

(ii) $A^*_{stk} > A^*_{arb}$: If $p^a \geq 2c^b_0$ ($A^*_{arb} = E$) or $k \geq \frac{2}{T_H}$ ($A^*_{stk} = \min(\frac{cp^aE}{2c^b_0}, E)$ for some $c \leq 1$), then the property does not hold. Otherwise, $A^*_{stk} = \min(\frac{cp^aE}{2c^b_0}, E)$ for some $c > 1$ and $A^*_{arb} = \frac{p^aE}{2c^b_0} < E$, so the property holds.

(iii) $\frac{R^*}{A^*} \geq 2$: Stacking always uses the full free regulation, which implies $\frac{R^*}{A^*} \geq 2$.

(iv) $R^*_{stk} > R^*_{reg}$: When (1) $x^*_H > x^*_L > 0$ or (3) $x^*_H = x^*_L > 0$, $R^*_{stk} = R^*_{reg}$. When (2) $x^*_H = x^*_L = 0$, the inequality holds if and only if $p^a > (T_L - 1)\underline{p}^r + (T_H - 1)\bar{p}^r$ (or $p^a[1 + k(\frac{T_L - T_H}{T})] > (T - 2)p^r$) when $A^*_{stk} = \frac{p^a + \underline{p}^r + \underline{p}^r}{2c^b_0}E < E$, and it holds if and only if $2c^b_0 > Tp^r$ when $A^*_{stk} = E$ ($\frac{p^a + \underline{p}^r + \underline{p}^r}{2c^b_0}E \geq E$).

(v) Cost-saving synergy: From Proposition 2.2, we have a positive cost saving for $k \leq \frac{1}{T_H - 1}$, $p^a \leq \frac{2c^b_0}{kT_H}$ because $x^*_L = x^*_H$. For $k > \frac{1}{T_H - 1}$ or $p^a > \frac{2c^b_0}{kT_H}$ ($x^*_H > x^*_L > 0$), $x^*_L = \frac{\underline{p}^r E}{c^b_0}$, $x^*_H = \frac{\bar{p}^r E}{c^b_0} - \frac{2A^*}{T_H}$. We have a positive cost saving if and only if $\frac{a^*_L + a^*_H}{2} > x^*_H - x^*_L$. This inequality is equivalent to $k < \frac{5T_L + T_H}{(4T_H - 3)T_L + T_H}$ if $\frac{T_H p^a (1-k)^+}{2(T_H - 2)} < c^b_0$ ($A^* < E$) and $\frac{2T_H T_L p^a k}{T_H + 5T_L} < c^b_0$ if $c^b_0 \leq \frac{T_H p^a (1-k)}{2(T_H - 2)}$ ($A^* = E$). Combining the conditions yields $k < \frac{5T_L + T_H}{(4T_H - 3)T_L + T_H}$ and $p^a < \frac{(T_H + 5T_L)c^b_0}{2T_L T_H k}$.

(vi) $\Pi^*_{stk} > \Pi^*_{arb} + \Pi^*_{reg}$: From Theorem A.1, it is straightforward to derive $\Delta\Pi := \Pi^*_{stk} - [\Pi^*_{arb} + \Pi^*_{reg}]$. When $x^*_H > x^*_L > 0$ ($k > \frac{1}{T_H - 1}$ or $p^a > \frac{2c^b_0}{kT_H}$), $\Delta\Pi$ can be written in the form $c_1(p^a)^2 + c_2 p^a + c_3$, defined over some interval for p^a. Then it is easy to check that the quadratic function has negative values at the boundaries, concluding that we never have superlinear gains.

When $x^*_H = x^*_L$ ($k \leq \frac{1}{T_H - 1}$, $p^a \leq \frac{2c^b_0}{kT_H}$), $\Delta\Pi$ can be written in the form $c_1(p^a)^2 + c_2 p^a \underline{p}^r + c_3(\underline{p}^r)^2 + c_4 p^a + c_5 \underline{p}^r + c_6$. Establishing cases with superlinear profit gain requires careful applications of the quadratic formula to establish the range of p^a where the property holds. Somewhat tedious enumeration of cases for the optimal solution yields the conditions in Corollary A.1.

□

Benefit of stacking. We now derive the upper bound on stacking's performance under correlated prices. In fact, we can show that correlated prices almost always (whenever $T_L > T_H$) have some set of prices $(\underline{p}, \bar{p}, p^r_0, k)$ that improve over the best achievable S under the base model. For analytical simplicity, we focus on $T_H \geq 4$ ($\frac{1}{T_H - 1} < \frac{1}{\sqrt{2T_H}}$), but the case of $T_H = 2$ can be done similarly (in this case, $\frac{1}{T_H - 1} > \frac{1}{\sqrt{2T_H}}$). We will first assume that energy is non-binding (Lemma A.3, Theorem A.2, and Corollary A.2) and then study the effect of binding energy constraint on S ratios (Corollary A.3).

Lemma A.3. *In the correlated price setting with non-binding energy capacity, ratios* $\frac{\Pi^*_{arb}}{\Pi^*_{stk}}$, $\frac{\Pi^*_{arb}}{\Pi^*_{reg}}$, *and* $\frac{\Pi^*_{stk}}{\Pi^*_{reg}}$ *are increasing in* $\bar{p}$.

Proof. Let $p^a := \bar{p} - \underline{p}, \underline{p}^r := p_0^r + k\underline{p}$, and $\alpha = \frac{T+2k(T_L-T_H)+k^2(T-2T_LT_H)}{4c_0^b(T-2)}E > 0$. Then we obtain the following:

$$\Pi^*_{arb} = \frac{(p^a)^2 E}{4c_0^b},$$
$$\Pi^*_{reg} = \frac{T_L(\underline{p}^r)^2 + T_H(\underline{p}^r + kp^a)^2}{2c_0^b}E,$$
$$\Pi^*_{stk} = \begin{cases} \Pi^*_{reg} + \frac{T_H((1-k)^+)^2}{4c_0^b(T_H-2)}(p^a)^2 E, & \text{if Case 1 } (x^*_H > x^*_L > 0), \\ \frac{E}{c_0^b}(\underline{p}^r + \frac{1+k}{2}p^a)^2, & \text{if Case 2 } (x^*_H = x^*_L = 0), \text{ and} \\ \Pi^*_{reg} + \alpha(p^a)^2, & \text{if Case 3 } (x^*_H = x^*_L > 0). \end{cases}$$

Here, cases 1 through 3 correspond to the three columns of the statement of the optimal stacking solution in Theorem A.1. The expressions for Π^*_{reg} and all three cases of Π^*_{stk} are of the form $a + bp^a + c(p^a)^2$ for constants $a, b, c > 0$, so it is immediate that Π^*_{arb}/Π^*_{reg} and Π^*_{arb}/Π^*_{stk} are strictly increasing in p^a. Similarly, for cases 1 and 3 we have $\Pi^*_{stk}/\Pi^*_{reg} = 1 + d(p^a)^2/\Pi^*_{reg}$ for some constant $d \geq 0$; the fact that $\Pi^*_{reg} = a + bp^a + c(p^a)^2$ for constants $a, b, c > 0$ implies that Π^*_{stk}/Π^*_{reg} is increasing in p^a for these two cases (strictly increasing except when $k \geq 1$ in Case 1).

For Case 2, we can establish that Π^*_{stk}/Π^*_{reg} is strictly increasing in p^a via differentiation, noting from the statement of Theorem A.1 that $x^*_H = x^*_L = 0$ requires $k \leq \frac{1}{T_H - 1} \leq 1$:

$$\frac{\partial(\Pi^*_{stk}/\Pi^*_{reg})}{\partial p^a} = \frac{\frac{E^2}{2(c_0^b)^2}(\underline{p}^r + \frac{1+k}{2}p^a)}{(\Pi^*_{reg})^2}\left(T(\underline{p}^r)^2 + k(\underline{p}^r)^2(T_L - T_H) + T_H k p^a \underline{p}^r \underbrace{(1-k)}_{\geq 0}\right) > 0.$$

□

Using Lemma A.3, we can also derive the relative performance of stacking when energy capacity is not binding.

Theorem A.2 (Upper bound on stacking's performance: Correlated prices)**.** *For fixed $T_L, T_H \geq 4, \underline{p}, p_0^r, k$, and non-binding energy capacity, $S = \frac{\Pi^*_{stk}}{\max(\Pi^*_{arb}, \Pi^*_{reg})}$ is up-down in $\bar{p}$; its maximum value is the value of $\frac{\Pi^*_{stk}}{\Pi^*_{reg}}$, evaluated at*

$$\bar{p} = \bar{p}_1 := \begin{cases} \frac{2T_H p_0^r k + \underline{p} + \underline{p}^r\sqrt{2T - 4k^2 T_L T_H}}{1 - 2k^2 T_H}, & \text{if } k \leq \frac{1}{\sqrt{2T_H}}, \\ \infty, & \text{otherwise}, \end{cases}$$

achieving value

$$\max S = \begin{cases} 1 + \frac{T+2k(T_L-T_H)-k^2(2T_LT_H-T)}{T-2}, & \text{if } k \le \frac{1}{T_H-1}, \\ 1 + \frac{T_H(1-k)^2}{T_H-2}, & \text{if } \frac{1}{T_H-1} \le k \le \frac{1}{\sqrt{2T_H}}, \text{ and} \\ 1 + \frac{((1-k)^+)^2}{2(T_H-2)k^2}, & \text{if } k \ge \frac{1}{\sqrt{2T_H}}. \end{cases}$$

This maximum value is up-down in k and maximized at $k = \frac{T_L-T_H}{2T_LT_H-T}$. For fixed T_L and T_H, S achieves a maximum value of $\max S = \frac{2T-2+\frac{(T_L-T_H)^2}{2T_LT_H-T}}{T-2}$.

Proof. For fixed $T_L, T_H, \underline{p}, p_0^r$ and k, we know from Lemma A.3 that $\frac{\Pi^*_{arb}}{\Pi^*_{reg}}$ is increasing in $\bar{p}$ from a minimum value of 0 for $\bar{p} = \underline{p}$ up to a limiting value of $\frac{1}{2T_Hk^2}$ as $\bar{p} \to \infty$. Therefore, when $k \ge \frac{1}{\sqrt{2T_H}}$, regulation-only is the best competitor; otherwise, there is a unique $\bar{p}$ at which the two competitors have equal profits, which can be easily computed as $\bar{p} = \bar{p}_1$.

When $k \le \frac{1}{T_H-1}$, then by Lemma A.3 S is up-down in $\bar{p}$, with a maximum value at $\bar{p} = \bar{p}_1$ (or equivalently, $\frac{p^a}{\underline{p}^r} = \frac{2T_Hk+\sqrt{2T-4k^2T_HT_L}}{1-2k^2T_H}$), which is the price at which $\Pi^*_{arb} = \Pi^*_{reg}$. At this point, stacking always has $x^*_H = x^*_L > 0$ (that is, $\frac{p^a}{\underline{p}^r} < \frac{T-2}{1-k(T_H-1)}$). To see this, we first note that $k \le \frac{1}{T_H-1} < \frac{T_H-1}{2T_H}$, which implies that

$$2k^2T_H < k(T_H-1).$$

Further, $2T_Hk+\sqrt{2T-4k^2T_HT_L} < T-2$ is equivalent to $f(T_H,T_L,k) := 4k^2T_HT-4T_H(T-2)k+(T-2)^2-2T > 0$. Then f decreases in k (for fixed T_L and T_H) and increases in T_L (for fixed T_H and k). Thus

$$f(T_H,T_L,k) \ge f(T_H,T_H,\frac{1}{T_H-1}) = [T_H-(T_H-1)^2][2T_H-(T_H-1)^2] > 0.$$

Then combining these leads to $\frac{2T_Hk+\sqrt{2T-4k^2T_HT_L}}{1-2k^2T_H} \le \frac{T-2}{1-k(T_H-1)}$.

Then from the argument at the beginning of the proof of Lemma A.3, we have:

$$\Pi^*_{stk} = \Pi^*_{reg} + \Pi^*_{arb} \cdot \frac{T+2k(T_L-T_H)-k^2(2T_LT_H-T)}{T-2},$$

which implies that

$$\max S = 1 + \frac{T+2k(T_L-T_H)-k^2(2T_LT_H-T)}{T-2}.$$

Since $\max S$ is up-down in k, it is maximized at $k = \frac{T_L-T_H}{2T_LT_H-T} (< \frac{1}{T_H-1})$, achieving the grand

maximum ratio:

$$\max S = \frac{2T - 2 + \frac{(T_L - T_H)^2}{2T_L T_H - T}}{T - 2}.$$

When $\frac{1}{T_H - 1} < k < \frac{1}{\sqrt{2T_H}}$, then again S is up-down in $\bar{p}$, with a maximum value at $\bar{p} = \bar{p}_1$. At this point, we have $x_H^* > x_L^* > 0$ from Theorem A.1. From the argument at the beginning of the proof of Lemma A.3, we have:

$$\Pi_{stk}^* = \Pi_{reg}^* + \Pi_{arb}^* \cdot \frac{T_H(1-k)^2}{(T_H - 2)},$$

and therefore S achieves maximum value $1 + \frac{T_H(1-k)^2}{T_H - 2}$, which is decreasing in k.

When $k \geq \frac{1}{\sqrt{2T_H}}$, the best competitor is always regulation-only; since $\frac{\Pi_{stk}^*}{\Pi_{reg}^*}$ is increasing in $\bar{p}$ from Lemma A.3, we know it is maximized at $\bar{p} = \infty$. Π_{stk}^* is in Case 1, so S is maximized at value $1 + \frac{((1-k)^+)^2}{2(T_H - 2)k^2}$, which is decreasing in k.

□

Theorem A.2 implies that the relative performance of stacking can improve under correlated prices compared to the uncorrelated setting ($\max S \to 2$ as $T \to \infty$).

Corollary A.2. *In the limit as $T \to \infty$, keeping T_H fixed,* $\max S \to 2 + \frac{1}{2T_H - 1}$.

It can be easily checked that Corollary A.2 remains consistent with $T_H = 2$ (with the same maximizer $k = \frac{T_L - T_H}{2T_L T_H - T}$, $\max S \to 2 + \frac{1}{2T_H - 1}$).

Theorem A.2 and Corollary A.2 assume non-binding energy capacity. With binding energy capacity, we can show that the maximum S ratio is still upper bounded by $\frac{2T - 2 + \frac{(T_L - T_H)^2}{2T_L T_H - T}}{T - 2}$.

Corollary A.3 (Upper bound on stacking's performance: Correlated prices)**.** $maxS \leq \frac{2T - 2 + \frac{(T_L - T_H)^2}{2T_L T_H - T}}{T - 2}$.

Proof. When energy capacity is binding for stacking but not for standalone arbitrage ($p^a < 2c_0^b$) or when $\Pi_{arb}^* < \Pi_{reg}^*$, the S ratio is upper-bounded by the S ratio under no energy constraint. Also, if $x_H^* > x_L^* > 0$ at optimality, then Corollary A.1 implies that $\Delta\Pi = \Pi_{stk}^* - [\Pi_{arb}^* + \Pi_{reg}^*] < 0$, concluding that the S ratio should decrease and become smaller than 2. Moreover, for $\frac{1}{T_H} \leq k < \frac{1}{T_H - 1}$, $p^a \geq 2c_0^b$ implies $x_H^* > x_L^* > 0$. As a result, the remainder of this proof will focus on the following two cases when standalone arbitrage is energy-constrained ($p^a \geq 2c_0^b$), $k \leq \frac{1}{T_H}$, and $\Pi_{arb}^* > \Pi_{reg}^*$ ($p^a - c_0^b > \frac{(\underline{p}^r)^2 T_L + (\bar{p}^r)^2 T_H}{2c_0^b}$):

- $x_H^* = x_L^* = 0$: if $k < \frac{1}{T_H}, \max(2c_0^b, c_0^b + \frac{T_L(\underline{p}^r)^2 + T_H(\bar{p}^r)^2}{2c_0^b}) \leq p^a \leq \frac{2c_0^b - T\underline{p}^r}{T_H k}$),

- $x_H^* = x_L^* > 0$: if $k < \frac{1}{T_H}, \max(2c_0^b, \frac{2c_0^b - T\underline{p}^r}{T_H k}, c_0^b + \frac{T_L(\underline{p}^r)^2 + T_H(\bar{p}^r)^2}{2c_0^b}) \le p^a \le \frac{2c_0^b}{T_H k}$.

In the first case, we claim

$$\frac{\Pi_{stk}^*}{\Pi_{arb}^*} = \frac{(p^a + \bar{p}^r + \underline{p}^r)E - c_0^b E}{p^a E - c_0^b E} = 1 + \frac{2\underline{p}^r + kp^a}{p^a - c_0^b} \le 2,$$

which is equivalent to show that

$$2\underline{p}^r + c_0^b \le (1-k)p^a.$$

From $p^a \le \frac{2c_0^b - T\underline{p}^r}{T_H k}$, it suffices to show $(1 - k + \frac{2T_H k}{T})p^a \ge \frac{T+4}{T}c_0^b$, which holds as follows:

$$\begin{aligned}(1 - k + \frac{2T_H k}{T})p^a &\ge (1 - k + \frac{2T_H k}{T}) \cdot 2c_0^b = \frac{T - (T_L - T_H)k}{T} \cdot 2c_0^b \ (\because p^a \ge 2c_0^b) \\ &> \frac{T - (T_L - T_H)\frac{1}{T_H}}{T} \cdot 2c_0^b = \frac{TT_H - (T_L - T_H)}{TT_H} \cdot 2c_0^b \ (\because k < \frac{1}{T_H}) \\ &\ge \frac{T+4}{T}c_0^b \ (\because T_H \ge 2).\end{aligned}$$

In the second case, we claim

$$\frac{\Pi_{stk}^*}{\Pi_{arb}^*} = \frac{\frac{(\underline{p}^r T_L + \bar{p}^r T_H)^2 E}{2c_0^b T} + (1 + \frac{(T_L - T_H)k}{T})p^a E - c_0^b(1 - \frac{2}{T})E}{p^a E - c_0^b E} \le \frac{2T - 2 + \frac{(T_L - T_H)^2}{2T_L T_H - T}}{T-2},$$

which is equivalent to show that

$$\begin{aligned}\frac{(T\underline{p}^r + T_H k p^a)^2}{2c_0^b T} \le &\frac{p^a[T^2 + k(2T_L - 2T_H - T_L^2 + T_H)^2 + \frac{T(T_L - T_H)^2}{2T_L T_H - T}]}{(T-2)T} \\ &+ \frac{c_0^b[-T^2 - 2T + 4 - \frac{T(T_L - T_H)^2}{2T_H T_L - T}]}{T(T-2)}.\end{aligned}$$

Since the left-hand-side is increasing in $\underline{p}^r$ for fixed p^a, while the right-hand-side is independent of $\underline{p}^r$, it suffices to show that the inequality holds at $\underline{p}^r = \frac{-kT_H p^a + \sqrt{(kT_H p^a)^2 - T[T_H(kp^a)^2 - 2p^a c_0^b + 2(c_0^b)^2]}}{T}$ (when $\Pi_{arb}^* = \Pi_{reg}^*$), which yields a quadratic in-

equality in terms of p^a:

$$T_L T_H k^2 (p^a)^2 + 2c_0^b [\frac{2T - k(T_L^2 - T_H^2 - 2T_L + 2T_H) + \frac{T(T_L - T_H)^2}{2T_H T_L - T}}{T-2}] p^a$$
$$- 2(c_0^b)^2 \frac{4T - 4 + \frac{T(T_L - T_H)^2}{2T_L T_H - T}}{T-2} \geq 0.$$

Then it is easy to algebraically check that the quadratic inequality holds for $2c_0^b \leq p^a \leq \frac{2c_0^b}{T_H k}$.

Combining these results conclude that the maximum ratio of S under a binding energy capacity is bounded by $\frac{2T-2+\frac{(T_L-T_H)^2}{2T_L T_H - T}}{T-2}$, which is the grand maximum from the non-binding case. □

A.3.2 Extension 2: Round-Trip Energy Efficiency (η^2)

In this section, we first derive the optimal actions and stopping threshold for standalone regulation with energy loss. Then we derive the optimal stacking actions.

As established in the proof of Theorem 2.3, the profit from the grid can be rewritten as a function of $A = T_H a_H$ and $X = T_L d_L + T_H d_H$, where $d_L := r_L - a_L$ and $d_H := r_H - a_H$ are the excess regulation from the grid's perspective in the low-price and high-price periods. Then the profit from the grid can be rewritten as $\tilde{p}^a A + \tilde{p}^x X$, for $\tilde{p}^a = \bar{p} - \frac{p}{\eta^2} + p^r(1 + \frac{1}{\eta^2})$ and $\tilde{p}^x = \frac{p^r}{2}(\frac{1}{\eta^2} + 1) - \frac{p}{2}(\frac{1}{\eta^2} - 1)$.

While it is straightforward that the degradation cost to provide some amount A of arbitrage and no excess regulation is always $\frac{c_0^b}{E} A^2/\eta^2$, the degradation cost to provide some positive amount of excess regulation $X > 0$ varies depending on how that excess regulation is distributed between the two periods.

Lemma A.4. *For fixed $A \geq 0$ and $X > 0$, the optimal degradation cost $deg(A, X)$ to provide this amount of service satisfies the following (Table A.3).*

Var.	Cases		
	$x_L > x_H = 0$	$x_L > x_H > 0$	$x_L = x_H > 0$
cond.	$\eta < \eta^*, X \leq c_2 A$	$\eta < \eta^*, X > c_2 A$	$\eta \geq \eta^*$
d_H^*	0	$\frac{T_H}{2T_L c_3}(X - c_2 A)$	X/c_1
$deg(A, X)$	$k_1 A^2 + k_2 AX + k_3 X^2$	$k_4 A^2 + k_5 AX + k_6 X^2$	$k_7 A^2 + k_8 AX + k_9 X^2$

Table A.3: Optimal degradation cost $deg(A, X)$.

Here, we define $\eta^* := \sqrt{1 - 2/T_L}$, $c_1 = \eta^2 T_L + T_H$, $c_2 = \frac{T_L(1-\eta^2)-2}{\eta^2}$, $c_3 = \frac{T_H^2}{4\eta^2} - \frac{T_H^2}{2} + \frac{T_H^2 \eta^2}{4} -$

$\frac{T_H^2}{2\eta^2 T_L} + \frac{T_H^2}{T_L} + \frac{T_H\eta^2}{2} > 0$,[8] $k_1 = \frac{c_0^b}{\eta^2 E}$, $k_2 = \frac{2c_0^b}{\eta^2 T_L E}$, $k_3 = \frac{c_0^b}{2\eta^2 T_L E}$, $k_4 = \frac{T_H^2(T_L-2)+T_H T_L^2\eta^4}{2\eta^4 c_3 T_L^2} \cdot \frac{c_0^b}{E}$, $k_5 = \frac{T_H^2(T_L-2)(1/\eta^2-1)+2T_H T_L\eta^2}{2\eta^2 c_3 T_L^2} \cdot \frac{c_0^b}{E}$, $k_6 = \frac{T_H^2(T_L-2)(1/\eta-\eta)^2+2T_H T_L\eta^2}{8\eta^2 c_3 T_L^2} \cdot \frac{c_0^b}{E}$, $k_7 = \frac{c_0^b}{\eta^2 E}$, $k_8 = \frac{2\eta^2+T_H(1-\eta^2)}{\eta^2 c_1} \cdot \frac{c_0^b}{E}$, and $k_9 = \frac{T_H^2(1-\eta^2)^2+2\eta^2 T_H(2-\eta^2)+2\eta^4 T_L}{4\eta^2 c_1^2} \cdot \frac{c_0^b}{E}$. All k_i constants are strictly positive.

Proof. The degradation cost function is defined as:

$$\frac{c_0^b}{E}\left(D^2 + 2D\max(x_L, x_H) + \frac{T_L}{2}x_L^2 + \frac{T_H}{2}x_H^2\right).$$

Note that $x_L = d_L/\eta$ and $x_H = d_H\eta$, and further that $d_L = \frac{X - T_H d_H}{T_L}$, due to the fact that we need to provide the full excess regulation X across the two regions. $x_L \geq x_H$ when $d_H \leq X/c_1$, while $x_L < x_H$ when $d_H > X/c_1$. Noting that $D = \frac{T_H}{2}d_H(\frac{1}{\eta} - \eta) + \frac{A}{\eta}$, the degradation can be expressed as a function of d_H. When $d_H > X/c_1$ and therefore $x_H > x_L$, degradation costs are always increasing in d_H:

$$\begin{aligned}
deg(d_H) &= \frac{c_0^b}{E}\left(D^2 + 2Dx_H + \frac{T_L}{2}x_L^2 + \frac{T_H}{2}x_H^2\right), \\
deg'(d_H) &= \frac{c_0^b}{E}\left(2D(D' + x'_H) + 2D'x_H + T_L x_L x'_L + T_H x_H x'_H\right) \\
&= \frac{c_0^b}{E}\left(2D(D' + x'_H) + \frac{T_H}{\eta}(x_H - x_L)\right) > 0.
\end{aligned}$$

As a result, we focus on optimizing over $d_H \in [0, X/c_1]$, where $x_L \leq x_H$. In this region, the degradation takes the form

$$\begin{aligned}
deg(d_H) &= \frac{c_0^b}{E}\left(D^2 + 2Dx_L + \frac{T_L}{2}x_L^2 + \frac{T_H}{2}x_H^2\right) \\
&= \frac{c_0^b}{E}\left((\frac{A^2}{\eta^2} + \frac{2AX}{\eta^2 T_L} + \frac{X^2}{2\eta^2 T_L}) + \underbrace{\frac{T_H}{T_L}(c_2 A - X)}_{:=\beta} d_H + c_3 d_H^2\right).
\end{aligned}$$

The degradation function is strictly convex in d_H, meaning the degradation cost will be minimized at endpoint $d_H = X/c_1$ iff the degradation function is non-increasing at that

[8] $c_3 = \frac{T_H^2}{4}(1/\eta - \eta)^2 + \frac{T_H^2}{T_L}(1 - \frac{1}{2\eta^2}) + \frac{T_H\eta^2}{2}$. This is clearly positive as long as $1 - \frac{1}{2\eta^2} \geq 0$. If $1 - \frac{1}{2\eta^2} < 0$, then c_3 is minimized at $T_L = T_H$, taking value $c_3 = \frac{T_H^2}{4}(1/\eta - \eta)^2 + \frac{T_H}{2}(\eta^2 + 2 - 1/\eta^2) = \frac{T_H}{4}((T_H - 2)(1/\eta - \eta)^2 + 4\eta^2) > 0$.

point. The derivative at that point is

$$\frac{c_0^b}{E}\left(\beta + \frac{2Xc_3}{c_1}\right) = \frac{c_0^b}{E}\underbrace{\left(\frac{T_H^2}{2c_1}X(\frac{1}{\eta^2}-1) + \frac{T_H}{\eta^2}A\right)}_{>0}\left(1 - \frac{2}{T_L} - \eta^2\right).$$

We conclude that $d_H^* = X/c_1$ iff $\eta \geq \eta^* := \sqrt{1-2/T_L}$.

When $\eta < \eta^*$, then $d_H^* = 0$ iff the degradation cost is non-decreasing in d_H at $d_H = 0$. This is equivalent to $\beta \geq 0$, or $X \leq c_2 A$. Otherwise, d_H^* lies between 0 and X/c_1; the first-order condition tells us in this case that $d_H^* = -\frac{\beta}{2c_3}$. The k_i constants follow by evaluating $deg(d_H^*)$ for each of the three cases; by inspection all are strictly positive. □

A.3.2.1 Optimal Standalone Regulation with Energy Loss

From Lemma A.4, we state the optimal standalone regulation under energy loss.

Theorem A.3. *Optimal standalone regulation under energy loss provides no service for* $\eta < \eta_{reg} := \sqrt{\frac{(\underline{p}-p^r)^+}{\underline{p}+p^r}}$*, and otherwise satisfies the following:*

Var.	Cases	
	$x_L^* = x_H^* > 0$	$x_L^* > x_H^* > 0$
cond.	$\eta^* \leq \eta \leq 1$	$\eta_{reg} \leq \eta < \eta^*$
X^*	$\tilde{p}^x/(2k_9)$	$\tilde{p}^x/(2k_6)$

for $\eta^* := \sqrt{1-2/T_L}$ and for constants $k_6, k_9 > 0$ from the statement of Lemma A.4.

Table A.4: Optimal standalone regulation.

Proof. For standalone regulation ($A = 0$), Lemma A.4 establishes that the optimal degradation cost to provide fixed excess regulation quantity X is $deg(0, X) = cX^2$, where constant c takes value k_9 for $\eta \geq \eta^*$ (the $x_L = x_H = 0$ case) and takes value k_6 for $\eta < \eta^*$ (the $x_L > x_H > 0$ case). Then the optimal profit for fixed X is $\Pi(X) = \tilde{p}^x X - cX^2$, where $\tilde{p}^x \geq 0$ iff $\eta \geq \eta_{reg}$ (see Theorem 2.3). Then from the first-order conditions $X^* = (\tilde{p}^x)^+/(2c)$. □

A.3.2.2 Optimal Stacking with Energy Loss

Optimal structure. We first state the optimal structure of stacking under energy loss.

Theorem A.4. *Optimal stacking under energy loss provides no service* ($A^* = X^* = 0$) *for* $\eta < \eta_{stk} := \sqrt{\frac{(\underline{p}-p^r)^+}{\overline{p}+p^r}}$*, provides free regulation only* ($A^* = \frac{\eta^2 \tilde{p}^a E}{2c_0^b}$, $X^* = 0$) *for* $\eta_{stk} \leq \eta < \eta_{reg} := \sqrt{\frac{(\underline{p}-p^r)^+}{\underline{p}+p^r}}$*, and otherwise satisfies the following (Table A.5).*

Var.	Cases	
	(1a) $x_L^* = x_H^* > 0$, $A^* > 0$	(1b) $x_L^* = x_H^* > 0$, $A^* = 0$
cond.	$\eta \geq \eta^*$, $d_1\tilde{p}^x < p^a \leq d_2\tilde{p}^x$	$\eta \geq \eta^*$, $p^a \leq d_1\tilde{p}^x$
A^*	$\min(\frac{c_1^2E^2}{2(T-2)}(2k_9\tilde{p}^a - k_8\tilde{p}^x)/(c_0^b)^2, \eta E)$	0
X^*	$(\tilde{p}^x - k_8A^*)/(2k_9)$	$\tilde{p}^x/(2k_9)$
	(2a) $x_L^* > x_H^* > 0$, $A^* > 0$	(2b) $x_L^* > x_H^* > 0$, $A^* = 0$
cond.	$\eta < \eta^*$, $d_3\tilde{p}^x < p^a \leq d_4\tilde{p}^x$	$\eta < \eta^*$, $p^a \leq d_3\tilde{p}^x$
A^*	$\min(\frac{\eta^2c_3T_L^2E^2}{T_H(T_L-2)}(2k_6\tilde{p}^a - k_5\tilde{p}^x)/(c_0^b)^2, \eta E)$	0
X^*	$(\tilde{p}^x - k_5A^*)/(2k_6)$	$\tilde{p}^x/(2k_6)$
	(3) $x_L^* > x_H^* = 0$	(4) $x_L^* = x_H^* = 0$
cond.	$\eta < \eta^*, d_4\tilde{p}^x < p^a \leq d_5\tilde{p}^x$	$\tilde{p}^x < \begin{cases} \min(p^a/d_2, \eta E k_8), & \text{if } \eta \geq \eta^* \\ \min(p^a/d_5, \eta E k_2), & \text{if } \eta < \eta^* \end{cases}$
A^*	$\min(\frac{\eta^2T_LE}{2(T_L-2)}(\tilde{p}^a - 2\tilde{p}^x)/c_0^b, \eta E)$	$\min(\eta^2\tilde{p}^aE/(2c_0^b), \eta E)$
X^*	$(\tilde{p}^x - k_2A^*)/(2k_3)$	0

Table A.5: Optimal stacking with energy loss.

Here, we define

$$\eta^* := \sqrt{1 - 2/T_L},$$

$$d_1 = \frac{2T_H\eta^2(1-\eta^2)(T-2)}{T_H^2(1-\eta^2)^2 + 2\eta^2T_H(2-\eta^2) + 2\eta^4T_L},$$

$$d_2 = \begin{cases} \frac{2\eta^2(T-2)}{2\eta^2+T_H(1-\eta^2)} & \text{if } \eta E k_8 \leq \tilde{p}^x \\ \infty & \text{if } \eta E k_8 > \tilde{p}^x \end{cases},$$

$$d_3 = \frac{2T_H(T_L-2)(\eta^2-\eta^4)}{2T_L\eta^4 + T_H(T_L-2)(1-\eta^2)^2},$$

$$d_4 = \begin{cases} \frac{2\eta^2}{1-\eta^2} & \text{if } \tilde{p}^x \leq \frac{c_0^b(T_L-2)(1-\eta^2)}{\eta^3T_L} \\ \infty & \text{if } \tilde{p}^x > \frac{c_0^b(T_L-2)(1-\eta^2)}{\eta^3T_L} \end{cases},$$

$$d_5 = \begin{cases} T_L - 2 & \text{if } \tilde{p}^x \leq \eta E k_2 \\ \infty & \text{if } \eta E k_2 \leq \tilde{p}^x \leq \frac{c_0^b(T_L-2)(1-\eta^2)}{\eta^3T_L} \end{cases},$$

and constants k_i and c_i from Lemma A.4.

Proof. As established in Theorem 2.3, $\tilde{p}^a, \tilde{p}^x < 0$ when $\eta < \eta_{stk}$, so no service will be provided in this case. Further, when $\eta_{stk} \leq \eta < \eta_{reg}$ then $\tilde{p}^a \geq 0, \tilde{p}^x < 0$, so only free regulation will be used ($X^* = 0$). As a result, we focus the proof of this theorem on the case where $\eta \geq \eta_{reg}$, meaning $\tilde{p}^a, \tilde{p}^x \geq 0$.

In the case of $\eta \geq \eta^*$, Lemma A.4 establishes that $x_L^* = x_H^*$, and the optimal degradation cost is $k_7A^2 + k_8AX + k_9X^2$ for $k_7, k_8, k_9 > 0$, which yields profit function

$$\Pi(A, X) = (\tilde{p}^a A - k_7 A^2) + (\tilde{p}^x - k_8 A)X - k_9 X^2.$$

For fixed A, it is immediate that $X^* = (\tilde{p}^x - k_8 A)^+/(2k_9)$, yielding the following optimal profit as a function of A:

$$\Pi(A) = \begin{cases} \frac{(\tilde{p}^x)^2}{4k_9} + (\tilde{p}^a - \frac{k_8\tilde{p}^x}{2k_9})A + (\frac{k_8^2}{4k_9} - k_7)A^2, & \text{if } A < \tilde{p}^x/k_8, \text{ and} \\ \tilde{p}^a A - k_7 A^2, & \text{if } A \geq \tilde{p}^x/k_8. \end{cases}$$

Noting that $\frac{k_8^2}{4k_9} - k_7 = \frac{-(T-2)}{2k_9c_1^2}(\frac{c_0^b}{E})^2 < 0$, we conclude that $\Pi(A)$ is a strictly concave function with a continuous, piecewise linear, decreasing derivative. Given the energy constraint $A \leq \eta E$ and derivatives

$$\Pi'(0) = \tilde{p}^a - (2 + d_1)\tilde{p}^x \text{ and}$$
$$\Pi'(\tilde{p}^x/k_8) = \tilde{p}^a - (2 + d_2)\tilde{p}^x,$$

it is clear that $A^* = 0$ when $\tilde{p}^a \leq (2 + d_1)\tilde{p}^x$, $A^* \in (0, \tilde{p}^x/k_8)$ when $(2 + d_1)\tilde{p}^x < \tilde{p}^a$ and $\tilde{p}^a < (2 + d_2)\tilde{p}^x$ or $\eta E \leq \tilde{p}^x/k_8$, and $A^* \geq \tilde{p}^x/k_8$ and therefore $X^* = 0$ when $\tilde{p}^a \geq (2 + d_2)\tilde{p}^x$ and $\eta E \geq \tilde{p}^x k_8$. Noting that $\tilde{p}^a = 2\tilde{p}^x + p^a$, condition $\tilde{p}^a \leq (2+c)\tilde{p}^x$ is equivalent to $p^a \leq c\tilde{p}^x$ for any c. In each region, the optimal A^* follows immediately from the first-order conditions and the energy constraint $A \leq \eta E$.

In the case of $\eta < \eta^*$ (which implies $T_L > 2$), Lemma A.4 establishes two separate cases for $x_L^* > x_H^*$, which differ in whether $x_H^* = 0$. These cases combine to yield profit function

$$\Pi(A, X) = \begin{cases} (\tilde{p}^a A - k_1 A^2) + (\tilde{p}^x - k_2 A)X - k_3 X^2, & \text{if } X \leq c_2 A, \text{ and} \\ (\tilde{p}^a A - k_4 A^2) + (\tilde{p}^x - k_5 A)X - k_6 X^2, & \text{if } X > c_2 A. \end{cases}$$

For fixed A, $\Pi(A, X)$ is a strictly concave function of X with a continuous, piecewise linear, decreasing derivative, with derivative value $\tilde{p}^x - \frac{c_0^b(T_L-2)(1-\eta^2)}{\eta^4 T_L E}A$ at $X = c_2 A$. From this characterization, it follows that $X^* = (\tilde{p}^x - k_2 A)^+/(2k_3)$ when $\tilde{p}^x - \frac{c_0^b(T_L-2)(1-\eta^2)}{\eta^4 T_L E}A \leq 0$, and otherwise $X^* = (\tilde{p}^x - k_5 A)/(2k_6)$. This yields the following optimal profit as a function of A:

$$\Pi(A) = \begin{cases} \frac{(\tilde{p}^x)^2}{4k_6} + (\tilde{p}^a - \frac{k_5\tilde{p}^x}{2k_6})A + (\frac{k_5^2}{4k_6} - k_4)A^2, & \text{if } A < \frac{\eta^4 T_L E}{c_0^b(T_L-2)(1-\eta^2)}\tilde{p}^x, \\ \frac{(\tilde{p}^x)^2}{4k_3} + (\tilde{p}^a - \frac{k_2\tilde{p}^x}{2k_3})A + (\frac{k_2^2}{4k_3} - k_1)A^2, & \text{if } \frac{\eta^4 T_L E}{c_0^b(T_L-2)(1-\eta^2)}\tilde{p}^x \le A < \tilde{p}^x/k_2, \text{ and} \\ \tilde{p}^a A - k_1 A^2, & \text{if } A \ge \tilde{p}^x/k_2. \end{cases}$$

Noting that $\frac{k_2^2}{4k_3} - k_1 = \frac{-(T_L-2)}{\eta^2 T_L} \cdot \frac{c_0^b}{E} < 0$ and $\frac{k_5^2}{4k_6} - k_4 = \frac{-2(T_L-2)}{T_H(T_L-2)(1/\eta-\eta)^2+2T_L\eta^2} \cdot \frac{c_0^b}{E} < 0$, $\Pi(A)$ is a strictly concave function with a continuous, piecewise linear, decreasing derivative. Given the energy constraint and derivatives

$$\begin{aligned} \Pi'(0) &= \tilde{p}^a - (2+d_3)\tilde{p}^x, \\ \Pi'(\frac{\eta^4 T_L E}{c_0^b(T_L-2)(1-\eta^2)}\tilde{p}^x) &= \tilde{p}^a - (2+d_4)\tilde{p}^x, \text{ and} \\ \Pi'(\tilde{p}^x/k_2) &= \tilde{p}^a - (2+d_5)\tilde{p}^x, \end{aligned}$$

it is clear that $A^* = 0$ when $p^a \le d_3\tilde{p}^x$, $A^* \in (0, \frac{\eta^4 T_L E}{c_0^b(T_L-2)(1-\eta^2)}\tilde{p}^x)$ and therefore $x_L^* > x_H^* > 0$ when $d_3\tilde{p}^x < p^a$ and $p^a < d_4\tilde{p}^x$ or $\eta E \le \frac{\eta^4 T_L E}{c_0^b(T_L-2)(1-\eta^2)}\tilde{p}^x$, $A^* \in [\frac{\eta^4 T_L E}{c_0^b(T_L-2)(1-\eta^2)}\tilde{p}^x, \tilde{p}^x/k_2)$ and therefore $x_L^* > x_H^* = 0$ when $d_4\tilde{p}^x \le p^a$, $\eta E \ge \frac{\eta^4 T_L E}{c_0^b(T_L-2)(1-\eta^2)}\tilde{p}^x$, and $p^a < d_5\tilde{p}^x$ or $\eta E \le \tilde{p}^x/k_2$, and $A^* \ge \tilde{p}^x/k_2$ and therefore $x_L^* = x_H^* = 0$ when $p^a \ge d_5\tilde{p}^x$ and $\eta E > \tilde{p}^x/k_2$. In each region, the optimal A^* follows immediately from the first-order conditions and the energy constraint $A \le \eta E$.

□

Note that $d_1 \le \bar{d}$ when $\eta \ge \eta^*$ and $d_2 \le \bar{d}$ when $\eta \le \eta^*$. We now prove that the most of the main properties remain consistent with the round-trip energy efficiency $\eta^2 < 1$ ($\frac{R^*}{A^*} := \infty$ for $A^* = 0$).

Corollary A.4. *With the round-trip energy efficiency $\eta^2 \in [0, 1)$, the following hold for stacking:*

- *R^* increases in p^a when $\tilde{p}^x < \begin{cases} \min(p^a/d_2, \eta E k_8), & \eta \ge \eta^* \\ \min(p^a/d_5, \eta E k_2), & \eta < \eta^* \end{cases}$, $p^a \le -\underline{p}(1-\frac{1}{\eta^2}) - p^r(1+\frac{1}{\eta^2}) + 2c_0^b/\eta$,*
- *A^* increases in p^r when $\tilde{p}^x < \begin{cases} \min(p^a/d_2, \eta E k_8), & \eta \ge \eta^* \\ \min(p^a/d_5, \eta E k_2), & \eta < \eta^* \end{cases}$, $p^a \le -\underline{p}(1-\frac{1}{\eta^2}) - p^r(1+\frac{1}{\eta^2}) + 2c_0^b/\eta$,*
- *$\frac{R^*}{A^*} \ge 2$,*

- $x_L^* = x_H^*$ *when* $\eta \geq \eta^*$ *or* $\tilde{p}^x < \min(p^a/d_5, \eta E k_2)$,
- $A^* > 0$ *when* $\eta > \eta^*, p^a > d_1\tilde{p}^x$ *or* $\eta < \eta^*, p^a > d_3\tilde{p}^x$,
- $A_{stk}^* > A_{arb}^*$ *when* $\eta_{stk} < \eta < \eta_{arb}$ *or* $\frac{\bar{p}\eta^2 - \underline{p}}{2c_0^b} < \eta$, $p^a > \begin{cases} \max(\bar{p}_1 - \underline{p}, d_1\tilde{p}^x), & \eta > \eta^* \\ \max(\bar{p}_2 - \underline{p}, d_2\tilde{p}^x), & \eta < \eta^* \end{cases}$, *where*

$$\bar{p}_1 = \frac{(\frac{1}{\eta^2} - \eta^2)T_H(T-2)p^r - [(\frac{1}{\eta} - \eta)^2 T_H(T_L - 2) - 4T_H(1-\eta^2) - 2T\eta^2 + 2T - 4]\underline{p}}{2[2\eta^2 - 2T_H(\eta^2 - 1) + \frac{T_H^2}{2}(\frac{1}{\eta} - \eta)^2]},$$
$$\bar{p}_2 = \frac{(\frac{1}{\eta^2} - \eta^2)T_H(T_L - 2)p^r - 2[T_L - 2 - T_L\eta^2]\underline{p}}{4\eta^2 + (T_L - 2)T_H(\frac{1}{\eta} - \eta)^2},$$

- $R_{stk}^* > R_{reg}^*$ *when* $\tilde{p}^x < \begin{cases} \min(p^a[\frac{c_0^b}{2k_9\eta^2 E} - 2]^{-1}, 4k_9\eta E), & \eta \geq \eta^* \\ \min(p^a[\frac{c_0^b}{2k_6\eta^2 E} - 2]^{-1}, 4k_6\eta E), & \eta < \eta^* \end{cases}$,
- *Positive cost-saving synergy when one of the following holds:*
  - $\eta \geq \eta^*, d_1\tilde{p}^x < p^a$
  - $\eta < \eta^*, \tilde{p}^x < \min(p^a/d_5, \eta E k_2)$
  - $\eta < \eta^*, d_3\tilde{p}^x < p^a < d_4\tilde{p}^x, \eta^2 T + 4T_H\eta + T_H(T_L - 2)\eta_1(\frac{\eta_1}{2} - 2) > 0$
  - $\eta < \eta^*, d_4\tilde{p}^x < p^a \leq d_5\tilde{p}^x$, *and* $\frac{-s_1 s_2}{s_1 s_3 + s_4}p' < p^a < \frac{2(T_L-2)c_0^b}{\eta T_L}$ *or* $s_5 > s_6 p', p^a > \frac{2(T_L-2)c_0^b}{\eta T_L}$

  where $s_1 = \frac{\eta^2 T_L E}{2c_0^b(T_L-2)}, s_2 = \frac{\eta_2 E}{8c_0^b}(\eta_1 - 4), s_3 = \frac{\eta(\eta+4)E}{4c_0^b(T_L-2)}, s_4 = \frac{T_H}{2}(\frac{\eta^2 T_L E}{2c_0^b T_H(T_L-2)})^2, s_5 = 4c_0^b(T\eta + 4T_H), s_6 = T_L T_H \eta_2(4 - \eta_1)$, *and* $p' = p^r - \frac{\eta_1}{\eta_2}\underline{p}$.

Proof. Clearly, the first two properties only holds when energy capacity is not binding. Also, from (2.17) – (2.18), $R^* = (A^* + \frac{X^*}{2}) \cdot (1 + \frac{1}{\eta^2})$. Then those properties are direct from restating the unconstrained optimal A^* and R^* for each region in the form $c_1\bar{p} + c_2\underline{p} + c_3 p^r$ and signing the region-specific coefficients:

- $A_{1a}^* = [\frac{T\eta^2 + 2T_H\eta_1\eta + \frac{T_H^2}{2}\eta_1^2}{2(T-2)\frac{c_0^b}{E}}]\bar{p} + [\frac{\eta_1^2 T_H E}{4c_0^b} - \frac{T\eta^2 + 2T_H\eta_1\eta + \frac{T_H^2}{2}\eta_1^2}{2(T-2)\frac{c_0^b}{E}}]\underline{p} + [-\frac{\eta_1\eta_2 T_H E}{4c_0^b}]p^r$ $(c_1 > 0, c_2 < 0, c_3 < 0)$ and $R_{1a}^* = \frac{[-T_H\eta_1\eta_2]\bar{p} + [-T_L\eta_1\eta_2]\underline{p} + [\eta_2^2 T]p^r}{4\frac{c_0^b}{E}}$ $(c_1 < 0, c_2 < 0, c_3 > 0)$;
- $A_{1b}^* = 0$ and $R_{1b}^* = -\frac{\eta_1(\frac{1+\eta^2}{2})^2(T_L + \frac{T_H}{\eta^2})^2}{\frac{c_0^b}{E}\eta_2[\frac{(T_H\eta_1)^2}{2} + 2T_H\eta_1\eta + T\eta^2]}\underline{p} + \frac{(\frac{1+\eta^2}{2})^2(T_L + \frac{T_H}{\eta^2})^2}{c^b[\frac{(T_H\eta_1)^2}{2} + 2T_H\eta_1\eta + T\eta^2]}p^r$ $(c_1 = 0, c_2 < 0, c_3 > 0)$;

- $A^*_{2a} = [\frac{T_L\eta^2 E}{2c_0^b(T_L-2)} + \frac{\eta_1^2 T_H E}{4c_0^b}]\bar{p} + [-\frac{T_L\eta^2 E}{2c_0^b(T_L-2)}]\underline{p} + [\frac{-\eta_1\eta_2 T_H E}{4c_0^b}]p^r$ $(c_1 > 0, c_2 < 0, c_3 < 0)$ and $R^*_{2a} = \frac{[-T_H\eta_1\eta_2]\bar{p}+[-T_L\eta_1\eta_2]\underline{p}+[\eta_2^2 T]p^r}{4\frac{c_0^b}{E}}$ $(c_1 < 0, c_2 < 0, c_3 > 0)$;
- $A^*_{2b} = 0$ and $R^*_{2b} = -\frac{\eta_1\eta_2 T_L E}{4c_0^b}[\frac{\frac{T_H T_L}{2}\eta_1^2+T\eta^2-T_H\eta_1^2}{\frac{T_H T_L}{2}\eta_1^2+T_L\eta^2-T_H\eta_1^2}]\underline{p} + \frac{\eta_2^2 T_L E}{4c_0^b}[\frac{\frac{T_H T_L}{2}\eta_1^2+T\eta^2-T_H\eta_1^2}{\frac{T_H T_L}{2}\eta_1^2+T_L\eta^2-T_H\eta_1^2}]p^r$ $(c_1 = 0, c_2 < 0, c_3 > 0)$;
- $A^*_3 = \frac{\eta^2 T_L E}{2(T_L-2)c_0^b}(\bar{p}-\underline{p})$ and $R^*_3 = \frac{\eta^2 T_L E}{4c_0^b}[-(\frac{1}{\eta^2}-1)\underline{p} + p^r(1+\frac{1}{\eta^2})](1+\frac{1}{\eta^2})$ $(A^*_3 : c_1 > 0, c_2 < 0, c_3 = 0$ and $R^*_3 : c_1 = 0, c_2 < 0, c_3 > 0)$;
- $A^*_4 = \frac{\eta^2\bar{p}-\underline{p}+(1+\eta^2)p^r}{2\frac{c_0^b}{E}}$ $(c_1 > 0, c_2 < 0, c_3 > 0)$ and $R^*_4 = \frac{\eta^2\bar{p}-\underline{p}+(1+\eta^2)p^r}{2\frac{c_0^b}{E}}(1+\frac{1}{\eta^2})$ $(c_1 > 0, c_2 < 0, c_3 > 0)$,

where $\eta_1 = \frac{1}{\eta} - \eta$ and $\eta_2 = \frac{1}{\eta} + \eta$.

Then A^* (R^*) increases in p^r (p^a) if and only if the energy capacity is not binding and we are in Region 4, i.e., $\tilde{p}^x < \begin{cases} \min(p^a/d_2, \eta E k_8), & \eta \geq \eta^* \\ \min(p^a/d_5, \eta E k_2), & \eta < \eta^* \end{cases}$, $p^a \leq -\underline{p}(1-\frac{1}{\eta^2}) - p^r(1+\frac{1}{\eta^2}) + 2c_0^b/\eta$.

From Theorem A.4, $x^*_L = x^*_H$ and $A^* > 0$ are direct. Also, $R^* = (A^* + \frac{X^*}{2}) \cdot (1+\frac{1}{\eta^2})$ and $\frac{R^*}{A^*} \geq 1 + \frac{1}{\eta^2} \geq 2$, which implies that the ratio always strictly exceeds 2 when $\eta < 1$.

$A^*_{stk} > A^*_{arb} = \min(\frac{\bar{p}\eta^2-\underline{p}}{2c_0^b}E, \eta E)$: Clearly, this property only holds when standalone arbitrage is unconstrained ($A^*_{stk} < \eta E$, or equivalently, $\frac{\bar{p}\eta^2-\underline{p}}{2c_0^b} < \eta$). When stacking is energy-constrained and standalone arbitrage is not, the property always holds. Thus, we now focus on unconstrained solutions for both stacking and standalone arbitrage ($A^*_{stk},\ A^*_{arb} < \eta E$). It is obvious that $A^*_4 \geq A^*_{arb}$ holds. Also, $A^*_3 > A^*_{arb} \Leftrightarrow 2\eta^2\bar{p} > [\eta^2 T_L - (T_L-2)]\underline{p}$ always holds since $\eta^2 T_L - (T_L-2) < 0$ when $\eta < \eta^*$. We now see the remaining cases (1a) and (2a). For Case (1a) ($\eta \geq \eta^*, d_1\tilde{p}^x < p^a$ are required), $A^*_{1a} > A^*_{arb} \Leftrightarrow 2[2\eta^2 + 2T_H\eta_1\eta + \frac{T_H^2}{2}\eta_1^2]\bar{p} + [\eta_1^2 T_H(T_L-2) - 4T_H\eta_1\eta - 2T\eta^2 + 2T - 4]\underline{p} > \eta_1\eta_2 T_H(T-2)p^r$. For Case (2a) ($\eta < \eta^*, d_3\tilde{p}^x < p^a$ are required), $A^*_{2a} > A^*_{arb} \Leftrightarrow [4\eta^2 + (T_L-2)T_H(\frac{1}{\eta}-\eta)^2]\bar{p} + 2[T_L - 2 - T_L\eta^2]\underline{p} > (\frac{1}{\eta^2} - \eta^2)T_H(T_L-2)p^r$. Combining these, we have necessary and sufficient conditions for $A^*_{stk} > A^*_{arb}$.

$R^*_{stk} > R^*_{reg}$: When $\eta \geq \eta^*$, we compare R^*_{1a} and R^*_4 with $R^*_{reg} = R^*_{1b}$ (subscripts represent corresponding cases). Then $R^*_{stk} > R^*_{reg}$ holds if and only if

$$R^*_{1a} > R^*_{reg} \Leftrightarrow (A^*_{1a} + \frac{X^*_{1a}}{2})(1+\frac{1}{\eta^2}) > \frac{\tilde{p}^x}{4k_9}(1+\frac{1}{\eta^2}) \Leftrightarrow 4k_9 > k_8,$$
$$R^*_4 > R^*_{reg} \Leftrightarrow A^*_4 > \frac{\tilde{p}^x}{4k_9} \Leftrightarrow \min(\frac{\eta^2\tilde{p}^a E}{2c_0^b}, \eta E) > \frac{\tilde{p}^x}{4k_9}.$$

It can be checked that $4k_9 \leq k_8$, so the first set is empty. Since $4k_9\eta E < k_8\eta E$, the property holds for $\eta > \eta^*$ if and only if $\tilde{p}^a > \frac{c_0^b \tilde{p}^x}{2\eta^2 E k_9},\ \tilde{p}^x < 4k_9\eta E$.

When $\eta_{reg} \leq \eta < \eta^*$, we compare R_{2a}^*, R_3^*, and R_4^* with $R_{reg}^* = R_{2b}^*$ and obtain the following:

$$
\begin{aligned}
R_{2a}^* > R_{reg}^* &\Leftrightarrow (A_{2a}^* + \frac{X_{2a}^*}{2})(1 + \frac{1}{\eta^2}) > \frac{\tilde{p}^x}{4k_6}(1 + \frac{1}{\eta^2}) \Leftrightarrow 4k_6 > k_5, \\
R_3^* > R_{reg}^* &\Leftrightarrow A_3^*(1 - \frac{k_2}{4k_3}) > \frac{\tilde{p}^x}{4}(\frac{1}{k_6} - \frac{1}{k_3}), \\
R_4^* > R_{reg}^* &\Leftrightarrow A_4^* > \frac{\tilde{p}^x}{4k_6} \Leftrightarrow \min(\frac{\eta^2 \tilde{p}^a E}{2c_0^b}, \eta E) > \frac{\tilde{p}^x}{4k_6}.
\end{aligned}
$$

It can be checked that the first two sets are empty. Since $4k_6\eta E < k_2\eta E$, the property holds for $\eta < \eta^*$ if and only if $\tilde{p}^a > \frac{c_0^b \tilde{p}^x}{2\eta^2 E k_6},\ \tilde{p}^x < 4k_6\eta E$.

Positive cost saving: Clearly, we have positive cost-saving synergy for $\eta \geq \eta^*, p^a > d_1\tilde{p}^x$. There is no cost-saving synergy in Cases (1b) and (2b) since standalone regulation is optimal.

We now check the remaining of Cases (2a) and (3). For each case, we can state the optimal actions in terms of p', a_H^*, and $A^* = T_H \cdot a_H^*$. From Proposition 2.2, then the cost saving for Case (2a) becomes:

$$
\begin{aligned}
Cost - saving &= \frac{c_0^b}{E} \cdot A^* \cdot [\frac{a_L^* + a_H^*}{2} - (x_L^* - x_H^*)] && \text{(A.7)} \\
&= \underbrace{\frac{c_0^b}{E} A^* \cdot C_{2a} \cdot (a_H^* + \frac{\eta_1\eta_2 E}{4c_0^b} p')}_{>0} \cdot R_{2a}, && \text{(A.8)}
\end{aligned}
$$

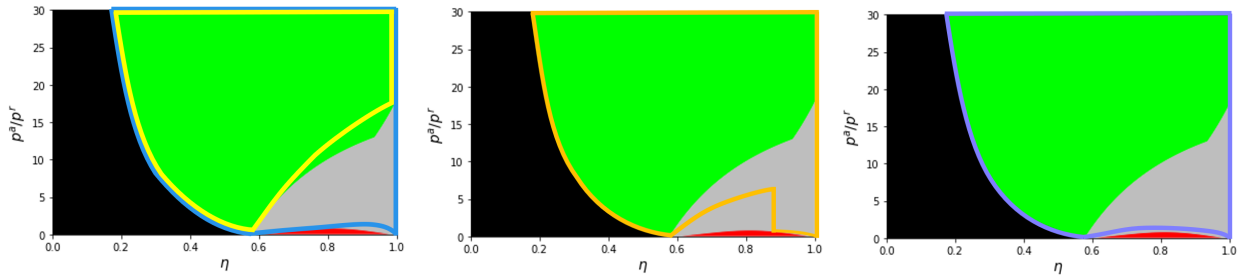
where $C_{2a} > 0$ is some positive constant and $R_{2a} := \eta^2 T + 4T_H\eta + T_H(T_L - 2)\eta_1(\frac{\eta_1}{2} - 2)$. Thus, we have positive cost saving if and only if $R_{2a} > 0$.

Similarly, the cost saving for Case (3) becomes:

$$
\begin{aligned}
Cost - saving &= \frac{c_0^b}{E} \cdot [A^*(\frac{a_L^*}{2} - x_L^*) + \frac{T_H}{2}(r_H^*)^2] && \text{(A.9)} \\
&= \underbrace{\frac{c_0^b}{E} \cdot C_3}_{>0} \cdot \underbrace{[a_H^* - \frac{T_L\eta}{T\eta + 4T_H} \cdot \frac{\eta_2(4 - \eta_1)E}{4c_0^b} p']}_{:= R_3}, && \text{(A.10)}
\end{aligned}
$$

where $C_3 > 0$ is some positive constant. Then signing R_3 leads to:

$$
\operatorname{sgn}(R_3) > 0 \Leftrightarrow \begin{cases} p^a > \frac{-s_1 s_2}{s_1 s_3 + s_4} p', & p^a < \frac{2(T_L - 2)c_0^b}{\eta T_L} \\ s_5 > s_6 p', & p^a \geq \frac{2(T_L - 2)c_0^b}{\eta T_L}, \end{cases} \tag{A.11}
$$



(a) $A^*_{stk} > A^*_{arb}, R^*_{stk} > R^*_{reg}$ (b) Positive cost-saving (c) $\Pi^*_{stk} > \Pi^*_{arb} + \Pi^*_{reg}$

Figure A.3: Illustration of Corollary A.4: (a) $A^*_{stk} > A^*_{arb}$ (blue), $R^*_{stk} > R^*_{reg}$ (yellow), (b) positive cost-saving (orange), (c) $\Pi^*_{stk} > \Pi^*_{arb} + \Pi^*_{reg}$ (purple). Adapted from Figure 2.8 (green: free regulation; black: no battery use; red: regulation-only; gray: excess regulation).

where $s_1 = \frac{\eta^2 T_L E}{2c_0^b(T_L-2)}, s_2 = \frac{\eta_2 E}{8c_0^b}(\eta_1 - 4), s_3 = \frac{\eta(\eta+4)E}{4c_0^b(T_L-2)}, s_4 = \frac{T_H}{2}(\frac{\eta^2 T_L E}{2c_0^b T_H(T_L-2)})^2, s_5 = 4c_0^b(T\eta + 4T_H)$, and $s_6 = T_L T_H \eta_2(4-\eta_1)$.

□

Synergistic behavior. Note that the synergistic behaviors under stacking can be dramatically expanded for $\eta < 1$. For example, consistent with the base model, the first two properties in Corollary A.4 hold when stacking is in the "free regulation-only region" (when the price of arbitrage is sufficiently high compared to the price of regulation). While under the base model this region only occurs when $\frac{p^a}{p^r} \geq T - 2$, the threshold for how high the arbitrage price needs to be to trigger this region actually gets looser as the battery gets less efficient when $p^r < \underline{p}$. Eventually ($\eta_{stk} < \eta \leq \eta_{reg}$), stacking always uses free regulation only regardless of the price of arbitrage.

Observation A.2. *If $\eta_{stk} < \eta \leq \eta_{reg}$, then $x^*_L = x^*_H = 0$ (free regulation-only region). That is, all the properties in Corollary A.4 hold.*

Figure 2.8 illustrates the expanded synergy when stacking is combined with inefficient batteries.

Benefit of stacking. Theorem 2.3 highlights that stacking can significantly enhance profitability with an inefficient battery, and the relative benefit of stacking, $S = \frac{\Pi^*_{stk}}{\max(\Pi^*_{arb}, \Pi^*_{reg})}$, is unbounded: $\max S = \infty$.

A.3.3 Extension 3: Non-Uniform Regulation Signal

A.3.3.1 Optimal Stacking: Trinary Signal (+1, 0, -1)

As stated in Section 2.6.3, we assume the regulation price $p^r(\alpha)$ to be an increasing

function of the dispatch-to-contract ratio α. For simplicity in exposition, we will omit the dependency when no confusion arises. We note that structural properties of optimal stacking remain unchanged when the regulation price is a function of α since we can derive optimal actions given p^a and p^r. All that changes is comparative statics on α, which we will state later. For simplicity, we present comparative statics under $p^r = c_1$ and $p^r = c_2 \cdot \alpha$.

Optimal structure. Similar to Lemma 2.1, it is easy to verify that $x^* := x_L^* = x_H^*$ for given arbitrage amount A, and the optimal actions are as follows:

Theorem A.5 (Optimal stacking: Trinary signal)**.** *With a trinary signal* $(+1, 0, -1)$ *and the dispatch-to-contract ratio* α*, the optimal arbitrage and regulation quantities and profit in the non-binding power setting are as follows:*

Var.	Cases		
cond.	$p^a \le 2(\frac{1}{\alpha}-1)p^r$	$2(\frac{1}{\alpha}-1)p^r \le p^a$ and $\{p^a \le \frac{T-2\alpha}{\alpha}p^r$ or $p^r \ge \frac{2c_0^b\alpha}{T}\}$	$p^a \ge \frac{T-2\alpha}{\alpha}p^r,\ p^r \le \frac{2c_0^b\alpha}{T}$
A^*	0	$\min(\frac{T(p^a-2(\frac{1}{\alpha}-1)p^r)}{2c_0^b(T-2)}E, E)$	$\min(\frac{p^a+2p^r}{2c_0^b}E, E)$
R^*	$\frac{p^rT}{c_0^b\alpha^2}E$	$\frac{p^rTE}{c_0^b\alpha^2} - \frac{2(1-\alpha)}{\alpha}A^*$	$2A^*$
x^*	$\frac{p^rE}{c_0^b\alpha}$	$\frac{p^rE}{c_0^b\alpha} - \frac{2A^*}{T}$	0
Π^*	$\frac{(p^r)^2TE}{2c_0^b\alpha^2}$	$p^aA^* - 2p^rA^*(\frac{1}{\alpha}-1)$ $+\frac{T(p^r)^2E}{2c_0^b\alpha^2} - \frac{c_0^b}{E}(A^*)^2(1-\frac{2}{T})$	$p^aA^* + 2p^rA^* - \frac{c_0^b}{E}(A^*)^2$

Table A.6: Optimal stacking (trinary signal).

Figure A.4 summarizes the structure of the optimal stacking.

Proof. From $x^* = x_L^* = x_H^*$, the profit function can be restated:

$$\Pi(A, x) = p^aA + 2p^rA + \frac{xT}{\alpha}p^r - \frac{c_0^b}{E}[A^2 + 2Ax + \frac{T}{2}x^2].$$

For fixed A, it is immediate that $x^* = (\frac{p^rE}{\alpha c_0^b} - \frac{2A}{T})^+$,yielding the following optimal profit as a function of A:

$$\Pi(A) = \begin{cases} p^aA + 2p^rA - \frac{c_0^b}{E}A^2, & \text{if } A > \frac{Tp^rE}{2\alpha c_0^b}, \text{ and} \\ p^aA - 2p^rA(\frac{1}{\alpha}-1) + \frac{T(p^r)^2E}{2c_0^b\alpha^2} - \frac{c_0^b}{E}A^2(1-\frac{2}{T}), & \text{if } A < \frac{Tp^rE}{2\alpha c_0^b}. \end{cases}$$

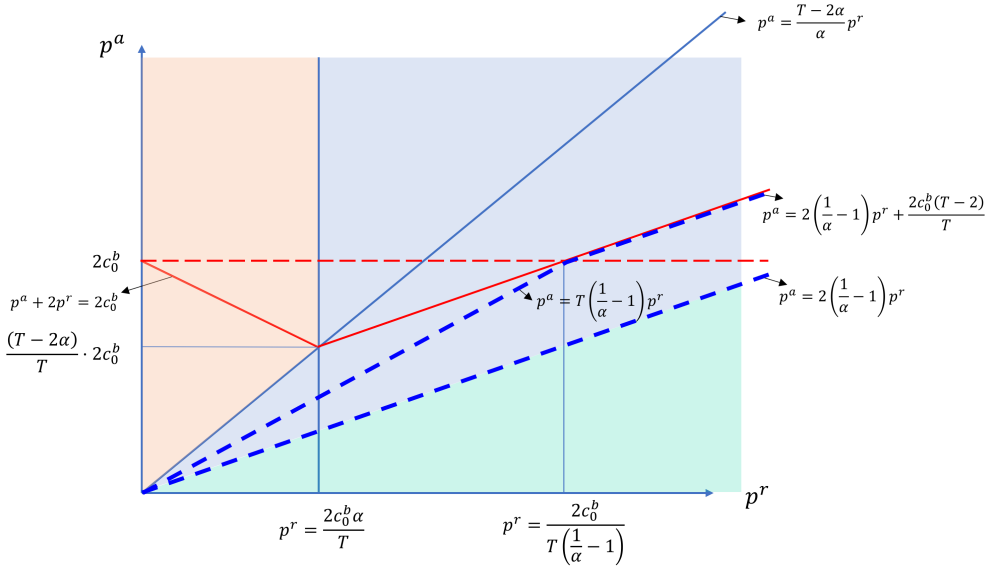


Figure A.4: Illustration of Theorem A.5 – Colors denote discrete regions: $A^* = 0$ (green), $A^* > 0,\ x^* = 0$ (orange), and $A^* > 0,\ x^* > 0$ (blue). Energy capacity is binding on the red line and above for stacking (solid) and standalone arbitrage (dashed). The subregion within the blue dashed lines denotes where $A^*_{stk} < A^*_{arb}$.

Thus, $\Pi(A)$ is a strictly concave function with a continuous, piecewise linear, decreasing derivative. Given derivatives

$$\Pi'(0) = p^a - 2(\frac{1}{\alpha} - 1)p^r \text{ and}$$
$$\Pi'(\frac{Tp^rE}{2\alpha c_0^b}) = p^a - \frac{T-2\alpha}{\alpha}p^r,$$

it is clear that $A^* = 0$ when $p^a \leq 2(\frac{1}{\alpha} - 1)p^r$ (or $\alpha \leq \frac{2p^r}{p^a+2p^r}$) and $A^* \geq \frac{Tp^rE}{2\alpha c_0^b}$ and therefore $x^* = 0$ when $p^a \geq \frac{T-2\alpha}{\alpha}p^r$ (or $\alpha \geq \frac{Tp^r}{p^a+2p^r}$).

□

From Theorem A.5, we immediately check the most of the properties still hold as follows ($\frac{R^*}{A^*} := \infty$ for $A^* = 0$).

Corollary A.5. *With the dispatch-to-contract ratio $\alpha \leq 1$, the following hold for stacking:*

- *R^* increases in p^a when $\frac{T-2\alpha}{\alpha}p^r \leq p^a < 2c_0^b - 2p^r$,*
- *A^* increases in p^r when $\frac{T-2\alpha}{\alpha}p^r \leq p^a < 2c_0^b - 2p^r$,*
- *Stacking always uses equal excess regulation: $x_L^* = x_H^*$,*

- $\frac{R^*}{A^*} \geq 2$,
- *Positive cost-saving synergy when* $p^a > \frac{2(1-\alpha)}{\alpha} p^r$,
- $A^*_{stk} > A^*_{arb}$ *when* $\frac{T(1-\alpha)}{\alpha} p^r < p^a < 2c_0^b$,
- $A^*_{stk} > 0$ *when* $p^a > \frac{2(1-\alpha)}{\alpha} p^r$,
- $R^*_{stk} > R^*_{reg}$ *when* $(\frac{T}{\alpha^2} - 2)p^r < p^a$ *and* $\frac{p^r T}{2\alpha^2} < c_0^b$,
- *Superlinear gains* $(\Pi^*_{stk} > \Pi^*_{arb} + \Pi^*_{reg})$ *when*
  (i) $\frac{T-\sqrt{T^2-2T}}{2} \leq \alpha < 1$, *and*
  $p^a > p^a_\alpha = \begin{cases} \frac{(1-\alpha)[T+\sqrt{T(T-2)}]}{\alpha} p^r, & p^r \leq \frac{2c_0^b \alpha (T-2)}{(1-\alpha)T[T-2+\sqrt{T(T-2)}]}, \\ 2c_0^b - \sqrt{8c_0^b[\frac{c_0^b}{T} - p^r(\frac{1}{\alpha} - 1)]}, & \frac{2c_0^b \alpha (T-2)}{(1-\alpha)T[T-2+\sqrt{T(T-2)}]} \leq p^r \leq \frac{c_0^b}{T(\frac{1}{\alpha}-1)}, \end{cases}$
  or (ii) $1/2 \leq \alpha < \frac{T-\sqrt{T^2-2T}}{2}$, $p^a > (\frac{T}{2\alpha^2} - 1)p^r$, $p^r \leq \frac{2c_0^b \alpha}{T}$,
  or (iii) $\alpha < 1/2$, $p^a > p^a_\alpha = \begin{cases} (\frac{T}{2\alpha^2} - 1)p^r, & p^r \leq \frac{4\alpha^2 c_0^b}{T+2\alpha^2}, \\ 2c_0^b - \sqrt{\frac{8(\alpha c_0^b)^2}{T} - \frac{2T}{\alpha^2}(p^r - \frac{2\alpha^2 c_0^b}{T})^2}, & \frac{4\alpha^2 c_0^b}{T+2\alpha^2} \leq p^r \leq \frac{4\alpha^2 c_0^b}{T}. \end{cases}$

Proof. Theorem A.5 immediately implies that the first five properties still hold.

$A^*_{stk} > A^*_{arb}$: This requires $A^*_{arb} < E$, which is equivalent to $\frac{p^a}{2} < c_0^b$. This holds when $x^* = 0$. When $x^* = \frac{E}{c_0^b}(\frac{T-2\alpha}{\alpha(T-2)} p^r - \frac{p^a}{T-2})$, it happens if and only if $p^a > \frac{T(1-\alpha)}{\alpha} p^r$, or equivalently, $\alpha > \frac{Tp^r}{p^a + Tp^r}$.

$A^*_{stk} > 0$: This holds if and only if $p^a > 2(\frac{1}{\alpha} - 1)p^r$, or equivalently, $\alpha > \frac{2p^r}{p^a + 2p^r}$.

$R^*_{stk} > R^*_{reg}$: When $x^* > 0$, $R^*_{stk} \leq R^*_{reg}$. When $x^* = 0$, $R^*_{stk} > R^*_{reg}$ holds if and only if $p^a > p^r(\frac{T}{\alpha^2} - 2)$, or equivalently, $\alpha > \sqrt{\frac{Tp^r}{p^a + 2p^r}}$ when $A^*_{stk} < E$ or $c_0^b > \frac{p^r T}{2\alpha^2}$ when $A^*_{stk} = E$. This leads to (i) $(\frac{T}{\alpha^2} - 2)p^r < p^a < 2c_0^b - 2p^r$ or (ii) $p^a \geq \max(\frac{T-2\alpha}{\alpha} p^r, 2c_0^b - 2p^r)$ and $\frac{p^r T}{2\alpha^2} < c_0^b$, which can be simplified as $(\frac{T}{\alpha^2} - 2)p^r < p^a$ and $\frac{p^r T}{2\alpha^2} < c_0^b$.

$\Pi^*_{stk} > \Pi^*_{arb} + \Pi^*_{reg}$: From Theorem A.5, it is straightforward to derive $\Delta\Pi := \Pi^*_{stk} - [\Pi^*_{arb} + \Pi^*_{reg}]$, which can be written in the form $c_1(p^a)^2 + c_2 p^a p^r + c_3(p^r)^2 + c_4 p^a + c_5 p^r + c_6$. Then the conditions for superlinear profit gains in Corollary A.5 can be derived from the enumeration of solutions for the quadratic formulas.

□

Synergistic behavior. From Theorem A.5, the condition for the $x^* = 0$ region requires the conditions $p^a \geq \frac{T-2\alpha}{\alpha} p^r$ and $p^r \leq \frac{2c_0^b \alpha}{T}$, which implies that the synergistic behavior is still present for sufficiently large α. For instance, consistent with Observation 2.3, the optimal arbitrage and regulation amounts are both monotonically increasing in p^a and p^r when $x^*_L = x^*_H = 0$. However, it requires a stronger condition than that of the base model ($\alpha = 1$)

under both constant and linear regulation price assumptions. This is because regulation becomes more attractive than arbitrage under the non-uniform signal.

Recall that under the base model, at least a small amount of arbitrage is always beneficial, since the sum of increased revenue and cost-saving for regulation is larger than the increased cost for arbitrage (Observation 2.4). However, when the dispatch-to-contract ratio α is sufficiently low ($p^a \leq 2(\frac{1}{\alpha}-1)p^r$), the cost-saving from regulation becomes marginal, making it optimal to provide regulation alone ($A^* = 0$). Note that under the constant price assumption, the benefits of stacking consistently diminish (i.e., $2(\frac{1}{\alpha}-1)p^r$ approaches infinity) as α approaches zero. In contrast, under the linear price assumption, stacking can still be beneficial as long as $p^a > 2(\frac{1}{\alpha}-1)p^r = 2(1-\alpha)c_2$, since the regulation price also diminishes when α approaches zero.

Benefit of stacking. When energy capacity is not binding ($p^a < 2c_0^b - 2p^r$ or $p^a < \min(2(\frac{1}{\alpha}-1)p^r + \frac{2c_0^b(T-2)}{T}, 2c_0^b)$), $\Pi^*_{stk} > \Pi^*_{arb} + \Pi^*_{reg}$ holds for $\alpha \in [1/2+\epsilon, 1]$ for some small $\epsilon = \frac{T-1-\sqrt{T^2-2T}}{2} > 0$. When $2(\frac{1}{\alpha}-1)p^r \leq p^a \leq \frac{T-2\alpha}{\alpha}p^r$, $\Pi^*_{stk} > \Pi^*_{arb} + \Pi^*_{reg}$ holds for $\alpha \in [1/2+\epsilon, 1]$ for some small $\epsilon = \frac{T-2}{[T-2+\sqrt{T^2-2T}]^2} > 0$. Thus, roughly speaking, the superlinear profit improvement still holds for $\alpha > 1/2$ with sufficiently large p^a.

Now we investigate stacking's performance compared to standalone services. First, with regulation being the only service, the (unconstrained) optimal amount of frequency regulation and the corresponding profit can be easily determined: $r^*_\alpha = \frac{p^r E}{c_0^b \alpha^2}$, $\Pi^*_{reg,\alpha} = \frac{(p^r)^2 TE}{2c_0^b\alpha^2}$. Then we can compare stacking's profitability as follows:

Corollary A.6 (Upper bound on stacking's performance: Trinary signal)**.** *Given dispatch-to-contract ratio α and non-binding energy capacity, $S = \frac{\Pi^*_{stk}}{\max(\Pi^*_{arb}, \Pi^*_{reg})}$ is as follows:*

$$S = \begin{cases} 1, & \text{if } \frac{p^a}{p^r} \leq 2(\frac{1}{\alpha}-1), \\ \frac{T+2\alpha^2-4\alpha}{T-2} - \frac{2(1-\alpha)\alpha}{T-2}\cdot\frac{p^a}{p^r} + \frac{1}{2(T-2)}(\frac{\alpha p^a}{p^r})^2, & \text{if } 2(\frac{1}{\alpha}-1) \leq \frac{p^a}{p^r} \leq \frac{\sqrt{2T}}{\alpha}, \\ \frac{T}{T-2} - \frac{4T(1-\alpha)}{\alpha(T-2)}\cdot\frac{p^r}{p^a} + \frac{2T(T+2\alpha^2-4\alpha)}{\alpha^2(T-2)}(\frac{p^r}{p^a})^2, & \text{if } \frac{\sqrt{2T}}{\alpha} \leq \frac{p^a}{p^r} \leq \frac{T-2\alpha}{\alpha}, \text{and} \\ 1 + 4\frac{p^r}{p^a} + 4(\frac{p^r}{p^a})^2, & \text{if } \frac{p^a}{p^r} \geq \frac{T-2\alpha}{\alpha}. \end{cases}$$

Similar to the result of the base model, $S \in [1, \frac{2T+2\alpha^2-4\alpha-2(1-\alpha)\sqrt{2T}}{T-2}]$, where $\max S = \frac{2T+2\alpha^2-4\alpha-2(1-\alpha)\sqrt{2T}}{T-2}$ is achieved at $\frac{p^a}{p^r(\alpha)} = \frac{\sqrt{2T}}{\alpha}$, which is increasing in α. However, with sufficiently large T, the decrease becomes negligible ($\max S \approx 2$). Since in the base model, the maximizer is achieved at $\frac{p^a}{p^r} = \sqrt{2T}$, the non-uniform signal may shift the peak either to the left or right (depending on the functional form of $p^r(\alpha)$). Recognizing the relationship between p^r and α may emphasize stacking's benefits — Considering the recent grid/market conditions, where frequency regulation is more profitable than arbitrage, the assumption

that regulation price being a function of α (e.g., linear price) may reduce frequency regulation's attractiveness, making arbitrage more comparable to regulation (recall that the ratio $S = \frac{\Pi^*_{stk}}{\max(\Pi^*_{arb}, \Pi^*_{reg})}$) improve as the two standalone services become more comparable and is maximized at $\Pi^*_{arb} = \Pi^*_{reg}$).

Below we consider the effect of binding energy capacity. Corollary A.6 assumes non-binding energy capacity. In the presence of binding energy capacity, we can show that the S ratio is still upper bounded by the grand maximum from the unbinding case ($\alpha = 1$).

Theorem A.6. *Given dispatch-to-contract ratio α and T, $S \leq \frac{2T-2}{T-2}$.*

Proof. When E is binding for stacking but not for standalone arbitrage or when $\Pi^*_{reg} > \Pi^*_{arb}$, the S ratio is upper-bounded by the S ratio under no energy constraint. Further, if $A^*_{stk} < A^*_{arb} = E$ and $x^* > 0$ (or $\max(2c^b_0, 2(\frac{1}{\alpha} - 1)p^r) \leq p^a \leq \frac{2c^b_0(T-2)}{T} + 2(\frac{1}{\alpha} - 1)p^r$), then Corollary A.5 implies that we never have superlinear profit gain ($\Pi^*_{stk} < \Pi^*_{arb} + \Pi^*_{reg}$), concluding that the S ratio is always strictly smaller than 2. We now focus on the two following cases where energy capacity is binding for both standalone arbitrage and stacking and $\Pi^*_{arb} > \Pi^*_{reg}$ ($p^a > c^b_0 + \frac{(p^r)^2 T}{2c^b_0 \alpha^2}$):

$$\Pi^*_{stk} = \begin{cases} p^a E + 2p^r E - c^b_0 E, & x^* = 0, \\ p^a E - 2p^r E(\frac{1}{\alpha} - 1) + \frac{T(p^r)^2 E}{2c^b_0 \alpha^2} - c^b_0 E(1 - \frac{2}{T}), & x^* > 0. \end{cases}$$

If $p^a \geq 2c^b_0,\ p^r \leq \frac{2c^b_0 \alpha}{T}$ ($x^* = 0$), then

$$\begin{aligned} \frac{\Pi^*_{stk}}{\Pi^*_{arb}} &\leq \frac{p^a E + \frac{4c^b_0 E\alpha}{T} - c^b_0 E}{p^a E - c^b_0 E} \ (\because p^r \leq \frac{2c^b_0 \alpha}{T}) \\ &\leq \frac{1}{1 - \frac{c^b_0}{p^a}} \\ &\leq 2 \ (\because p^a \geq 2c^b_0). \end{aligned}$$

If $p^a \geq \max(2c_0^b, \frac{2c_0^b(T-2)}{T} + 2(\frac{1}{\alpha}-1)p^r),\ p^r > \frac{2c_0^b\alpha}{T}$ $(x^* > 0)$, then

$$\begin{aligned}
\frac{\Pi^*_{stk}}{\Pi^*_{arb}} &\leq \frac{2(p^aE - c_0^bE) + \frac{2c_0^bE}{T} - 2p^rE(\frac{1}{\alpha}-1)}{p^aE - c_0^bE} \ (\because \frac{(p^r)^2TE}{2c_0^b\alpha^2} < p^aE - c_0^bE) \\
&= 2 + \frac{2}{T}[\frac{c_0^bE - p^rE(\frac{1}{\alpha}-1)T}{p^aE - c_0^bE}] \\
&\leq 2 + \frac{2}{T}[\frac{c_0^bE}{p^aE - c_0^bE}] \leq 2 + \frac{2}{T} \ (\because p^a \geq 2c_0^b) \\
&< \frac{2T-2}{T-2}.
\end{aligned}$$

Combining the above results concludes the proof. □

Though the grand maximum ($S = \frac{2T-2}{T-2}$ when $\alpha = 1$) cannot be improved under the binding energy capacity, the relative benefit of stacking over the best standalone for certain α can improve.

Observation A.3. *$S(\alpha) > \frac{2T+2\alpha^2-4\alpha-2(1-\alpha)\sqrt{2T}}{T-2}$ can happen where $\frac{2T+2\alpha^2-4\alpha-2(1-\alpha)\sqrt{2T}}{T-2}$ is the maximum S ratio under non-binding energy capacity in Corollary A.6.*

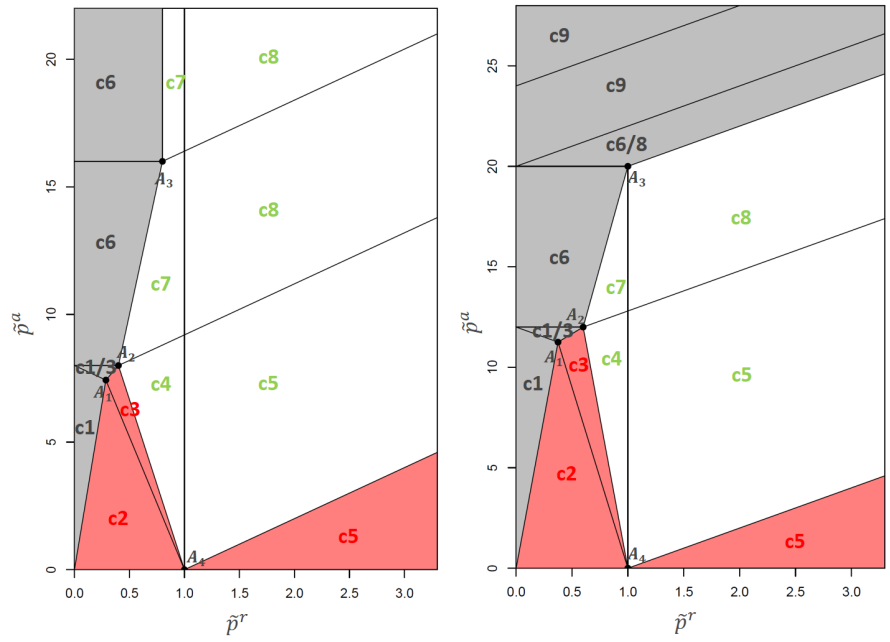
This situation arises when $A^*_{stk} = \frac{TE(p^a-2(\frac{1}{\alpha}-1)p^r)}{2c_0^b(T-2)} < A^*_{arb} = E$ — the limited capacity restricts standalone arbitrage (which outperforms standalone regulation, i.e., $\Pi^*_{arb} > \Pi^*_{reg}$), while stacking remains unaffected by the energy constraint due to its ability to balance the quantities of the two services ($A^*_{stk} = \frac{T(p^a-2(\frac{1}{\alpha}-1)p^r)}{2c^b(T-2)}$). Consequently, this leads to an augmentation in the S ratio. Numerically, the increase in the S ratio (i.e., $S(\alpha) - \frac{2T+2\alpha^2-4\alpha-2(1-\alpha)\sqrt{2T}}{T-2}$) can be as high as 4%.

A.3.4 Extension 4: Stacking when Power is Binding

A.3.4.1 Optimal Stacking: Power is Binding

Below we provide a detailed description of the comparative statics. We normalize service prices by the degradation coefficient c_0^b and the energy-to-power ratio. A.1.1.2).

Lemma A.5. *Define $\tilde{p}^a := \frac{p^aE}{c_0^bP}$ and $\tilde{p}^r := \frac{p^rE}{c_0^bP}$ to be the prices of the services, normalized by c_0^b and energy-to-power ratio. Then for a fixed arbitrage amount A, the optimal profit of the*



(a) $T_L \geq 2T_H$ (b) $T_L \leq 2T_H$

Figure A.5: Illustration of Lemma A.5. The colored regions denote $x_L^* = x_H^* > 0$ (pink), $x_L^* = x_H^* = 0$ (gray), and $x_L^* > x_H^*$ (white). $A_1 = (\frac{T_H}{T}, \frac{T_H(T-2)}{T})$, $A_2 = (\frac{T_H}{T_L}, T_H)$, $A_3 = \begin{cases} (\frac{2T_H}{T_L}, 2T_H), & T_L \geq 2T_H \\ (1, T_L), & T_L \leq 2T_H \end{cases}$, $A_4 = (1, 0)$ where $T_L = 20, T_H = 8$ and $T_L = 20, T_H = 12$ are used for (a) and (b), respectively.

stacked model with power constraints becomes:

$$\Pi(A) = \begin{cases} (p^a + 2p^r)A - \frac{c_0^b}{E}A^2, & \textit{if } (c1) \\ \frac{T(p^r)^2E}{2c_0^b} + p^aA - \frac{c_0^b}{E}(1 - \frac{2}{T})A^2, & \textit{if } (c2) \\ TP(p^r - \frac{\frac{c_0^b}{E}P}{2}) + (p^a + \frac{2T_L(\frac{c_0^b}{E}P - p^r)}{T_H})A - \frac{c_0^b}{E}(1 + \frac{2(T_L - T_H)}{T_H^2})A^2, & \textit{if } (c3) \\ (\frac{(p^r)^2T_LE}{2c_0^b} + p^rT_HP - \frac{c_0^bT_HP^2}{2E}) + (p^a - 2p^r + 2\frac{c_0^b}{E}P)A - \frac{c_0^b}{E}(1 - \frac{2}{T_L} + \frac{2}{T_H})A^2, & \textit{if } (c4) \\ TP(p^r - \frac{\frac{c_0^b}{E}P}{2}) + (p^a - 2p^r + 2\frac{c_0^b}{E}P)A - \frac{c_0^b}{E}(1 - \frac{2}{T_L} + \frac{2}{T_H})A^2, & \textit{if } (c5) \\ p^rPT_H + p^aA - \frac{c_0^b}{E}A^2, & \textit{if } (c6) \\ (p^rPT_H + \frac{T_L(p^r)^2E}{2c_0^b}) + (p^a - 2p^r)A - \frac{c_0^b}{E}(1 - \frac{2}{T_L})A^2, & \textit{if } (c7) \\ (p^rPT - \frac{c_0^bP^2T_L}{2E}) + (p^a - 2p^r)A - \frac{c_0^b}{E}(1 - \frac{2}{T_L})A^2, & \textit{if } (c8) \\ p^rPT + (p^a - 2p^r)A - \frac{c_0^b}{E}A^2, & \textit{if } (c9) \end{cases}$$

where conditions $(c1)$ – $(c9)$ *are defined as follows:*

- *Region 1:* $0 \le A \le \frac{PT_H}{2}$:
  - *(c1):* $\tilde{p}^r \le \frac{T_H}{T}, A \ge \frac{Tp^rE}{2c_0^b}$,
  - *(c2):* $\tilde{p}^r \le \frac{T_H}{T}, A < \frac{Tp^rE}{2c_0^b}$ *or* $\frac{T_H}{T} < \tilde{p}^r < 1, A < \frac{\frac{c_0^b}{E}P - p^r}{2\frac{c_0^b}{E}(1/T_H - 1/T)}$,
  - *(c3):* $\frac{T_H}{T} < \tilde{p}^r \le \frac{T_H}{T_L}, A \ge \frac{\frac{c_0^b}{E}P - p^r}{2\frac{c_0^b}{E}(1/T_H - 1/T)}$ *or* $\frac{T_H}{T_L} < \tilde{p}^r < 1, \frac{\frac{c_0^b}{E}P - p^r}{2\frac{c_0^b}{E}(1/T_H - 1/T)} \le A \le \frac{\frac{c_0^b}{E}P - p^r}{2\frac{c_0^b}{E}(1/T_H - 1/T_L)}$,
  - *(c4):* $\frac{T_H}{T_L} < \tilde{p}^r < 1, A > \frac{\frac{c_0^b}{E}P - p^r}{2\frac{c_0^b}{E}(1/T_H - 1/T_L)}$,
  - *(c5):* $\tilde{p}^r \ge 1$,
- *Region 2:* $\frac{PT_H}{2} < A \le \min(PT_H, \frac{PT_L}{2})$:
  - *(c6):* $\tilde{p}^r \le \frac{T_H}{T_L}$ *or* $\frac{T_H}{T_L} < \tilde{p}^r < \min(\frac{2T_H}{T_L}, 1), A \ge \frac{T_Lp^rE}{2c_0^b}$,
  - *(c7):* $T_L > 2T_H, \frac{2T_H}{T_L} \le \tilde{p}^r < 1$ *or* $\frac{T_H}{T_L} < \tilde{p}^r < \min(\frac{2T_H}{T_L}, 1), A < \frac{T_Lp^rE}{2c_0^b}$,
  - *(c8):* $\tilde{p}^r \ge 1$,
- *Region 3:* $\frac{PT_L}{2} < A \le PT_H$:
  - *(c9):* $T_L < 2T_H$.

The optimal solutions under conditions $(c1)$ – $(c9)$ *follow the properties listed in Table A.7.*

All proofs of results stated in Appendix A.3.4.1 are provided in Appendix A.3.4.2. From Lemma A.5, Figure A.5 is derived. Table A.7 provides specific conditions required for the key properties to hold.

Properties	Regions†								
	$(c1)$	$(c2)$	$(c3)$	$(c4)$	$(c5)$	$(c6)$	$(c7)$	$(c8)$	$(c9)$
$x_L^* = x_H^* > 0$	×	✓	$\tilde{p}^r > \frac{T_H}{T_L}$ or $A < \frac{PT_H}{2}$	×	×	×	×	×	×
$x_L^* = x_H^* = 0$	✓	×	$\tilde{p}^r \leq \frac{T_H}{T_L}$ and $A = \frac{PT_H}{2}$	×	×	✓	×	$2T_H \geq T_L$ and $A = \frac{PT_L}{2}$	✓
P unconstrained in both periods	✓	✓	×	×	×	×	×	×	×
P constrained in both periods	×	×	×	×	✓	✓	×	✓	✓
Uses all available free regulation	✓	✓	✓	✓	✓	×	×	×	×
$\frac{\partial^2 \Pi(A)}{\partial p^r \partial A} > 0$	✓	×	×	×	×	×	×	×	×
$\frac{\partial R^*}{\partial A} > 0$	✓	×	×	×	×	×	×	×	×
$\frac{R^*}{A} \geq 2$	✓	✓	✓	✓	✓	×	✓	✓	×
$\Pi'_{stk}(A) > \Pi'_{arb}(A)$‡	✓	✓	✓	×	×	×	×	×	×
$R^*_{stk} > R^*_{reg}$	✓	×	×	×	×	✓	×	×	✓
Cost-saving synergy	✓	✓	✓	✓	✓	✓	✓	✓	✓

Table A.7: Properties of the optimal power-constrained solution for fixed arbitrage amount A when $T_L > T_H$.

†: Regions $(c1)$ – $(c9)$ defined in Lemma A.5.
‡: Define $\Pi_{arb}(A) = p^a A - \frac{c_0^b}{E} A^2$.

Observation A.4 (Guaranteed cost-saving synergy with binding P)**.** *According to Proposition A.1, a limited power capacity may lead to negative cost-saving synergy when excess regulation values are highly imbalanced: $x_L^* > x_H^*$. We read from Table A.7 that such an imbalance will never occur if the high-price period is sufficiently long relative to the low-price period ($T_H > \frac{3T}{8}$).*

Proposition A.1 states properties of the optimal solution with a power limit P but no energy limit E.

Proposition A.1. *At optimality, the stacked model with finite power capacity P but no energy limit E satisfies the following when $T_L > T_H$:*

- *Optimal excess regulation:*

- *Positive excess regulation in equal quantities between the two time periods* ($x_H^* = x_L^* > 0$, $A^* > 0$) *is optimal iff*

$$\tilde{p}^a < \begin{cases} (T-2)\tilde{p}^r, & \text{if } \tilde{p}^r \leq \frac{T_H}{T}, \\ \frac{2T_L}{T_H}\tilde{p}^r + (T_H - 2), & \text{if } \frac{T_H}{T} < \tilde{p}^r \leq \frac{T_H}{T_L}, \text{ and} \\ \frac{T_L T_H}{T_L - T_H}(1 - \tilde{p}^r), & \text{if } \frac{T_H}{T_L} < \tilde{p}^r < 1, \end{cases}$$

- *Free regulation only* ($x_H^* = x_L^* = 0$) *is optimal iff*

$$\tilde{p}^a \geq \begin{cases} (T-2)\tilde{p}^r, & \text{if } \tilde{p}^r \leq \frac{T_H}{T}, \\ \frac{2T_L}{T_H}\tilde{p}^r + (T_H - 2), & \text{if } \frac{T_H}{T} < \tilde{p}^r \leq \frac{T_H}{T_L}, \\ T_L\tilde{p}^r, & \text{if } \frac{T_H}{T_L} < \tilde{p}^r < \min(\frac{2T_H}{T_L}, 1), \text{ and} \\ 2\tilde{p}^r + T_L - 2, & \text{if } \tilde{p}^r \geq 1, T_L \leq 2T_H, \end{cases}$$

- *Regulation-only* ($r_H^* = r_L^* = P$, $A^* = 0$) *is optimal iff* $\tilde{p}^r \geq 1$, $\tilde{p}^a \leq 2(\tilde{p}^r - 1)$.
- *In all other cases, the stacked model satisfies* $x_L^* > x_H^*$.

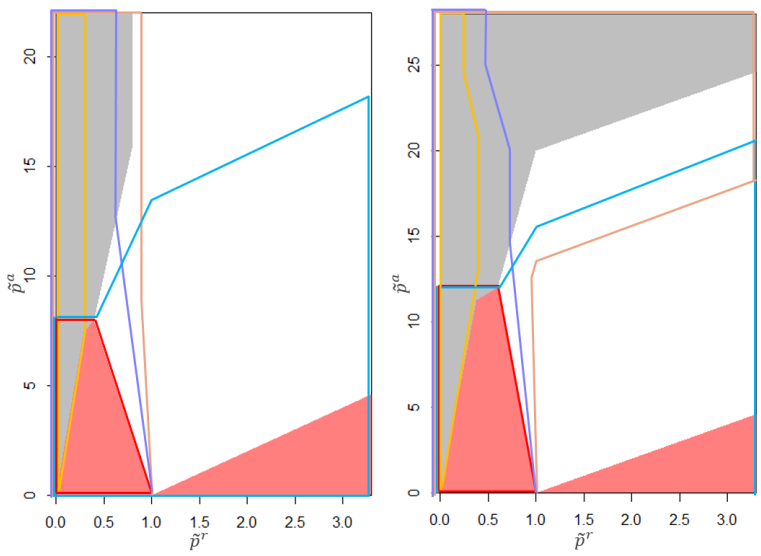
- *Power constraints:*
  - *Stacking is power unconstrained in both time periods iff*

$$\tilde{p}^a < \begin{cases} T_H - 2\tilde{p}^r, & \text{if } \tilde{p}^r \leq \frac{T_H}{T}, \text{ and} \\ \frac{(T-2)T_H}{T_L}(1 - \tilde{p}^r), & \text{if } \frac{T_H}{T} < \tilde{p}^r < 1, \end{cases}$$

  - *Stacking is power constrained in both time periods either when* $\tilde{p}^r \geq 1$ *or when* $\tilde{p}^r < 1$, $\tilde{p}^a \geq T_L$, *and* $T_L \leq 2T_H$.
  - *Stacking uses all available free regulation* ($r_L^* \geq a_L^*, r_H^* \geq a_H^*$) *iff*

$$\tilde{p}^a \leq \begin{cases} T_H, & \text{if } \tilde{p}^r \leq \frac{T_H}{T_L}, \text{ and} \\ 2\tilde{p}^r + T_H(1 - \frac{2}{T_L}), & \text{if } \tilde{p}^r > \frac{T_H}{T_L}. \end{cases}$$

- *Key properties:*
  - A^* (R^*) *is strictly increasing in* p^r (p^a) *when* $\tilde{p}^r < \frac{T_H}{T}$, $(T-2)\tilde{p}^r \leq \tilde{p}^a \leq -2\tilde{p}^r + T_H$,
  - $A_{stk}^* > A_{arb}^*$ *when* $\tilde{p}^a < \min(T_H, \frac{T_L T_H}{T_L - T_H}(1 - \tilde{p}^r))$,
  - $R_{stk}^* > R_{reg}^*$ *when* $\begin{cases} \tilde{p}^r < \min(\frac{\tilde{p}^a}{T-2}, \frac{T_H}{T}), T_L \geq 2T_H, \text{ or} \\ \tilde{p}^r < \min(\frac{\tilde{p}^a}{T-2}, \frac{T_H}{T}, \frac{T-\tilde{p}^a}{T-2}), T_L < 2T_H, \text{ or} \\ \frac{T-\tilde{p}^a}{T-2} \leq \tilde{p}^r < \frac{T_L - T_H}{T}, T_L < 2T_H, \end{cases}$



(a) $T_L \geq 2T_H$ (b) $T_L \leq 2T_H$

Figure A.6: Illustration of Proposition A.1. The shaded regions denote $x_L^* = x_H^* > 0$ (pink), $x_L^* = x_H^* = 0$ (gray), and $x_L^* > x_H^*$ (white). The subregions within colored lines denote where each property holds: $A_{stk}^* > A_{arb}^*$ (red), $R_{stk}^* > R_{reg}^*$ (yellow), $\frac{R^*}{A^*} \geq 2$ (blue), positive cost-saving (orange), and superlinear profit (purple).

- $\frac{R^*}{A^*} \geq 2$ *when* $\tilde{p}^a \leq \tilde{p}_1^a = \begin{cases} T_H, & \text{if } \tilde{p}^r < \frac{T_H}{T_L} \\ \frac{T_L+2}{2}\tilde{p}^r + \frac{T_H(T_L-2)}{2T_L}, & \text{if } \frac{T_H}{T_L} \leq \tilde{p}^r < 1 \\ 2\tilde{p}^r + \frac{T}{2}(1 - \frac{2}{T_L}), & \text{if } \tilde{p}^r \geq 1, T_L < 3T_H \\ \infty, & \text{if } \tilde{p}^r \geq 1, T_L \geq 3T_H, \end{cases}$
- $A^* > 0$ *when* $\tilde{p}^a > 2(\tilde{p}^r - 1)$.

Based on Proposition A.1, Figure A.6 represents regions where each synergistic property holds for the case when energy is not binding for stacking. Most of the synergistic properties (e.g., positive cost-saving) continue to hold even when power is binding. Some properties hold more broadly under wide peaks ($T_L \leq 2T_H$) than under narrow peaks ($T_L \geq 2T_H$). For instance, the regions where stacking achieves positive cost savings are expanded; Observation A.4 states that stacking always results in a positive cost saving when $T_H > \frac{3T}{8}$.

Naturally, the optimal stacking solution characterized by Proposition A.1 may select an infeasible amount of arbitrage for finite energy capacity E ($A^* > E$). However, since A^* is monotone increasing in $\tilde{p}^a$ for fixed $\tilde{p}^r$, it is always possible in such situations to select some $\tilde{p}_E^a < \tilde{p}^a$ such that the optimal solution to the energy-constrained problem with normalized price of arbitrage $\tilde{p}^a$ exactly matches the optimal solution to the energy-

unconstrained problem considered in Proposition A.1 with normalized price of arbitrage $\tilde{p}_E^a$. Proposition A.2 formalizes this notion.

Proposition A.2 (Equivalence of the optimal structure)**.** *The optimal solution of a problem with power constraint P, energy constraint E, normalized regulation price $\tilde{p}^r$, and normalized arbitrage price $\tilde{p}^a$ is exactly the same as the optimal solution to a problem with power constraint P, no enforced energy constraint, normalized regulation price $\tilde{p}^r$, and normalized arbitrage price* $\min(\tilde{p}^a, \tilde{p}_E^a)$*, for some $\tilde{p}_E^a$ that depends on E/P and $\tilde{p}^r$.*
In particular, when $E/P \geq T_H$, then

$$\tilde{p}_E^a = \infty.$$

When $\frac{T_L}{2} \leq E/P < T_H$ and $T_L < 2T_H$, then

$$\tilde{p}_E^a = 2\tilde{p}^r + 2E/P.$$

When $\frac{T_H}{2} \leq E/P < \min(\frac{T_L}{2}, T_H)$, then

$$\tilde{p}_E^a = \begin{cases} 2E/P, & \text{if } 0 \leq \tilde{p}^r \leq \frac{2}{T_L}E/P, \text{ and} \\ 2\tilde{p}^r + 2(1 - \frac{2}{T_L})E/P, & \text{if } \tilde{p}^r \geq \frac{2}{T_L}E/P. \end{cases}$$

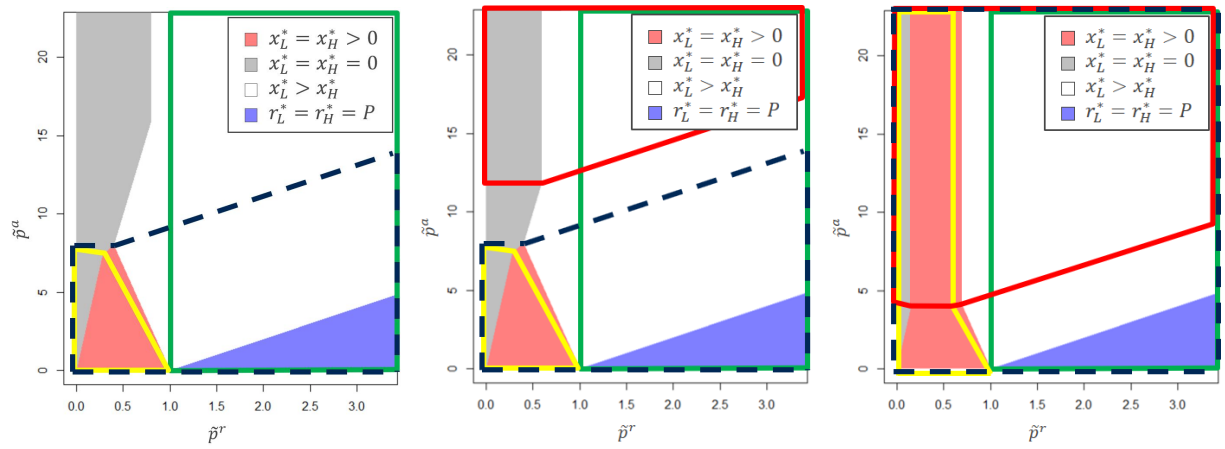
Finally, when $E/P < \frac{T_H}{2}$, then

$$\tilde{p}_E^a = \begin{cases} 2E/P - 2\tilde{p}^r, & \text{if } 0 \leq \tilde{p}^r \leq \frac{2}{T}E/P, \\ 2(1 - \frac{2}{T})E/P, & \text{if } \frac{2}{T}E/P \leq \tilde{p}^r \leq 1 - \frac{2T_L}{T_H T}E/P, \\ 2(1 + \frac{2(T_L - T_H)}{T_H^2})E/P - \frac{2T_L(1-\tilde{p}^r)}{T_H}, & \text{if } 1 - \frac{2T_L}{T_H T}E/P \leq \tilde{p}^r \leq 1 - \frac{2(T_L - T_H)}{T_L T_H}E/P, \text{ and} \\ 2(1 - \frac{2}{T_L} + \frac{2}{T_H})E/P - 2(1 - \tilde{p}^r), & \text{if } \tilde{p}^r \geq 1 - \frac{2(T_L - T_H)}{T_L T_H}E/P. \end{cases}$$

Figures A.7 – A.8 characterize optimal battery operations such as when $x_L^* = x_H^*$ vs. $x_L^* > x_H^*$ (etc.) as a function of $\tilde{p}^a$ and $\tilde{p}^r$ for $T_L \geq 2T_H$ and $T_L < 2T_H$, respectively.[9]

Next, we state the implications of limited power/energy capacity. Clearly, both energy and power capacity affect the optimal structure and the benefit of stacking (e.g., synergistic properties). Figure A.8 illustrates the optimal structure of different energy-to-power ratios for $T_L < 2T_H$, where the bottom of the red outlined region marks $\tilde{p}_E^a$ for a given $\tilde{p}^r$. The key properties of stacking established in Proposition A.1 (e.g., the optimal solution structure, $\frac{R^*}{A^*} \geq 2$, positive cost-saving) then immediately follow by reading the relevant property for

[9] Appendix A.3.4.3 describes comparative statics with respect to other key parameters (e.g., p^a and c^b).



(a) $E/P > T_H$ (b) $\frac{T_H}{2} < E/P \leq T_H$ (c) $E/P \leq \frac{T_H}{2}$

Figure A.7: Illustration of optimal battery operations ($T_L \geq 2T_H$). Power is unconstrained within the yellow line, power is constrained in both time periods within the green line, and otherwise, power is constrained only in the high-price period. Energy is constrained within the red line. Maximum free regulation is used in both time periods within the black dashed area. The blue area denotes regulation alone ($A^* = 0$). $T_L = 20$ and $T_H = 8$ are used.

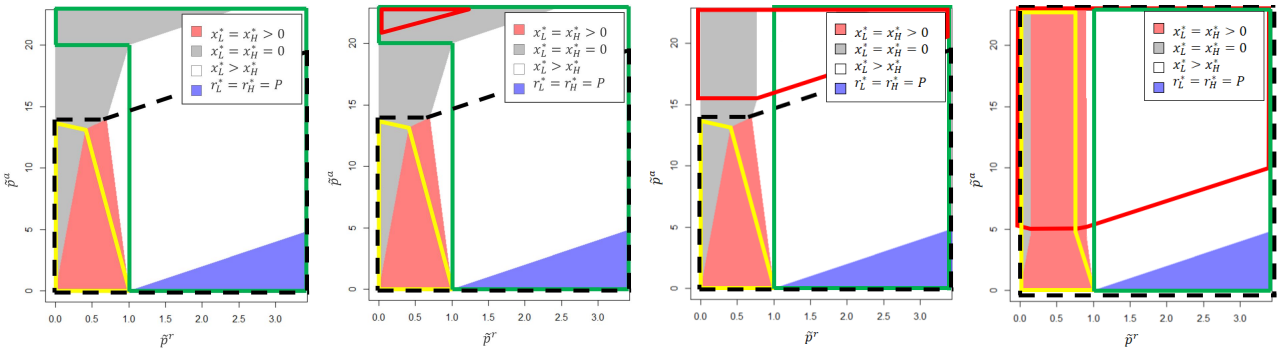
$\tilde{p}_E^a$ instead of $\tilde{p}^a$. Further, Figure A.9 illustrates the effect of limited energy capacity by comparing $E/P < \frac{T_H}{2}$ and $E/P > T_H$. Some key observations are as follows:

- A binding energy capacity may limit or expand some of the synergistic behaviors. As shown in Figure A.9, the range for $R_{stk}^* > R_{reg}^*$ becomes smaller under limited energy capacity, while the ranges for $A_{stk}^* > A_{arb}^*$ and positive cost-saving become expanded.
- Relative benefits of stacking can be stronger under a binding energy capacity: Interestingly, stacking's performance relative to standalone services can be stronger under a binding energy capacity as opposed to non-binding capacity. This is exemplified in the expanded regions where stacking achieves superlinear profit improvement: the purple regions ($\Pi_{stk}^* > \Pi_{arb}^* + \Pi_{reg}^*$) are larger when $E/P < \frac{T_H}{2}$ compared to the unconstrained setting as shown in Figure A.9. Intuitively, when arbitrage prices are high, the limited energy capacity constrains standalone arbitrage more than it constrains stacking since stacking has the option to shift to the regulation service.

A.3.4.2 Proof of Lemma A.5 and Propositions A.1 – A.2

We will use regions and notations introduced in Lemma A.5.

Proof of Lemma A.5:



(a) $E/P > T_H$ (b) $\frac{T_L}{2} < E/P \leq T_H$ (c) $\frac{T_H}{2} < E/P \leq \frac{T_L}{2}$ (d) $E/P \leq \frac{T_H}{2}$

Figure A.8: Illustration of the optimal battery operation ($T_L < 2T_H$). Power is unconstrained within the yellow line, power is constrained in both time periods within the green line, and otherwise, power is constrained only in the high-price period. Energy is constrained within the red line. Maximum free regulation is used in both time periods within the black dashed area. The blue area denotes regulation alone ($A^* = 0$). $T_L = 20$ and $T_H = 14$ are used.

We begin by deriving $\Pi(A)$, the optimal profit as a function of fixed arbitrage amount A, for different ranges of A values. Given this characterization, we determine the conditions that yield the various properties of interest.

Region 1: $0 \leq A \leq PT_H/2$

For $A \leq PT_H/2$, both the low-price and high-price periods have sufficient power to provide the full amount of free regulation; at optimality both will do so. Defining the total amount of excess regulation sold to the grid as $X := T_L x_L + T_H x_H$ and observing that we sell $R = 2A + X$ total regulation, note that the battery generates a profit from the grid of $(p^a + 2p^r)A + p^r X$. It is straightforward that the degradation-minimizing way to provide X amount of excess regulation is to provide it evenly between the two periods ($x_L = x_H = X/T$) if doing so does not violate the power constraint ($X \leq T(P - 2a_H)$), and it's otherwise optimal to provide the maximum physically possible excess regulation in the high-price period and the remainder in the low-price period ($x_H = P - 2a_H$, $x_L = X/T_L - T_H P/T_L + 2a_L$). Allocating the excess

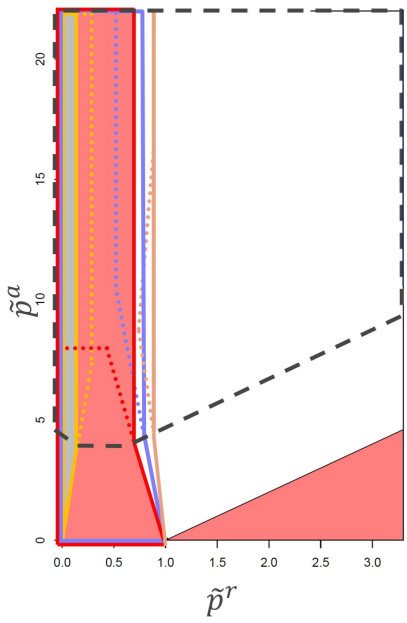


Figure A.9: Illustration of Propositions A.1 – A.2 ($T_L \geq 2T_H$). The limited energy capacity shifts the range where each of the properties holds, as seen by comparing the regions in solid lines ($E/P < \frac{T_H}{2}$) and the regions in dotted lines (unconstrained setting). Colors denote properties $A^*_{stk} > A^*_{arb}$ (red), $R^*_{stk} > R^*_{reg}$ (yellow), positive cost-saving (orange), and superlinear profit (purple). Energy is constrained within the black dashed line for the $E/P < \frac{T_H}{2}$ case.

regulation in this way yields the following optimal profit for fixed A and X:

$$\Pi(A,X) = \begin{cases} c_1 + (p^r - \frac{2c_0^b A}{TE})X - \frac{c_0^b}{2TE}X^2, & \text{if } 0 \le X \le T(P - \frac{2A}{T_H}) \\ c_2 + (p^r - \frac{c_0^b(4A - T_H P)}{T_L E})X - \frac{c_0^b}{2T_L E}X^2, & \text{if } T(P - \frac{2A}{T_H}) \le X \le TP - 4A \end{cases}, \text{ for}$$

$$c_1 = (p^a + 2p^r)A - \frac{c_0^b}{E}A^2 \text{ and}$$

$$c_2 = (p^a + 2p^r)A - \frac{c_0^b}{E}[A^2(1 + \frac{6}{T_L} + \frac{2}{T_H}) + \frac{T_H T P^2}{2T_L} - \frac{2P(2T_H + T_L)}{T_L}A].$$

For fixed A, $\Pi(A,X)$ is a continuous, concave function. Its derivative is a piecewise linear, strictly decreasing function with a discontinuity at $X = T(P - 2a_H)$:

$$\begin{aligned} \Pi'(A,0) &= p^r - \frac{2c_0^b A}{TE}, \\ \Pi'_-(A, T(P-2a_H)) &= p^r - \frac{c_0^b}{E}P + 2\frac{c_0^b}{E}A(\frac{1}{T_H} - \frac{1}{T})), \\ \Pi'_+(A, T(P-2a_H)) &= p^r - \frac{c_0^b}{E}P + 2\frac{c_0^b}{E}A(\frac{1}{T_H} - \frac{1}{T_L})), \text{ and} \\ \Pi'(A, TP - 4A) &= p^r - \frac{c_0^b}{E}P. \end{aligned}$$

When $p^r \ge \frac{c_0^b}{E}P$ ($\tilde{p}^r \ge 1$), then $X^* = TP - 4A$ and the maximum possible regulation is provided in both time periods; otherwise, a smaller amount is used. Using $0 \le A \le PT_H/2$, we have $p^r - \frac{c_0^b PT_H}{TE} \le \Pi'(A,0) \le p^r$, $p^r - \frac{c_0^b}{E}P \le \Pi'_-(A, T(P-2a_H)) \le p^r - \frac{c_0^b PT_H}{TE}$, and $p^r - \frac{c_0^b}{E}P \le \Pi'_+(A, T(P-2a_H)) \le p^r - \frac{c_0^b PT_H}{T_L E}$.

Signing $\Pi'(A,X)$ at these points yields a complete characterization of X^* given a fixed A. Each of these conditions has a natural interpretation. In ($c1$), only free regulation is used in both time periods ($x_L^* = x_H^* = 0$), and neither time period has power binding for $A < PT_H/2$. In ($c2$), an equal, positive amount of excess regulation is used in both time periods ($x_L^* = x_H^* > 0$), and neither time period has power binding. In ($c3$), an equal, positive amount of excess regulation is used in both time periods ($x_L^* = x_H^* > 0$), and power is binding in the high-price time period (but not in the low-price period, unless $T_L = T_H$ or $A = 0$). In ($c4$), an unequal amount of excess regulation is used ($x_L^* > x_H^*$), and power is binding in the high-price period but not in the low-price period. In ($c5$), the maximum physically possible excess regulation is provided, resulting in binding power in both time periods (in this case $x_L^* > x_H^*$, except when $T_L = T_H$ or $A = 0$).

Given this characterization, we can state $\Pi(A)$, the optimal profit for fixed A:

$$\Pi(A) = \begin{cases} (p^a + 2p^r)A - \frac{c_0^b}{E}A^2, & (c1), \\ \frac{T(p^r)^2E}{2c_0^b} + p^aA - \frac{c_0^b}{E}(1 - \frac{2}{T})A^2, & (c2), \\ TP(p^r - \frac{c_0^bP}{2E}) + (p^a + \frac{2T_L(\frac{c_0^b}{E}P - p^r)}{T_H})A - \frac{c_0^b}{E}(1 + \frac{2(T_L - T_H)}{T_H^2})A^2, & (c3), \\ (\frac{(p^r)^2T_LE}{2c_0^b} + p^rT_HP - \frac{c_0^bT_HP^2}{2E}) + (p^a - 2p^r + 2\frac{c_0^b}{E}P)A - \frac{c_0^b}{E}(1 - \frac{2}{T_L} + \frac{2}{T_H})A^2, & (c4), \\ TP(p^r - \frac{c_0^bP}{2E}) + (p^a - 2p^r + 2\frac{c_0^b}{E}P)A - \frac{c_0^b}{E}(1 - \frac{2}{T_L} + \frac{2}{T_H})A^2, & (c5). \end{cases}$$

Region 2: $PT_H/2 < A \leq \min(PT_H, PT_L/2)$

In this region, the high-price time period does not have enough power to use all of its free regulation, while the low-price period has enough power for all of its free regulation. At optimality both will use as much free regulation as possible. Then $r_L = a_L + x_L$ and $r_H = P - a_H$; if we define $X = T_Lx_L$ to be the amount of excess regulation sold to the grid, then $R = T_Lr_L + T_Hr_H = X + PT_H$. This means that the total profit from the grid is $p^aA + p^r(X + PT_H)$. The optimal profit for fixed A and $0 \leq X \leq PT_L - 2A$ immediately follows:

$$\Pi(A, X) = (p^rPT_H + p^aA - \frac{c_0^b}{E}A^2) + (p^r - \frac{2c_0^bA}{T_LE})X - \frac{c_0^b}{2T_LE}X^2.$$

For fixed A, $\Pi(A, X)$ is concave, with derivatives $\Pi'(A, 0) = p^r - \frac{2c_0^bA}{T_LE}$ and $\Pi'(A, PT_L - 2A) = p^r - \frac{c_0^b}{E}P$. From $PT_H/2 < A \leq \min(PT_H, PT_L/2)$, we have $\max(p^r - \frac{2c_0^bPT_H}{T_LE}, p^r - \frac{c_0^b}{E}P) \leq \Pi'(A, 0) < p^r - \frac{c_0^bPT_H}{T_LE}$. Signing $\Pi'(A, X)$ at these points yields a complete characterization of X^* given a fixed A:

$$X^* = \begin{cases} 0, & (c6) : \tilde{p}^r \leq \frac{T_H}{T_L} \text{ or } \frac{T_H}{T_L} < \tilde{p}^r < \min(\frac{2T_H}{T_L}, 1), A \geq \frac{T_Lp^rE}{2c_0^b}, \\ \frac{T_Lp^rE}{c_0^b} - 2A, & (c7) : T_L > 2T_H, \frac{2T_H}{T_L} \leq \tilde{p}^r < 1 \text{ or } \frac{T_H}{T_L} < \tilde{p}^r < \min(\frac{2T_H}{T_L}, 1), A < \frac{T_Lp^rE}{2c_0^b}, \\ PT_L - 2A, & (c8) : \tilde{p}^r \geq 1. \end{cases}$$

Again, each condition has a natural interpretation. In $(c6)$, only free regulation is used in both time periods ($x_L^* = x_H^* = 0$), and the high-price period has power binding (the low-price period is not power binding for $A < TP_L/2$). In $(c7)$, excess regulation is provided in the low-price period alone ($x_L^* > x_H^* = 0$); the high-price period has power binding but the low-price period does not. In $(c8)$, the maximum physically possible excess regulation is provided ($x_L^* > x_H^* = 0$), resulting in binding power in both time periods.

Given this characterization, we can state $\Pi(A)$, the optimal profit for fixed A:

$$\Pi(A) = \begin{cases} p^r PT_H + p^a A - \frac{c_0^b}{E} A^2, & \text{if } (c6), \\ (p^r PT_H + \frac{T_L (p^r)^2 E}{2c_0^b}) + (p^a - 2p^r)A - \frac{c_0^b}{E}(1 - \frac{2}{T_L})A^2, & \text{if } (c7), \\ (p^r PT - \frac{c_0^b P^2 T_L}{2E}) + (p^a - 2p^r)A - \frac{c_0^b}{E}(1 - \frac{2}{T_L})A^2, & \text{if } (c8). \end{cases}$$

Region 3: $PT_L/2 < A \leq PT_H$

In this region (c9), which only occurs when $T_L < 2T_H$, the battery does not have sufficient power to use all available free regulation in either time period. At optimality, the battery will use its full power to provide free regulation, meaning $r_L = P - a_L$, $r_H = P - a_H$, and $R = PT - 2A$. This means the total profit from the grid is $(p^a - 2p^r)A + p^r PT$, and the optimal profit for fixed A is

$$\Pi(A) = p^r PT + (p^a - 2p^r)A - \frac{c_0^b}{E} A^2, \qquad \text{if } (c9).$$

Given the optimal X^* and R^* under fixed A for conditions $(c1)$ – $(c9)$, it is straightforward to establish the properties listed in Table A.7.

□

Proof of Proposition A.1:

Optimal excess regulation and power constraints

(1) Properties of the optimal solution: $\tilde{p}^r \leq \frac{T_H}{T}$

When $\tilde{p}^r \leq \frac{T_H}{T}$, $\Pi(A)$ follows condition $(c2)$ for $0 \leq A < \frac{Tp^r E}{2c_0^b}$, condition $(c1)$ for $\frac{Tp^r E}{2c_0^b} \leq A \leq \frac{PT_H}{2}$, condition $(c6)$ for $\frac{PT_H}{2} < A \leq \min(PT_H, \frac{PT_L}{2})$, and condition $(c9)$ for $T_L < 2T_H, \frac{PT_L}{2} < A \leq PT_H$. By inspection, $\Pi(A)$ is a concave function with a piecewise linear,

decreasing derivative that has discontinuities at $A = \frac{PT_H}{2}$ and $A = \frac{PT_L}{2}$. Further,

$$\begin{aligned}
\Pi'(0) &= p^a, \\
\Pi'(\frac{Tp^rE}{2c_0^b}) &= p^a - (T-2)p^r, \\
\Pi'_-(\frac{PT_H}{2}) &= p^a + 2p^r - \frac{c_0^b}{E}PT_H, \\
\Pi'_+(\frac{PT_H}{2}) &= p^a - \frac{c_0^b}{E}PT_H, \\
\Pi'_-(\frac{PT_L}{2}) &= p^a - \frac{c_0^b}{E}PT_L, \\
\Pi'_+(\frac{PT_L}{2}) &= p^a - 2p^r - \frac{c_0^b}{E}PT_L, \text{ and} \\
\Pi'(PT_H) &= \begin{cases} p^a - 2\frac{c_0^b}{E}PT_H, & T_L \geq 2T_H \\ p^a - 2p^r - 2\frac{c_0^b}{E}PT_H, & T_L < 2T_H \end{cases}.
\end{aligned}$$

(2) Properties of the optimal solution: $\frac{T_H}{T} < \tilde{p}^r \leq \frac{T_H}{T_L}$

When $\frac{T_H}{T} < \tilde{p}^r \leq \frac{T_H}{T_L}$, $\Pi(A)$ follows condition $(c2)$ for $0 \leq A < \frac{\frac{c_0^b}{E}P - p^r}{2\frac{c_0^b}{E}(1/T_H - 1/T)}$, condition $(c3)$ for $\frac{\frac{c_0^b}{E}P - p^r}{2\frac{c_0^b}{E}(1/T_H - 1/T)} \leq A \leq \frac{PT_H}{2}$, condition $(c6)$ for $\frac{PT_H}{2} < A \leq \min(PT_H, \frac{PT_L}{2})$, and condition $(c9)$ for $T_L < 2T_H$, $\frac{PT_L}{2} < A \leq PT_H$. By inspection, $\Pi(A)$ is a concave function with a piecewise linear, decreasing derivative that has discontinuities at $A = \frac{PT_H}{2}$ and $A = \frac{PT_L}{2}$. Further,

$$\begin{aligned}
\Pi'(0) &= p^a, \\
\Pi'(\frac{\frac{c_0^b}{E}P - p^r}{2\frac{c_0^b}{E}(1/T_H - 1/T)}) &= p^a - \frac{(T-2)T_H}{T_L}(\frac{c_0^b}{E}P - p^r), \\
\Pi'_-(\frac{PT_H}{2}) &= p^a - \frac{2T_L}{T_H}p^r - \frac{c_0^b}{E}P(T_H - 2), \\
\Pi'_+(\frac{PT_H}{2}) &= p^a - \frac{c_0^b}{E}PT_H, \text{ and} \\
\Pi'_-(\frac{PT_L}{2}) &= p^a - \frac{c_0^b}{E}PT_L.
\end{aligned}$$

$\Pi'_+(\frac{PT_L}{2})$ and $\Pi'(PT_H)$ are the same as the previous case ($\tilde{p}^r \leq \frac{T_H}{T}$).

(3) Properties of the optimal solution: $\frac{T_H}{T_L} < \tilde{p}^r < 1$

When $\frac{T_H}{T_L} < \tilde{p}^r < 1$ (which implies $T_L > T_H$), $\Pi(A)$ follows condition $(c2)$ for $0 \leq A <$

$\frac{\frac{c_0^b}{E}P-p^r}{2\frac{c_0^b}{E}(1/T_H-1/T)}$, condition $(c3)$ for $\frac{\frac{c_0^b}{E}P-p^r}{2\frac{c_0^b}{E}(1/T_H-1/T)} \leq A \leq \frac{\frac{c_0^b}{E}P-p^r}{2\frac{c_0^b}{E}(1/T_H-1/T_L)}$, and condition $(c4)$ for $\frac{\frac{c_0^b}{E}P-p^r}{2\frac{c_0^b}{E}(1/T_H-1/T_L)} < A \leq \frac{PT_H}{2}$. When $T_L \leq 2T_H$ or $\frac{T_H}{T_L} < \tilde{p}^r < \frac{2T_H}{T_L}$, then $\Pi(A)$ follows condition $(c7)$ for $\frac{PT_H}{2} < A < \frac{T_L p^r E}{2c_0^b}$, condition $(c6)$ for $\frac{T_L p^r E}{2c_0^b} \leq A \leq \min(PT_H, \frac{PT_L}{2})$, and condition $(c9)$ for $T_L < 2T_H$, $\frac{PT_L}{2} < A \leq PT_H$. Otherwise $\Pi(A)$ follows condition $(c7)$ for $\frac{PT_H}{2} < A \leq PT_H$. By inspection, $\Pi(A)$ is a concave function with a piecewise linear, decreasing derivative that has a discontinuity at $A = \frac{PT_L}{2}$. Further,

$$
\begin{aligned}
\Pi'(0) &= p^a, \\
\Pi'(\frac{\frac{c_0^b}{E}P-p^r}{2\frac{c_0^b}{E}(1/T_H-1/T)}) &= p^a - \frac{(T-2)T_H}{T_L}(\frac{c_0^b}{E}P-p^r), \\
\Pi'(\frac{\frac{c_0^b}{E}P-p^r}{2\frac{c_0^b}{E}(1/T_H-1/T_L)}) &= p^a - \frac{T_L T_H}{T_L-T_H}(\frac{c_0^b}{E}P-p^r), \\
\Pi'(\frac{PT_H}{2}) &= p^a - 2p^r - \frac{c_0^b}{E}PT_H(1-\frac{2}{T_L}), \\
\Pi'(\frac{T_L p^r E}{2c_0^b}) &= p^a - T_L p^r, \text{ and} \\
\Pi'_-(\frac{PT_L}{2}) &= p^a - \frac{c_0^b}{E}PT_L.
\end{aligned}
$$

$\Pi'_+(\frac{PT_L}{2})$ and $\Pi'(PT_H)$ are the same as the first case $(\tilde{p}^r \leq \frac{T_H}{T})$.

(4) Properties of the optimal solution: $\tilde{p}^r \geq 1$

When $\tilde{p}^r \geq 1$, $\Pi(A)$ follows condition $(c5)$ for $0 \leq A < \frac{PT_H}{2}$, condition $(c8)$ for $\frac{PT_H}{2} \leq A \leq \min(PT_H, \frac{PT_L}{2})$, and condition $(c9)$ for $T_L < 2T_H$, $\frac{PT_L}{2} < A \leq PT_H$. $\Pi(A)$ is a concave function with a piecewise linear, decreasing derivative that has a discontinuity at $A = \frac{PT_L}{2}$. Further,

$$
\begin{aligned}
\Pi'(0) &= p^a - 2p^r + 2\frac{c_0^b}{E}P, \\
\Pi'(\frac{PT_H}{2}) &= p^a - 2p^r + \frac{c_0^b}{E}PT_H(1-\frac{2}{T_L}), \text{ and} \\
\Pi'_-(\frac{PT_L}{2}) &= p^a - 2p^r - \frac{c_0^b}{E}P(T_L-2).
\end{aligned}
$$

$\Pi'_+(\frac{PT_L}{2})$ and $\Pi'(PT_H)$ are the same as the first case $(\tilde{p}^r \leq \frac{T_H}{T})$.

Key properties (Proposition A.1)

Most properties follow straightforwardly by combining the results in Table A.7 with the $\Pi'(A)$ results presented in the proof of Proposition A.1. For instance, we read from Table A.7

that stacking uses all available free regulation under conditions ($c1$) – ($c5$). When $\tilde{p}^r \leq \frac{T_H}{T}$, this means the property holds for $A^* \leq \frac{PT_H}{2}$, and $\Pi'_+(\frac{PT_H}{2}) \leq 0$ gives the condition for the property to hold. Here, we present a few properties that don't follow immediately from the results in Table A.7.

Positive arbitrage amount ($A^* > 0$): Stacking uses a positive amount of arbitrage whenever $\Pi'(0) > 0$. Since $\Pi'(0) = p^a > 0$ for $\tilde{p}^r < 1$ and $\Pi'(0) = p^a - 2p^r + 2\frac{c_0^b}{E}P$ for $\tilde{p}^r \geq 1$, we conclude that stacking uses a positive amount of arbitrage whenever $\tilde{p}^a > 2(\tilde{p}^r - 1)$.

Superlinear profit gain ($\Pi^*_{stk} > \Pi^*_{arb} + \Pi^*_{reg}$): Superlinear profit gain holds whenever $\Pi(A)$ follows conditions ($c1$) (with $A < \frac{PT_H}{2}$) or ($c2$) due to the fact that the stacking solution is not power constrained in such situations (see Table A.7; as a result, superlinear profit follows by Proposition 2.4). Similarly, superlinear profit gain never holds when $\tilde{p}^r \geq 1$, as established in Lemma A.1.

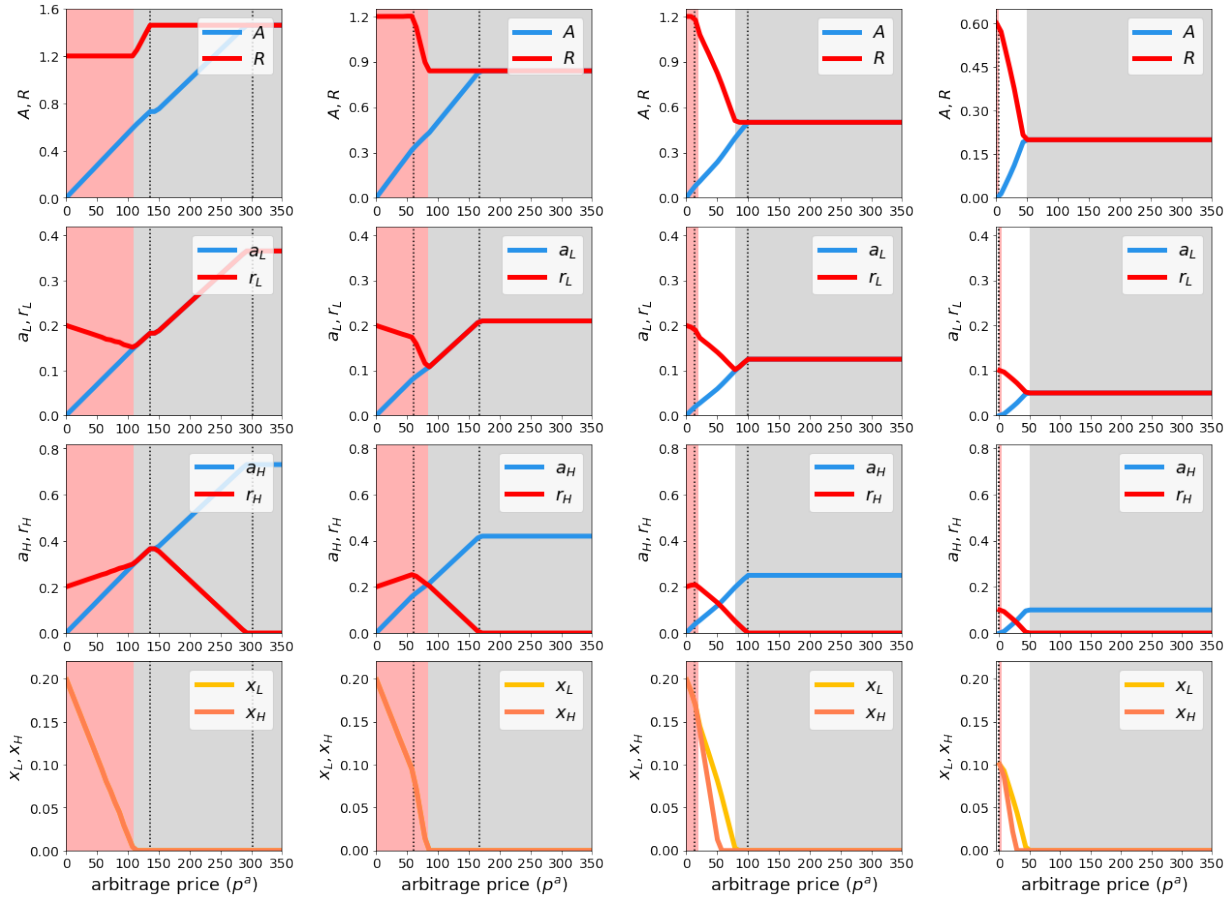
To establish when superlinear profit gain holds in other scenarios, we exhaustively checked the property under each of the remaining conditions — ($c1$) with $A = \frac{PT_H}{2}$, ($c3$), ($c4$), ($c6$), ($c7$), and ($c9$) with $\tilde{p}^r < 1$. The $\Pi'(A)$ results established thus far show that either A^* occurs at a corner point (e.g., $A^* = \frac{PT_H}{2}$ for $\tilde{p}^r \leq \frac{T_H}{T}$), in which case it holds for a range of p^a and p^r values, or otherwise A^* is a linear combination of p^a and p^r, which can be derived by solving $\Pi'(A) = 0$. In either case, $\Pi^*_{stk} - (\Pi^*_{arb} + \Pi^*_{reg})$ can be written in the form $c_1(p^a)^2 + c_2 p^a p^r + c_3(p^r)^2 + c_4 p^a + c_5 p^r + c_6$. Establishing cases with superlinear profit gain requires careful applications of the quadratic formula to establish the range of p^a where the property holds. Somewhat tedious enumeration of cases for the optimal solution yields the conditions in Proposition A.1. □

Proof of Proposition A.2:

If $E \geq PT_H$, then the energy constraint is never binding, and $\tilde{p}^a_E = \infty$ can be used in the statement of Proposition A.2. Otherwise, $\Pi(E)$ can follow any of the nine conditions ($c1$) – ($c9$), and we obtain Proposition A.2's result by setting $\tilde{p}^a_E$ to be a $\tilde{p}^a$ value such that $\Pi'(A) > 0$ for $A < E$ and $\Pi'(A) < 0$ for $A > E$. □

A.3.4.3 Comparative Statics (Binding Power Capacity)

Grid conditions evolve as technologies and policies change. For instance, [125] reported that PJM's grid conditions have changed dramatically (the number of active battery storage projects in the PJM increased from 1 to 71 between 2014 and 2020) due to battery-favorable developments such as FERC (Federal Energy Regulatory Commission) Order No. 755. We characterize grid/market conditions using comparative statics, providing forward-looking



(a) $\tilde{p}^r \leq \frac{T_H}{T}$ (b) $\frac{T_H}{T} \leq \tilde{p}^r \leq \frac{T_H}{T_L}$ (c) $\frac{T_H}{T_L} \leq \tilde{p}^r \leq 1$ (d) $\tilde{p}^r \geq 1$

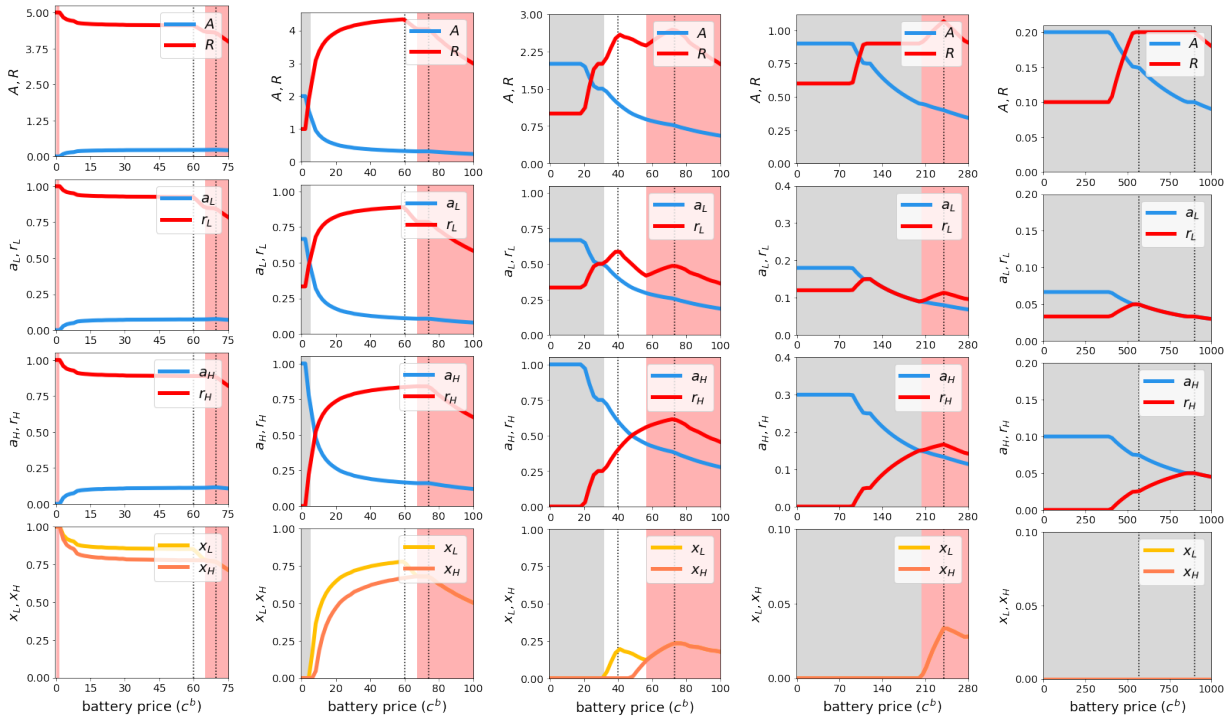
Figure A.10: Comparative statics (p^a effect). The backgrounds for $x_L^* = x_H^* > 0, x_L^* = x_H^* = 0$, and $x_L^* > x_H^* > 0$ are colored pink, gray, and white, respectively, and the dotted vertical lines show when the power capacity starts to bind in the high-price (left vertical line) and low-price (right vertical line) regions ($T_H = 8, T = 24, E = 2$).

guidance to decision makers about the effect of two key parameters, arbitrage price p^a and battery cell price c^b, on the optimal mix of arbitrage and regulation that they should provide with their battery.

p^a **effect.** The arbitrage price, p^a, has been changing over time, and these dynamics are expected to continue with increased renewable energy penetration.[10] Figure A.10 illustrates changes in the optimal mix as p^a increases. Depending on a battery's capacity, the optimal strategy can differ dramatically different from the non-binding setting (Figure 2.4a).

When $\frac{T_H}{T} \leq \tilde{p}^r \leq \frac{T_H}{T_L}$ (Figure A.10b), after the first dotted line ($a_H^* + r_H^* = P$), excess

[10]California and Texas recently observed increases in p^a as solar generation shapes electricity load into a 'duck curve' — the wholesale energy price has higher prices at the beginning and end of the day and a sharp decrease in prices (including occasionally negative prices) in the middle of the day [110].



(a) $p^a \leq 2p^r$ (b) $2p^r \leq p^a \leq \frac{2T_L p^r}{T_H}$ (c) $\frac{2T_L p^r}{T_H} \leq p^a \leq T_L p^r$ (d) $T_L p^r \leq p^a \leq (T-2)p^r$ (e) $p^a \geq (T-2)p^r$

Figure A.11: Comparative statics (c_0^b effect). The backgrounds for $x_L^* = x_H^* > 0, x_L^* = x_H^* = 0$, and $x_L^* > x_H^* > 0$ are colored pink, gray, and white, respectively, and the dotted vertical lines show when the power capacity starts to bind in the high-price (left vertical line) and low-price (right vertical line) regions.

regulation starts to decrease more rapidly than before, which leads to sharp decreases in both r_L and r_H. Eventually, r_L starts to increase again when $x_L = x_H = 0$ since all frequency regulation is free, and the amount of arbitrage being provided is increasing. Meanwhile, r_H continues to decrease due to the fact that power is binding in the high-price period, meaning any increase in the arbitrage amount must be matched with a corresponding decrease in regulation.

When $\frac{T_H}{T_L} \leq \tilde{p}^r \leq 1$ (Figure A.10c), on the other hand, there exists a region of p^a at which maintaining unequal excess $x_L^* > x_H^*$ is optimal as shown in non-shaded/white region. This enables a slower decrease in r_L compared to the rate that it would have decreased if $x_L = x_H$ is maintained. Note that performing more regulation (compared to the quantity under $x_L = x_H$) while having unequal excess be clearly beneficial when the regulation price is sufficiently high and the peak is narrow ($\tilde{p}^r \geq \frac{T_H}{T_L}$).

c_0^b effect. Recall that battery price and degradation coefficient (c^b) are proportional. The effect of changing c^b is very relevant, as battery prices have decreased precipitously in recent

years. Figure A.11c illustrates how complicated changes in the optimal mix can be as the relationship between excess regulation evolves: r_L changes in an up-down-up-down manner; r_H goes up and down. When the battery price is very high, both arbitrage and regulation increase as c^b decreases (unconstrained solution). However, once c^b is low enough so that power P is binding in the high-price period (right vertical line in Figure A.11c), the optimal profit needs to be carefully adjusted, and it is optimal to maintain equal excess by reducing both x_L and x_H.[11] This highlights that maintaining equal or unequal excess regulation is determined by the full consideration of market conditions (region length: T_H, T_L and service prices: p^a, p^r) and battery specifications (c^b and E/P ratio).

A.3.4.4 Two Common Models in Literature

Due to the iterative computations needed to compute degradation costs using the rainflow-counting algorithm, many papers have resorted to simpler models to estimate degradation costs. Below we describe the two common models in the literature.

No-Degradation Model

Interestingly, most stacking papers ignore the impacts of usage patterns on the degradation cost of batteries. Instead, they consider a fixed capital cost (e.g., up-front investment cost) and assume that a battery's degradation cost is independent of its usage profile [110, 63]. However, models that ignore cost of degradation may easily overestimate the benefits of stacking, since they do not account for increased battery utilization under stacking.

The no-degradation model maximizes the stacked revenue without consideration of usage-based battery degradation. Then, the objective function can be formulated as follows:

$$\max_{A, r_L, r_H} \quad p^a A + p^r r_L T_L + p^r r_H T_H. \tag{A.12}$$

The optimal action under the no-degradation model can be easily derived:

$$A^* = \begin{cases} 0, & \text{if } p^a \le 2p^r \\ \min(E, PT_H), & \text{if } p^a > 2p^r \end{cases},$$

$$r_i^* = P - a_i^* = \begin{cases} P, & \text{if } p^a \le 2p^r \\ P - \frac{\min(E, PT_H)}{T_i}, & \text{if } p^a > 2p^r \end{cases} \quad \text{for } i = L, H.$$

Under the no-degradation model, we always operate a battery at its maximum power capacity

[11] Note that r_L also should be decreased even though $r_L + a_L < P$ since the battery price is still burdensome. When c^b gets low enough, increasing r_L and having unequal excess becomes optimal as long as $r_L + a_L < P$. Once $r_L + a_L = P$, both regulation should be decreased in order to increase A.

and do either "no" arbitrage or "full" arbitrage. Unsurprisingly, this aggressive usage of batteries may lead to undesirable or even disastrous outcomes (we will see this).

Linear-Degradation Model

The linear-degradation model ($\beta = 1$) has been commonly used in the industry/literature to capture the tradeoff between increased revenue and degradation costs that comes from increased use of a battery. The obvious advantage of the linear-degradation model is its simplicity — under the rainflow-counting algorithm, this is equivalent to assuming that degradation is proportional to the total energy throughput (charging or discharging) of the battery [74, 213]. While a linear approximation of degradation is methodologically appealing (no need to rely on the iterative calculation of the rainflow-counting algorithm), it may easily lead to poor battery performance due to misrepresenting the actual (nonlinear) degradation process.

The objective function under the linear-degradation model is formulated as follows:

$$\max_{A, r_L, r_H} \quad p^a A + p^r r_L T_L + p^r r_H T_H - c^b_{lin}[A + \frac{T_L}{2} x_L + \frac{T_H}{2} x_H]. \tag{A.13}$$

where c^b_{lin} denotes the battery degradation coefficient under the linear degradation model.[12] Following [174], the linearized degradation coefficient c^b_{lin} is fitted as follows:

$$c^b_{lin} = \frac{c_{cell} \times E}{Nl \times E} = \frac{c_{cell}}{Nl}, \tag{A.14}$$

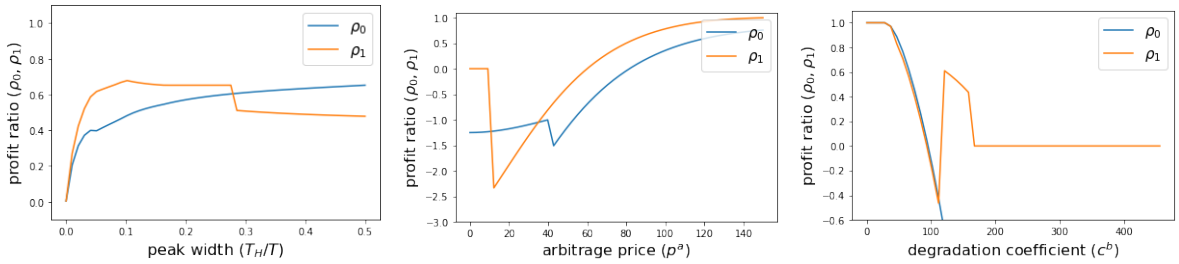
where c_{cell} is the battery cell price (\$/MWh), $l \in [0, 1]$ is the operable DOD range (as a fraction of the total energy capacity E), and N is the number of cycles that the battery can operate at the specified DOD range. Under the linear-degradation model, some of the dynamics are undesirable:

Lemma A.6 (Linear-degradation)**.** *The optimal regulation rates given a fixed arbitrage amount A satisfy the following:*

- *If $2p^r > c^b_{lin}$, $r^*_i(A) = P - a_i,\ i = L, H$.*
- *If $2p^r \leq c^b_{lin}$, $r^*_i(A) = \min(P - a_i, a_i),\ i = L, H$. Thus, $x^*_L = x^*_H = 0$.*

Proof. For each time period $i \in \{L, H\}$, $\frac{\partial \Pi}{\partial r_i} = \begin{cases} p^r T_i, & \text{if } r_i < a_i \\ (2p^r - c^b_{lin})\frac{T_i}{2}, & \text{if } r_i > a_i \end{cases}$. If $c^b_{lin} < 2p^r$, then it is always profitable to increase regulation, so we use the maximum physically possible

[12] Typically, c^b_{lin} is calibrated over a limited SOC range where linear fitting works relatively well, but at the sacrifice of batteries' maximum usability. For example, [174] assumes the linear degradation function by restricting the operable SOC region to 0–70% of energy capacity (the maximum DOD is upper bounded by 70% to avoid deep-cycle effects).



(a) peak width $\frac{T_H}{T}$ (b) arbitrage price p^a (c) degradation coefficient c_0^b

Figure A.12: Stacking performance under the two misspecified models ($\rho_0 = \frac{\Pi^*_{no}}{\Pi^*_{quad}}, \rho_1 = \frac{\Pi^*_{lin}}{\Pi^*_{quad}}$).
(a): $E = 1, P = 2, p^r = 10, p^a = 80, c_0^b = 150, c_{lin}^b = 75$, (b): $E = 1, P = 2, T_H = 4, T = 10, p^r = 20, c_0^b = 150, c_{lin}^b = 75$, (c): $E = 1, P = 0.25, T_H = 12, T = 40, p^r = 10, p^a = 60$, and $l = 0.5$ are used as parameters.

regulation in each time period. Otherwise, only free regulation is profitable, so we use the maximum physically possible free regulation in each time period. □

As stated in Section 3.3, a significant portion of the existing literature disregards the cost of degradation or uses a simplified (linearized) degradation function, and thus fails to capture the true impact of stacking on batteries' degradation costs. As we shall see, these models rely heavily on a battery's power or energy capacity; since stacking usually leads to increased battery usage, disregarding or incorrectly modeling degradation costs may lead to overuse of batteries. In this section and later in Appendix A.4, we numerically illustrate the effect of misspecification of degradation costs on stacking's performance.

Figure A.12 quantifies the performance of the two misspecified models across various values for the peak width $\frac{T_H}{T}$, arbitrage price p^a, and degradation coefficient c^b. In the figure, $\rho_0 = \frac{\Pi^*_{no}}{\Pi^*_{quad}}$ and $\rho_1 = \frac{\Pi^*_{lin}}{\Pi^*_{quad}}$ denote the portion of the optimal stacking profit that is achieved in the misspecified models, where Π^*_{quad} is the optimal stacking profit under the correct model specification and Π^*_{lin} and Π^*_{no} are the (true) stacking profits under the optimal solutions to the two misspecified models.

As expected, ρ_0 can be negative when either c^b is high or service prices are low. Interestingly, it is possible that $\rho_0 > \rho_1$ or $\rho_0, \rho_1 < 0$. For example, when $2p^r \leq c_{lin}^b$, the linear model may be too conservative and not use the battery at all, whereas the no-degradation model's (over-)optimism lets the battery operate, generating positive profit in some cases. On the other hand, a c_{lin}^b that is too small underestimates the true battery degradation coefficient c^b, which may lead to overusage of a battery and $\rho_1 < 0$. In the engineering literature on stacking, as stated in Section 2.2.2, increased utilization and diversified revenues are often

assumed to drive the economic feasibility of stacking. The comparative statics above highlight the importance of correctly characterizing the degradation costs, and that two common models from the industry/literature may result in a significant suboptimality.[13]

A.3.5 Details of Table 2.2

To summarize our modeling extensions, Table A.8 provides specific conditions (for simplicity, we exclusively compare cases when energy capacity is non-binding) required for the key properties established for the base model in Section 2.5 to continue to hold.

Properties	Base model	Correlated prices	Inefficiency $\eta \in (\eta_{stk}, 1]$	Trinary signal	$P, E < \infty$
A^* increases in p^r	$p^a \geq (T-2)p^r$	inc. in k ($k \leq \frac{1}{T_H-1}$), inc. in p_0^r ($k \leq \frac{p^a-(T-2)p_0^r}{(T_H-1)\bar{p}+(T_L-1)\underline{p}}$)	$p^a \geq \bar{d}\tilde{p}^x$	$p^a \geq \frac{T-2\alpha}{\alpha}p^r$	$(T-2)\tilde{p}^r \leq \tilde{p}^a \leq -2\tilde{p}^r + T_H$, $\tilde{p}^r < \frac{T_H}{T}^\star$
R^* increases in p^a	$p^a \geq (T-2)p^r$	$k \leq \frac{p^a-(T-2)p_0^r}{(T_H-1)\bar{p}+(T_L-1)\underline{p}}$	$p^a \geq \bar{d}\tilde{p}^x$, dec. in $\underline{p}$	$p^a \geq \frac{T-2\alpha}{\alpha}p^r$	$(T-2)\tilde{p}^r \leq \tilde{p}^a \leq -2\tilde{p}^r + T_H$, $\tilde{p}^r < \frac{T_H}{T}$
$A^*_{stk} > A^*_{arb}$	always	$k < \frac{2}{T_H}$	$p^a \geq \bar{d}\tilde{p}^x$ or $\eta > \hat{\eta}_A, p^a \leq \bar{d}\tilde{p}^x$	$p^a > \frac{T(1-\alpha)}{\alpha}p^r$	Prop A.1 – A.2
$R^*_{stk} > R^*_{reg}$	$p^a > (T-2)p^r$	$k \leq \frac{p^a-(T-2)p_0^r}{(T_H-1)\bar{p}+(T_L-1)\underline{p}}$	$p^a \geq \bar{d}\tilde{p}^x$ and $\eta > \eta^*$ or $\eta < \hat{\eta}_R$	$p^a > (\frac{T}{\alpha^2}-2)p^r$	Prop A.1 – A.2
$A^* > 0$	always	$k < 1$	$\eta \geq \eta^*, p^a \geq d_1\tilde{p}^x$ or $\eta < \eta^*, p^a \geq d_2\tilde{p}^x$	$p^a > \frac{2(1-\alpha)}{\alpha}p^r$	$\tilde{p}^a > 2(\tilde{p}^r - 1)$
$x^*_L = x^*_H$	always	$k \leq \frac{1}{T_H-1}$	$\eta \geq \eta^*$ or $p^a \geq \bar{d}\tilde{p}^x$	always	Prop A.1 – A.2
$\frac{R^*}{A^*}$ indpt. of c_0^b	always	always	always	always	dependent
$\frac{R^*}{A^*} \geq 2$	always	always	always	always	Prop A.1 – A.2
$\max S$ (large T)	2	$2 + \frac{1}{2T_H-1}$	∞	2	2
Cost-saving synergy	always	$k < \frac{5T_L+T_H}{(4T_H-3)T_L+T_H}$	$\eta \geq \eta^*$ or $p^a \geq \bar{d}\tilde{p}^x$	$p^a > \frac{2(1-\alpha)}{\alpha}p^r$	Prop A.1 – A.2
Superlinear profit	always	$k \leq \frac{2}{2T_H-1}$ or $k < \frac{T_L-T_H+\sqrt{T(T-2)}}{2T_LT_H-T}$, $p^a \leq \frac{B-\sqrt{B^2-AC}}{A}^\dagger$	suff. large p^a	$p^a > p^a_\alpha$	Prop A.1 – A.2

Table A.8: Key properties under the extensions considered (when c_0^b is sufficiently large).

†: See Corollary A.1 for constants A, B, and C;
‡: See Theorem A.4 and Corollary A.4;
*: $\tilde{p}^a = \frac{p^aE}{c_0^bP}$ and $\tilde{p}^r = \frac{p^rE}{c_0^bP}$ from Lemma A.5.

[13] [208] raises similar issues: the no-degradation model achieves negative profits (the battery is so overused that it must be replaced within 1-3 years), while the linear-degradation model tends to be too conservative, making the battery remain idle most of the time.

A.4 Numerical Results

In this section, we numerically check the sensitivity of our results to key modeling assumptions and evaluate the performance of stacking under various plausible situations, with the goal of establishing the realistically achievable benefits of stacking under current grid conditions and of confirming that the synergy properties predicted by our model continue to hold under more realistic data.

Section A.4.1 explains the operational dataset used for the numerical study. Section A.4.2 constructs comprehensive optimization problems for different operations (standalone services, time-exclusive stacking, and simultaneous stacking) and calibrates model parameters to reflect realistic grid/market circumstances and batteries' characteristics. Section A.4.3 reports the numerical results including illustrations of actual dispatching profiles (Section A.4.3.1) and extensive profitability analysis (Section A.4.3.2).

A.4.1 Dataset

A.4.1.1 Day-Ahead Energy/Regulation Price Dataset

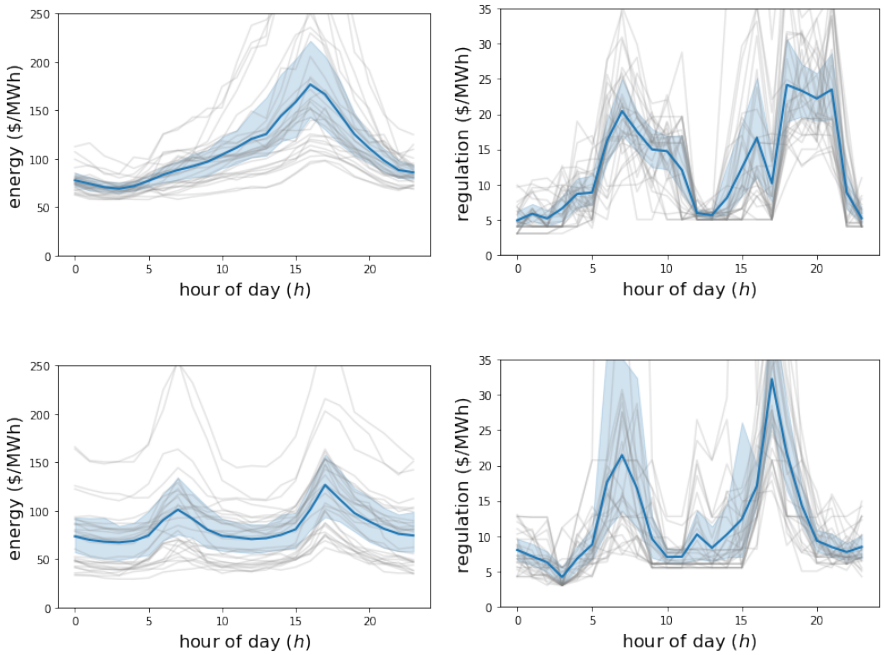


Figure A.13: Day-ahead (hourly) energy and regulation prices: (top) summer, (bottom) winter. Gray lines represent realized price patterns. The blue solid line and blue region specify the average prices and confidence interval, respectively (source: [135]).

Figure A.13 shows price patterns retrieved from the 2022 NYISO operational dataset ([135]). Note that the energy prices exhibit distinctive seasonality. During summer, energy prices tend to have a single peak per day quite consistently at 3 – 5 pm. During winter, energy prices tend to have two peaks consistently at 5 – 7 am and 5 – 7 pm. Despite the price uncertainty, the timing of peak price periods is quite predictable, which confirms the predictability of peak timing in Assumption 2.1. Regulation prices also have two peaks, which are correlated with price peaks during winter. Previous years (2019 – 2021) show similar patterns but have smaller price uncertainty compared to the year 2022. As detailed in Appendix A.4.2.2, we calibrated price parameters based on the historical price dataset.

A.4.1.2 Regulation Signal Dataset

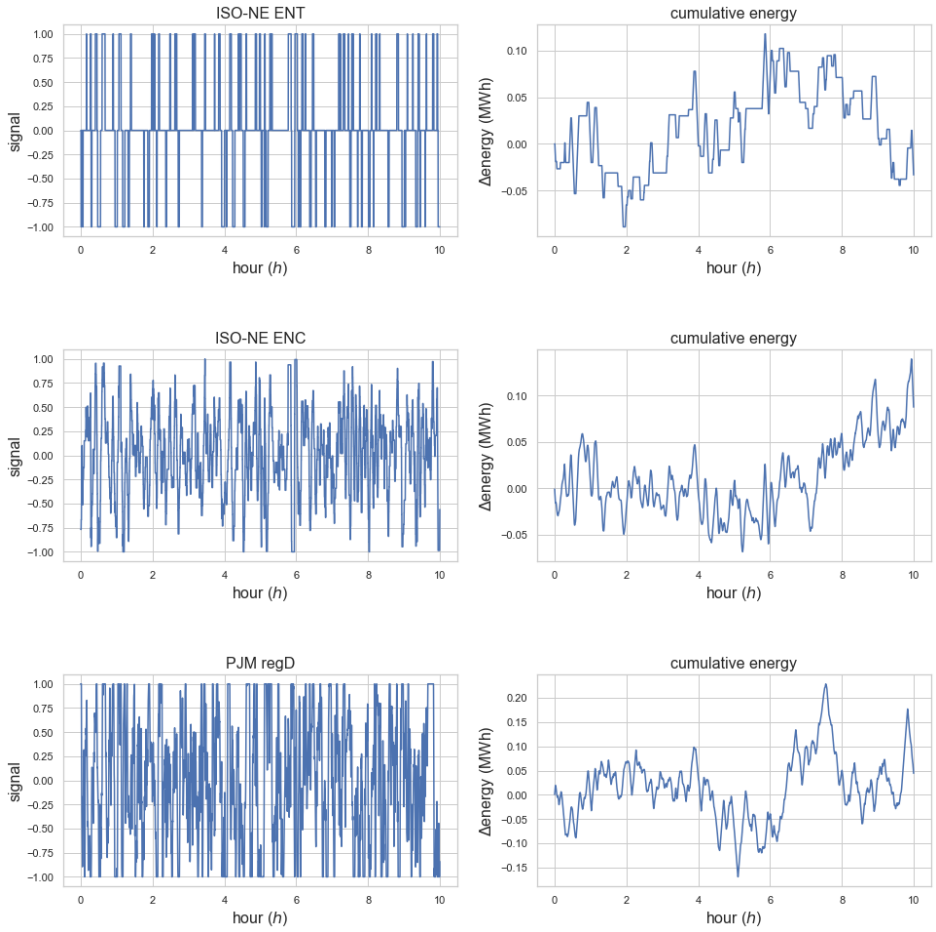


Figure A.14: Regulation signals and the corresponding net energy change under a unit capacity commitment: (top) ISO-NE trinary; (middle) ISO-NE continuous; (bottom) PJM regD.

As stated in Appendix A.1.2, the energy-neutrality guarantee level may differ across regulation signals and ISOs. Figure A.14 illustrates three different regulation signals for a single day from the ISO-NE simulated automatic generator control (AGC) dataset ([80]) and the PJM regulation signal dataset (Jan 1st, 2020; [149]), along with the corresponding net energy change assuming a unit capacity commitment. As detailed in Appendix A.4.2.2, we calibrated the characteristics of regulation signals based on the historical signal dataset.

A.4.2 Hourly Optimization Models

In numerical experiments, we formulate and solve optimization problems for each operation (standalone services, time-exclusive stacking, and simultaneous stacking), using realistic grid/market parameters and battery characteristics. In Appendix A.4.2.1, we first formulate an hourly optimization problem with intra-day price non-stationarity (expected hourly service prices p_i^e for energy and p_i^r for regulation), dispatch-to-contract ratio α, energy-neutrality (we assume energy neutrality will be restored within $2\Delta^c$ time units), battery power P, battery energy E, and battery round-trip efficiency η^2. We then evaluate the performance of the optimized schedule using real grid data (price profiles and regulation signals).

A.4.2.1 Hourly Optimization Model Formulation for Simultaneous Stacking

$$\max_{a_i,r_i,I_i,J_i,S_{max},S_{min},D} -\sum_{i=1}^{T_L} p_i^e a_i + \sum_{i=T_L+1}^{T} p_i^e a_i + \sum_{i=1}^{T} p_i^r r_i - \frac{c_0^b}{E}\left[D^2 + \sum_{i=1}^{T} \frac{(x_i\Delta^c)^2}{2\Delta^c}\right] \tag{A.15}$$

$$x_i = \begin{cases} \alpha(r_i - a_i)^+/\eta, & \forall i = 1,\cdots,T_L \\ \alpha(r_i - a_i)^+\eta, & \forall i = T_L+1,\cdots,T \end{cases} \tag{A.16}$$

$$S_1 = S_{T+1} \tag{A.17}$$

$$S_{i+1} = S_i \tag{A.18}$$

$$+ \begin{cases} I_i[\frac{\alpha}{2}[a_i(1/\eta+\eta) - r_i(1/\eta-\eta)] + (1-\alpha)a_i\eta] + J_i[a_i\eta], & \forall i = 1,\cdots,T_L \\ I_i[-\frac{\alpha}{2}[a_i(1/\eta+\eta) + r_i(1/\eta-\eta)] - (1-\alpha)a_i/\eta] + J_i[-a_i/\eta], & \forall i = T_L+1,\cdots,T \end{cases}$$

$$r_i - a_i \le MI_i,\ \forall i = 1,\cdots,T \tag{A.19}$$

$$a_i - r_i \le MJ_i,\ \forall i = 1,\cdots,T \tag{A.20}$$

$$I_i + J_i = 1,\ \forall i = 1,\cdots,T \tag{A.21}$$

$$S_{min} \le S_i - x_i\Delta^c,\ \forall i = 1,\cdots,T_L \tag{A.22}$$

$$S_{min} \le S_{i+1} - x_i\Delta^c,\ \forall i = T_L+1,\cdots,T \tag{A.23}$$

$$S_{max} \ge S_{i+1} + x_i\Delta^c,\ \forall i = 1,\cdots,T_L \tag{A.24}$$

$$S_{max} \ge S_i + x_i\Delta^c,\ \forall i = T_L+1,\cdots,T \tag{A.25}$$

$$D \ge S_{max} - S_{min} \tag{A.26}$$

$$D \le E \tag{A.27}$$

$$a_i + r_i \le P,\ \forall i = 1,\cdots,T_L \tag{A.28}$$

$$\frac{r_i - a_i}{\eta} \le P, \forall i = 1,\cdots,T_L \tag{A.29}$$

$$\frac{a_i + r_i}{\eta} \le P,\ \forall i = T_L+1,\cdots,T \tag{A.30}$$

$$I_i \in \{0,1\},\ \forall i = 1,\cdots,T \tag{A.31}$$

$$J_i \in \{0,1\},\ \forall i = 1,\cdots,T \tag{A.32}$$

$$a_i \ge 0,\ \forall i = 1,\cdots,T \tag{A.33}$$

$$r_i \ge 0,\ \forall i = 1,\cdots,T. \tag{A.34}$$

We optimally decide hourly service rates for arbitrage (a_i) and regulation (r_i) that the battery commits to provide the grid for each time interval i, requiring that the arbitrage rate be used to fill the battery during low-price periods 1 through T_L, while arbitrage be used to

discharge the battery during high-price periods $T_L + 1$ through T. S_i, the SOC level at the beginning of time interval i, evolves following eq. (A.18), where M is some large constant and the binary variables I_i and J_i differentiate whether excess regulation is strictly positive or not (e.g., when $r_i > a_i$, then $I_i = 1,\ J_i = 0$). As in the main model, we assume the battery operates over multiple days, so we require the starting and ending SOC to be equal. Degradation is estimated using the $+1, 0, -1, 0, \cdots$ pattern from Section 2.6.3, with the time spent at each signal level as $\alpha\Delta^c, (1-\alpha)\Delta^c, \alpha\Delta^c, \cdots$. D represents the largest cycle. The energy constraint in eq. (A.27) is more general than eq. (2.8) from Section 2.6.4, capturing the potential expansion of the largest cycle due to positive excess regulation. Eqs. (A.28) – (A.30) guarantee that the services combined are deliverable without violating the battery's power capacity. Since decision variables are defined from the grid's perspective ([19, 132]), the discharging (charging) rate is upper limited by $P\eta$ (P) after factoring in energy loss.

The benchmark models can be defined similarly with some adjustments below.

Time-exclusive stacking: Simultaneous stacking with eqs. (A.19) – (A.20) being replaced by:

$$a_i \leq MJ_i,\ \forall i = 1, \cdots, T, \tag{A.35}$$

$$r_i \leq MI_i,\ \forall i = 1, \cdots, T, \tag{A.36}$$

implying arbitrage and regulation can be only provided exclusively.

Regulation-Only: Time-exclusive stacking with additional constraints

$$a_i = 0,\ \forall i = T_L + 1, \cdots, T.$$

Note that we allow $a_i > 0$ for $i \leq T_L$ to allow energy replenishment to offset energy losses from providing regulation, as we did in Section 2.6.2.

Arbitrage-Only: Time-exclusive stacking with additional constraints

$$r_i = 0,\ \forall i = 1, \cdots, T.$$

A.4.2.2 Calibration of Model Parameters

To calibrate our models, we used real-world historical data from the NYISO day-ahead energy and regulation hourly price dataset from Jan 01, 2019 to Dec 31, 2022 and from the ISO-NE trinary/continuous regulation signal dataset, which includes data from before (2019 – 2020) and during (2021 – 2022) the global energy crisis. Other model parameters are calibrated using real-world operational data from multiple ISO/RTOs in the United States.

Type	Notation	Parameter	Value	Unit	Sources
Grid/market condition	p_i^e	energy hourly price ($i = 1, \cdots, 24$)	historical values	\$/MWh	[135]
	p_i^r	regulation hourly price ($i = 1, \cdots, 24$)	historical values	\$/MWh	[135]
	$2\Delta^c$	energy neutrality time period	1	hrs	[150, 81, 135]
	T_H	peak length	2	hrs	[150, 81, 135]
	T	total time length (winter/summer)	12 (w) / 24 (s)	hrs	[150, 81, 135]
	α	dispatch-to-contract ratio	0.6	-	[150, 81, 135]
Battery specification	β	degradation exponent	1.5–2.5‡	-	Table A.1
	c_0^b	degradation coefficient	150 (165)†	\$	[208], [21, 110]
	c_{lin}^b	linearized degradation coefficient ($l = 0.3$)	13.5 (14.9)†	\$/(MWh)	Table A.1, [144]
	c_{lin}^b	linearized degradation coefficient ($l = 0.5$)	37.5 (41.3)†	\$/(MWh)	Table A.1, [144]
	c_{lin}^b	linearized degradation coefficient ($l = 0.7$)	73.5 (80.9)†	\$/(MWh)	Table A.1, [174]
	l	DOD range for linear degradation models	0.3–0.7	-	[144, 174]
	P	power capacity	0.5	MW	[177]
	E	energy capacity	1	MWh	[177]
	η^2	round-trip efficiency	0.8 (0.7)‡	-	[52, 56]

Table A.9: Summary of the model parameters used in Appendix A.4.

Using the battery specifications from Key Capture Energy's Bulk Energy Storage Market Bridge Incentive (MBI) program in New York, we consider a lithium-ion BESS with energy capacity $E = 1$MWh and power capacity $P = 0.5$MW (see also [177, 54, 97] for typical grid-scale battery specifications). The round-trip efficiency is set to 80% (the average utility-scale battery's round-trip efficiency from [56]). For grid/market conditions, we take typical values reported or numerically fitted from the NYISO (as well as ISO-NE and PJM) operational datasets. The energy neutrality time period is set as $2\Delta^c = 1$ hour based on the empirically observed energy neutrality time in the ISO-NE trinary/continuous signals, as described in Appendix A.1.2. The peak length (two hours per peak) and timing are determined from the historical pattern in Figure A.13. Table A.9 summarizes all the model parameters used and the sources for our numerical study.

A.4.3 Results

A.4.3.1 Actual Dispatching Profiles and Capacity Utilization

Figure A.15 illustrates canonical examples of actual dispatching profiles under each operation (arbitrage only, regulation only, time-exclusive stacking, and simultaneous stacking) when optimizing using the models from Appendix A.4.2.1 and parameter estimates from Appendix A.4.2.2. For illustrative purposes, three different regulation signals are drawn for regulation-only and stacking. The overall performance over $N = 100$ randomly selected realizations of the regulation signal and price profiles is $S = \frac{\Pi_{stk}}{\max(\Pi_{arb}, \Pi_{reg})} = 1.23$ and $\frac{\Pi_{stk}}{\Pi_{te}} = 1.23$; for a fair comparison, the net energy change between the initial and final energy levels (due to the regulation signal not being exactly energy neutral throughout the course of the day) is

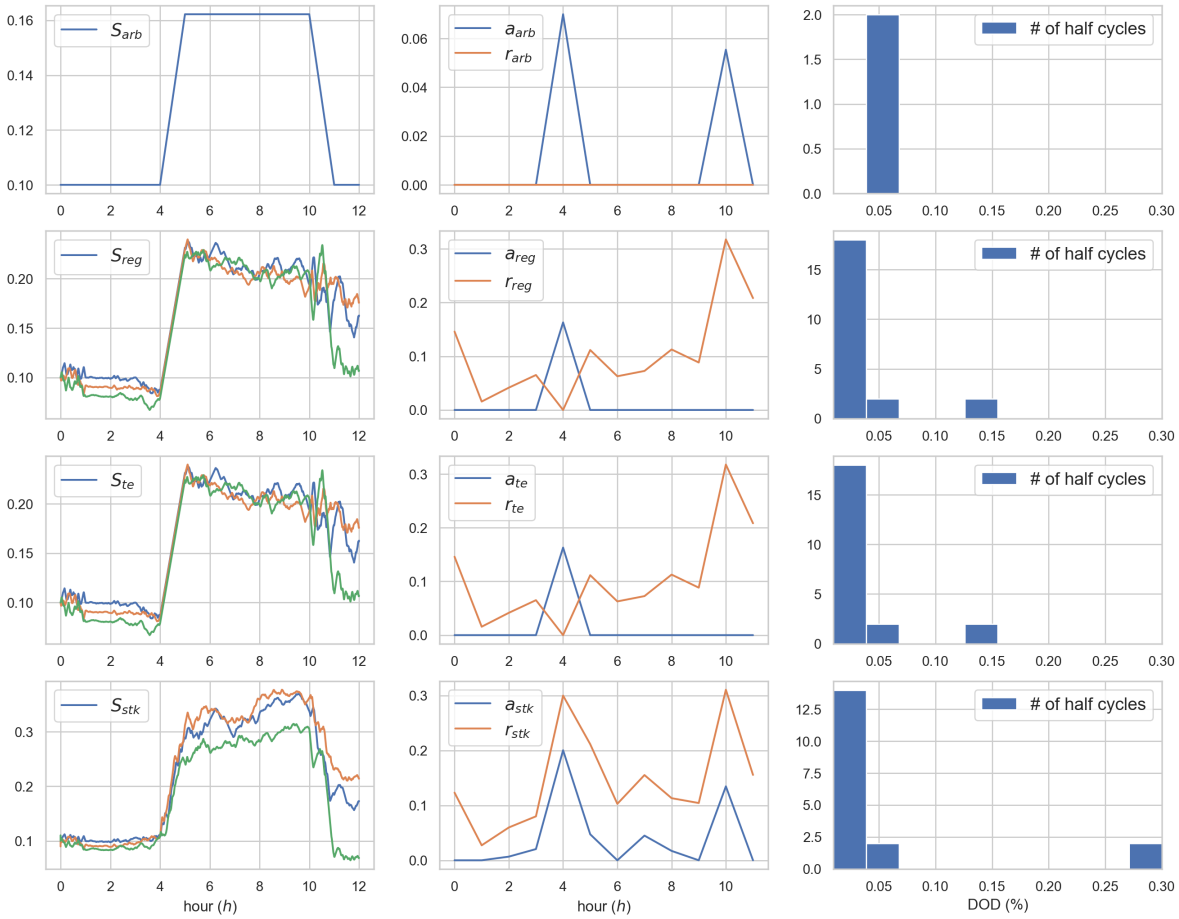


Figure A.15: Illustration of actual dispatching profile: each row sequentially represents arbitrage-only, regulation-only, time-exclusive stacking, and simultaneous stacking. The left, middle, and right columns represent the SOC levels (three realizations), provision rates for arbitrage/regulation, and the histogram of DOD sizes (the number of half cycles) from the rainflow counting algorithm for the blue realization of the regulation signal, respectively.

credited if positive and charged if negative, according to NYISO's accounting manual [136].

In Figure A.15, the histogram of DOD sizes (the right column) is obtained from the rainflow counting algorithm for the blue realization in the SOC plot (the left column). It shows that arbitrage-only has a single cycle (two half cycles of DOD = 6.1%); regulation-only has a single mid-sized cycle (10% < DOD < 20%) and many small cycles (DOD < 10%). Time-exclusive stacking coincides with regulation-only since regulation is much more attractive than arbitrage. On the other hand, simultaneous stacking has a large cycle (DOD = 27.1%) with many small-sized cycles (DOD < 10%). Note that simultaneous stacking provides much more service (and earns larger revenues) than other benchmark models, especially during the peak hours of periods 4 and 10, as shown in the second column. This is because simultaneous stacking benefits from cost-saving synergy by increasing both service rates at the same time.

A.4.3.2 Sensitivity Analysis

We further perform an extensive sensitivity analysis over a range of parameters to evaluate stacking's performance. Tables A.10 (for $\eta^2 = 0.8$) and A.11 (for $\eta^2 = 0.7$) show stacking's performance under different scenarios that reflect alternative assumptions and parameters (e.g., different times of the year and degradation functions). For each operation, we report the average performance of over $N = 100$ realizations, where the realizations of service prices and regulation signals are randomly drawn from the historical data. The findings are five-fold. First and foremost, the key lessons of the analytical work (e.g., degradation/energy replenishment cost savings and superlinear profit improvement) continue to hold using realistic grid/market parameters and battery characteristics, even when the two-price assumption is relaxed to hourly service prices. Second, the overall performance of stacking relative to standalone service tends to improve when the cost of degradation is less convex. Less convexity of the degradation function (when β is smaller) implies that frequency regulation carries a higher portion of the cost burden, as regulation cycles become more expensive. In such cases, stacking benefits more from cost-saving synergy. For example, when $\beta = 1.5$, the profit can be more than doubled ($S \approx 2.5$) compared to the profit of the best standalone service. Third, having multiple peaks (per day) implies higher arbitrage rates, which increases the maximum free regulation. This implies that stacking can be more important under ISO/RTOs typically having multiple peaks such as CAISO and NYISO. Fourth, as battery efficiency decreases and service prices decrease, S ratios tend to increase, emphasizing the expanded benefit of stacking under such circumstances. From the point of view of the likely market trajectory, this dependency may be particularly relevant, as many used car batteries with lower efficiency could soon be available for second-life uses. Lastly, the values of ρ_0, ρ_1 imply that the misspecified models (no- and linear-degradation models) suffer

severe suboptimality with real-world parameters, since they tend to have larger DODs; thus, accurately capturing the nonlinearity in the degradation costs becomes crucial. It is also noteworthy that the heuristic DOD restrictions used in the linear-degradation model may still perform poorly.

Figure A.16 shows that power/energy utilization for Table A.10 with three different degradation exponents $\beta \in \{1.7, 2.0, 2.3\}$, which confirms that both constraints are not likely to be binding under the service prices experienced in 2019 – 2020. Similar findings are also reported in other numerical studies (e.g., [144, 208]). [208] demonstrate that providing frequency regulation at full capacity can result in very early battery retirement (within less than 3 years) and significant monetary loss, as the investment cost of the battery cannot be recovered.

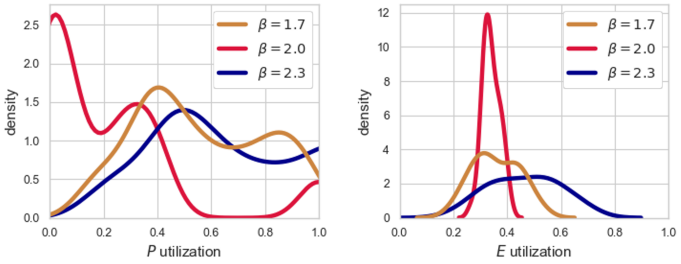
As of 2021 – 2022, however, power capacity is from time to time (roughly 5% of the time) binding due to exceptional service prices due to the energy crisis. As the degradation function becomes more convex (i.e., has a larger β), we tend to provide more regulation. Intuitively, this is the situation where frequency regulation becomes less demanding in terms of degradation costs; thus, the overall power usage increases, which also increases the maximum DOD (energy utilization).

A.4.3.3 Managerial Implications

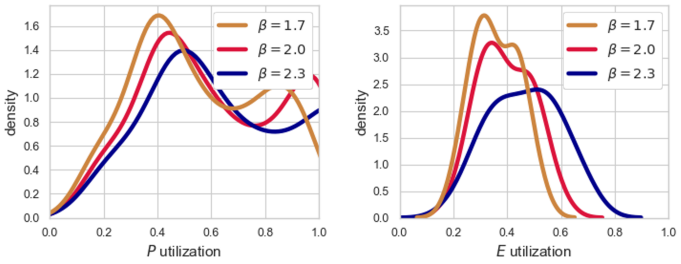
In this subsection, we will briefly discuss the potential managerial implications of this work for battery operators and practitioners. Specifically, we will address two key questions: (1) "Which ISO markets offer the greatest benefits for battery operators adopting stacking?" and (2) "Which types of batteries derive the greatest benefits from stacking in a given grid/market environment?".

For the first question, we analyze market environments with different characteristics such as varying peak widths (represented by $\frac{T_H}{T}$), energy-neutrality guarantees ($2\Delta^c$), and service price ratios ($\frac{p^a}{p^r}$), and we determine which ISO markets are most suitable for adopting the proposed stacking strategy, as measured by stacking's relative strength over standalone services. For the second question, we focus on identifying the relationship between battery type/characteristics and potential profit boost from stacking given some grid/market environment. Parameters such as longevity coefficient (z), round-trip efficiency (η^2), and power-to-energy ratio (P/E) play a crucial role in determining the batteries that are best suited for stacking.

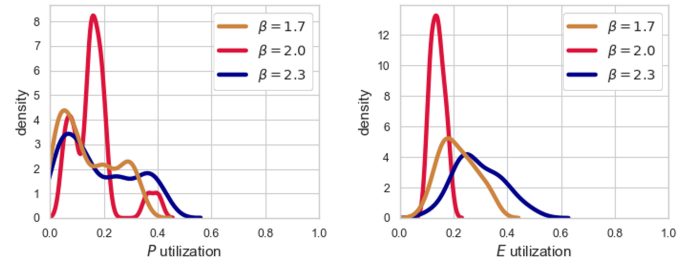
By addressing these questions and considering various factors, we aim to provide valuable insights to battery operators and practitioners, enabling them to make informed decisions about whether to make battery management system (BMS) upgrades to enable stacking.



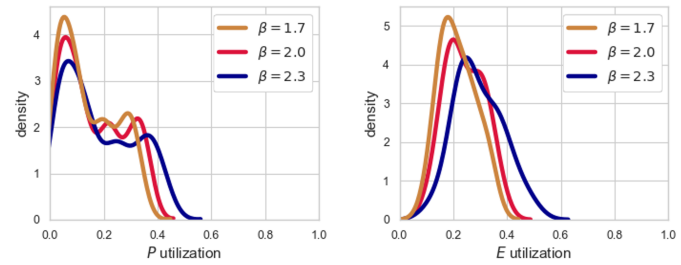
(a) NYISO 2021 – 2022 dataset (summer)



(b) NYISO 2021 – 2022 dataset (winter)



(c) NYISO 2019 – 2020 dataset (summer)



(d) NYISO 2019 – 2020 dataset (winter)

Figure A.16: Power and energy utilization density plot for Table A.10 under different degradation exponents $\beta = 1.7, 2.0, 2.3$.

(1) Which ISO markets offer the greatest benefits for battery operators adopting stacking?

Even though the total capacity of grid-scale BESS continues to grow in the U.S. (and globally), regional patterns such as weather conditions and ISO/RTO market structures can have a significant impact on the profitability of a battery. In fact, [54] reveals that the characteristics of grid-scale BESS in the U.S. vary significantly depending on their deployment locations. For instance, batteries located in CAISO and ISO-NE tend to have a lower power-to-energy ratio, typically consisting of 4-hour batteries. Conversely, batteries in PJM have a high power-to-energy ratio, with 1-hour batteries being the norm.[14]

Determining which battery operators should consider adopting the stacking strategy based on the ISO in which they operate is a crucial question in practice, since adopting stacking may require a shift in BMS technology to a provider like E3 or Fluence.

Figure A.17 shows stacking's relative profit $S = \frac{\Pi^*_{stk}}{\max(\Pi^*_{arb}, \Pi^*_{reg})}$ over various grid/market environments. Specifically, Figure A.17a varies the peak width $\frac{T_H}{T} \in [0.05, 0.5]$ and different service price ratios (by multiplying a constant to regulation prices p^r for fixed energy prices), while Figure A.17b varies the peak width and the energy-neutrality guarantee $2\Delta^c \in [0.125, 1]$. For each case, we report the average performance over $N = 100$ realizations, where the hourly energy/regulation prices and regulation signals are randomly sampled.

From Figure A.17a, stacking achieves the highest benefits in scenarios where the peak is wide (e.g., $\frac{T_H}{T} = 0.5$) and the regulation prices are lower than the current levels (e.g., p^r multiplier of 0.5).[15] This is because wide peaks enable the battery to better make use of cost-saving synergy, and reduced regulation prices relative to arbitrage prices (represented by the p^r multiplier being less than 1) make the profitability of providing regulation services more comparable to that of providing arbitrage services (recall that providing regulation is significantly more profitable compared to providing arbitrage services as of 2022).

From Figure A.17b, stacking yields greater benefits when the energy-neutrality guarantee is weaker (indicating a longer time to achieve energy neutrality while providing regulation services). This is because strong energy neutrality implies smaller regulation cycles, leading to lower degradation costs. Consequently, regulation services become even more favorable in comparison to arbitrage services, resulting in a smaller marginal benefit from stacking.

The obtained results provide insights about the ISO/RTOs where battery owners should

[14]Later in our discussion, we will provide a rationale for this discrepancy by demonstrating that the PJM market design strongly favors batteries providing regulation services over other types of services. As a result, this market structure has incentivized investment in batteries with high power-to-energy ratios to provide regulation services effectively.

[15]To construct service prices for different peak widths based on the historical data, we interpolated the historical prices by increasing/decreasing the number of data points used for interpolation on the extended/shortened periods, respectively.

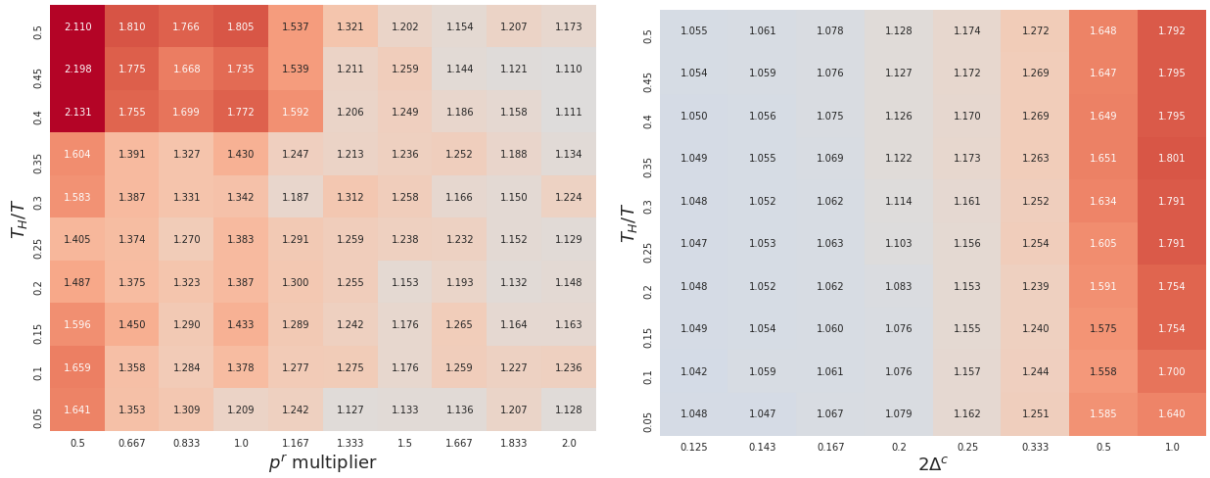
put particular emphasis on implementing stacking. For instance, batteries located in PJM, where regulation-to-arbitrage service price ratios are relatively high and the energy-neutrality condition is more strict, may experience fewer benefits from stacking. According to [125], PJM has observed high ratios of regulation prices to arbitrage prices. This is partly due to long-lasting market design failures, resulting in overpayment for regD resources compared to regA resources ([125]). Additionally, as stated in Appendix A.1.2, PJM initially enforced a strict energy neutrality requirement (15-minute neutrality; $2\Delta^c = 0.25$), which is more stringent than other ISO/RTOs. Even though the requirement has been recently relaxed to conditional neutrality within 30 minutes ($2\Delta^c \geq 0.5$), 80% of the time, energy neutrality is achieved within 30 minutes from the PJM's regulation signal dataset ([149]). On the other hand, batteries located in ISO-NE, where regulation-to-arbitrage service price ratios are relatively low and the energy-neutrality condition is less strict, may experience more benefits from stacking. The low regulation-to-arbitrage price ratio is partly due to price changes during the global energy crisis. According the ISO's annual report ([82]), ISO-NE observed average regulation capacity/service clearing prices of \$30.96/MW and \$0.27/mile in 2022, which are a 60.1% increase and a 28.7% increase from 2021, respectively, while the average day-ahead energy price was \$85.56/MWh in 2022, an 86% increase from 2021. Furthermore, the ISO-NE trinary signal dataset suggests weaker energy neutrality compared to PJM's regD signal, with energy neutrality achieved within 60 minutes 80% of the time ([80]).

These insights demonstrate how a battery's location may impact the attractiveness of implementing stacking. Batteries located in PJM, characterized by higher regulation prices and a historically strict energy-neutrality requirement, may experience limited benefits from stacking. Conversely, batteries located in ISO-NE, with lower regulation prices and a less stringent energy-neutrality condition, may enjoy greater advantages from the proposed stacking.

(2) Which types of batteries offer the greatest benefits from stacking?

[196] reported a fragmented battery energy storage systems (BESS) market in 2020. The majority of the market share was occupied by NMC (Nickel-Manganese-Cobalt) batteries, followed by NCA (Nickel-Cobalt-Aluminum Oxide), LFP (Lithium-Iron-Phosphate), and other types of batteries. However, the report also projected significant changes in the market share distribution in the near future, indicating potential shifts in the dominance of different battery types.

Additionally, it is anticipated that many electric vehicle (EV) batteries will retire from their initial use and become available as second-hand batteries after repurposing, as reported by [20]. It should be noted that repurposed batteries generally exhibit reduced longevity and



(a) $(\frac{T_H}{T}, p^r\text{multiplier})$ (b) $(\frac{T_H}{T}, 2\Delta^c)$

Figure A.17: Stacking's relative profit $S = \frac{\Pi^*_{stk}}{\max(\Pi^*_{arb}, \Pi^*_{reg})}$ with various grid/market environments. The NYISO 2021 – 2022 dataset (winter) is used. Other parameters are summarized in Table A.9. The p^r multiplier in pane (a) operates by multiplying historical regulation prices by some constant value while keeping historical energy prices fixed. The energy neutrality guarantees $2\Delta^c$ in pane (b) is varied by assuming the regulation signal is updated every $(4 \times \Delta)$ seconds for $\Delta = \{1/i | i = 1, \cdots, 8\}$ while using the historical regulation signal.

lower round-trip efficiency compared to new batteries. These factors need to be considered when evaluating the performance and viability of repurposed batteries for various applications.

Determining which battery types should most prioritize stacking is a crucial question in practice for battery operators. Figure A.18 shows stacking's relative profit $S = \frac{\Pi^*_{stk}}{\max(\Pi^*_{arb}, \Pi^*_{reg})}$ for different battery types. Specifically, Figure A.18a varies the battery's remaining cycle count $N \in [100, 4000]$ and round-trip efficiency $\eta^2 \in [0.72, 1]$, while Figure A.18b varies power-to-energy ratio ($P/E \in [0.125, 2.5]$) and round-trip efficiency. We report the average performance over $N = 100$ realizations, where the hourly energy/regulation prices and regulation signals are randomly sampled. We use the 2023 average cell price of \$152 ([21]) for a cell with E=1kWh, P=1kW, N=1000, and η^2=1.[16]

From Figure A.18a, batteries with lower efficiency and shorter life cycles, such as second-hand batteries, demonstrate the highest benefit from stacking. For instance, $S > 2.5$ is

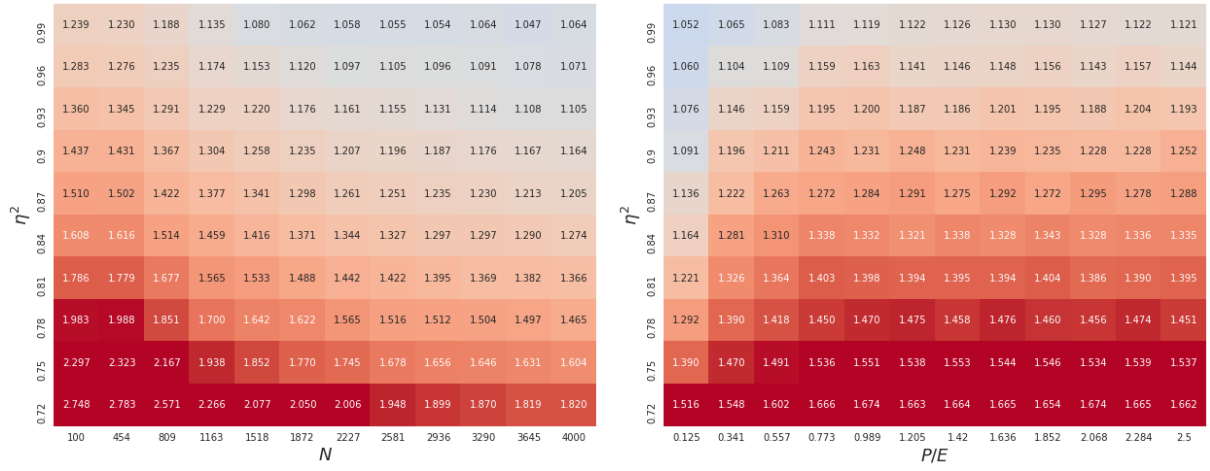
[16]We assume the cell price to be linear in power and energy, with the coefficient of power being roughly one-tenth of that of energy based on the empirical evidence on manufacturing costs ([166]). For a given (P, E), we further assume that the cell price is linear in η^2 and $\log N$, based on the longevity (cycle counts) and efficiency of six typical Li-ion battery chemistries ([173]). The final expression used for cell price is $(c_1 E + c_2 P)(\eta^2 + c_3 \log N)$ for c_1=\$100/MWh, c_2=\$10/MW, and c_3=\$0.055 (unit: \$).

possible for a scenario with $N \leq 809$ and $\eta^2 = 0.72$. This finding is consistent with our analytical modeling, and explained by energy replenishment cost-saving (see Section 2.6.2). This finding has significant implications, particularly in the context of the fast-growing cumulative capacity of used EV batteries. Stacking can contribute not only to improving the profitability of second-hand batteries but also to reducing greenhouse gas emissions and maintaining a sustainable power grid, as highlighted by [197].

Typical lithium-ion batteries, with cycle counts ranging between 500 – 2000 and round-trip efficiency of 0.8 – 0.9, exhibit significant benefits from stacking. The stacking benefit ratios (S) for such batteries fall within the range of [1.15,1.80]. For batteries with extended lifespans and high round-trip efficiency (e.g., 4000 cycles and $\eta^2 \geq 0.96$), the stacking benefit is reduced compared to other battery types. However, even in such cases, stacking still offers a minimum increase in profitability of 5%.

From Figure A.18b, batteries with high power-to-energy ratios (i.e., fast batteries) and lower round-trip efficiency tend to exhibit higher S ratios. Conversely, when a battery has very high efficiency and a very low power-to-energy ratio, the stacking strategy only improves profitability by approximately 5 percent compared to the best standalone service.

Overall, we provide valuable insights to battery operators and practitioners, enabling them to make informed decisions about (a) whether to make battery management system (BMS) upgrades to enable stacking and (b) which battery types should most prioritize stacking. Beyond battery operators, others who may benefit from these insights are BMS companies, who could use them to target marketing efforts.



(a) (N, η^2) (b) $(P/E, \eta^2)$

Figure A.18: Stacking's relative profit $S = \frac{\Pi^*_{stk}}{\max(\Pi^*_{arb}, \Pi^*_{reg})}$ with various battery types. $\beta = 2, \eta^2 \in [0.72, 1]$, and the NYISO 2021 – 2022 price dataset (winter) are used. Other parameters are summarized in Table A.9. $N \in [100, 4000]$ indicates the battery's remaining cycle count, while $P/E \in [0.125, 2.5]$ indicates the battery's power-to-energy ratio.

Table A.10: Sensitivity analysis: NYISO dataset ($\eta^2 = 0.8$)

(a) 2021 – 2022 dataset, summer (one-peak)											
β	Π^*_{stk}	Cost savings	S	$A^*_{stk} > A^*_{arb}$	$R^*_{stk} > R^*_{reg}$	$\frac{R^*}{A^*} \geq 2$	Superlinear profit	ρ_0	ρ_1 ($l = 0.3$)	ρ_1 ($l = 0.5$)	ρ_1 ($l = 0.7$)
1.5	46.24	32.07	1.78	✓	✓	✓	✓	< 0	0.78	< 0	< 0
1.7	66.05	34.65	1.34	✓	✓	✓	✓	< 0	0.65	< 0	< 0
2.0	103.85	43.03	1.16	✓	✓	✓	✓	< 0	0.50	< 0	0.19
2.3	141.05	53.82	1.10	✓	✓	✓	✓	< 0	0.41	0.43	0.25
2.5	160.47	47.38	1.09	×	✓	✓	✓	< 0	0.36	0.62	0.27
(b) 2021 – 2022 dataset, winter (two-peak)											
β	Π^*_{stk}	Cost savings	S	$A^*_{stk} > A^*_{arb}$	$R^*_{stk} > R^*_{reg}$	$\frac{R^*}{A^*} \geq 2$	Superlinear profit	ρ_0	ρ_1 ($l = 0.3$)	ρ_1 ($l = 0.5$)	ρ_1 ($l = 0.7$)
1.5	67.23	44.52	2.43	✓	✓	✓	✓	< 0	0.58	< 0	< 0
1.7	84.13	38.34	1.64	✓	✓	✓	✓	< 0	0.42	< 0	< 0
2.0	119.07	36.42	1.28	✓	✓	✓	✓	< 0	0.30	< 0	0.11
2.3	153.43	40.78	1.15	✓	✓	✓	✓	< 0	0.23	0.48	0.14
2.5	171.67	36.70	1.12	✓	✓	✓	✓	< 0	0.22	0.70	0.15
(a) 2019 – 2020 dataset, summer (one-peak)											
β	Π^*_{stk}	Cost savings	S	$A^*_{stk} > A^*_{arb}$	$R^*_{stk} > R^*_{reg}$	$\frac{R^*}{A^*} \geq 2$	Superlinear profit	ρ_0	ρ_1 ($l = 0.3$)	ρ_1 ($l = 0.5$)	ρ_1 ($l = 0.7$)
1.5	3.20	2.68	2.49	✓	✓	✓	✓	< 0	< 0	< 0	< 0
1.7	6.30	3.38	1.98	✓	✓	✓	✓	< 0	< 0	< 0	< 0
2.0	13.40	5.02	1.42	✓	✓	✓	✓	< 0	0.26	< 0	0.18
2.3	22.00	7.13	1.25	×	✓	✓	✓	< 0	0.38	< 0	0.24
2.5	27.61	8.66	1.19	×	✓	✓	✓	< 0	0.37	< 0	0.36
(b) 2019 – 2020 dataset, winter (two-peak)											
β	Π^*_{stk}	Cost savings	S	$A^*_{stk} > A^*_{arb}$	$R^*_{stk} > R^*_{reg}$	$\frac{R^*}{A^*} \geq 2$	Superlinear profit	ρ_0	ρ_1 ($l = 0.3$)	ρ_1 ($l = 0.5$)	ρ_1 ($l = 0.7$)
1.5	5.65	4.78	2.20	✓	✓	✓	✓	< 0	< 0	< 0	< 0
1.7	9.80	4.92	2.10	✓	✓	✓	✓	< 0	< 0	< 0	< 0
2.0	18.20	5.22	1.84	×	✓	✓	✓	< 0	0.38	< 0	< 0
2.3	27.64	5.72	1.50	×	✓	✓	✓	< 0	0.60	< 0	< 0
2.5	33.52	6.30	1.39	×	✓	✓	✓	< 0	0.61	< 0	< 0

Note: The linearized coefficient c^b_{lin} is calibrated over three different operable DOD ranges ($l = 0.3, 0.5, 0.7$ representing 30%, 50%, and 70% of DOD, respectively). The hourly energy/regulation prices and regulation signals are randomly sampled ($N = 100$) for profitability analysis. $T_H = 2$ and $T = 12$ and 24 are used for winter and summer, respectively. $c^b_0 = 165$ and $c^b_0 = 150$ are used for degradation coefficients in 2019 – 2020 and 2021 – 2022, respectively, factoring in a drop in battery prices. Other parameters are summarized in Table A.9. Power and energy utilization are presented in Figure A.16.

Table A.11: Profitability analysis: NYISO dataset ($\eta^2 = 0.7$)

(a) 2021 – 2022 dataset, summer (one-peak)											
β	Π^*_{stk}	Cost savings	S	$A^*_{stk} > A^*_{arb}$	$R^*_{stk} > R^*_{reg}$	$\frac{R^*}{A^*} \geq 2$	Superlinear profit	ρ_0	ρ_1 ($l = 0.3$)	ρ_1 ($l = 0.5$)	ρ_1 ($l = 0.7$)
1.5	27.55	28.84	2.14	✓	✓	✓	✓	< 0	< 0	< 0	< 0
1.7	39.47	37.27	1.70	✓	✓	✓	✓	< 0	< 0	< 0	< 0
2.0	64.76	46.31	1.21	✓	✓	✓	✓	< 0	0.25	< 0	< 0
2.3	90.95	56.32	1.14	✓	✓	✓	✓	< 0	0.51	< 0	< 0
2.5	103.41	49.13	1.13	✓	✓	✓	✓	< 0	0.52	< 0	< 0
(b) 2021 – 2022 dataset, winter (two-peak)											
β	Π^*_{stk}	Cost savings	S	$A^*_{stk} > A^*_{arb}$	$R^*_{stk} > R^*_{reg}$	$\frac{R^*}{A^*} \geq 2$	Superlinear profit	ρ_0	ρ_1 ($l = 0.3$)	ρ_1 ($l = 0.5$)	ρ_1 ($l = 0.7$)
1.5	51.04	39.86	2.99	✓	✓	✓	✓	< 0	< 0	< 0	< 0
1.7	63.64	41.15	2.19	✓	✓	✓	✓	< 0	< 0	< 0	< 0
2.0	92.48	45.36	1.53	✓	✓	✓	✓	< 0	0.15	< 0	< 0
2.3	121.14	62.73	1.31	✓	✓	✓	✓	< 0	0.21	< 0	< 0
2.5	133.84	57.63	1.20	✓	✓	✓	✓	< 0	0.23	< 0	< 0
(a) 2019 – 2020 dataset, summer (one-peak)											
β	Π^*_{stk}	Cost savings	S	$A^*_{stk} > A^*_{arb}$	$R^*_{stk} > R^*_{reg}$	$\frac{R^*}{A^*} \geq 2$	Superlinear profit	ρ_0	ρ_1 ($l = 0.3$)	ρ_1 ($l = 0.5$)	ρ_1 ($l = 0.7$)
1.5	2.08	2.96	3.08	✓	✓	✓	✓	< 0	< 0	< 0	< 0
1.7	4.05	5.33	2.66	✓	✓	✓	✓	< 0	< 0	< 0	< 0
2.0	8.48	7.66	2.09	✓	✓	✓	✓	< 0	< 0	< 0	< 0
2.3	13.94	11.74	1.51	✓	✓	✓	✓	< 0	< 0	< 0	< 0
2.5	17.55	13.25	1.34	✓	✓	✓	✓	< 0	< 0	< 0	< 0
(b) 2019 – 2020 dataset, winter (two-peak)											
β	Π^*_{stk}	Cost savings	S	$A^*_{stk} > A^*_{arb}$	$R^*_{stk} > R^*_{reg}$	$\frac{R^*}{A^*} \geq 2$	Superlinear profit	ρ_0	ρ_1 ($l = 0.3$)	ρ_1 ($l = 0.5$)	ρ_1 ($l = 0.7$)
1.5	3.94	5.24	2.86	✓	✓	✓	✓	< 0	< 0	< 0	< 0
1.7	6.04	6.32	2.19	✓	✓	✓	✓	< 0	< 0	< 0	< 0
2.0	13.14	8.95	1.92	✓	✓	✓	✓	< 0	< 0	< 0	< 0
2.3	18.92	10.77	1.78	✓	✓	✓	✓	< 0	< 0	< 0	< 0
2.5	24.14	13.63	1.52	✓	✓	✓	✓	< 0	< 0	< 0	< 0

Note: The parameters are the same as those used in Table A.10.

APPENDIX B

Proofs in Chapter 3

B.1 Empirical Evidence of Performance Degradation

This section provides technical details and experimental/empirical evidence on battery performance degradation, focusing on energy capacity degradation and round-trip energy efficiency fade.

B.1.1 Charge-Discharge Curve and Shifts of Curves

In the engineering literature, a charge-discharge curve (also known as a voltage-capacity curve) is used to measure a battery's performance metrics (e.g., capacity, round-trip efficiency).

A charge-discharge curve is determined by the battery's voltage and capacity. The voltage is the amount of power that has been applied to the battery, whereas the capacity is the amount of energy that the battery can store. The voltage and capacity are the two most important factors in the charge-discharge curve. The charge-discharge curve is determined by the voltage, capacity, and the battery's internal resistance. The internal resistance is the resistance in the circuit that is powering the battery. Understanding the voltage-capacity curve is a critical aspect of quantifying battery characteristics.

As a battery experiences battery degradation, the charge-discharge curve shifts, which affects the battery's performance metrics. Thus, it is important to understand how the use of the battery affects the charge-discharge curve and to understand how to prolong the life of the battery.

B.1.1.1 Energy Capacity

In the engineering literature, a voltage-capacity curve is typically used to define DOD under capacity degradation. Specifically, a certain voltage range is used to define DOD. For

instance, a battery's current capacity (maximum energy that can be stored) is defined by the taper voltages (or thresholds). Then a full DOD (100%) corresponds to the voltage from upper and lower limits (e.g., [42] uses 4.2 and 3.0V).

B.1.1.2 Round-Trip Energy Efficiency

The area under the charging curve (for a specified voltage range) corresponds to the charging energy. The area under the discharge curve (for a specified voltage range) corresponds to the discharging energy. Typically, the round-trip energy efficiency is defined as the ratio between discharging energy over charging energy over a full voltage range:

$$x^2 := \frac{D}{C}, \tag{B.1}$$

where D and C represent discharging and charging energy (MWh), respectively.

B.1.2 Capacity Degradation and Cost Amortization

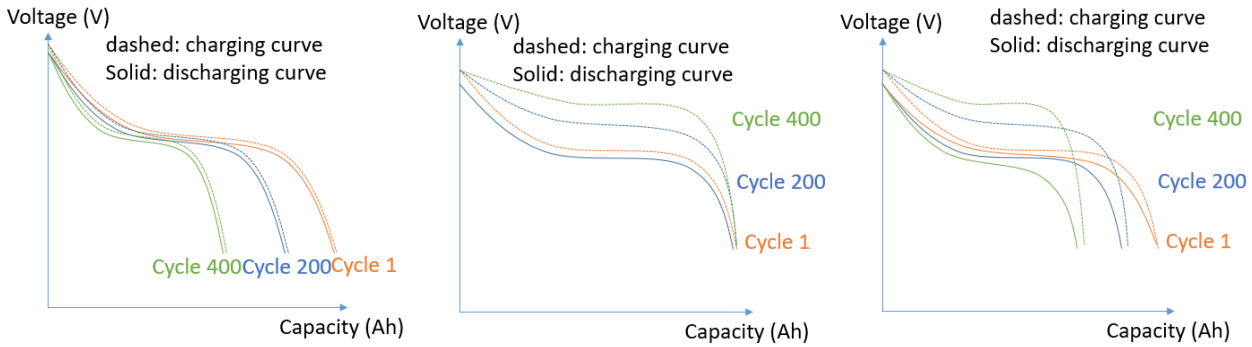
Several engineering papers have experimentally tested the effect of DOD on degradation, most often by relating the expected number of cycles N_i that a battery can provide before it is completely degraded if operated at DOD level u_i ($0 \leq u_i \leq 1$). This is called the Wöhler curve or the SN curve showing the relationship between the stress level (S) and the number of cycles (N); see [167] and [51] for two representative studies of this form. Though many functional forms for this relationship have been explored, the most commonly adopted form assumes

$$N_i = \left(\frac{1}{z u_i}\right)^{\beta}, \tag{B.2}$$

where $z > 0$ and $\beta > 1$ are constants that do not depend on the DOD. Rewriting (B.2), the cost of a single cycle of DOD u_i can be characterized by the degradation cost function $\Phi(u_i) : [0, 1] \to \mathbb{R}$ ([205]):

$$\begin{aligned} \Phi(u_i) &= \underbrace{c_{cell} \cdot E}_{\text{battery price}} \cdot \frac{1}{N_i} = c_{cell} \cdot E \cdot (z u_i)^{\beta} \\ &= \underbrace{(c^b \cdot E)}_{\substack{\text{The cost of} \\ \text{a full cycle}}} \cdot u_i^{\beta} \\ &= k \cdot u_i^{\beta}, \end{aligned} \tag{B.3}$$

where



(a) capacity degradation only (b) efficiency degradation only (c) both degradation

Figure B.1: Different performance degradation patterns

- $c^b := c_{cell} \cdot z^\beta$ (\$/MWh) is the battery degradation coefficient and represents the cost of operating a battery with capacity $E = 1$ MWh for a single full DOD cycle ($u = 1$),
- z (unitless) is the longevity coefficient from the Wöhler curve,
- β (unitless) is the degradation growth exponent from the Wöhler curve,
- c_{cell} (\$/MWh) is the battery cell price per unit of energy capacity,
- E (MWh) is the battery capacity, and
- $k := c^b \cdot E$ is the battery degradation coefficient, incorporating the battery capacity E.

B.1.3 General Relationship Between Capacity and Efficiency Degradation

Various research papers have focused on numerically identifying and quantifying the relationship between capacity degradation and energy efficiency degradation. Indeed, the empirical investigation reveals intriguing variations in performance degradation patterns among different battery types, as depicted in Figure B.1. The data analysis demonstrates that certain batteries exhibit more pronounced capacity degradation compared to efficiency degradation, as depicted in Figure B.1a. In these cases, the battery's capacity experiences a substantial decline over time, while the efficiency degradation remains relatively modest.

Conversely, for certain battery types, specific portions of the battery experience significant efficiency degradation while exhibiting only modest capacity degradation, as depicted in Figure B.1b.

Furthermore, the investigation also uncovers batteries that display both capacity and efficiency degradation, as illustrated in Figure B.1c. In these cases, both aspects of battery performance degrade noticeably over time, suggesting a correlated degradation pattern.

The variations in performance degradation patterns among different battery types emphasize the importance of understanding the specific characteristics and behaviors of each battery technology. By comprehending these degradation patterns, researchers and industry experts can develop tailored strategies for optimal battery control and management.

Building upon the observed variations in performance degradation patterns among different battery types, we conduct an analytical study focusing on three distinct degradation patterns: (1) capacity degradation only, (2) efficiency degradation only, and (3) correlated degradation.

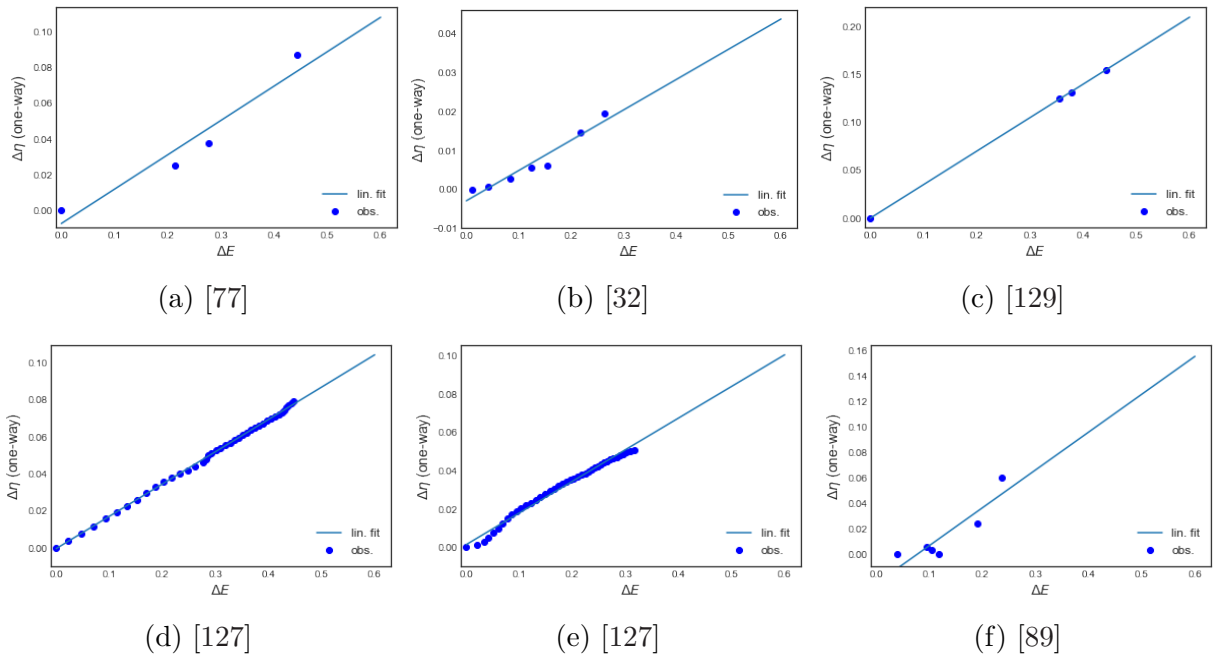
For each degradation pattern, we aim to gain a deeper understanding of the underlying dynamics and quantify their impact on battery control decisions. This analytical investigation allows us to derive insights into the optimal strategies and decision-making processes for managing batteries under each degradation pattern. By understanding the unique characteristics and challenges associated with each degradation pattern, we can develop tailored approaches and policies to optimize battery control, prolong battery life, and enhance overall system performance.

B.1.4 Linear Relationship Between Capacity Decrement and Efficiency Decrement

Various research papers have focused on numerically identifying and quantifying the relationship between capacity degradation and energy efficiency degradation. In many cases, these relationships have been characterized using power functions, including linear and quadratic functions. These empirical findings provide valuable insights into understanding the joint degradation behavior of batteries and can be utilized for modeling, prediction, and optimization purposes.

In our empirical investigation, we focus on exploring the relationship between energy capacity degradation and efficiency degradation. To gather data for this analysis, we extensively review and analyze over 30 published papers from the literature. These papers provide valuable insights into the performance degradation of batteries and often report charging/discharging curves, typically represented in voltage-Ampere plots.

To utilize the data from these curves, we employ a process of digitization. By converting the charging/discharging curves into digital formats, we can extract the necessary information for our analysis. Specifically, we calculate and quantify the energy capacity degradation



(a) [77] (b) [32] (c) [129]

(d) [127] (e) [127] (f) [89]

Figure B.2: Experimental/empirical evidence on the linear relationship between ΔE and Δx.

by measuring the area under the discharging curve. This energy capacity is a key metric that reflects the amount of energy that can be stored and subsequently released by the battery. Additionally, we evaluate the efficiency degradation by calculating the round-trip efficiency. This metric is determined by comparing the discharging capacity (the energy released during discharge) to the charging capacity (the energy input during charging). The round-trip efficiency indicates how effectively the battery converts stored energy back into usable power.

By systematically analyzing the digitized charging/discharging curves and calculating the energy capacity degradation and round-trip efficiency, we aim to gain empirical insights into the relationship between these two degradation factors. Based on the digitization and fitting from regressions, we noticed that a linear function reasonably captures the relationship between ΔE (capacity decrement) and Δx (one-way efficiency decrement) as shown in Figure B.2.[1]

[1] Alternatively, one may model ΔE and Δx^2 (round-trip efficiency decrement), which leads to very similar lessons (in terms of optimal policy, etc.).

B.2 Proofs of Statements (Main)

B.2.1 Section 3.4.1: Capacity-Degradation-Only

Justification of Fluid Approximation

A discrete-time formulation allows us to describe the setting clearly and to derive a corresponding continuous-time representation. We operate a battery over T days, with an aim to maximize the cumulative discounted arbitrage revenue.

For each day $i \in \{1, \cdots, T\}$, let E_i denote the battery's current capacity and u_i the depth-of-discharge (DOD). Let $x \in (0, 1]$ represent the one-way efficiency; it remains constant regardless of battery utilization. Under this setup, discharging an amount $E_i u_i$ of energy from the battery effectively results in selling $E_i u_i x$ units at the high price $\bar{p}$. This also implies that $\frac{E_i u_i}{x}$ units of energy must be purchased at the low price $\underline{p}$. The resulting arbitrage margin is:

$$\bar{p} \cdot E_i u_i x - \underline{p} \cdot \frac{E_i u_i}{x} = p^a E_i u_i,$$

where $p^a := \bar{p}x - \underline{p}/x > 0$ denotes the effective profit per unit of discharge, as defined in (3.1). We use $\delta \geq 0$ to denote a (daily) discount factor. Then a discrete optimization problem can be stated as follows:

$$\begin{aligned} \max_{u_i \in [0,1], 1 \leq i \leq T} \ & \sum_{i=1}^{T} e^{-\delta i} p^a E_i u_i \\ s.t. \ & E_{i+1} = E_i[1 - \Delta t \cdot \Phi(u_i)] \\ & \Phi(u_i) = k u_i^2, \end{aligned} \tag{B.4}$$

The (discounted) revenue and degradation dynamics on day i can be expressed as follows:[2]

$$\begin{aligned} r_i :=& e^{-\delta i} p^a E_i u_i, \text{ and} \\ E_{i+1} - E_i :=& - E_i \cdot \Delta t \cdot \Phi(u_i). \end{aligned}$$

The discounted revenue r_i immediately follows from (3.1). The multiplicative degradation dynamics is a discrete counterpart of (3.4) based on empirical/experimental evidence ([204, 158]). Both revenue r_i and degradation $\Phi(u_i)$ are increasing in u_i, which implies that aggressive use of a battery (larger u_i) generates more revenue but also incurs more degradation. Thus, an ideal policy should strike a balance between immediate revenue, obtained by

[2]We assume the quadratic degradation based on several empirical papers (e.g., [204]). In practice, non-quadratic functions were also reported depending on the combination of a battery's chemistry and manufacturer. Appendix B.3.1 performs a detailed sensitivity analysis, where we show that overall lessons such as optimal policy structure remain the same for any convex degradation.

exploiting/front-loading the battery, and future opportunities, achieved by delaying its use until later.

Though this model can be readily optimized via dynamic programming (DP), the clean analytical results we seek in this work can be better obtained via a fluid approximation. The fluid approximation takes advantage of the fact that a battery typically operates over many days (usually over several years) and each day takes up a small fraction of total revenue and degradation. The following lemma leads to the limiting optimization problem (see the proof for a formal description).

Lemma B.1. *Assume that the battery is used over $N := M \times T$ days, with one cycle per day, for some multiplier $M \geq 1$. We gradually increase M from 1 to infinity, while normalizing the arbitrage price, battery duration (or cycle count), and discounting factor. The fluid approximation leads to the following limiting optimization problem:*

$$\begin{aligned} \max_{u(t)\in[0,1],0\leq t\leq T} \ & \int_0^T e^{-\delta t} p^a u(t) E(t) dt \\ s.t. \ & \dot{E}(t) = -E(t)\Phi(u(t)) \\ & \Phi(u(t)) := k u(t)^2, \end{aligned} \tag{B.5}$$

where $r(t) := e^{-\delta t} p^a E(t) u(t)$ and $\dot{E}(t)$ are the discounted immediate revenue rate and the (quadratic) capacity degradation dynamics, respectively, at time t.

Proof of Lemma B.1

For the fluid approximation, we now introduce a multiplier $M \geq 1$. We assume that the battery is used over $N := M \times T$ days, with one cycle per day, under a constant arbitrage price $p^a := \bar{p} - \underline{p}$. We gradually increase M from 1 to infinity, while normalizing the arbitrage price, battery duration (or cycle count), and discounting factor: we decrease p^a to p^a/M, increase the battery duration (or cycle count), and decrease the discounting factor. Formally, for cycle $i \in \{1, \cdots, N\}$, we define the corresponding revenue function $\tilde{r}(i)$ and degradation function $\tilde{d}(i)$ as follows:

$$\begin{aligned} \tilde{r}_i &:= p^a E_i u_i e^{-\delta i \cdot \Delta t} \cdot \Delta t = \frac{p^a}{M} E_i u_i e^{-\delta i/M}, \text{ and} \\ \tilde{d}_i &:= E_{i+1} - E_i = -E_i k u_i^2 \cdot \Delta t = -\frac{k}{M} E_i u_i^2, \end{aligned}$$

for $\Delta t := \frac{T}{N} = \frac{1}{M}$.

Next, we study the limiting dynamics by assuming $M \to \infty$ (infinitely many cycles) or

$\Delta t \to 0$. We define $t := \frac{i}{M} = i\Delta t$, so that $t \in [0, T]$. We also define the following dynamics:

$$r(t) := \lim_{M\to\infty} \frac{\tilde{r}(i)}{\Delta t} = e^{-\delta t} p^a E(t) u(t), \text{ and}$$
$$d(E, u, t) := \lim_{M\to\infty} \frac{\tilde{d}(i)}{\Delta t} = -kE(t)u(t)^2 = \dot{E}(t),$$

where $r(t), \dot{E}(t), E(t)$, and $u(t)$ follow the definitions used in Lemma B.1.

We can then approximate the continuous-time system in Lemma B.1 by:

$$E_{i+1} = E_i + d(E_i, u_i, i\Delta t) \cdot \Delta t,$$

and the cumulative revenue by:

$$S(T, E_N) + \sum_{i=1}^{N-1} r(E_i, u_i, i\Delta t) \cdot \Delta t.$$

The remainder of the proof then follows directly from the derivation of the Hamilton-Jacobi-Bellman (HJB) equation in Section 2.2.1 of [171], which shows that applying dynamic programming (DP) to the discrete-time formulation yields the fluid approximation in the limit. □

Based on Lemma B.1, we employ optimal control theory, a mathematical framework for determining optimal policies in dynamic systems.

Proof of Theorem 3.1

We first state the detailed version of Theorem 3.1.

Theorem B.1 (Capacity-degradation-only: Finite horizon)**.** *For capacity-degradation-only under a finite horizon T, it is either optimal to run the battery at full DOD for the whole horizon ($k \le \delta$ or $k > \delta$, $T \le \frac{\log(\frac{2k}{k-\delta})}{k+\delta}$) or to otherwise operate the battery at partial DOD until time*

$$t_A = T - \frac{\log(\frac{2k}{k-\delta})}{k+\delta}$$

and at full DOD afterwards. The following hold at optimality:

	Cases		
	$k > \delta, T > \frac{\log(\frac{2k}{k-\delta})}{k+\delta}$		$k \le \delta$ or $k > \delta,\ T \le \frac{\log(\frac{2k}{k-\delta})}{k+\delta}$
	Discounted ($\delta > 0$)	Undiscounted ($\delta = 0$)	
$u^*(t)$	$\begin{cases} \left[\frac{k\left(e^{2\delta(t_A-t)}-1\right)+\delta}{\delta e^{2\delta(t_A-t)}}\right]^{-\frac{1}{2}}, & 0 \le t \le t_A, \\ 1, & t_A \le t \le T. \end{cases}$	$\begin{cases} [1+2k(t_A-t)]^{-\frac{1}{2}}, & 0 \le t \le t_A, \\ 1, & t_A \le t \le T. \end{cases}$	1
$p(t)e^{\delta t}$	$\begin{cases} \frac{p^a}{2k}\left[\frac{k\left(e^{2\delta(t_A-t)}-1\right)+\delta}{\delta e^{2\delta(t_A-t)}}\right]^{\frac{1}{2}}, & 0 \le t \le t_A, \\ \frac{p^a}{k+\delta}(1-e^{-(k+\delta)(T-t)}), & t_A \le t \le T. \end{cases}$	$\begin{cases} \frac{p^a}{2k}[1+2k(t_A-t)]^{\frac{1}{2}}, & 0 \le t \le t_A, \\ \frac{p^a}{k}(1-e^{-k(T-t)}), & t_A \le t \le T. \end{cases}$	$\frac{p^a}{k+\delta}(1-e^{-(k+\delta)(T-t)})$
$E^*(t) =$	$\begin{cases} \sqrt{\frac{k(e^{2\delta(t_A-t)}-1)+\delta}{k(e^{2\delta t_A}-1)+\delta}}, & 0 \le t \le t_A, \\ e^{-k(t-t_A)}\sqrt{\frac{\delta}{k(e^{2\delta t_A}-1)+\delta}}, & t_A \le t \le T. \end{cases}$	$\begin{cases} \sqrt{\frac{2k(t_A-t)+1}{2kt_A+1}}, & 0 \le t \le t_A, \\ \frac{e^{-k(t-t_A)}}{\sqrt{2kt_A+1}}, & t_A \le t \le T. \end{cases}$	e^{-kt}
$A^*(t)$	$\begin{cases} e^{\delta(t_A-t)}\sqrt{\frac{\delta}{k(e^{2\delta t_A}-1)+\delta}}, & 0 \le t \le t_A, \\ e^{-k(t-t_A)}\sqrt{\frac{\delta}{k(e^{2\delta t_A}-1)+\delta}}, & t_A \le t \le T. \end{cases}$	$\begin{cases} \frac{1}{\sqrt{2kt_A+1}}, & 0 \le t \le t_A, \\ \frac{e^{-k(t-t_A)}}{\sqrt{2kt_A+1}}, & t_A \le t \le T. \end{cases}$	e^{-kt}
$R^*_{cum} =$	$\frac{p^a}{2k}\sqrt{\frac{k(e^{2\delta t_A}-1)+\delta}{\delta e^{2\delta t_A}}}$	$\frac{p^a}{2k}\sqrt{2kt_A+1}$	$p^a(\frac{1-e^{-(k+\delta)T}}{k+\delta})$

Table B.1: Capacity-degradation-only (finite horizon).

Proof. We first state Hamiltonian. The Hamiltonian is a function of the capacity $E(t)$, the control $u(t)$, the shadow price $p(t)$, and time t:

$$\begin{aligned} H(E(t), u(t), p(t), t) &= r(t) + p(t)\dot{E}(t) \\ &= e^{-\delta t}p^a u(t)E(t) + p(t)(-kE(t)u^2(t)). \end{aligned} \tag{B.6}$$

$r(t) = e^{-\delta t}p^a u(t)E(t)$ is the immediate revenue rate at time t and $\dot{E}(t) = -kE(t)u^2(t)$ is the (multiplicative) capacity degradation dynamics.

According to the Pontryagin maximum principle, an optimal control trajectory $\{u^*(t)|t \in [0,T]\}$ satisfies the following necessary conditions:

$$\begin{aligned} [M] &: H(E^*(t), u^*(t), p(t), t) = \max_{0 \le u(t) \le 1} H(E^*(t), u(t), p(t), t), \\ [ODE] &: \dot{E}^*(t) = \nabla_{p(t)} H(E^*(t), u^*(t), p(t), t) = -kE^*(t)(u^*(t))^2, \\ [ADJ] &: \dot{p}(t) = -\nabla_{E(t)} H(E^*(t), u^*(t), p(t), t) = -e^{-\delta t}p^a u^*(t) + kp(t)(u^*(t))^2, \\ [T] &: p(T) = 0. \end{aligned} \tag{B.7}$$

Here, $p(t)$ denotes the shadow price of capacity discounted to time 0 (also known as the "present-value shadow price"), which is derived from the Hamiltonian using the Pontryagin maximum principle. For simplicity, we also define $\tilde{p}(t) := p(t)e^{\delta t}$, which denotes the shadow price of $E(t)$ evaluated at time t (also known as "current-value shadow price").

From $[M]$, we have

$$u^*(t) = \min(\frac{e^{-\delta t}p^a}{2kp(t)}, 1). \tag{B.8}$$

In a time range for which $\tilde{p}(t) \geq \frac{p^a}{2k}$ for all t in the range, $[ADJ]$ of (B.7) and (B.8) yield

$$u^*(t) = \frac{p^a}{2k\tilde{p}(t)} \text{ and}$$
$$p(t)\dot{p}(t) = -\frac{e^{-2\delta t}(p^a)^2}{4k}.$$

This is a first-order nonlinear ODE, so

$$\tilde{p}(t) = p(t)e^{\delta t} = \begin{cases} \sqrt{\frac{(p^a)^2}{4k\delta} - \frac{C_1}{e^{-2\delta t}}}, & \text{if } \delta > 0, \text{ and} \\ \sqrt{C_2 - \frac{(p^a)^2 t}{2k}}, & \text{if } \delta = 0, \end{cases}$$

for some constants C_1 and C_2.

In a time range for which $p(t)e^{\delta t} \leq \frac{p^a}{2k}$ for all t in the range, $[ADJ]$ of (B.7) and (B.8) yield

$$u^*(t) = 1 \text{ and}$$
$$\dot{p}(t) - kp(t) = -e^{-\delta t}p^a.$$

This is a standard first-order linear ODE, and we have

$$p(t)e^{\delta t} = \frac{p^a}{k+\delta} - C_3 e^{(k+\delta)t},$$

for some constant C_3.

We proceed to establish the optimal solution trajectory backward in time from the end of horizon $t = T$. Note that $p(T) = 0$, and by the continuity of $p(t)$ there is a time range extending backward in time from $t = T$ for which $\frac{p^a}{e^{-\delta t}} \leq \frac{p^a}{2k}$ and therefore $u^*(t) = 1$. Obtaining $p(T) = 0$ requires

$$C_3 = \frac{p^a}{(k+\delta)e^{(k+\delta)T}}, \tag{B.9}$$

meaning that in this time range

$$p(t)e^{\delta t} = \frac{p^a}{k+\delta}(1 - e^{-(k+\delta)(T-t)}).$$

$p(t)e^{\delta t}$ is strictly monotone decreasing, so $u^*(t) = 1$ for all $t \in [0, T]$ whenever $p(0) \leq \frac{p^a}{2k}$, or equivalently whenever $e^{-(k+\delta)T} \geq \frac{k-\delta}{2k}$. We conclude that $u^*(t) = 1$ for the full time horizon whenever $k \leq \delta$ or $k > \delta$ and $T \leq \frac{\log(\frac{2k}{k-\delta})}{k+\delta}$. In this case it is straightforward via $[ODE]$ of (B.7) that $E^*(t) = e^{-kt}$.

The remainder of the proof will focus on the case when $k > \delta$ and $T > \frac{\log(\frac{2k}{k-\delta})}{k+\delta}$. Going backward in time from $t = T$, we reach $p(t)e^{\delta t} = \frac{p^a}{2k}$ at time $t_A = T - \frac{\log(\frac{2k}{k-\delta})}{k+\delta}$; recall that $u^*(t) < 1$ for $p(t)e^{\delta t} > \frac{p^a}{2k}$. By the continuity of $p(t)e^{\delta t}$, we get

$$C_1 = \frac{(k-\delta)(p^a)^2}{4k^2\delta}e^{-2\delta t_A} > 0 \text{ and}$$
$$C_2 = \frac{(p^a)^2(1+2kt_A)}{4k^2} > 0.$$

$C_1,\ C_2 > 0$ confirms that $p(t)e^{\delta t}$ is strictly decreasing for $t \leq t_A$ with the selected C_1 and C_2, establishing the optimal structure—we have $p(t)e^{\delta t} > \frac{p^a}{2k}$ for $t \in [0, t_A)$ with the C_1 and C_2 selected above, followed by $p(t)e^{\delta t} < \frac{p^a}{2k}$ for $t \in (t_A, T]$ with the C_3 selected in (B.9).

$[ODE]$ of (B.7) defines a first-order linear ODE that can be used to straightforwardly establish $E^*(t)$ under initial condition $E(0) = 1$.

□

Proof of Lemma 3.1

We will prove the result by showing that $\bar{R}(u)$ is either strictly monotone increasing or has an up-down pattern with a unique maximizer $u \in (0, 1)$. We begin with monotone change of variable $y := ku^2 + \delta$, for $y \in (\delta, k + \delta]$. Then

$$\bar{r}(y) = p^a\sqrt{\frac{y-\delta}{ky^2}}(1 - e^{-Ty}), \text{ and}$$
$$\bar{r}'(y) = \underbrace{\frac{p^a}{2ky^3\sqrt{\frac{y-\delta}{ky^2}}}}_{>0} \times \underbrace{\Big[-y + 2\delta + e^{-Ty}[2T(y-\delta)y + (y-2\delta)]\Big]}_{:=f(y)}.$$

We proceed by signing $f(y)$ for $y \in (\delta, k+\delta]$. From

$$\begin{aligned} f'(y) =& \frac{g(y)-h(y)}{h(y)}, \text{ for} \\ g(y) :=& 1 + (3T + 2T^2\delta)y - 2T^2y^2 \text{ and} \\ h(y) :=& e^{Ty} > 0, \end{aligned}$$

we read that $f'(y)$ takes the same sign as $g(y) - h(y)$. Noting that $g(y) - h(y)$ is a strictly concave function that takes negative values for sufficiently large y and that takes value 0 and has a positive derivative at $y = 0$, we conclude that $f'(y)$ has a positive-negative pattern for $y \in (0, \infty)$. Over our range $y \in (\delta, k+\delta]$, $f(y)$ is either strictly increasing, strictly decreasing, or strictly increasing up to a unique maximizer and then strictly decreasing afterwards.

Since $\bar{r}(\delta) = 0$ and $f(\delta) > 0$, we conclude from the possible patterns of $f(y)$ that $\bar{r}(y)$ is either strictly increasing up to a maximum at $y = k + \delta$ ($\bar{u} = 1$), or up-down with a maximizer at the unique $y \in (\delta, k+\delta)$ at which $f(y) = 0$. The optimal DOD will be 1 whenever $f(k+\delta) \geq 0$ and smaller otherwise. From

$$f(k+\delta) = -(k-\delta) + e^{-T(k+\delta)}[2Tk(k+\delta) + (k-\delta)],$$

we can straightforwardly derive the conditions leading to full DOD.

□

Proof of Lemma 3.2

The revenue for the optimal policy can be read from Theorem B.1 (the R^*_{cum} row), while the optimal revenue for the fixed-DOD policy is established in (3.8), either by setting $\bar{u} = 1$ when indicated in Lemma 3.1, or otherwise by setting $\bar{u}$ to be the unique $u \in (0, 1)$ satisfying $\bar{r}'(u) = 0$. Note that both revenue functions are continuous at $\delta = 0$; we prove the monotonicity result across all $\delta > 0$. This yields the following ratio of optimal revenues:

$$S(\delta) = \begin{cases} 1, & \text{if } k \leq \delta \text{ or } k > \delta > 0,\ e^{T(k+\delta)} \leq \frac{2k}{k-\delta}, \\ \frac{2\sqrt{\delta k}(1-e^{-(k+\delta)T})}{(k+\delta)\sqrt{1-2e^{-2\delta T}(\frac{k-\delta}{2k})\frac{k-\delta}{k+\delta}}}, & \text{if } k > \delta > 0,\ \frac{2k}{k-\delta} \leq e^{T(k+\delta)} \leq \frac{k-\delta+2Tk(k+\delta)}{k-\delta}, \text{ and} \\ \frac{2\sqrt{\delta k}\bar{u}(1-e^{-(k\bar{u}^2+\delta)T})}{(k\bar{u}^2+\delta)\sqrt{1-2e^{-2\delta T}(\frac{k-\delta}{2k})\frac{k-\delta}{k+\delta}}}, & \text{if } k > \delta > 0,\ e^{T(k+\delta)} > \frac{k-\delta+2Tk(k+\delta)}{k-\delta}. \end{cases}$$

The first case corresponds to both strategies using full-DOD for the full horizon, the next case corresponds to fixed-DOD alone using full DOD for the whole horizon, and the last case

corresponds to neither using full DOD for the full horizon. Note that $\bar{u}$ is a function of δ in this expression. We seek to establish that $S(\delta)$ is an increasing function of δ.

For the case when $k > \delta$ and $\frac{2k}{k-\delta} \leq e^{T(k+\delta)} \leq \frac{k-\delta+2Tk(k+\delta)}{k-\delta}$, the derivative with respect to δ immediately gives the result:

$$S'(\delta) = \underbrace{\frac{-2k}{(k+\delta)^2\sqrt{\delta/k}\big(1-2e^{-2\delta T}\big(\frac{k-\delta}{2k}\big)^{\frac{k-\delta}{k+\delta}}\big)^{3/2}}}_{<0} \times \underbrace{N_1(e^{-(k+\delta)T}, \frac{k-\delta}{2k})}_{\leq 0 \text{ (Lemma B.2)}},$$

for $N_1(R, L)$ defined in Lemma B.2.

When $k > \delta$ and $e^{T(k+\delta)} \geq \frac{k-\delta+2Tk(k-\delta)}{k-\delta}$, we use the fact that $\bar{u}$ satisfies the FOC for (3.8) to prove the result:

$$S'(\delta) = \frac{\partial S}{\partial \delta} + \underbrace{\frac{\partial S}{\partial \bar{u}}}_{\substack{=0 \\ (FOC)}} \cdot \frac{\partial \bar{u}}{\partial \delta}$$

$$= \underbrace{\frac{\bar{u}(\delta k)^{-\frac{1}{2}}}{(\bar{u}^2+\delta/k)(1-e^{-(k\bar{u}^2+\delta)T}[1+(k\bar{u}^2+\delta)T])[1-2(\frac{k-\delta}{2k})^{\frac{k-\delta}{k+\delta}}e^{-2\delta T}]^{\frac{3}{2}}}}_{>0} \times \underbrace{N_2(e^{-(k\bar{u}^2+\delta)T}, \frac{k-\delta}{2k})}_{\geq 0 \text{ (Lemma B.3)}},$$

for $N_2(R, L)$ defined in Lemma B.3.

□

The proof of Lemma 3.2 relies on establishing the sign of $N_1(R, L)$ and $N_2(R, L)$, two bivariate functions defined over a closed subset of $\mathbb{R}^2$ in Lemmas B.2 and B.3, respectively.

Lemma B.2. *For $L \in (0.0.5]$ and $0 < R \leq L$, define*

$$\begin{aligned} N_1(R, L) := &- L + \big(-2(1-2L)\log R + \frac{1-2L}{1-L}\log L + 1\big)L^{\frac{L}{1-L}}R^{\frac{1-2L}{1-L}} \\ &+ (L + (1-2L)\log R)R + \big(-\frac{1-2L}{1-L}\log L - 1\big)L^{\frac{L}{1-L}}R^{\frac{2-3L}{1-L}}. \end{aligned}$$

Then $N_1(R, L) \leq 0$.

It is straightforward that $N_1(R, \frac{1}{2}) = 0$ for any R. Consider any $0 < L < 0.5$. We will prove $N_1(R; L) \leq 0$ for this fixed L and for all $0 < R \leq L$ by treating N_1 as a univariate function

of R and taking derivatives:

$$N_1'(R;L) = L^{\frac{L}{1-L}} R^{-\frac{L}{1-L}}[-2(1-2L) + \frac{1-2L}{1-L}(\frac{1-2L}{1-L}\log L + 1) - \frac{2(1-2L)^2}{1-L}\log R]$$
$$+ (1-L) + (1-2L)\log R + (-\frac{1-2L}{1-L}\log L - 1)\frac{2-3L}{1-L} L^{\frac{L}{1-L}} R^{\frac{1-2L}{1-L}}, \quad \text{and}$$
$$N_1''(R;L) = \frac{g(R;L)}{R^{\frac{1}{1-L}}},$$

where

$$g(R;L) := (1-2L)R^{\frac{L}{1-L}} + L^{\frac{L}{1-L}}\left[\frac{(1-2L)(-6L^2+7L-2)}{(1-L)^2} - \frac{L(1-2L)^2}{(1-L)^3}\log L\right.$$
$$\left. + \frac{2L(1-2L)^2}{(1-L)^2}\log R - \frac{(2-3L)(1-2L)^2 R}{(1-L)^3}\log L - \frac{(2-3L)(1-2L)R}{(1-L)^2}\right].$$

We proceed by signing $g(R;L)$ for our fixed L and any $0 < R \leq L$, again by taking derivatives:

$$g'(R;L) = \frac{L}{1-L}(1-2L)R^{-\frac{1-2L}{1-L}}$$
$$+ L^{\frac{L}{1-L}}[\frac{2L(1-2L)^2}{(1-L)^2 R} - \frac{(2-3L)(1-2L)^2}{(1-L)^3}\log L - \frac{(2-3L)(1-2L)}{(1-L)^2}], \text{ and}$$
$$g''(R;L) = -\frac{L}{1-L}(\frac{1-2L}{1-L})(1-2L)R^{-\frac{2-3L}{1-L}} - L^{\frac{L}{1-L}}[\frac{2L(1-2L)^2}{(1-L)^2R^2}] < 0.$$

Having established $g(R;L)$ as a concave function of R, we next sign g and g' at the maximum R value of $R = L$ for our selected $L \in (0, 0.5)$:

$$g(L;L) = \frac{-(1-2L)^2 L^{\frac{L}{1-L}}}{(1-L)^2} \times \underbrace{(1-L+L\log L)}_{>0 \text{ for } 0<L<0.5} < 0, \text{ and}$$
$$g'(L;L) = \frac{(1-2L)^2 L^{\frac{L}{1-L}}}{(1-L)^3} \times \underbrace{(1-L-(2-3L)\log L)}_{>0 \text{ for } 0<L<0.5} > 0.$$

We conclude that $g(R;L)$ increases up to a negative value at $R = L$, indicating that $g(R;L) < 0$ for all $0 < R \leq L$. The negative sign of $g(R;L)$ indicates that $N_1(R;L)$ is a concave function of R. It is easy to check that $N_1(L;L) = N_1'(L;L) = 0$, meaning N_1 increases in R up to a value of 0 at $R = L$ and satisfies $N_1(R;L) \leq 0$ for all $0 < R \leq L$.

□

Lemma B.3. *For $L \in (0, 0.5]$ and $0 < R \leq \frac{L}{L - \log R}$, define*

$$\begin{aligned} N_2(R, L) :=& 2(R - R\log R - 1)R\log R \\ &+ R^{\frac{R-2R\log R-1}{R-R\log R-1}}(1-R)(R - R\log R - 1) \cdot \frac{L^{\frac{L}{1-L}}[-(1-L) + (1-2L)\log L]}{(1-L)^2} \\ &- R^{\frac{R-2R\log R-1}{R-R\log R-1}}\left[(1-R)^2 + (R - 2R\log R - 1)\log R\right] \cdot 2L^{\frac{L}{1-L}}. \end{aligned}$$

Then $N_2(R, L) \geq 0$.

The first two terms of $N_2(R, L)$ are positive, while the last is negative. For fixed L, $N_2(R; L) \geq 0$ can be written as the ratio between the positive and negative parts being greater than or equal to 1:

$$c_1 f(R) + c_2 g(R) \geq 1,$$

where

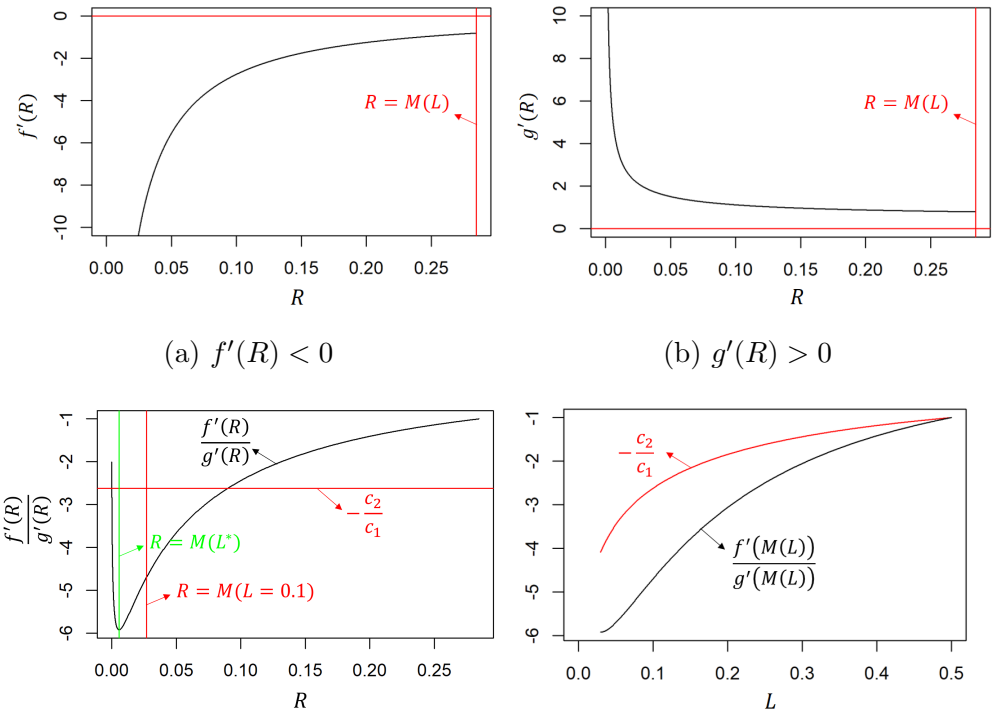
$$\begin{aligned} c_1 &= \frac{1}{2L^{\frac{L}{1-L}}}, \\ c_2 &= \frac{1 - L - (1-2L)\log L}{2(1-L)^2}, \\ f(R) &= \frac{2R(R - R\log R - 1)\log R}{R^{\frac{R-2R\log R-1}{R-R\log R-1}}\left[(1-R)^2 + (R - 2R\log R - 1)\log R\right]}, \text{ and} \\ g(R) &= \frac{-(1-R)(R - R\log R - 1)}{(1-R)^2 + (R - 2R\log R - 1)\log R}. \end{aligned}$$

We accomplish this by arguing that the function $c_1 f(R) + c_2 g(R)$ has an up-down shape in R (or a more simple monotone shape) and therefore must achieve its minimum value at either $R = 0$ or $R = \frac{L}{L - \log R} := M(L)$, at which point the ratio exceeds 1. For the boundary conditions, if $R \to 0$, then $N_2 \to 0^+$ (the ratio approaches 1^+); if $R = M(L)$, then the result is direct from B.2 using the continuity of S.

We now argue that $c_1 f(R) + c_2 g(R)$ has an up-down shape in R. It is easy to algebraically see that $f(R)$ is a decreasing function of R, and $g(R)$ is an increasing function of R (their derivatives in Figures B.3a – B.3b). The derivative of $c_1 f(R) + c_2 g(R)$ is therefore

$$\underbrace{g'(R)}_{>0}(c_2 + c_1 \frac{f'(R)}{g'(R)}),$$

which will be increasing whenever $\frac{f'(R)}{g'(R)} > -\frac{c_2}{c_1}$, and it will be decreasing whenever $\frac{f'(R)}{g'(R)} <$



(a) $f'(R) < 0$ (b) $g'(R) > 0$

(c) $\frac{f'(R)}{g'(R)}$ $(L = 0.1)$ (d) $-\frac{c_2}{c_1} \geq \frac{f'(M(L))}{g'(M(L))}$

Figure B.3: Figures for the proof of Lemma 3.2

$-\frac{c_2}{c_1}$.

It is straightforward to derive the univariate function $\frac{f'(R)}{g'(R)}$, which we plot below between $R = 0$ and $R = M(0.5) \approx 0.285$ (that is the largest value that R can take across all L values) in Figure B.3c. The figure shows that it is a down-up function that begins at -2 ($R = 0$) and ends at -1 ($R = M(0.5)$). Also on this plot are two red lines, corresponding to our problem instance for $L = 0.1$. The horizontal line captures $-\frac{c_2}{c_1}$ evaluated at $L = 0.1$, while the vertical line captures $R = M(0.1)$. We can see that $\frac{f'(R)}{g'(R)}$ starts above $-\frac{c_2}{c_1}$ and then falls below it as R increases from 0 to $M(0.1)$, meaning our positive-to-negative ratio has an up-down pattern for $L = 0.1$ (as desired). What remains is to prove that this is the case for all L between 0 and 0.5; we split this analysis into two cases. Define L^* to be the unique value of L such that $\frac{f'(R)}{g'(R)}$ achieves its minimum at $M(L^*)$. Numerically, $L^* \approx 0.0297$.

Case 1: $0 \leq L \leq L^*$. This is the case where $M(L)$ is so small that $\frac{f'(R)}{g'(R)}$ is a strictly decreasing function between $R = 0$ and $R = M(L)$. Then our positive-to-negative ratio must be monotone increasing (if $-\frac{c_2}{c_1} \leq \frac{f'(M(L))}{g'(M(L))}$), monotone decreasing (if $-\frac{c_2}{c_1} \geq -2$), or up-down (otherwise).

Case 2: $L^* < L \leq 0.5$. In this case, it is easy to see that $-\frac{c_2}{c_1}$ always exceeds $\frac{f'(M(L))}{g'(M(L))}$

across all L (in Figure B.3d, the red line is $-\frac{c_2}{c_1}$ and the black line is $\frac{f'(M(L))}{g'(M(L))}$). Specifically, $-\frac{c_2}{c_1} - \frac{f'(M(L))}{g'(M(L))} = -L_2 - \frac{f'(M(L))}{g'(M(L))}$ increases then decreases in L, with the difference minimized when $L \to 0.5$ (or $\delta \to 0$ and $R \to M(0.5)$). From $L = 0.5$ and $R = M(0.5)$ (i.e., $R - 2R\log R = 1$), we have $L_2 \to -1$ and $\frac{f'(M(L))}{g'(M(L))} \to -1$.

Combining the two cases implies that $c_1 f(R) + c_2 g(R)$ must either have an up-down pattern (if $-\frac{c_2}{c_1} < -2$) or a monotone decreasing pattern (otherwise), concluding the proof. □

Proof of Corollary 3.2

Without time discounting, we have $k > \delta = 0$, so $S = 1$ whenever $T \leq \frac{\log 2}{k}$. Otherwise, we can read the optimal revenue of the two approaches from Theorem B.1 (the R^*_{cum} row) and (3.8), yielding revenue ratio:

$$S = \frac{2(1 - e^{-Tk\bar{u}^2})}{\bar{u}\sqrt{1 + 2Tk - 2\log 2}}.$$

From Lemma 3.1, we know $\bar{u} = 1$ if horizon T is sufficiently short ($e^{Tk} \leq 2Tk + 1$), and $\bar{u} < 1$ otherwise and solves the first-order condition for the maximization problem in (3.8). We will derive bounds on S by considering fixed k and studying the trajectory of S as T is increased from $\frac{\log 2}{k}$.

For $T > \frac{\log 2}{k}$ and $e^{Tk} \leq 2Tk + 1$, we have $\bar{u} = 1$ and

$$S'(T) = \underbrace{\frac{-2k}{(1 + 2Tk - 2\log 2)^{3/2}}}_{<0} \times \underbrace{[1 - 2e^{-Tk}(1 + Tk - \log 2)]}_{>0 \text{ (for any } T > \frac{\log 2}{k})} < 0.$$

For $T > \frac{\log 2}{k}$ and $e^{Tk} > 2Tk + 1$, then $\bar{u} < 1$ satisfies the FOC on (3.8):

$$e^{Tk\bar{u}^2} = 1 + 2Tk\bar{u}^2. \tag{B.10}$$

The equation $e^a = 1 + 2a$ has a unique positive solution, so solving (B.10) leads to

$$\begin{aligned} \bar{u} =& \sqrt{\frac{a}{Tk}}, \text{ for} \\ a :=& -W_{-1}(-\frac{1}{2\sqrt{e}}) - \frac{1}{2} \approx 1.2564, \end{aligned} \tag{B.11}$$

where W_{-1} is the Lambert W function with branch index -1. Then whenever $e^{Tk} > 2Tk + 1$,

we have

$$S = \frac{2(1-e^{-a})}{\sqrt{a(2-\frac{2\log 2-1}{Tk})}}.$$

We conclude that S is monotone decreasing across all T and minimized as $T \to \infty$, approaching the infimum:

$$\sqrt{\frac{2}{a}}(1-e^{-a}) \approx 0.9025.$$

□

B.2.2 Section 3.4.2: Unified Model (In the Presence of Efficiency Degradation)

We first state the Hamiltonian for the unified model.

$$\begin{aligned} H(E(t), u(t), p(t), t) &= r(t) + p(t)\dot{E}(t) \\ &= e^{-\delta t}u(t)E(t)p^a(x(t)) + p(t)(-kE(t)u^2(t)), \end{aligned}$$

where $r(t) = e^{-\delta t}u(t)E(t)p^a(x(t))$ is the immediate revenue rate at time t, $\dot{E}(t) = -E(t)\Phi(u(t)) = -E(t)ku^2(t)$ is the system dynamics, $p^a(x(t)) = \bar{p}x(t) - \underline{p}/x(t)$ is the effective profit, and $x(t) = a(E(t)) = \alpha_0 + \alpha_1 E(t)$ is the efficiency at time t. According to the Pontryagin maximum principle, an optimal control trajectory $\{u^*(t)|t \in [0,T]\}$ satisfies the following necessary conditions:

$$\begin{aligned} [M] &: H(E^*(t), u^*(t), p(t), t) = \max_{0\le u(t)\le 1} H(E^*, u, p, t), \\ [ODE] &: \dot{E}^*(t) = \nabla_{p(t)} H(E^*(t), u^*(t), p(t), t) = -kE^*(t)(u^*(t))^2, \\ [ADJ] &: \dot{p}(t) = -\nabla_{E(t)} H(E^*(t), u^*(t), p(t), t) \\ &\quad = -e^{-\delta t}u^*(t)[2\bar{p}x^*(t) - \alpha_0(\bar{p} + \frac{\underline{p}}{(x^*(t))^2})] + kp(t)(u^*(t))^2, \\ [T] &: p(T) = 0. \end{aligned} \tag{B.12}$$

As before, we define $\tilde{p}(t) = p(t)e^{\delta t} = p(t)e^{\delta t}$ as the current-value shadow price and $\tilde{H}(t) = \frac{H(t)}{e^{-\delta t}}$ to be the current-value Hamiltonian.

$$\tilde{H}(t) := \frac{r(t)}{e^{-\delta t}} + \tilde{p}(t)\dot{E}(t).$$

Taking the time derivative of $\tilde{H}(t)$ yields ([171]):

$$\frac{d\tilde{H}(t)}{dt} = -\delta\tilde{p}(t)\dot{E}(t). \tag{B.13}$$

Throughout the chapter, we drop "*" from various terms for readability, but whenever we refer to $E(t)$ or $x(t)$ below, these should be understood to be the optimal trajectories $E^*(t)$ and $x^*(t)$.

From $[M]$, maximizing the Hamiltonian leads to:

$$u^*(t) = \min\Big(\frac{e^{-\delta t}p^a(x(t))}{2kp(t)}, 1\Big) = \min\Big(\frac{p^a(x(t))}{2k\tilde{p}(t)}, 1\Big). \tag{B.14}$$

Recall from Section 3.4.2 that we have defined $\underline{x} := \sqrt{\frac{p}{\bar{p}}}$ as the shut-off efficiency. We incur a loss when operating the battery if $x(t) < \underline{x}$, so we focus on batteries with $\alpha_0 + \alpha_1 > \underline{x}$, and our optimal trajectory will satisfy $x(t) \geq \underline{x}$.

In the time range for which $\tilde{p}(t) > \frac{p^a(x(t))}{2k}$, $u^*(t)$ is unconstrained and set by the first-order condition:

$$\begin{aligned}
u^*(t) &= \frac{p^a(x(t))}{2k\tilde{p}(t)} \\
[u^*(t)]' &= \frac{1}{2k}\cdot\frac{\tilde{p}(t)\dot{x}(t)[\bar{p} + \underline{p}/x^2(t)] - \dot{\tilde{p}}(t)p^a(x(t))}{[\tilde{p}(t)]^2} \\
&= \underbrace{\frac{p^a(x(t))}{2k\tilde{p}(t)}}_{=u^*(t)}\cdot\left[\frac{\dot{x}(t)[\bar{p} + \underline{p}/x^2(t)]}{p^a(x(t))} - \frac{\dot{\tilde{p}}(t)}{\tilde{p}(t)}\right].
\end{aligned}$$

From $x(t) = \alpha_0 + \alpha_1 E(t)$, $[ODE]$ of (B.12) and (B.14) yield:

$$\begin{aligned}
\dot{x}(t) &= -\frac{(x(t) - \alpha_0)[p^a(x(t))]^2}{4k(\tilde{p}(t))^2} \\
&= -k(x(t) - \alpha_0)[u^*(t)]^2.
\end{aligned} \tag{B.15}$$

From $[ADJ]$ of (B.12) and (B.14), we have:

$$\dot{p}(t) = \frac{e^{-2\delta t} p^a(x(t))}{4kp(t)} \Big[p^a(x(t)) - 2[2\bar{p}x(t) - \alpha_0(\bar{p} + \frac{\underline{p}}{x^2(t)})] \Big], \tag{B.16}$$

$$\begin{aligned} \dot{\tilde{p}}(t) &= \big[p(t)e^{\delta t}\big]' = \frac{\dot{p}(t)}{e^{-\delta t}} + \delta \tilde{p}(t) \\ &= \delta \tilde{p}(t) + \frac{p^a(x(t))}{4k\tilde{p}(t)} \Big[p^a(x(t)) - 2[2\bar{p}x(t) - \alpha_0(\bar{p} + \frac{\underline{p}}{x^2(t)})] \Big], \text{ and} \end{aligned} \tag{B.17}$$

$$\begin{aligned} \frac{\dot{\tilde{p}}(t)}{\tilde{p}(t)} &= \delta + \frac{(\bar{p}x(t) - \underline{p}/x(t))^2}{4k[\tilde{p}(t)]^2} \left[1 - \frac{2[2\bar{p}x(t) - \alpha_0(\bar{p} + \underline{p}/x^2(t))]}{\bar{p}x(t) - \underline{p}/x(t)} \right] \\ &= \delta + k[u^*(t)]^2 \cdot \left[1 - \frac{2[2\bar{p}x(t) - \alpha_0(\bar{p} + \underline{p}/x^2(t))]}{\bar{p}x(t) - \underline{p}/x(t)} \right]. \end{aligned}$$

Putting it all together, we have:

$$\begin{aligned} \frac{[u^*(t)]'}{u^*(t)} &= z(x(t), u^*(t)), \text{ for} \\ z(x,u) &:= \frac{1}{p^a(x)} \cdot \left[ku^2[2\bar{p}x - \alpha_0\bar{p} - \alpha_0\underline{p}/x^2] - \delta(p^a(x)) \right] \\ &= \frac{1}{p^a(x)} \cdot \left[ku^2[(p^a(x)) + (x - \alpha_0)(\bar{p} + \underline{p}/x^2)] - \delta(p^a(x)) \right] \\ &= ku^2 \Bigg[1 + \underbrace{\frac{(x - \alpha_0)(\bar{p} + \underline{p}/x^2)}{p^a(x)}}_{:=h(x)} \Bigg] - \delta. \end{aligned} \tag{B.18}$$

The behavior of $h(x)$ will be critical to establish the patterns of $u^*(t)$ over time. For $\underline{x} \leq x \leq 1$, we have

$$\begin{aligned} h'(x) =& \frac{f(x)}{[p^a(x)]^2 x^4}, \text{ where} \\ f(x) :=& \alpha_0[\bar{p}^2x^4 + 4\bar{p}\underline{p}x^2 - \underline{p}^2] - 4\bar{p}\underline{p}x^3. \end{aligned} \tag{B.19}$$

In any time range for which $\tilde{p}(t) \leq \frac{p^a(x(t))}{2k}$ (i.e., $u^*(t) = 1$), $[ODE]$ of (B.12) yields:

$$\begin{aligned} E(t) &= C_1 e^{-kt}, \\ x(t) &= \alpha_0 + \alpha_1 C_1 e^{-kt}, \text{ and} \\ \dot{x}(t) &= -k\alpha_1 C_1 e^{-kt} = -k(x(t) - \alpha_0), \end{aligned} \tag{B.20}$$

for some constant $C_1 > 0$. Then

$$\begin{aligned}\dot{p}(t) - kp(t) &= -e^{-\delta t}[2\bar{p}x(t) - \alpha_0(\bar{p} + \frac{\underline{p}}{x^2(t)})] \\ &= -e^{-\delta t}[\bar{p}(2dC_1e^{-kt} + \alpha_0) - \frac{\underline{p}\alpha_0}{(\alpha_0 + \alpha_1 C_1 e^{-kt})^2}].\end{aligned} \tag{B.21}$$

Noting that $\dot{p}(t) = e^{-\delta t}[-\delta\tilde{p}(t) + \tilde{p}'(t)]$, this can be written as:

$$\tilde{p}'(t) - (k+\delta)\tilde{p}(t) = -[2\bar{p}x(t) - \alpha_0(\bar{p} + \frac{\underline{p}}{x^2(t)})] \tag{B.22}$$

In general, there is no closed-form solution for the unified model.

Proof of Theorem 3.2

Recall from (B.23) – (B.24) that

$$\begin{aligned}\tilde{H}(t) &= p^a(t)u(t)E(t) \cdot (1 - 1/2) \\ &= \frac{r(t)}{e^{-\delta t}} \cdot (1 - 1/2) \\ &= \tilde{H}(0) \cdot e^{-\delta t},\end{aligned}$$

yielding

$$r(t) = r(0)e^{-2\delta t}.$$

□

We first state a technical lemma (Lemma B.4), which we will use to prove Theorem 3.3.

Lemma B.4. *The function* $f(x) := \alpha_0[\bar{p}^2x^4 + 4\bar{p}\underline{p}x^2 - \underline{p}^2] - 4\bar{p}\underline{p}x^3$ *defined in* (B.19)*, over the domain* $\sqrt{\frac{\underline{p}}{\bar{p}}} = \underline{x} \le x \le 1$*, exhibits the following patterns depending on the energy prices* $\bar{p}$ *and* $\underline{p}$ *and the efficiency intercept term* α_0*.*

- *If* $\alpha_0 \le \min\{\underline{x}, \frac{4\bar{p}\underline{p}}{\bar{p}^2+4\bar{p}\underline{p}-\underline{p}^2}\}$*, then* $f(x) \le 0$ *for* $x \in [\underline{x}, 1]$*,*
- *If* $\underline{x} < \alpha_0 < \frac{4\bar{p}\underline{p}}{\bar{p}^2+4\bar{p}\underline{p}-\underline{p}^2}$ *(a case only possible when* $\underline{x} > \sqrt{2} - 1 \approx 0.4142$*), then* $f(x)$ *follows a positive - negative pattern for* $x \in [\underline{x}, 1]$*,*
- *If* $\frac{4\bar{p}\underline{p}}{\bar{p}^2+4\bar{p}\underline{p}-\underline{p}^2} < \alpha_0 < \underline{x}$ *(a case only possible when* $\underline{x} < \sqrt{2} - 1 \approx 0.4142$*), then* $f(x)$ *follows a negative - positive pattern for* $x \in [\underline{x}, 1]$*,*

- *If* $\max\{\underline{x}, \frac{4\bar{p}\underline{p}}{\bar{p}^2+4\bar{p}\underline{p}-\underline{p}^2}\} \leq \alpha_0 < \sqrt{9/8} \cdot \underline{x}$*, then either* $f(x)$ *follows either a positive or positive - negative - positive pattern for* $x \in [\underline{x}, 1]$*,*

- *If* $\alpha_0 \geq \sqrt{9/8} \cdot \underline{x}$*, then* $f(x) > 0$ *for* $x \in [\underline{x}, 1]$*.*

Proof. From $\bar{p}^2x^4 + 4\bar{p}\underline{p}x^2 - \underline{p}^2 \geq 4\underline{p}^2 > 0$, the result is immediate for $\alpha_0 \leq 0$. The remainder of the proof will focus on the $\alpha_0 > 0$ case. Note that $f(x)$ is a quartic function with

$$\begin{aligned}
f'(x) &= 4\bar{p}x[\alpha_0\bar{p}x^2 - 3\underline{p}x + 2\alpha_0\underline{p}], \\
f''(x) &= 4\bar{p}[3\alpha_0\bar{p}x^2 - 6\underline{p}x + 2\alpha_0\underline{p}], \\
f(0) &= -\alpha_0\underline{p}^2,\ f'(0) = 0,\ f''(0) = 8\alpha_0\bar{p}\underline{p}, \\
f(\underline{x}) &= 4\underline{p}^2(\alpha_0 - \underline{x}),\ f'(\underline{x}) = 12\sqrt{\bar{p}\underline{p}}\underline{p}(\alpha_0 - \underline{x}),\ f''(\underline{x}) = 4\bar{p}\underline{p}(5\alpha_0 - 6\underline{x}), \\
f(1) &= \alpha_0(\bar{p}^2 + 4\bar{p}\underline{p} - \underline{p}^2) - 4\bar{p}\underline{p}, \text{ and} \\
f'(1) &= 4\bar{p}[\alpha_0(\bar{p} + 2\underline{p}) - 3\underline{p}].
\end{aligned}$$

Thus, $f(\underline{x})$ and $f'(\underline{x})$ both take the sign of $\alpha_0 - \underline{x}$, while $f(1)$ takes the sign of $\alpha_0 - \frac{4\bar{p}\underline{p}}{\bar{p}^2+4\bar{p}\underline{p}-\underline{p}^2}$. Additionally, we have $f'(x)/x \geq 0$ for all x when $\alpha_0 \geq \sqrt{9/8} \cdot \underline{x}$, while $f'(x)/x$ follows a positive - negative - positive pattern for all x when $0 < \alpha_0 < \sqrt{9/8} \cdot \underline{x}$.

We proceed through our cases:

- If $0 < \alpha_0 < \min\{\underline{x}, \frac{4\bar{p}\underline{p}}{\bar{p}^2+4\bar{p}\underline{p}-\underline{p}^2}\}$, then $f(\underline{x}), f'(\underline{x}), f(1) < 0$. From the positive - negative - positive shape of $f'(x)/x$ across all x, we conclude that $f'(x)$ has either a negative or a negative-positive pattern for $x \in [\underline{x}, 1]$, yielding $f(x) < 0$ for $x \in [\underline{x}, 1]$.

- If $\underline{x} < \alpha_0 < \frac{4\bar{p}\underline{p}}{\bar{p}^2+4\bar{p}\underline{p}-\underline{p}^2}$, then $f(\underline{x}), f'(\underline{x}) > 0$ and $f(1) < 0$. From the positive - negative - positive shape of $f'(x)/x$ across all x, we conclude that $f'(x)$ has either a positive - negative or a positive - negative - positive pattern for $x \in [\underline{x}, 1]$, yielding a positive - negative pattern for $f(x)$ when $x \in [\underline{x}, 1]$.

- If $\frac{4\bar{p}\underline{p}}{\bar{p}^2+4\bar{p}\underline{p}-\underline{p}^2} < \alpha_0 < \underline{x}$, then $f(\underline{x}), f'(\underline{x}) < 0$ and $f(1) > 0$. From the positive - negative - positive shape of $f'(x)/x$ across all x, we conclude that $f'(x)$ has a negative-positive pattern for $x \in [\underline{x}, 1]$, yielding a negative - positive pattern for $f(x)$ when $x \in [\underline{x}, 1]$.

- If $\max\{\underline{x}, \frac{4\bar{p}\underline{p}}{\bar{p}^2+4\bar{p}\underline{p}-\underline{p}^2}\} < \alpha_0 < \sqrt{9/8} \cdot \underline{x}$, then $f(\underline{x}), f'(\underline{x}), f(1) > 0$, while $f'(x)/x$ takes a positive - negative - positive pattern across all x. As a result, $f(x)$ takes either a positive or positive - negative - positive pattern when $x \in [\underline{x}, 1]$.

- If $\alpha_0 \geq \sqrt{9/8} \cdot \underline{x}$, then $f'(x)/x \geq 0$ for all x and $f(\underline{x}) > 0$, meaning $f(x) > 0$ for all $x \in [\underline{x}, 1]$.

□

Proof of Theorem 3.3

Under an infinite horizon, we have $\tilde{p}(t) = f(x(t))$ for some strictly monotone increasing function $f(x)$. In this setting, the only mechanism by which time t impacts the current-value shadow price is through the battery efficiency $x(t)$. This is not true for a finite horizon case, where $\tilde{p}(t)$ also depends on the remaining time until the end of the horizon. With this, we rewrite our system dynamics explicitly in terms of the efficiency $x(t)$. In particular, note that:

$$\begin{aligned}\tilde{p}'(t) &= \frac{d}{dt} f(x(t)) \\ &= f'(x(t)) \cdot x'(t).\end{aligned}$$

In the scenario where the optimal DOD is set by the first-order condition (aka $u^*(t) < 1$), we have expressions for $\tilde{p}'(t)$ from (B.17) and for $x'(t)$ from (B.15). Combining them yield:

$$f'(x) = \frac{\delta f(x) + \frac{\bar{p}x - \underline{p}/x}{4kf(x)}[(\bar{p}x - \underline{p}/x) - 2[2\bar{p}x - \alpha_0(\bar{p} + \underline{p}/x^2)]]}{\frac{-(x-\alpha_0)(\bar{p}x - \underline{p}/x)^2}{4kf^2(x)}}.$$

This is a first-order nonlinear ODE, with solution

$$\begin{aligned}f(x;c) =& \frac{(x-\alpha_0)(\bar{p}x - \underline{p}/x)^2}{\sqrt{c + g(x)}}, \text{ for} \\ g(x) :=& \frac{2\delta k}{3} \cdot \left(\bar{p}^2 x^3(3x - 4\alpha_0) - 12\bar{p}\underline{p}x(x - 2\alpha_0) + 12\underline{p}^2(\log x + \alpha_0/x)\right), \text{ and} \\ g'(x) =& \frac{2\delta k}{3} \cdot \left(3\bar{p}^2 x^2(3x - 4\alpha_0) + 3\bar{p}^2 x^3 - 12\bar{p}\underline{p}(2x - 2\alpha_0) + 12\underline{p}^2(1/x - \alpha_0/x^2)\right) \\ =& 12(\bar{p}x - \underline{p}/x)^2(x - \alpha_0) \geq 0, \ x \in [\max(\underline{x}, \alpha_0), 1].\end{aligned}$$

Since $g(x)$ is an increasing function over $x \in [\max(\underline{x}, \alpha_0), 1]$, any $c \geq -g(\max(\underline{x}, \alpha_0))$ defines a valid DOD trajectory $u(t;c)$, with associated payoffs for a unit-capacity battery of efficiency x given by $f(x;c)$:

$$\begin{aligned}u(t;c) =& j(x(t);c), \text{ for} \\ j(x;c) :=& \frac{\sqrt{c + g(x)}}{2k \cdot (x - \alpha_0) \cdot (\bar{p}x - \underline{p}/x)}.\end{aligned}$$

Since $f(x;c)$ is a decreasing function of c, we conclude that our optimal trajectory must have $c = c^*$ for $c^* := -g(\max(\underline{x}, \alpha_0))$. The following lemma characterizes the limiting behavior of $j(x;c)$ as x approaches $\max(\underline{x}, \alpha_0)$.

Lemma B.5. *In the limit as $x \to \max(\underline{x}, \alpha_0)^+$, the function $j(x;c)$ satisfies:*

$$\lim_{x \to \max(\underline{x}, \alpha_0)^+} j(x; c^*) = \begin{cases} 0, & \underline{x} \geq \alpha_0, \\ \sqrt{\delta/k}, & \underline{x} < \alpha_0. \end{cases}$$

We provide the proof of Lemma B.5 at the end.

If $\underline{x} \geq \alpha_0$, then the battery will eventually reach the shut-off efficiency $\underline{x}$ given sufficient usage, beyond which it is no longer profitable to operate. Lemma B.5 provides the intuitive result that the battery slows down as it approaches the shut-off efficiency. However, under an infinite horizon, the battery never completely shut offs—early stopping is ruled out by Theorem 3.5.

If $\underline{x} < \alpha_0$, then the battery cannot reach the shut-off efficiency, even under unbounded usage. While $E(t)$ becomes arbitrarily small, the condition $x(t) \geq \alpha_0$ ensures that the shut-off efficiency is never attained. Lemma B.5 again offers a natural intuition that the system behavior begins to resemble that of the capacity-degradation-only model. This is consistent with the fact that $x(t)$ converges to α_0, so the dynamics approach those of a model where efficiency is fixed at α_0.

In the scenario where the optimal DOD is constrained (aka $u^*(t) = 1$), recall (B.20) and (B.21):

$$\begin{aligned} \dot{p}(t) - kp(t) &= -e^{-\delta t}[2\bar{p}x(t) - \alpha_0(\bar{p} + \frac{\underline{p}}{x^2(t)})], \\ \dot{x}(t) &= -k\alpha_1 C_1 e^{-kt} = -k(x(t) - \alpha_0), \end{aligned}$$

for some constant $C_1 > 0$. From $\dot{p}(t) = e^{-\delta t}[-\delta\tilde{p}(t) + \tilde{p}'(t)]$, this can be written as:

$$\tilde{p}'(t) - (k + \delta)\tilde{p}(t) = -[2\bar{p}x(t) - \alpha_0(\bar{p} + \frac{\underline{p}}{x^2(t)})].$$

Noting that $\tilde{p}(t) = f(x(t))$ and $\tilde{p}'(t) = f'(x(t)) \cdot x'(t)$, this can be written as a function of $x(t)$ only:

$$f'(x(t)) = \frac{(k + \delta)f(x(t)) - [2\bar{p}x(t) - \alpha_0(\bar{p} + \underline{p}/x^2(t))]}{-k(x(t) - \alpha_0)},$$

which is a linear ODE.

Lastly, we proceed to characterize the possible patterns of $u^*(x)$. Each of the five cases from Lemma B.4 yield possible behaviors for $u^*(x)$ (or equivalently, $u^*(t)$ across time). These possible patterns are governed by the regions of $f(x)$ from Lemma B.4 as well as whether $u^*(t)$ is increasing or decreasing at the end of the horizon. Below we show that it is increasing in Cases 2, 4, and 5 and decreasing for Cases 1 and 3.

From (B.18) and (B.19), when $f(x) > 0$, it follows that $h'(x) > 0$, so $h(x(t))$ is a decreasing function of time. This makes regions with decreasing $u^*(t)$ "sticky" — once $k[u^*(t)]^2$ begins to decline, the entire term $k[u^*(t)]^2 \cdot [1 + h(x(t))]$ continues to decrease and remains below δ, causing $u^*(t)$ to keep decreasing. A symmetric argument shows that increasing $u^*(t)$ is also "sticky" when $f(x) < 0$.

If $\underline{x} \geq \alpha_0$, then $x(t) \to \underline{x}$ and $u^*(t) \to 0$ as $t \to \infty$.

If $\underline{x} < \alpha_0$, then $x(t) \to \alpha_0$ and $u^*(t) \to \min(\sqrt{\delta/k}, 1)$ as $t \to \infty$. Clearly, when $u^*(t) \to 1$, it approaches 1 from below . In the case $\delta < k$ (i.e., $u^*(t) \to \sqrt{\delta/k}$), observe from (B.18) that

$$[u^*(t)]'/u^*(t) = k[u^*(t)]^2 \cdot [1 + h(x(t))] - \delta,$$

with $h(x(t)) > 0$. Therefore, whenever $u^*(t) > \sqrt{\delta/k}$, we have $[u^*(t)]'/u^*(t) > 0$ for the remainder of the horizon. This contradicts the convergence $u^*(t) \to \sqrt{\delta/k}$. Thus, we conclude that $u^*(t)$ approaches $\sqrt{\delta/k}$ from below as $t \to \infty$ and always satisfies $u^*(t) < \sqrt{\delta/k}$ for all t.

Combining the results above, we conclude with the following pattern:

- Case 1: Sticky increases always yield monotone decreasing for $u^*(t)$.
- Case 2: region of sticky increase followed by region of sticky decrease yields monotone increasing or down - up patterns for $u^*(t)$.
- Case 3: Sticky decreases followed by region of sticky increase always yields monotone decreasing or up - down patterns for $u^*(t)$.
- Case 4: Region of sticky decrease followed by region of sticky increase followed by region of sticky decrease yields monotone increasing or down - up or up - down - up patterns for $u^*(t)$.
- Case 5: Sticky decreases always yield monotone increasing patterns for $u^*(t)$.

Proof of Lemma B.5

We begin by analyzing the case $\underline{x} \geq \alpha_0$, followed by the case $\underline{x} < \alpha_0$.

$$\lim_{x\to \underline{x}^+} j(x;c^*) = \lim_{x\to \underline{x}^+} \frac{\sqrt{g(x)-g(\underline{x})}}{2k(x-\alpha_0)(\bar{p}x-\underline{p}/x)}$$
$$= \lim_{x\to \underline{x}^+} \underbrace{\frac{1}{2k(x-\alpha_0)}}_{>0} \cdot \sqrt{\underbrace{\frac{g(x)-g(\underline{x})}{(\bar{p}x-\underline{p}/x)^2}}_{:=A_1(x)}}$$

where

$$A_1(x) = \frac{\frac{2\delta k}{3}\left[3\bar{p}(\bar{p}x^4 - 4\underline{p}x^2 + 3\underline{p}\underline{x}^2) - 4\alpha_0\bar{p}(\bar{p}x^3 - 6\underline{p}x + 5\underline{p}\underline{x}) + 12\underline{p}^2(\log(\frac{x}{\underline{x}} + \frac{\alpha_0}{x} - \frac{\alpha_0}{\underline{x}}))\right]}{(\bar{p}x-\underline{p}/x)^2}.$$

Since both denominator and numerator of $A_1(x)$ approach zero as $x \to \underline{x}$, we use L'hopital's rule to obtain:

$$\lim_{x\to \underline{x}^+} A_1(x) = \lim_{x\to \underline{x}^+} \underbrace{\frac{2\delta k}{3} \cdot \frac{1}{2(\bar{p}+\underline{p}/x^2)}}_{>0} \cdot \underbrace{\frac{3\bar{p}(4\bar{p}x^3 - 8\underline{p}x) - 4\alpha_0\bar{p}(3\bar{p}x^2 - 6\underline{p}) + 12\underline{p}^2 \cdot \frac{x-\alpha_0}{x^2}}{(\bar{p}x-\underline{p}/x)}}_{:=B_1(x)}.$$

Again, both denominator and numerator of $B_1(x)$ approach zero as $x \to \underline{x}$. Thus, we use L'hopital's rule to show:

$$\lim_{x\to \underline{x}^+} B_1(x) = \lim_{x\to \underline{x}^+} \frac{3\bar{p}(12\bar{p}x^2 - 8\underline{p}) - 4\alpha_0\bar{p}(6\bar{p}x) + 12\underline{p}^2\frac{-x^2+2\alpha_0 x}{x^4}}{(\bar{p}+\underline{p}/x^2)} = 0.$$

Then we conclude that $\lim_{x\to \underline{x}^+} j(x;c^*) = 0$.

We now proceed with the case of $\underline{x} < \alpha_0$.

$$\lim_{x\to \alpha_0^+} j(x;c^*) = \lim_{x\to \alpha_0^+} \frac{\sqrt{g(x)-g(\alpha_0)}}{2k(x-\alpha_0)(\bar{p}x-\underline{p}/x)}$$
$$= \lim_{x\to \alpha_0^+} \underbrace{\frac{1}{2k(\bar{p}x-\underline{p}/x)}}_{>0} \cdot \sqrt{\underbrace{\frac{g(x)-g(\alpha_0)}{(x-\alpha_0)^2}}_{:=A_2(x)}}$$

where

$$A_2(x) = \frac{\frac{2\delta k}{3}\left[\bar{p}^2(3x^4 - 4\alpha_0 x^3 + \alpha_0^4) - 12\bar{p}\underline{p}(x-\alpha_0)^2 + 12\underline{p}^2(\log(\frac{x}{\alpha_0}) + \frac{\alpha_0}{x} - 1)\right]}{(x-\alpha_0)^2}.$$

Since both denominator and numerator of $A_2(x)$ approach zero as $x \to \alpha_0$, we use L'hopital's rule to obtain:

$$\lim_{x\to\alpha_0^+} A_2(x) = \lim_{x\to\alpha_0^+} \underbrace{\frac{2\delta k}{3}\cdot\frac{1}{2}}_{>0} \cdot \underbrace{\frac{\bar{p}^2(12x^3 - 12\alpha_0 x^2) - 24\bar{p}\underline{p}(x-\alpha_0) + 12\underline{p}^2(1/x - \alpha_0/x^2)}{(x-\alpha_0)}}_{:=B_2(x)}.$$

Again, both denominator and numerator of $B_2(x)$ approach zero as $x \to \alpha_0$. Thus, we use L'hopital's rule to show:

$$\lim_{x\to\alpha_0^+} B_2(x) = \lim_{x\to\alpha_0^+} \frac{\bar{p}^2(36x^2 - 24\alpha_0 x) - 24\bar{p}\underline{p} + 12\underline{p}^2 \cdot \frac{-x^2+2\alpha_0 x}{x^4}}{1} = 12[p^a(\alpha_0)]^2.$$

Then we conclude that $\lim_{x\to\alpha_0^+} j(x;c^*) = \frac{1}{2kp^a(\alpha_0)} \cdot \sqrt{\frac{\delta k}{3}\cdot 12[p^a(\alpha_0)]^2} = \sqrt{\delta/k}$. □

Proof of Theorem 3.5

We first prove (1) the existence of $\hat{t}$, and then (2) establish the patterns of $u^*(t)$ over time.

Step (1). Existence of $\hat{t}$.

If $u^*(t) = 1$ for all $t \in [0,T]$, then the result holds immediately. Otherwise, we are in the $u^*(t) < 1$ region for some $t \in [0,T)$, and we proceed to show that there always exists a transition from $u^*(t) < 1$ to $u^*(t) = 1$ when t is sufficiently close to T. For notational simplicity, we interchangeably write the effective profit of providing $x(t)$ units of arbitrage service, originally defined as $p^a(x(t))$, as a function of time:

$$p^a(t) := \bar{p}x(t) - \frac{\underline{p}}{x(t)}.$$

If $p^a(T) > 0$ then it is immediate that we use the battery for the full horizon and that $u^*(t) = 1$ for a positive length of time at the end of the horizon, as $u^*(t) = \min\{1, \frac{p^a(t)}{2k\tilde{p}(t)}\}$ and $\tilde{p}(T) = 0$. We focus the remainder of the proof on the case where $p^a(T) = 0$.

Part 1: $u^*(t) = 1$ Leading up to the Shut-Off Efficiency

Define $\tau := \inf\{t : p^a(t) = 0\}$, with $\tau \leq T$. In Part 1 we seek to show that there exists some $\hat{t} < \tau$ such that $u^*(t) = 1$ for all $t \in [\hat{t}, \tau)$.

(B.18) states whenever $u^*(t) < 1$ that

$$\frac{[u^*(t)]'}{u^*(t)} = k[u^*(t)]^2 \cdot [1 + h(x(t))] - \delta, \text{ for}$$
$$h(x) := \frac{(x - \alpha_0)(\bar{p} + \underline{p}/x^2)}{\bar{p}x - \underline{p}/x}.$$

Since $h(x)$ grows unboundedly large as x approaches the shut-off efficiency $\underline{x}$, there exists some $t^* < \tau$ such that $1 + h(x(t)) > \delta/k$ for any $t \in [t^*, \tau)$. If there exists some $\hat{t} \in [t^*, \tau)$ at which $u^*(\hat{t}) = 1$, then (B.18) tells us that $u^*(t) = 1$ for all $t \in [\hat{t}, \tau)$, completing the result. We proceed by contradiction to rule out the possibility that $u^*(t) < 1$ for all $t \in [t^*, \tau)$ to complete Part 1.

In our unified model, the revenue rate is given by $r(t) = e^{-\delta t} p^a(t) u(t) E(t)$, and the system dynamics are given by $\dot{E}(t) = f(t) = ku^2(t)E(t)$ (function arguments are dropped for notational simplicity; note that r and f are both functions of state $E(t)$ and action $u(t)$). The first-order condition in (B.14) implies that $p^a(t) = 2\tilde{p}(t)ku(t)$, meaning that our revenue rate and the incurred future costs satisfy $p^a(t)u(t)E(t) = 2\tilde{p}(t)f(t)$ whenever $u^*(t) < 1$. We immediately observe that

$$\tilde{H}(t) = p^a(t)u(t)E(t) \cdot (1 - 1/2) \text{ and} \tag{B.23}$$
$$\begin{aligned}\tilde{H}'(t) &= p^a(t)u(t)E(t) \cdot (-\delta/2) \\ &= -\delta \cdot \tilde{H}(t).\end{aligned} \tag{B.24}$$

Since the rate of change in $\tilde{H}(t)$ is proportional to its current value, we conclude that $\tilde{H}(t)$ follows exponential decay in a region where $u^*(t) < 1$: $\tilde{H}(t) = \tilde{H}(0) \cdot e^{-\delta t}$. Then $\tilde{H}(t)$ decreases down to some $\tilde{H}(\tau) > 0$ over $t \in [t^*, \tau)$, which is only possible if $u(t)$ grows unboundedly large as t approaches τ (since $p^a(\tau) = 0$). This contradicts $u^*(t) < 1$ for all $t \in [t^*, \tau)$, completing Part 1.

Part 2: Using the Full Horizon

Assume for a contradiction that $\tau < T$, meaning the battery reaches its shutoff efficiency before the end of the finite horizon T. For any sufficiently small $\epsilon > 0$, we know from Part 1 that $u^*(t) = 1$ for $t \in [\tau - \epsilon, \tau]$. Define $\underline{E} := (\underline{x} - \alpha_0)/d$ to be the shut-off energy; we know

that $E(\tau) = \underline{E}$. From $E'(t) = -kE(t)$ when $u^*(t) = 1$, we have $E(\tau - \epsilon) = \underline{E} \cdot e^{k\epsilon}$.

Consider now a battery operating at fixed DOD $0 < u \leq 1$ from an initial energy of $\underline{E} \cdot e^{k\epsilon}$ until the battery is depleted (its energy reaches $\underline{E}$). For notational simplicity, we'll consider the battery as beginning to operate from time $t = 0$. From $E'(t) = -ku^2E(t)$, we have

$$E(t) = \underline{E} \cdot e^{k(\epsilon - u^2 t)},$$

meaning that the battery operates over $t \in [0, \epsilon/u^2]$ before being fully exhausted. Defining $q := u^2 t/\epsilon$ to indicate the proportion of the horizon, we can rewrite

$$E(q) = \underline{E} \cdot e^{k\epsilon(1-q)}.$$

Via $x(t) = \alpha_0 + \alpha_1 E(t)$ and $p^a(t) = \bar{p}x(t) - \underline{p}/x(t)$, it is straightforward to derive the expressions for the margin both as a function of time ($p^a(t)$) and as a function of the proportion of the horizon ($p^a(q)$).

Define $R(u)$ to be the total discounted revenue over horizon $t \in [0, \epsilon/u^2]$ when operating at fixed DOD u. Then

$$\begin{aligned} R(u) &= \int_0^{\epsilon/u^2} e^{-\delta t} \cdot u \cdot E(t) \cdot p^a(t)\ dt \\ &= \int_0^1 e^{-\delta\epsilon q/u^2} \cdot \frac{\epsilon}{u} \cdot E(q) \cdot p^a(q)\ dq, \text{ so} \\ R'(u) &= \int_0^1 \underbrace{\frac{e^{-\delta\epsilon q/u^2}\epsilon E(q)p^a(q)}{u^4}}_{\geq 0} \cdot \underbrace{(2\delta\epsilon q - u^2)}_{<0 \text{ for suff. small } \epsilon > 0} \quad dq \end{aligned}$$

For arbitrary $0 < u < 1$, there is some sufficiently small $\epsilon > 0$ such that $R(u)$ is strictly decreasing from u to 1, meaning the discounted revenue can be increased by operating at DOD u over time range $[\tau - \epsilon, \tau + \epsilon(1/u^2 - 1)]$ instead of operating at DOD 1 over time range $[\tau - \epsilon, \tau]$. We conclude that it's never optimal to reach the shutoff efficiency before time T.

Step (2). Patterns of $u^*(t)$ over time.

Next, we establish the possible behaviors of $u^*(t)$ over time. As shown above, $u^*(t)$ is always increasing as t approaches T. Using this fact, we can characterize how each of five cases from Lemma B.4 yield possible behaviors for $u^*(t)$ across time.

- Case 1: Sticky increases always yield monotone increasing or down - up patterns for $u^*(t)$.

- Case 2: region of sticky increase followed by region of sticky decrease yields monotone increasing or down - up patterns for $u^*(t)$.
- Case 3: Sticky decreases followed by region of sticky increase always yields monotone increasing or down - up or up - down - up patterns for $u^*(t)$.
- Case 4: Region of sticky decrease followed by region of sticky increase followed by region of sticky decrease yields monotone increasing or down - up or up - down - up patterns for $u^*(t)$.
- Case 5: Sticky decreases always yield monotone increasing patterns for $u^*(t)$.

Summarizing this yields the three possible patterns ($u^*(t)$ is either monotone increasing, down-up, or up-down-up in t).

□

Proof of Theorem 3.6

The proof follows immediately from Lemma B.4 and Theorem 3.5.

□

B.3 Generalization/Extension

In this section, we investigate several extensions to our base model. These include (1) other forms of degradation and (2) multiple price models.

B.3.1 Section 3.5.1: Sensitivity Analysis on Degradation Functions

Capacity-degradation-only: Power function

In this subsection, we perform a sensitivity analysis on the quadratic degradation assumption used in Section 3.4.1 to see if other convex functions would change/reserve the property. Consider any convex power function with the order $\beta > 1$ for the system dynamics. Then the optimization problem becomes:

$$\begin{aligned} \max_{0\le u(t)\le 1} \int_0^T e^{-\delta t} p^a u(t) E(t) dt \\ \text{s.t. } \dot{E}(t) = -kE(t)u(t)^\beta, \end{aligned} \tag{B.25}$$

where $p^a := \bar{p}x - \frac{p}{x}$ is the efficiency-adjusted arbitrage price. By definition, the arbitrage quantity at time t is $A(t) = xu(t)E(t)$, defined from the grid's perspective (we assume $x = 1$ in this section). The Hamiltonian is a function of the capacity E, the control u, the shadow price p, and time t:

$$\begin{aligned} H(E(t), u(t), p(t), t) &= r(t) + p(t)\dot{E}(t) \\ &= e^{-\delta t} p^a u(t) E(t) + p(t)(-kE(t)u^\beta(t)). \end{aligned} \tag{B.26}$$

$r(t) = e^{-\delta t}u(t)E(t)$ is the immediate revenue rate at time t and $\dot{E}(t) = -kE(t)u^\beta(t)$ is the (multiplicative) capacity degradation dynamics. According to the Pontryagin maximum principle, an optimal control trajectory $\{u^*(t)|t \in [0, T]\}$ satisfies the following necessary conditions:

$$\begin{aligned} [M] &: H(E^*(t), u^*(t), p(t), t) = \max_{0 \le u(t) \le 1} H(E^*(t), u(t), p(t), t), \\ [ODE] &: \dot{E}^*(t) = \nabla_{p(t)} H(E^*(t), u^*(t), p(t), t) = -kE^*(t)(u^*(t))^\beta, \\ [ADJ] &: \dot{p}(t) = -\nabla_{E(t)} H(E^*(t), u^*(t), p(t), t) = -e^{-\delta t} p^a u^*(t) + kp(t)(u^*(t))^\beta, \\ [T] &: p(T) = 0. \end{aligned} \tag{B.27}$$

We then obtain Theorem B.2, which extends Theorem 3.1 (with the quadratic assumption) to any power function with the order $\beta > 1$.

Theorem B.2 (**Capacity-degradation-only: Finite horizon and** $\beta > 1$)**.** *For capacity-degradation-only under a finite horizon T, it is either optimal to run the battery at full DOD for the whole horizon ($\delta \ge (\beta - 1)k$ or $\delta < (\beta - 1)k$, $T \le \frac{\log(\frac{\beta k}{\beta k - k - \delta})}{k + \delta}$) or to otherwise operate the battery at partial DOD until time*

$$t_A = T - \frac{\log(\frac{\beta k}{\beta k - k - \delta})}{k + \delta}$$

and at full DOD afterwards. The following hold at optimality:

	Cases		
	$(\beta-1)k > \delta, T > \frac{\log(\frac{\beta k}{\beta k-k-\delta})}{k+\delta}$)		$(\beta-1)k \le \delta$ or $(\beta-1)k > \delta,\ T \le \frac{\log(\frac{\beta k}{\beta k-k-\delta})}{k+\delta}$
	Discounted ($\delta > 0$)	Undiscounted ($\delta = 0$)	
$u^*(t)$	$\begin{cases} \left[\frac{(\beta-1)k\left(e^{\frac{\beta\delta(t_A-t)}{\beta-1}}-1\right)+\delta}{\delta e^{\frac{\beta\delta(t_A-t)}{\beta-1}}}\right]^{-\frac{1}{\beta}}, & 0 \le t \le t_A, \\ 1, & t_A \le t \le T. \end{cases}$	$\begin{cases} [1+\beta k(t_A-t)]^{-\frac{1}{\beta}}, & 0 \le t \le t_A, \\ 1, & t_A \le t \le T. \end{cases}$	1
$p(t)e^{\delta t}$	$\begin{cases} \frac{p^a}{\beta k}\left[\frac{(\beta-1)k\left(e^{\frac{\beta\delta(t_A-t)}{\beta-1}}-1\right)+\delta}{\delta e^{\frac{\beta\delta(t_A-t)}{\beta-1}}}\right]^{\frac{\beta-1}{\beta}}, & 0 \le t \le t_A, \\ \frac{p^a}{k+\delta}(1-e^{-(k+\delta)(T-t)}), & t_A \le t \le T. \end{cases}$	$\begin{cases} \frac{p^a}{\beta k}[1+\beta k(t_A-t)]^{\frac{\beta-1}{\beta}}, & 0 \le t \le t_A, \\ \frac{p^a}{k}(1-e^{-k(T-t)}), & t_A \le t \le T. \end{cases}$	$\frac{p^a}{k+\delta}(1-e^{-(k+\delta)(T-t)})$
$E^*(t)$	$\begin{cases} \left[\frac{(\beta-1)k\left(e^{\frac{\beta\delta(t_A-t)}{\beta-1}}-1\right)+\delta}{(\beta-1)k\left(e^{\frac{\beta\delta t_A}{\beta-1}}-1\right)+\delta}\right]^{\frac{1}{\beta}}, & 0 \le t \le t_A, \\ e^{-k(t-t_A)}\left[\frac{\delta}{(\beta-1)k\left(e^{\frac{\beta\delta t_A}{\beta-1}}-1\right)+\delta}\right]^{\frac{1}{\beta}}, & t_A \le t \le T. \end{cases}$	$\begin{cases} [\frac{\beta k(t_A-t)+1}{\beta k t_A+1}]^{\frac{1}{\beta}}, & 0 \le t \le t_A, \\ e^{-k(t-t_A)}[\frac{1}{1+\beta k t_A}]^{\frac{1}{\beta}}, & t_A \le t \le T. \end{cases}$	e^{-kt}
$A^*(t)$	$\begin{cases} e^{\frac{\delta(t_A-t)}{\beta-1}}\left[\frac{\delta}{(\beta-1)k\left(e^{\frac{\beta\delta t_A}{\beta-1}}-1\right)+\delta}\right]^{\frac{1}{\beta}}, & 0 \le t \le t_A, \\ e^{-k(t-t_A)}\left[\frac{\delta}{(\beta-1)k\left(e^{\frac{\beta\delta t_A}{\beta-1}}-1\right)+\delta}\right]^{\frac{1}{\beta}}, & t_A \le t \le T. \end{cases}$	$\begin{cases} [\frac{1}{\beta k t_A+1}]^{\frac{1}{\beta}}, & 0 \le t \le t_A, \\ e^{-k(t-t_A)}[\frac{1}{\beta k t_A+1}]^{\frac{1}{\beta}}, & t_A \le t \le T. \end{cases}$	e^{-kt}
R^*_{cum}	$\frac{p^a}{\beta k}\left[\frac{(\beta-1)k\left(e^{\frac{\beta\delta t_A}{\beta-1}}-1\right)+\delta}{\delta e^{\frac{\beta\delta t_A}{\beta-1}}}\right]^{\frac{\beta-1}{\beta}}$	$\frac{p^a}{\beta k}\left(\beta k t_A+1\right)^{\frac{\beta-1}{\beta}}$	$p^a(\frac{1-e^{-(k+\delta)T}}{k+\delta})$

Table B.2: Capacity-degradation-only (finite horizon; $\beta > 1$)

The following time dynamics occur across the time horizon:

- Optimal DOD $u^*(t)$ is strictly monotone increasing for $t \in [0, t_A)$,
- The shadow price of energy capacity $p(t)$, as well as that shadow price normalized by the time discounting, $p(t)e^{\delta t}$, are strictly monotone decreasing across the full horizon, and
- The optimal amount of energy to sell to the grid, $A^*(t)$, is strictly monotone decreasing across the full horizon under time discounting ($\delta > 0$), but under the undiscounted model it is a constant for $t \in [0, t_A]$ and then strictly monotone decreasing for $t > t_A$.

Proof. From $[M]$, we have

$$u^*(t) = \min((\frac{e^{-\delta t}p^a}{\beta k p(t)})^{\frac{1}{\beta-1}}, 1). \tag{B.28}$$

In a time range for which $p(t)e^{\delta t} \ge \frac{p^a}{\beta k}$ for all t in the range, $[ADJ]$ of (B.27) and (B.28)

yield

$$u^*(t) = (\frac{e^{-\delta t}p^a}{\beta k p(t)})^{\frac{1}{\beta-1}} \text{ and}$$
$$p(t)\dot{p}(t) = -k^{\frac{1}{1-\beta}}(\beta-1)(\frac{e^{-\delta t}p^a}{\beta})^{\frac{\beta}{\beta-1}}p(t)^{\frac{\beta-2}{\beta-1}}.$$

This is a first-order nonlinear ODE, so

$$p(t)e^{\delta t} = \begin{cases} [\frac{\beta^{\frac{-\beta}{\beta-1}}(\beta-1)k^{\frac{1}{1-\beta}}(p^a)^{\frac{\beta}{\beta-1}}}{\delta} - C_1 e^{\frac{\delta\beta t}{\beta-1}}]^{\frac{\beta-1}{\beta}}, & \text{if } \delta > 0, \text{ and} \\ [C_2 - (\frac{p^a}{\beta k})^{\frac{1}{\beta-1}}p^a t]^{\frac{\beta-1}{\beta}}, & \text{if } \delta = 0, \end{cases}$$

for some constants C_1 and C_2.

In a time range for which $p(t)e^{\delta t} \leq \frac{p^a}{\beta k}$ for all t in the range, $[ADJ]$ of (B.27) and (B.28) yield

$$u^*(t) = 1 \text{ and}$$
$$\dot{p}(t) - kp(t) = -e^{-\delta t}p^a.$$

This is a standard first-order linear ODE, and we have

$$p(t)e^{\delta t} = \frac{p^a}{k+\delta} - C_3 e^{(k+\delta)t},$$

for some constant C_3.

We proceed to establish the optimal solution trajectory backward in time from the end of horizon $t = T$. Note that $p(T) = 0$, and by the continuity of $p(t)$ there is a time range extending backward in time from $t = T$ for which $p(t)e^{\delta t} \leq \frac{p^a}{\beta k}$ and therefore $u^*(t) = 1$. Obtaining $p(T) = 0$ requires

$$C_3 = \frac{p^a}{(k+\delta)e^{(k+\delta)T}}, \tag{B.29}$$

meaning that in this time range

$$p(t)e^{\delta t} = \frac{p^a}{k+\delta}(1 - e^{-(k+\delta)(T-t)}).$$

$p(t)e^{\delta t}$ is strictly monotone decreasing, so $u^*(t) = 1$ for all $t \in [0, T]$ whenever $p(0) \leq \frac{p^a}{\beta k}$, or equivalently whenever $e^{-(k+\delta)T} \geq \frac{(\beta-1)k-\delta}{\beta k}$. We conclude that $u^*(t) = 1$ for the full time horizon whenever $(\beta-1)k \leq \delta$ or $(\beta-1)k > \delta$ and $T \leq \frac{\log(\frac{\beta k}{\beta k-k-\delta})}{k+\delta}$. In this case it is

straightforward via $[ODE]$ of (B.27) that $E^*(t) = e^{-kt}$.

The remainder of the proof will focus on the case when $(\beta-1)k > \delta$ and $T > \frac{\log(\frac{\beta k}{\beta k-k-\delta})}{k+\delta}$. Going backward in time from $t = T$, we reach $p(t)e^{\delta t} = \frac{p^a}{\beta k}$ at time $t_A = T - \frac{log(\frac{\beta k}{\beta k-k-\delta})}{k+\delta}$; recall that $u^*(t) < 1$ for $p(t)e^{\delta t} > \frac{p^a}{\beta k}$. By the continuity of $p(t)e^{\delta t}$, we get

$$C_1 = e^{\frac{-\delta\beta t_A}{\beta-1}}[\frac{\beta^{\frac{-\beta}{\beta-1}}(\beta-1)k^{\frac{1}{1-\beta}}}{\delta} - (\beta k)^{\frac{-\beta}{\beta-1}}](p^a)^{\frac{\beta}{\beta-1}} > 0 \text{ and}$$
$$C_2 = (\frac{p^a}{\beta k})^{\frac{\beta}{\beta-1}}(1+\beta k t_A) > 0.$$

$C_1,\ C_2 > 0$ confirms that $p(t)e^{\delta t}$ is strictly decreasing for $t \le t_A$ with the selected C_1 and C_2, establishing the optimal structure—we have $p(t)e^{\delta t} > \frac{p^a}{\beta k}$ for $t \in [0, t_A)$ with the C_1 and C_2 selected above, followed by $p(t)e^{\delta t} < \frac{p^a}{\beta k}$ for $t \in (t_A, T]$ with the C_3 selected in (B.29).

$[ODE]$ of (B.27) defines a first-order linear ODE that can be used to straightforwardly establish $E^*(t)$ under initial condition $E(0) = 1$.

□

Consistent with Corollary 3.1, Corollary B.1 below shows that the fixed-DOD policy remains optimal for any convex function when $T \to \infty$.

Corollary B.1 (**Capacity-degradation-only: Infinite horizon**). *With $T \to \infty$, discount $\delta > 0$, and capacity-degradation-only for any power convex function, a fixed-DOD is optimal:*

$$u^*(t) = \min\left(\left[\frac{\delta}{(\beta-1)k}\right]^{\frac{1}{\beta}}, 1\right), \text{ and}$$
$$p(t)e^{\delta t} = \begin{cases} \frac{p^a}{k+\delta} & \text{if } (\beta-1)k \le \delta, \text{ and} \\ \frac{(\beta-1)p^a}{\beta\delta}(\frac{\delta}{k(\beta-1)})^{\frac{1}{\beta}} & \text{if } (\beta-1)k > \delta. \end{cases}$$

Theorem B.2 and Corollary B.1 provide theoretical justifications for the simple heuristics that have been used in the literature/practice under some special cases of the capacity-degradation-only model. Thus, we confirmed that all the lessons (e.g., a fixed-DOD is optimal) in Section 3.4.1 (quadratic degradation) still hold even if we consider any convex power degradation function. One natural follow-up question is whether these heuristics still continue to work well under efficiency degradation, a question we will address in Section 3.4.2.

Heuristic (Fixed-DOD). Corollary B.1 states that a fixed-DOD policy is optimal under the special case of the infinite horizon. In this subsection, we evaluate the performance of the fixed-DOD policy under a finite horizon.

Given some fixed-DOD level (i.e., $u(t) = u$ for $0 \le t \le T$), the system dynamic of (B.27) implies

$$E(t) = e^{-ku^\beta t}.$$

Plugging $E(t)$ into the objective function (B.25), the best DOD level u can be selected as the constant maximizing the revenue over the full horizon:

$$R_{cum}^{DOD} := \max_{0\le u\le 1} \bar{R}(u) = \frac{p^a u}{ku^\beta + \delta}[1 - e^{-T(ku^\beta+\delta)}], \tag{B.30}$$

where $\bar{R}(u)$ is the full-horizon discounted revenue associated with a fixed-DOD level u under the capacity-degradation-only model. Let $\bar{u}$ be the optimal fixed-DOD level, aka, $\bar{u} := \arg\max_{0\le u\le 1} \bar{R}(u)$. We can show the uniqueness of it.

Lemma B.6. *$\bar{R}(u)$ in (B.30) has a unique maximizer $0 < \bar{u} \le 1$, which uses the full DOD ($\bar{u} = 1$) if the discount factor is high ($\delta \ge (\beta-1)k$) or if the time horizon is short ($\delta < (\beta-1)k$, $e^{-T(k+\delta)}[\beta Tk(k+\delta) + k(\beta-1) - \delta] \ge [(\beta-1)k - \delta]$), and a smaller DOD otherwise.*

Proof. We will prove the result by showing that $\bar{R}(u)$ is either strictly monotone increasing or has an up-down pattern with a unique maximizer $u \in (0, 1)$. We begin with monotone change of variable $y := ku^\beta + \delta$, for $y \in (\delta, k+\delta]$. Then

$$\begin{aligned}
\bar{r}(y) &= p^a(\frac{y-\delta}{ky^\beta})^{\frac{1}{\beta}}(1 - e^{-Ty}), \text{ and} \\
\bar{r}'(y) &= \underbrace{\frac{p^a}{\beta k y^{\beta+1}}(\frac{y-\delta}{ky^\beta})^{\frac{1}{\beta}-1}}_{>0} \times \underbrace{\Big[(1-\beta)y + \beta\delta + e^{-Ty}[\beta T(y-\delta)y + (\beta-1)y - \beta\delta]\Big]}_{:=f(y)}.
\end{aligned}$$

We proceed by signing $f(y)$ for $y \in (\delta, k+\delta]$. From

$$\begin{aligned}
f'(y) =& \frac{g(y) - (\beta-1)h(y)}{h(y)}, \text{ for} \\
g(y) :=& (\beta-1) + [(\beta+1)T + \beta T^2\delta]y - \beta T^2 y^2 \text{ and} \\
h(y) :=& e^{Ty} > 0,
\end{aligned}$$

we read that $f'(y)$ takes the same sign as $g(y) - (\beta-1)h(y)$. Noting that $g(y) - (\beta-1)h(y)$ is a strictly concave function that takes negative values for sufficiently large y and that takes value 0 and has a positive derivative at $y = 0$, we conclude that $f'(y)$ has a positive-negative pattern for $y \in (0, \infty)$. Over our range $y \in (\delta, k+\delta]$, $f(y)$ is either strictly increasing, strictly

decreasing, or strictly increasing up to a unique maximizer and then strictly decreasing afterwards.

Since $\bar{r}(\delta) = 0$ and $f(\delta) > 0$, we conclude from the possible patterns of $f(y)$ that $\bar{r}(y)$ is either strictly increasing up to a maximum at $y = k + \delta$ ($\bar{u} = 1$), or up-down with a maximizer at the unique $y \in (\delta, k + \delta)$ at which $f(y) = 0$. The optimal DOD will be 1 whenever $f(k + \delta) \geq 0$ and smaller otherwise. From

$$f(k+\delta) = -[(\beta-1)k - \delta] + e^{-T(k+\delta)}[\beta Tk(k+\delta) + k(\beta-1) - \delta],$$

we can straightforwardly derive the conditions leading to full DOD.

□

In general, $\bar{u}$ and the corresponding cumulative revenue $r(\bar{u})$ do not have closed-form expressions, but $\bar{u}$ can easily be found numerically. In the numerical section, we compare the performance of this heuristic with dynamic approaches.

We now study the performance of the heuristic compared to the optimal policy for the undiscounted problem.

Corollary B.2. *Under capacity-degradation-only and no discounting, S decreases in kT. The lower bound on S is $a^{\frac{1-\beta}{\beta}}\beta^{\frac{1}{\beta}}(1-e^{-a})$ where $a = -W_{-1}\left(-\frac{e^{\frac{1}{\beta}-1}(\beta-1)}{\beta}\right) - \frac{\beta-1}{\beta} > 0$.*

Proof. Without time discounting, we have $(\beta-1)k > \delta = 0$, so $S = 1$ whenever $T \leq \frac{\log(\frac{\beta}{\beta-1})}{k}$. Otherwise, we can read the optimal revenue of the two approaches from Theorem B.2 (the R^*_{cum} row) and (B.30), yielding revenue ratio:

$$S = \frac{\beta(1-e^{-Tk\bar{u}^\beta})}{\bar{u}^{\beta-1}[1+\beta kT - \beta\log(\frac{\beta}{\beta-1})]^{\frac{\beta-1}{\beta}}}.$$

From Lemma B.6, we know $\bar{u} = 1$ if horizon T is sufficiently short ($e^{Tk} \leq 1 + \frac{\beta Tk}{\beta-1}$), and $\bar{u} < 1$ otherwise and solves the first-order condition for the maximization problem in (B.30). We will derive bounds on S by considering fixed k and studying the trajectory of S as T is increased from $\frac{\log(\frac{\beta}{\beta-1})}{k}$.

For $T > \frac{\log(\frac{\beta}{\beta-1})}{k}$ and $e^{Tk} \leq 1 + \frac{\beta Tk}{\beta-1}$, we have $\bar{u} = 1$ and

$$S'(T) = \underbrace{\frac{-\beta k}{(1+\beta Tk - \beta\log(\frac{\beta}{\beta-1}))^{\frac{2\beta-1}{\beta}}}}_{<0} \times \underbrace{[(\beta-1) - \beta e^{-Tk}(1+Tk-\log(\frac{\beta}{\beta-1}))]}_{>0 \text{ for any } T > \frac{\log(\frac{\beta}{\beta-1})}{k}} < 0.$$

For $T > \frac{\log(\frac{\beta}{\beta-1})}{k}$ and $e^{Tk} > 1 + \frac{\beta Tk}{\beta-1}$, then $\bar{u} < 1$ satisfies the FOC on (B.30):

$$e^{Tk\bar{u}^\beta} = 1 + \frac{\beta}{\beta - 1} Tk\bar{u}^\beta. \tag{B.31}$$

Solving (B.31) yields the unique solution:

$$\begin{aligned} \bar{u} =& \big[\frac{a}{Tk}\big]^{\frac{1}{\beta}} \text{ for} \\ a :=& - W_{-1}\left(-\frac{e^{\frac{1}{\beta}-1}(\beta-1)}{\beta}\right) - \frac{\beta-1}{\beta} > 0, \end{aligned} \tag{B.32}$$

where W_{-1} is the Lambert W function with branch index -1. Then whenever $e^{Tk} > 1 + \frac{\beta Tk}{\beta-1}$, we have

$$S = \frac{\beta(1-e^{-a})}{[a \cdot \frac{1+\beta Tk - \beta\log(\frac{\beta}{\beta-1})}{Tk}]^{\frac{\beta-1}{\beta}}}.$$

We conclude that S is monotone decreasing aross all T and minimized as $T \to \infty$, approaching the infimum:

$$a^{\frac{1-\beta}{\beta}} \beta^{\frac{1}{\beta}} (1 - e^{-a}).$$

□

Heuristic (Fixed-A). In this subsection, we evaluate the performance of the constant A policy with $\beta > 1$.

Given some constant service quantity A, let t_A denote the smallest time $t \in [0, T]$ such that $E(t) = A$ ($t_A := \infty$ if $E(T) > A$). For $t \le t_A$, $u(t) = \frac{A}{E(t)}$. Also, the system dynamic of (B.25) implies

$$E(t) = (1 - \beta k t A^\beta)^{\frac{1}{\beta}}. \tag{B.33}$$

For $t_A < t \le T$, providing A amount of service becomes infeasible due to the limited energy capacity. Thus, we have $u(t) = 1$ and the system dynamic of (B.25) implies

$$E(t) = Ae^{-k(t-t_A)}. \tag{B.34}$$

Also, we have

$$t_A = \begin{cases} \frac{1-A^\beta}{\beta k A^\beta}, & \text{if } (1+\beta kT)^{-\frac{1}{\beta}} \leq A, \text{ and} \\ \infty, & \text{otherwise.} \end{cases}$$

Plugging (B.33) – (B.34) into the objective function (B.25), the best service level A can be selected as the constant maximizing the revenue over the full horizon. Note that if $(1+\beta kT)^{-\frac{1}{\beta}} > A$, then

$$\begin{aligned} &:= \max_{0 \leq A \leq (1+\beta kT)^{-\frac{1}{\beta}}} \int_0^T e^{-\delta t} p^a A dt \\ &= \max_{0 \leq A \leq (1+\beta kT)^{-\frac{1}{\beta}}} \frac{p^a A}{\delta}(1 - e^{-\delta T}), \end{aligned}$$

which implies that the optimal service quantity always satisfies $A \geq (1+\beta kT)^{-\frac{1}{\beta}}$.

Thus, we have

$$\begin{aligned} R^A_{cum} &:= \max_{(1+\beta kT)^{-\frac{1}{\beta}} \leq A \leq 1} \left[\int_0^{t_A} e^{-\delta t} p^a A dt + \int_{t_A}^T e^{-\delta t} p^a A e^{-k(t-t_A)} dt \right] \\ &= \max_{(1+\beta kT)^{-\frac{1}{\beta}} \leq A \leq 1} \underbrace{p^a A \left[\frac{1}{\delta}(1 - e^{-\delta \frac{1-A^\beta}{\beta k A^\beta}}) - \frac{e^{\frac{1-A^\beta}{\beta A^\beta}}}{k+\delta}(e^{-(k+\delta)T} - e^{-(k+\delta)\frac{1-A^\beta}{\beta k A^\beta}}) \right]}_{:=\bar{r}(A)}. \end{aligned}$$

Let $\bar{A} := \arg\max_{0 \leq A \leq 1} \bar{r}(A)$. We can numerically study the performance of the heuristic compared to the optimal policy. Let $S(\delta) := \frac{R^A_{cum}}{R^\star_{cum}}$ be the ratio between the cumulative discounted revenues from the fixed-A heuristic at optimal level $\bar{A}$ and optimal dynamic policy, respectively, under some discount factor $\delta > 0$.

Unified model: Power function

We perform a sensitivity analysis on the quadratic degradation assumption used in Section 3.4.2 to see if other convex functions would change/reserve the property. Similar to the previous section, we consider a convex power function with the order $\beta > 1$ for the system dynamics. Then the optimization problem becomes:

$$\begin{aligned} &\max_{0 \leq u(t) \leq 1} \int_0^T e^{-\delta t} [\bar{p} E(t) u(t) x(t) - \underline{p} \frac{E(t) u(t)}{x(t)}] dt \\ \text{s.t. } &\dot{E}(t) = -k E(t) u(t)^\beta \\ &x(t) = a(E(t)) = \alpha_0 + \alpha_1 E(t). \end{aligned}$$

We first state the Hamiltonian.

$$\begin{aligned} H(E(t), u(t), p(t), t) &= r(t) + p\dot{E}(t) \\ &= e^{-\delta t} u(t) E(t) p^a(x(t)) + p(t)(-kE(t)u^\beta(t)), \end{aligned}$$

where $r(t) = e^{-\delta t} u(t) E(t) p^a(x(t))$ is the immediate revenue rate at time t and $\dot{E}(t) = -kE(t)u^\beta(t)$ is the system dynamics. According to the Pontryagin maximum principle, an optimal control trajectory $\{u^*(t) | t \in [0, T]\}$ satisfies (we omit the time-dependency of the variables for simplicity):

$$\begin{aligned} [M] &: H(E^*(t), u^*(t), p(t), t) = \max_{0 \le u(t) \le 1} H(E^*(t), u(t), p(t), t), \\ [ODE] &: \dot{E}(t) = \nabla_{p(t)} H(E^*(t), u^*(t), p(t), t) = -kE^*(t)(u^*)^\beta(t), \\ [ADJ] &: \dot{p}(t) = -\nabla_{E(t)} H(E^*(t), u^*(t), p(t), t) \\ &\quad = -e^{-\delta t} u(t)[2\bar{p}x(t) - \alpha_0(\bar{p} + \frac{\underline{p}}{x^2(t)})] + kp(t)u^\beta(t), \\ [T] &: p(T) = 0. \end{aligned} \tag{B.35}$$

From $[M]$, maximizing the Hamiltonian leads to:

$$u^*(t) = \min\left(\left[\frac{p^a(x(t))}{\beta k \tilde{p}(t)} \right]^{\frac{1}{\beta - 1}}, 1 \right), \tag{B.36}$$

for $\tilde{p}(t) = p(t)e^{\delta t}$ and $x(t) \ge \underline{x}$, where $\underline{x} = \sqrt{\frac{\underline{p}}{\bar{p}}}$ is the shut-off efficiency.

If $u^*(t) = 1$, then

$$\dot{E}(t) = -kE(t)$$

leads to

$$\begin{aligned} E(t) &= C_1 e^{-kt} \text{ and} \\ x(t) &= \alpha_0 + \alpha_1 C_1 e^{-kt}, \end{aligned}$$

for some constant $C_1 > 0$. Then

$$\dot{p}(t) - kp(t) = -e^{-\delta t}[\bar{p}(2C_1 d e^{-kt} + \alpha_0) - \frac{\underline{p}\alpha_0}{(\alpha_0 + C_1 d e^{-kt})^2}].$$

In general, there's no closed-form solution for this.

If $u^*(t) < 1$, then we have

$$\dot{p}(t) = \frac{e^{\frac{-\delta\beta t}{\beta-1}}[p^a(x(t))]^{\frac{1}{\beta-1}}}{\beta^{\frac{\beta}{\beta-1}}(kp(t))^{\frac{1}{\beta-1}}}[p^a(x(t)) - \beta[2\bar{p}x(t) - \alpha_0(\bar{p} + \frac{\underline{p}}{x^2(t)})]], \tag{B.37}$$

$$\begin{aligned}\dot{\tilde{p}}(t) &= \frac{\dot{p}(t)}{e^{-\delta t}} + \delta\tilde{p}(t) \\ &= \delta\tilde{p}(t) + \frac{[p^a(x(t))]^{\frac{1}{\beta-1}}}{\beta^{\frac{\beta}{\beta-1}}(k\tilde{p}(t))^{\frac{1}{\beta-1}}}[p^a(x(t)) - \beta[2\bar{p}x(t) - \alpha_0(\bar{p} + \frac{\underline{p}}{x^2(t)})]],\end{aligned} \tag{B.38}$$

$$\begin{aligned}\frac{\dot{\tilde{p}}(t)}{\tilde{p}(t)} &= \delta + \frac{[p^a(x(t))]^{\frac{\beta}{\beta-1}}}{\beta^{\frac{\beta}{\beta-1}}k^{\frac{1}{\beta-1}}[\tilde{p}(t)]^{\frac{\beta}{\beta-1}}}\left[1 - \frac{\beta[2\bar{p}x(t) - \alpha_0(\bar{p} + \frac{\underline{p}}{x^2(t)})]}{p^a(x(t))}\right] \\ &= \delta + k[u^*(t)]^\beta \cdot \left[1 - \frac{\beta[2\bar{p}x(t) - \alpha_0(\bar{p} + \frac{\underline{p}}{x^2(t)})]}{p^a(x(t))}\right], \quad \text{and} \\ \dot{x}(t) &= -\frac{e^{\frac{-\delta\beta t}{\beta-1}}(x(t) - \alpha_0)[p^a(x(t))]^{\frac{\beta}{\beta-1}}}{\beta^{\frac{\beta}{\beta-1}}k^{\frac{1}{\beta-1}}p^{\frac{\beta}{\beta-1}}(t)} = -\frac{(x(t) - \alpha_0)[p^a(x(t))]^{\frac{\beta}{\beta-1}}}{\beta^{\frac{\beta}{\beta-1}}k^{\frac{1}{\beta-1}}\tilde{p}^{\frac{\beta}{\beta-1}}(t)}.\end{aligned} \tag{B.39}$$

Now we proceed with the unconstrained solution.

Theorem B.3 (**Unified: Unconstrained solution**). *When $u^*(t) < 1$, the optimal battery control under the unified degradation model is described as follows:*

- *The optimal DOD $u^*(t)$ satisfies:*

$$\frac{[u^*(t)]'}{u^*(t)} = ku^\beta\left[1 + \underbrace{\frac{(x - \alpha_0)(\bar{p} + \underline{p}/x^2)}{p^a(x)}}_{=h(x)}\right] - \frac{\delta}{\beta - 1}. \tag{B.40}$$

- *The discounted revenue rate $r(t) := e^{-\delta t}p^a(t)E(t)u(t)$ satisfies:*

$$r(t) = r(0)e^{-\delta t \cdot \frac{\beta}{\beta-1}}.$$

The overall structure of the optimal policy remains unchanged from the main model. For instance, (B.40) implies that when time discounting is negligible ($\delta \approx 0$), $u^*(t)$ is monotone increasing. Also, if $\delta = 0$, then the revenue rate $r(t)$ remains constant whenever $u^*(t) < 1$. Theorem B.3 also shows how both discount rate δ and degradation elasticity β play a role in how we distribute revenue across time. For a fixed β, a larger δ implies faster decline of $r(t)$. Conversely, for a fixed δ, as β increases (i.e., as the degradation rate becomes more sensitive to changes in DOD), the effective decay factor $\frac{\beta}{\beta-1}$ decreases toward 1, so $r(t)$ decays more slowly over time. Furthermore, Theorem B.4 below extends Theorem 3.5.

Theorem B.4 (**Unified: Finite horizon,** $\beta > 1$)**.** *Under the unified model with a finite horizon T, the optimal control satisfies the following:*

- *There exists $0 \leq \hat{t} < T$ such that $u^*(t) = 1$ for all $t \in [\hat{t}, T]$, and*
- *The optimal DOD $u^*(t)$ is either monotone increasing, down-up, or up-down-up in t.*

Proof. Following the logic used for the proof of Theorem 3.5, we can show the existence of $\hat{t}$. Since the function $h(x)$ from (B.40) remains the same as the quadratic degradation case, the remainder of the proof follows directly from the proof of Theorem 3.5.

□

B.3.1.1 General Convex Functions

Capacity-degradation-only: General convex function

Theorem B.5 (**Capacity-degradation-only: Finite horizon**)**.** *For capacity-degradation-only under a finite horizon T with a convex increasing degradation function $\Phi(u)$, the following dynamics occurs across the time horizon:*

- *Optimal DOD $u^*(t)$ is either (i) $u^*(t) = 1$ for any $t \in [0, T]$ or (ii) $u^*(t)$ is strictly monotone increasing for $t \in [0, t_A)$ and $u^*(t) = 1$ for $t \in [t_A, T]$,*
- *The shadow price of energy capacity $p(t)$, as well as that shadow price normalized by the time discounting, $p(t)e^{\delta t}$, are strictly monotone decreasing across the full horizon.*

Proof of Theorem B.5

The Hamiltonian for the discounted capacity-degradation-only problem is $e^{-\delta t}p^a u(t)E(t) - p(t)\Phi(u(t))E(t)$, where $p(t)$ is the shadow price for energy capacity. The optimality condition indicates that $u^*(t)$ maximizes the Hamiltonian for each time t. From the derivative of the Hamiltonian with respect to $u(t)$, $u^*(t) = 1$ when $e^{-\delta t}p^a \geq p(t)\Phi'(u(t) = 1)$. For unconstrained cases ($u^*(t) < 1$), setting the derivative of the Hamiltonian with respect to $u(t)$ equal to 0 yields:

$$\Phi'(u(t))p(t) = e^{-\delta t}p^a. \tag{B.41}$$

Throughout this section, we drop "*" from various terms for readability, but whenever we refer to $E(t)$ or $u(t)$ below, these should be understood to be the optimal trajectories $E^*(t)$

and $u^*(t)$. Lastly, our optimality conditions provide a necessary condition (labeled [ADJ] in our chapter) for the evolution of the shadow price:

$$p'(t) = -e^{-\delta t}p^a \cdot u(t) + p(t) \cdot \Phi(u(t)). \tag{B.42}$$

From (B.41), taking the derivative with respect to t yields:

$$\Phi''(u(t))u'(t)p(t) + \Phi'(u(t))p'(t) = e^{-\delta t}p^a(-\delta). \tag{B.43}$$

Plugging (B.42) into (B.43) leads to:

$$\begin{aligned}
&\Phi''(u(t))u'(t)p(t) + \Phi'(u(t))[-e^{-\delta t}p^a \cdot u(t) + p(t) \cdot \Phi(u(t))] = e^{-\delta t}p^a(-\delta) \\
\Leftrightarrow\ &\Phi''(u(t))u'(t)p(t) = e^{-\delta t}p^a[u(t)\Phi'(u(t)) - \Phi(u(t)) - \delta].
\end{aligned}$$

We then read that $\text{sgn}(u'(t)) = \text{sgn}(g(t))$ for $g(t) := u(t)\Phi'(u(t)) - \Phi(u(t)) - \delta$. Note that

$$\begin{aligned}
g'(t) &= u'(t)\Phi'(u(t)) + u(t)\Phi''(u(t))u'(t) - \Phi'(u(t))u'(t) \\
&= \underbrace{u(t)\Phi''(u(t))}_{\geq 0}u'(t),
\end{aligned}$$

which implies $\text{sgn}(g'(t)) = \text{sgn}(u'(t))$. Thus, $g(t)$ is increasing (decreasing) whenever $u(t)$ is increasing (decreasing).

Then we can prove by contradiction that the only possible case is $u(t)$ increasing. If $u(t)$ is decreasing for some $\tilde{t} \in [0, T]$, i.e., $u'(\tilde{t}) < 0$, then $g(\tilde{t}) < 0$, and $g'(\tilde{t}) < 0$. This implies that $g(t) < 0$ (i.e., $u(t)$ is decreasing) for any $t \in [\tilde{t}, T]$. This contradicts the fact that $u^*(t) = 1$ when t is sufficiently close to T, under no salvage. This implies that the only possible patterns for $u^*(t)$ either (i) $u^*(t) = 1$ for the entire period or (ii) $u^*(t)$ is monotone increasing in t and stays at $u^*(t) = 1$ for the remaining time.

Lastly, from (B.41), $\Phi'(u(t))\tilde{p}(t) = p^a$. This implies that $\tilde{p}(t)$ and $p(t)$ are both strictly monotone decreasing.

□

Corollary B.3 (**Capacity-degradation-only: Infinite horizon**). *With $T \to \infty$, discount $\delta > 0$, convex increasing degradation function, and capacity-degradation-only, a fixed-DOD is optimal.*

Proof. From (B.41), $\Phi'(u(t))\tilde{p}(t) = p^a$. Under the infinite problem ($T \to \infty$), the current-value shadow price $\tilde{p}(t)$, the marginal value of capacity measured at time t, remains constant

since the value-to-go function is proportional only to the capacity $E(t)$. This implies that a fixed-DOD is optimal.

□

B.3.1.2 Autonomous System and DOD-Elasticity of Degradation

Let's consider a general optimal control problem:

$$\begin{aligned} \max_{u\in\Omega(t)} \left\{ J = \int_0^T F(x,u,t)dt + S(x(T),T) \right\} \\ s.t.\ \dot{x} = f(x,u,t), \\ x(0) = x_0. \end{aligned}$$

The system is called autonomous if F, f, S, and Ω are not explicit functions of time t. Then the following can be shown.

Lemma B.7 (**Autonomous system; [171]**). *For an autonomous problem, the Hamiltonian is constant along the optimal path, i.e.,* $\frac{dH}{dt} = 0$.

In the following, we analyze how the elasticity of the degradation function influences the structural characteristics of each model.

B.3.1.3 Capacity-Degradation-Only

Lemma B.8. *When providing A total arbitrage across some time range $[t_1, t_2]$ under arbitrary strictly convex degradation function $f(u)$, it is degradation-minimizing to keep quantity $A(t) \cdot [1 - \frac{1}{\epsilon(A(t)/E(t))}]$ constant over $t \in [t_1, t_2]$, where $A(t)$ is the rate of arbitrage at time t and $\epsilon(u) := f'(u)u/f(u)$ is the elasticity of the degradation function.*

Proof. We seek to solve the following optimal control problem:

$$\begin{aligned} \max_{A(t),E(t),W(t)} \quad & E(t_2) \\ \text{s.t.} \quad & E'(t) = -f(\frac{A(t)}{E(t)}) \cdot E(t) \\ & W'(t) = A(t) \\ & W(t_1) = 0, W(t_2) = A, E(t_1) = E_0. \end{aligned}$$

Define $\lambda(t)$ to be the shadow price of energy capacity $E(t)$ and μ to be the shadow price of

cumulative arbitrage $W(t)$. This enables us to write the Hamiltonian:

$$H(E, A, \lambda, \mu) = -\lambda f(\frac{A}{E})E + \mu A.$$

Note that μ is a constant (not a function of time t) because the Hamiltonian is independent of cumulative work $W(t)$ (work has the same value regardless of when it is completed).

Via the first-order condition,

$$\lambda(t) f'(\frac{A^*(t)}{E(t)}) = \mu, \text{ so}$$
$$H(E(t), A^*(t), \lambda(t), \mu) = \mu A^*(t)[1 - \frac{1}{\epsilon(A^*(t)/E(t))}].$$

We conclude the result by noting that the Hamiltonian is constant along the optimal path in an autonomous system. □

Observation B.1. *When providing A total arbitrage across some time range $[t_1, t_2]$ under a degradation function with constant elasticity ($f(u) = ku^\beta$ for $\beta > 1$), it is optimal to evenly spread arbitrage across time time period, setting $A(t) = A/(t_2 - t_1)$.*

Theorem B.6 (**Elasticity: Arbitrage quantity**). *For the unconstrained, undiscounted capacity-degradation-only model with a convex increasing degradation function $\Phi(u)$, the optimal arbitrage quantity satisfies the following:*

- *A constant amount policy is optimal ($A^*(t) = c$ for some c) if and only if DOD-elasticity of degradation is constant for any $u < 1$ (i.e., $\Phi(u)$ is a power function),*
- *$A^*(t)$ is decreasing if and only if DOD-elasticity of degradation is increasing in u,*
- *$A^*(t)$ is increasing if and only if DOD-elasticity of degradation is decreasing in u.*

B.3.1.4 Examples

Constant elasticity (Power function): It is well known that Φ has constant elasticity β if and only if Φ is a power function of the form $\Phi(u) = ku^\beta$ for some constant $c > 0$. In other words, the "constant revenue" phenomenon for the undiscounted, capacity-degradation-only model happens if and only if DOD-elasticity of degradation is constant at $\beta > 1$ (convex)—when DOD level rises by 1%, degradation rises by β%.

We have already established that any strictly convex, power degradation function yields the "constant revenue" phenomenon for the undiscounted, capacity-degradation-only model. Theorem B.6 implies that power functions are the only class of degradation functions that

yield the phenomenon for this model. Theorem B.6 also implies that we see increasing (decreasing) $A^*(t)$ if and only if the DOD-elasticity of degradation is decreasing (increasing) over time.

Increasing elasticity (Exponential function): Let's consider $\Phi(u) = \frac{e^{\beta u}-1}{e^{\beta}-1}$ for some $\beta > 0$ (convex increasing). In this case, DOD-elasticity of degradation, denoted by $\epsilon(u)$, becomes u-dependent:

$$\epsilon(u) = \frac{\beta u}{1 - e^{-\beta u}} > 1, \ u \in (0, 1].$$

Obviously, a constant revenue policy is no longer optimal. Note that $\epsilon(u)$ is increasing in u (i.e., $\Phi(u)$ has increasing elasticity) from

$$\epsilon'(u) = \frac{e^{\beta u} - 1 - \beta u}{\frac{e^{\beta u}}{\beta} \times (1 - e^{-\beta u})^2} > 0 \ (\because e^{\beta u} > 1 + \beta u \text{ for any } u > 0).$$

Intuitively, this implies that a unit percentage increase in DOD leads to a larger percentage increase in the degradation rate as u_t becomes larger. Since $u^*(t)$ is strictly increasing in t for any convex increasing degradation under a finite horizon (Theorem B.5), the immediate revenue function is then strictly decreasing in t.

Decreasing elasticity: Decreasing elasticity is equivalent to

$$\begin{aligned} \epsilon'(u) < 0 \Leftrightarrow & [\Phi''(u) + \frac{\Phi'(u)}{u}]\Phi(u) < [\Phi'(u)]^2 \\ \Leftrightarrow & \frac{\Phi''(u)}{\Phi'(u)} + \frac{1}{u} < \frac{\Phi'(u)}{\Phi(u)}. \end{aligned}$$

Let's consider the following degradation function:

$$\Phi(u) = \begin{cases} u^2, & \text{if } 0 \le u \le 1/2, \text{ and} \\ u^2 + 3u - \frac{3}{2}, & \text{if } 1/2 \le u \le 1. \end{cases} \tag{B.44}$$

It can be easily checked that $\Phi(u)$ satisfies $\Phi(u) > 0, \Phi'(u) > 0, \Phi''(u) > 0$. Also, $\Phi(u)$ has constant elasticity for $0 \le u < 1/2$, increasing elasticity at $u = 1/2$, and decreasing elasticity for $1/2 < u \le 1$. Clearly, $u^*(t)$ is monotone increasing until it reaches 1 and remains so afterward (Theorem B.5). $A^*(t)$ is constant, then decreases in t, then increases in t until $u^*(t)$ reaches 1, at which point $A^*(t)$ begins to decrease thereafter.

B.3.1.5 Unified Model

Let's check for our unified model. Let $\Phi(u)$ denote the functional form of our degradation model, which is assumed to be any increasing, convex function of u. Below, we show that the elasticity of the degradation function determines the structural property of the optimal revenue rate.

Lemma B.9. *When providing R total revenue across some time range $[t_1, t_2]$ under arbitrary strictly convex degradation function $f(u)$, it is degradation-minimizing to keep quantity $r(t) \cdot [1 - \frac{1}{\epsilon(A(t)/E(t))}]$ constant over $t \in [t_1, t_2]$, where $r(t) := p^a(t)E(t)u(t)$ is the rate of revenue at time t, $A(t) = E(t)u(t)$ is the rate of arbitrage at time t, and $\epsilon(u) := f'(u)u/f(u)$ is the elasticity of the degradation function.*

Proof. We seek to solve the following optimal control problem:

$$\begin{aligned}
\max_{r(t),E(t),W(t)} \quad & E(t_2) \\
\text{s.t.} \quad & E'(t) = -f(\frac{A(t)}{E(t)}) \cdot E(t) \\
& W'(t) = r(t) \\
& r(t) = A(t)[\bar{p}(\alpha_0 + \alpha_1 E(t)) - \frac{\underline{p}}{\alpha_0 + \alpha_1 E(t)}] \\
& W(t_1) = 0, W(t_2) = R, E(t_1) = E_0.
\end{aligned}$$

Define $\lambda(t)$ to be the shadow price of energy capacity $E(t)$ and μ to be the shadow price of cumulative revenue $W(t)$. We can assume $A(t)$ is the primary control variable that we optimize. Then $r(t)$ is determined by $A(t)$ and $E(t)$ via the relationship above. This enables us to write the Hamiltonian:

$$H(E, A, \lambda, \mu) = -\lambda f(\frac{A}{E})E + \mu A[\bar{p}(\alpha_0 + \alpha_1 E) - \frac{\underline{p}}{\alpha_0 + \alpha_1 E}].$$

Note that μ is a constant (not a function of time t) because the Hamiltonian is independent of cumulative work $W(t)$ (work has the same value regardless of when it is completed).

Via the first-order condition,

$$\begin{aligned}
\lambda(t) f'(\frac{A^*(t)}{E(t)}) &= \mu[\bar{p}(\alpha_0 + \alpha_1 E(t)) - \frac{\underline{p}}{\alpha_0 + \alpha_1 E(t)}], \text{ so} \\
H(E(t), A^*(t), \lambda(t), \mu) &= \mu A^*(t)[\bar{p}(\alpha_0 + \alpha_1 E(t)) - \frac{\underline{p}}{\alpha_0 + \alpha_1 E(t)}][1 - \frac{1}{\epsilon(A^*(t)/E(t))}].
\end{aligned}$$

We conclude the result by noting that the Hamiltonian is constant along the optimal path in an autonomous system. □

Observation B.2. *When providing R total arbitrage revenue across some time range $[t_1, t_2]$ under a degradation function with constant elasticity ($f(u) = ku^\beta$ for $\beta > 1$), it is optimal to evenly spread revenue across time time period, setting $r(t) = R/(t_2 - t_1)$.*

Theorem B.7 (**Elasticity: Revenue rate**). *For the unconstrained, undiscounted unified model with a convex increasing degradation function $\Phi(u)$, the optimal revenue rate satisfies the following:*

- *A constant revenue policy is optimal ($r^*(t) = c$ for some c) if and only if DOD-elasticity of degradation is constant for any $u < 1$ (i.e., $\Phi(u)$ is a power function),*
- *$r^*(t)$ is decreasing if and only if DOD-elasticity of degradation is increasing in u,*
- *$r^*(t)$ is increasing if and only if DOD-elasticity of degradation is decreasing in u.*

Proof. The Hamiltonian is again the instantaneous revenue, $p^a(x(t))u(t)E(t)$, minus the cost of the resources used, given by:

$$H = E(t)[p^a(x(t))u(t) - p(t) \cdot \Phi(u(t))]. \tag{B.45}$$

By applying the definition of DOD-elasticity $\epsilon(u) = \frac{\Phi'(u)u}{\Phi(u)}$, the resource cost term can be rewritten as $p(t)E(t)\Phi(u(t)) = p(t)E(t) \cdot \frac{u(t)\Phi'(u(t))}{\epsilon(u(t))}$. This allows us to express the Hamiltonian with the term $u(t)E(t)$ factored out:

$$H = u(t)E(t)[p^a(x(t)) - p(t) \cdot \frac{\Phi'(u(t))}{\epsilon(u(t))}]. \tag{B.46}$$

For an unconstrained soltuion, FOC implies:

$$p(t) = \frac{p^a(x(t))}{\Phi'(u(t))}, \tag{B.47}$$

which means that, at the optimum $u^*(t)$, the marginal revenue equals the marginal cost. Then substituting the FOC back into the Hamiltonian yields:

$$H = u(t)E(t)p^a(x(t))[1 - \frac{1}{\epsilon(u(t))}]. \tag{B.48}$$

Thus, under an autonomous system (with a constant Hamiltonian), a constant elasticity implies a constant $p^a(x(t))u(t)E(t)$ (constant revenue).

□

B.3.2 Multiple Prices

B.3.2.1 Capacity-Degradation-Only (N-Price Setting)

We first consider capacity-degradation-only. We generalize the arbitrage price to have N possible values: $P(t) \in \{p_1^a, \cdots, p_N^a\}$, where each price $p_i^a := \bar{p}_i x - \frac{p_i}{x}$ occurs with probability p_i for all $i \in [N] := \{1, \cdots, N\}$. Without loss of generality, we assume $p_1^a \leq \cdots \leq p_N^a$. Let u_i denote the DOD level associated with the price p_i^a. Then the optimization problem for capacity-degradation-only over the T time period becomes:

$$\begin{aligned} \max_{0 \leq u_i(t) \leq 1} \int_0^T e^{-\delta t} E(t) \sum_{i=1}^N p_i p_i^a u_i(t) dt \\ \text{s.t. } \dot{E}(t) = -E(t) \sum_{i=1}^N p_i \Phi(u_i(t)) \\ \Phi(u_i(t)) = k u_i(t)^2 \text{ for all } i \in [N]. \end{aligned}$$

Then the expected arbitrage quantity (or throughput) at time t is then

$$A(t) = E(t) \sum_{i=1}^N p_i u_i(t).$$

The Hamiltonian is a function of the capacity E, the control $\mathbf{u}(t) = (u_1(t), \cdots, u_N(t))$, the shadow price $p(t)$, and time t with the functional form

$$\begin{aligned} H(E(t), \mathbf{u}(t), p(t), t) &= r(E(t), \mathbf{u}(t), t) + p(t)\dot{E}(t) \\ &= e^{-\delta t} E(t) [\sum_{i=i}^N p_i p_i^a u_i(t)] + p(t)[-kE(t)(\sum_{i=1}^N p_i u_i^2(t))], \end{aligned} \tag{B.49}$$

where $r(E(t), \mathbf{u}(t), t) = e^{-\delta t} E(t) [\sum_{i=i}^N p_i p_i^a u_i(t)]$ is the immediate revenue function at time t and $\dot{E}(t) = -kE(t)(\sum_{i=1}^N p_i u_i^2(t))$ is the capacity degradation dynamics. According to the Pontryagin maximum principle, an optimal control trajectory $\{\mathbf{u}^*(t) | t \in [0, T]\}$ satisfies the

following necessary conditions:

$$
\begin{aligned}
[M] &: H(E^*(t), \mathbf{u}^*(t), p(t), t) = \max_{0 \le u_i(t) \le 1, i \in [N]} H(E^*(t), \mathbf{u}(t), p(t), t), \\
[ODE] &: \dot{E}^*(t) = \nabla_{p(t)} H(E^*(t), \mathbf{u}^*(t), p(t), t) = -kE(t)(\sum_{i=1}^{N} p_i u_i^2(t)), \\
[ADJ] &: \dot{p}(t) = -\nabla_{E(t)} H(E^*(t), \mathbf{u}^*(t), p(t), t) \\
&\quad = -e^{-\delta t}[\sum_{i=1}^{N} p_i p_i^a u_i^*(t)] + kp(t)[\sum_{i=1}^{N} p_i (u_i^*(t))^2], \\
[T] &: p(T) = 0.
\end{aligned}
\tag{B.50}
$$

From $[M]$, we have

$$
u_i^*(t) = \min(\frac{e^{-\delta t} p_i^a}{2kp(t)}, 1), \ \forall i \in [N]. \tag{B.51}
$$

Case 1. If $p(t) \le \frac{e^{-\delta t} p_1^a}{2k}$, then

$$
\begin{aligned}
u_i^*(t) &= 1, \ \forall i \in [N] \text{ and} \\
\dot{p}(t) &= \sum_{i=1}^{N} [-e^{-\delta t} p_i^a + kp(t)] p_i.
\end{aligned}
$$

We then have

$$
\begin{aligned}
p(t) &= \frac{e^{-\delta t} \sum_{i=1}^{N} p_i p_i^a}{k + \delta} - C_3 e^{kt} \text{ and} \\
E(t) &= A(t) = C_4 e^{-kt},
\end{aligned}
$$

for some constants C_3 and $C_4 > 0$.

Case n ($\forall n \in [2, \cdots, N]$). If $\frac{e^{-\delta t} p_{n-1}^a}{2k} \le p(t) \le \frac{e^{-\delta t} p_n^a}{2k}$, then

$$
\begin{aligned}
u_i^*(t) &= \begin{cases} 1, & \text{if } i \in [n, n+1, \cdots, N], \\ \frac{e^{-\delta t} p_i^a}{2kp(t)}, & \text{if } i \in [1, 2, \cdots, n-1], \end{cases} \quad \text{and} \\
\dot{p}(t) &= \sum_{i=n}^{N} [-e^{-\delta t} p_i^a + kp(t)] p_i - \sum_{i=1}^{n-1} \frac{e^{-2\delta t} p_i (p_i^a)^2}{4kp(t)}.
\end{aligned}
$$

Case $N+1$. If $p(t) \geq \frac{e^{-\delta t} p_N^a}{2k}$,

$$p(t)\dot{p}(t) = -\sum_{i=1}^{N} p_i \frac{(p_i^a)^2 e^{-2\delta t}}{4k},$$

which is a first-order nonlinear ODE, yielding

$$p(t) = \sqrt{\frac{e^{-2\delta t}\sum_{i=1}^{N} p_i (p_i^a)^2}{4k\delta} - C_1} \text{ and}$$
$$u_i^*(t) = \frac{e^{-\delta t} p_i^a}{2k\sqrt{\frac{e^{-2\delta t}\sum_{i=1}^{N} p_i (p_i^a)^2}{4k\delta} - C_1}}, \text{ for all } i \in [N],$$

for some constant C_1. Then we have

$$\frac{\dot{E}(t)}{E(t)} = -\frac{1}{-\frac{4kC_1}{e^{-2\delta t}\sum_{i=1}^{N} p_i (p_i^a)^2} + 1/\delta},$$

meaning

$$E(t) = C_2 \sqrt{\frac{e^{-2\delta t}}{4k\delta}\sum_{i=1}^{N} p_i (p_i^a)^2 - C_1},$$

for some constant $C_2 > 0$.

We now establish some structural properties. We first consider a finite horizon ($T < \infty$).

Theorem B.8. *Under the N-price setting with capacity-degradation-only, the following properties hold:*

- *The current-value shadow price $p(t)e^{\delta t}$ decreases in t,*
- *The optimal DOD $u_i^*(t)$ increases in t for all $i \in [N]$, and*
- *$u_i^*(t) \leq u_j^*(t)$ for all $i, j \in [N]$ such that $i < j$.*

Proof. For all $i, j \in [N]$ such that $i < j$, $u_i^*(t) \leq u_j^*(t)$ is immediate from (B.51).

We now proceed to show that $p(t)e^{\delta t}$ decreases in t, which is equivalent to show that $u_i^*(t)$ increases in t for all $i \in [N]$. For a finite T, $p(T) = 0$ implies that we are always in the $u_i^*(t) = 1,\ \forall i \in [N]$ region (Case 1) when t is sufficiently close to T. Also, the constant C_3

becomes:

$$C_3 = \frac{\sum_{i=1}^N p_i p_i^a}{(k+\delta)e^{T(k+\delta)}} > 0$$
$$p(t)e^{\delta t} = \frac{\sum_{i=1}^N p_i p_i^a}{k+\delta}(1 - e^{-(k+\delta)(T-t)}).$$

Thus, $p(t)e^{\delta t}$ is strictly monotone decreasing in this region. Going backward in time, the transition happens at time

$$t_A = T - \frac{\log(\frac{2k\sum_{i=1}^N p_i p_i^a}{2k\sum_{i=1}^N p_i p_i^a - p_1^a(k+\delta)})}{k+\delta},$$

if $\frac{2k}{k+\delta} > \frac{p_1^a}{\sum_{i=1}^N p_i p_i^a}$ and $T > \frac{1}{k+\delta}\log[\frac{2k\sum_{i=1}^N p_i p_i^a}{2k\sum_{i=1}^N p_i p_i^a - (k+\delta)p_1^a}]$. Otherwise (i.e., $\frac{2k}{k+\delta} \le \frac{p_1^a}{\sum_{i=1}^N p_i p_i^a}$ or $\frac{2k}{k+\delta} > \frac{p_1^a}{\sum_{i=1}^N p_i p_i^a}$ and $T \le \frac{1}{k+\delta}\log[\frac{2k\sum_{i=1}^N p_i p_i^a}{2k\sum_{i=1}^N p_i p_i^a - (k+\delta)p_1^a}]$), we always in the $u_i^*(t) = 1,\ \forall i \in [N]$ case.

For Case n ($\forall n \in [2, \cdots, N]$), we have

$$\begin{aligned}
\mathrm{sgn}([p(t)e^{\delta t}]') &= \dot{p}(t)e^{-\delta t} + p(t)e^{-\delta t}\delta \\
&= -\sum_{i=1}^{n-1}\frac{e^{-\delta t}p_i(p_i^a)^2}{4kp(t)} + \sum_{i=n}^{n}[-e^{-2\delta t}p_i^a + kp(t)e^{-\delta t}]p_i + p(t)e^{-\delta t}\delta \\
&= g(p(t)) - \sum_{i=n}^{N} e^{-2\delta t}p_i^a p_i,
\end{aligned}$$

where $g(p) = -\frac{D_1}{p} + D_2 p$, $D_1 = \sum_{i=1}^{n-1}\frac{e^{-\delta t}p_i(p_i^a)^2}{4k} > 0$, and $D_2 = e^{-\delta t}[\sum_{i=n}^N kp_i + \delta] > 0$.

Then $g(p)$ is increasing in p since $g'(p) = \frac{D_1}{p^2} + D_2 > 0$. Thus, $g(p)$ is maximized at $p = \frac{e^{-\delta t}p_n^a}{2k}$, which leads to

$$\begin{aligned}
\mathrm{sgn}([p(t)e^{\delta t}]') &\le g(p = \frac{e^{-\delta t}p_n^a}{2k}) - \sum_{i=n}^{N} e^{-2\delta t}p_i p_i^a \\
&= \frac{e^{-2\delta t}}{2p_n^a}\underbrace{\left[-\sum_{i=1}^{n-1}p_i(p_i^a)^2 + (p_n^a)^2[\frac{\delta}{k} + \sum_{i=n}^{N}(p_i - \frac{2p_i^a p_i}{p_n^a})]\right]}_{:=D_3}.
\end{aligned}$$

We now show $D_3 \le 0$, which is equivalent to show $\frac{\delta}{k} \le -\sum_{i=n}^N p_i(1 - \frac{2p_i^a}{p_n^a}) + \sum_{i=1}^{n-1}p_i(\frac{p_i^a}{p_n^a})^2$. We use the fact that Case n happens only if $2k\sum_{i=1}^N p_i p_i^a > p_1^a(k+\delta)$, or equivalently,

$\frac{\delta}{k} < 2\sum_{i=1}^{N} \frac{p_i p_i^a}{p_1^a} - 1$. We are done if we can show

$$-\sum_{i=n}^{N} p_i(1 - \frac{2p_i^a}{p_n^a}) + \sum_{i=1}^{n-1} p_i(\frac{p_i^a}{p_n^a})^2 \leq 2\sum_{i=1}^{N} \frac{p_i p_i^a}{p_1^a} - 1,$$

or equivalently,

$$\sum_{i=1}^{n-1} p_i[\frac{(p_i^a)^2 p_1^a + (p_n^a)^2 p_1^a - 2p_i^a (p_n^a)^2}{(p_n^a)^2 p_1^a}] \leq \sum_{i=n}^{N} [2p_i p_i^a \frac{p_n^a - p_i^a}{p_1^a p_n^a}]. \tag{B.52}$$

We use mathematical induction. When $N = 2$, the inequality (B.52) can be restated as

$$p_1 < \underbrace{\frac{2(p_2^a)^2}{(p_2^a - p_1^a)(2p_2^a + p_1^a)}}_{>1},$$

which always holds. Now assume the inequality (B.52) holds for some $N \geq 2$. Then we have

$$\begin{aligned}\sum_{i=1}^{n-1} p_i[\frac{(p_i^a)^2 p_1^a + (p_n^a)^2 p_1^a - 2p_i^a (p_n^a)^2}{(p_n^a)^2 p_1^a}] &\leq \sum_{i=n}^{N+1} [2p_i p_i^a \frac{p_n^a - p_i^a}{p_1^a p_n^a}] \\ &= \sum_{i=n}^{N} [2p_i p_i^a \frac{p_n^a - p_i^a}{p_1^a p_n^a}] + 2(1 - p_1 - \cdots - p_N)\frac{p_{N+1}^a - p_1^a}{p_1^a}.\end{aligned}$$

Redefining $p_i := p_i/(1 - p_{N-1})$ yields $\sum_{i=1}^{N} p_i = 1$. Then it is straightforward to check that the inequality holds, which concludes $\text{sgn}([p(t)e^{\delta t}]') \leq 0$.

For Case $N + 1$, applying the same logic from the proof of Theorem 3.1 leads to $C_1 > 0$, which implies that $p(t)e^{\delta t}$ is strictly monotone decreasing in this region.

□

Theorem B.8 characterizes the optimal DOD policy both across different arbitrage prices at a fixed time and over time for a fixed price. First, at any given time t, the battery is used more intensively when the arbitrage price is higher. Second, as we approach the end of the horizon, battery usage intensifies, reflecting the monotonicity of the optimal DOD sequence $(u_1^*(t), \cdots, u_N^*(t))$ over time. Figure B.4(a) at the end of Section 3.5.2 shows the optimal system dynamics of the capacity-degradation-only model under multiple energy prices.

Next, consistent with Section 3.4.1, we consider two special cases: (1) $\delta = 0$ (no discounting) and (2) $T \to \infty$ (infinite horizon). When $\delta = 0$, the optimal arbitrage quantity $A^*(t)$ remains constant as long as capacity is not binding, which again confirms that the constant A (constant throughput) policy commonly used in practice and literature can be

near-optimal.

Corollary B.4 (**No discount**). *Under the N-price setting with $\delta \to 0$ and capacity-degradation-only, a constant throughput A policy is optimal as long as the battery capacity is not binding at the highest arbitrage price p_N^a.*

Under the infinite horizon, the current-value shadow price, $p(t)e^{\delta t}$, remains constant because the value-to-go function is proportional only to the capacity $E(t)$. As a result, the optimal DOD sequence remains constant over time.

Corollary B.5 (**Infinite horizon: N-price**). *In the N-price setting with the infinite horizon and capacity-degradation-only, the current-value shadow price $p(t)e^{\delta t}$ is constant for all t:*

$$
\begin{aligned}
&p(t)e^{\delta t} \\
&= \begin{cases}
\sqrt{\frac{\sum_{i=1}^{N} p_i (p_i^a)^2}{4\delta k}}, & \frac{(p_N^a)^2}{\sum_{i=1}^{N} p_i (p_i^a)^2} < k/\delta, \\
\tilde{p}_0 := \frac{\sum_{i=n}^{N} p_i p_i^a + \sqrt{(\sum_{i=n}^{N} p_i p_i^a)^2 + [\delta/k + \sum_{i=n}^{N} p_i] \cdot [\sum_{i=1}^{n-1} p_i (p_i^a)^2]}}{2[\delta + k \sum_{i=n}^{N} p_i]}, & \frac{p_1^a}{\sum_{i=1}^{N} p_i p_i^a} < \frac{2k}{k+\delta}, \frac{(p_N^a)^2}{\sum_{i=1}^{N} p_i (p_i^a)^2} \geq k/\delta, \\
\frac{\sum_{i=1}^{N} p_i p_i^a}{k+\delta}, & \frac{p_1^a}{\sum_{i=1}^{N} p_i p_i^a} \geq \frac{2k}{k+\delta},
\end{cases}
\end{aligned}
$$

for some index $n \in [2, \cdots, N]$. A fixed-DOD strategy $u^* = (u_1^*, \cdots, u_N^*)$ is optimal for all t:

$$
\begin{cases}
u_i^* = \frac{p_i^a}{\sqrt{\frac{k \sum_{i=1}^{N} p_i (p_i^a)^2}{\delta}}} < 1, \forall i \in [N], & \frac{(p_N^a)^2}{\sum_{i=1}^{N} p_i (p_i^a)^2} < k/\delta, \\
u_i^* = \frac{p_i^a}{2k\tilde{p}_0} < 1, \forall i < n \text{ and } u_i^* = 1, \forall i \geq n & \frac{p_1^a}{\sum_{i=1}^{N} p_i p_i^a} < \frac{2k}{k+\delta}, \frac{(p_N^a)^2}{\sum_{i=1}^{N} p_i (p_i^a)^2} \geq k/\delta, \text{ and} \\
u_i^* = 1, \forall i \in [N], & \frac{p_1^a}{\sum_{i=1}^{N} p_i p_i^a} \geq \frac{2k}{k+\delta}.
\end{cases}
$$

Proof. The optimal solution in which all DOD pairs are either unconstrained or constrained corresponds directly to Cases 1 and $N+1$, respectively. We now turn to the intermediate case where the DOD for the lowest-price pairs is unconstrained, while it is constrained for the highest-price pairs. Following the same logic as in the single-price setting, the current-value shadow price remains constant under an infinite horizon. From $\tilde{p}'(t) = 0$, we obtain:

$$\sum_{i=n}^{N} [-p_i^a + k\tilde{p}] p_i - \sum_{i=1}^{n-1} \frac{p_i (p_i^a)^2}{4k\tilde{p}} = -\delta\tilde{p},$$

which can be rewritten as a quadratic equation in $\tilde{p}$:

$$4k[\delta + k \sum_{i=n}^{N} p_i](\tilde{p})^2 - 4k \sum_{i=n}^{N} p_i p_i^a \tilde{p} - \sum_{i=1}^{n-1} p_i (p_i^a)^2 = 0.$$

□

This implies that the battery allocates more utilization to higher and more frequent arbitrage prices: increasing p_i^a while holding other p_j^a values fixed tends to increase u_i^* and lower u_j^* for all $j \neq i$ (i.e., $\frac{\partial u_i^*}{\partial p_i^a} > 0$ and $\frac{\partial u_j^*}{\partial p_i^a} < 0$ for all $j \neq i$). Additionally, increasing p_i (while proportionally normalizing the other p_j values to maintain their sum at one) tends to increase u_i^* and decrease u_j^* for all $j \neq i$.

Next, we examine the unconstrained case where the battery's energy capacity is not binding for any p_i^a (i.e., $u_N^*(t) < 1$). In this case, the dynamics coincide with those of the base model. Specifically, there exists p^a such that $\sum_{i=1}^N p_i (p_i^a)^2 = (p^a)^2$, and the corresponding degradation dynamics and revenue rate are exactly the same. This implies, for instance, the 90.25% optimality of the fixed-DOD heuristic continues to hold.

In summary, the key structural properties in the base capacity-degradation-only model (with a single arbitrage price) continue to hold when the arbitrage price can take N values.

B.3.2.2 Unified Model (N-Price Setting)

We now consider a unified degradation model, where capacity and efficiency degradation are linearly correlated: $x(t) = \alpha_0 + \alpha_1 E(t)$, with $\alpha_0 + \alpha_1 \leq 1$. For simplicity, we assume a constant low energy price $\underline{p}$, and N possible high energy prices, such that $\bar{P}(t) \in \{\bar{p}_1, \bar{p}_2, \cdots, \bar{p}_N\}$, where each high price $\bar{p}_i$ occurs with probability p_i. Without loss of generality, we assume $\bar{p}_1 \leq \bar{p}_2 \leq \cdots \leq \bar{p}_N$.[3] Under this setup, let $(u_1(t), \cdots, u_N(t))$ denote the DOD allocation at time t associated with the high price vector $(\bar{p}_1, \cdots, \bar{p}_N)$. Then the optimization problem for the unified model is given by:

$$\max_{0 \leq u_i(t) \leq 1} \int_0^T e^{-\delta t} \left[\sum_{i=1}^N p_i \cdot p_i^a(x(t)) u_i(t) \right] E(t) dt$$

$$\text{s.t. } \dot{E}(t) = -E(t)[\sum_{i=1}^N p_i \Phi(u_i(t))]$$

$$x(t) = \alpha_0 + \alpha_1 E(t)$$

$$\Phi(u_i(t)) = k u_i(t)^2 \text{ for all } i \in [N].$$

[3]The result trivially holds for $\{(\bar{p}_1, \underline{p}_1), \cdots, (\bar{p}_N, \underline{p}_N)\}$ (with p_i being the probability of $(\bar{p}_i, \underline{p}_i)$ to be the energy price pair) as long as $\bar{p}_i x - \frac{\underline{p}_i}{x} \leq \bar{p}_j x - \frac{\underline{p}_j}{x}$ holds for any $i < j$ and $x \in (0, 1]$.

We first state the Hamiltonian. Let $\mathbf{u}(t) := (u_1(t), \cdots, u_N(t))$. Then we have

$$\begin{aligned} H(E(t), \mathbf{u}(t), p(t), t) &= r(E(t), \mathbf{u}(t), t) + p(t)\dot{E}(t) \\ &= \sum_{i=1}^{N} p_i[e^{-\delta t} p_i^a(x(t)) u_i(t) E(t) + p(t)(-kE(t)u_i^2(t))], \end{aligned}$$

where $r(E(t), \mathbf{u}(t), t) = e^{-\delta t}[\sum_{i=1}^{N} p_i p_i^a(x(t)) u_i(t)]E(t)$ is the immediate revenue rate at time t and $\dot{E}(t) = -kE(t)(\sum_{i=1}^{N} p_i u_i^2(t))$ is the system dynamics. According to Pontryagin maximum principle, an optimal control trajectory $\{(u_1^*(t), \cdots, u_N^*(t)) | t \in [0, T]\}$ satisfies the following necessary conditions:

$$\begin{aligned} &[M] : H(E^*(t), \mathbf{u}^*(t), p, t) = \max_{0 \le u_i \le 1, i \in [N]} H(E^*(t), \mathbf{u}(t), p(t), t), \\ &[ODE] : \dot{E}(t) = \nabla_{p(t)} H(E^*(t), \mathbf{u}^*(t), p(t), t) = -kE^*(t)(\sum_{i=1}^{N} p_i (u_i^*(t))^2), \\ &[ADJ] : \dot{p}(t) = -\nabla_{E(t)} H(E^*(t), \mathbf{u}^*(t), p(t), t) = -e^{-\delta t}[\sum_{i=1}^{N} p_i p_i^a(x(t)) u_i(t)] \\ &\qquad - e^{-\delta t}\alpha_1 E(t)[\sum_{i=1}^{N} p_i(\bar{p}_i + \frac{p}{x^2(t)})u_i(t)] + p(t)k(\sum_{i=1}^{N} p_i u_i^2(t)), \\ &[T] : p(T) = 0. \end{aligned} \tag{B.53}$$

From $[M]$, maximizing Hamiltonian leads to:

$$u_i^*(t) = \min(\frac{e^{-\delta t} p_i^a(x(t))}{2p(t)k}, 1), \ \forall i \in [N]. \tag{B.54}$$

The overall structure of the optimal policy remains unchanged from the single-price unified model (Section 3.4.2). For instance, without time discounting, the optimal DOD $u_i^*(t)$ monotonically increases over time for all $i \in [N]$, and the expected arbitrage revenue rate remains constant over time as long as capacity is not binding for all price pairs (i.e., $u_N^*(t) < 1$).

Theorem B.9 (**No discount: N-price**). *When $\delta = 0$ and under the unified model with the N-price setting, $u_i^*(t)$ is monotone increasing in t for all $i \in [N]$. Also, when $u_N^*(t) < 1$, the expected arbitrage revenue rate $r(t) := \sum_{i=1}^{N} p_i p_i^a(x(t)) u_i^*(t) E(t)$, remains constant.*[4]

[4]For alternative degradation function $\Phi(u)$, see Theorem B.7; in particular, $r(t)$ increases (decreases) over time when $\Phi(u)$ is decreasing (increasing) in u.

Proof. To show that $\dot{r}(t) = 0$ for $u_N^*(t) < 1$, we plug (B.54) into $r(t)$:

$$\begin{aligned}
r(t) &= \frac{(x(t) - \alpha_0)P}{2p(t)k\alpha_1}, \\
\dot{r}(t) &= \frac{p(t)\dot{x}(t)[P + (x(t) - \alpha_0)Q] - \dot{p}(t)(x(t) - \alpha_0)P}{2\alpha_1 k p^2(t)}, \text{ for} \\
P &= \sum_{i=1}^{N} p_i [p_i^a(x(t))]^2 \text{ and} \\
Q &= 2\sum_{i=1}^{N} p_i p_i^a(x(t))(\bar{p}_i + \underline{p}/x^2(t)).
\end{aligned}$$

From (B.53) and $\dot{x}(t) = \alpha_1 \cdot \dot{E}(t)$, it is easy to algebraically check that

$$\begin{aligned}
\dot{x}(t) &= -\frac{(x(t) - \alpha_0)}{4p^2(t)k} P \text{ and} \\
\dot{p}(t) &= -\frac{1}{4p(t)k}[A + (x(t) - \alpha_0)Q].
\end{aligned}$$

This implies that the numerator equals zero, concluding the proof.

□

For the general discounted setting, we consider the unconstrained case in which the battery capacity is sufficient for the most prolific price pair (i.e., $u_N^*(t) < 1$), so that the optimal DOD for each price pair is determined by the first-order condition.

Theorem B.10 (**Unconstrained: N-price**). *When $u_N^*(t) < 1$, the optimal battery control under the unified model with the N-price setting is described as follows:*

- *The expected discounted revenue rate $r(t) := \sum_{i=1}^{N} e^{-\delta t} p_i p_i^a(x(t)) u_i^*(t) E(t)$ satisfies:*

$$r(t) = r(0)e^{-2\delta t}.$$

- *The optimal DOD $u^*(t)$ satisfies:*

$$\begin{aligned}
\frac{[u_i^*(t)]'}{u_i^*(t)} = -\delta + \sum_{j \neq i}^{N} k p_j u_j^2 \left[1 + \frac{2(x - \alpha_0)(\bar{p}_j + \underline{p}/x^2)}{p_j^a} - \frac{(x - \alpha_0)(\bar{p}_i + \underline{p}/x^2)}{p_i^a}\right] \\
+ k p_i u_i^2 \left[1 + \frac{(x - \alpha_0)(\bar{p}_i + \underline{p}/x^2)}{p_i^a}\right]. \qquad \text{(B.55)}
\end{aligned}$$

Proof. For the unconstrained solution (i.e., $u_N^*(t) = \frac{p_N^a(t)}{2k\tilde{p}(t)} < 1$), we have:

$$E'(t) = -f(t) = -E(t) \cdot \sum_{j=1}^{N} kp_j(u_j^*(t))^2 \text{ for}$$
$$p_i^a(t) = 2k\tilde{p}(t)u_i^*(t), \ \forall i \in [N].$$

Then we have:

$$2\tilde{p}(t)f(t) = E(t) \cdot \sum_{j=1}^{N} p_j p_j^a(t) u_j^*(t),$$
$$\tilde{H}(t) = \sum_{i=1}^{N} p_i^a(t) u_i^*(t) E(t)(1 - 1/2),$$

yielding

$$r(t) = r(0)e^{-2\delta t}.$$

For the optimal DOD, note that:

$$x'(t) = -(x(t) - \alpha_0) \times \sum_{i=1}^{N} p_i \frac{(p_i^a)^2}{4k\tilde{p}^2(t)},$$
$$p'(t) = \sum_{i=1}^{N} \frac{p_i e^{-2\delta t}(p_i^a)}{4kp(t)} \left[p_i^a - 2[2\bar{p}_i x - \alpha_0(\bar{p}_i + \frac{\underline{p}}{x^2})] \right],$$

yielding:

$$\begin{aligned}
\tilde{p}'(t) &= \frac{p'(t)}{e^{-\delta t}} + \delta\tilde{p}(t) \\
&= \delta\tilde{p}(t) + \sum_{i=1}^{N} \frac{p_i p_i^a}{4k\tilde{p}(t)} \left[p_i^a - 2[2\bar{p}_i x - \alpha_0(\bar{p}_i + \frac{\underline{p}}{x^2})] \right], \\
\frac{\tilde{p}'(t)}{\tilde{p}(t)} &= \delta + \sum_{i=1}^{N} \frac{p_i p_i^a}{4k\tilde{p}^2(t)} \left[p_i^a - 2[2\bar{p}_i x - \alpha_0(\bar{p}_i + \frac{\underline{p}}{x^2})] \right] \\
&= \delta + \sum_{i=1}^{N} \frac{p_i (p_i^a)^2}{4k\tilde{p}^2(t)} \left[1 - \frac{2[2\bar{p}_i x - \alpha_0(\bar{p}_i + \frac{\underline{p}}{x^2})]}{p_i^a} \right] \\
&= \delta + \sum_{i=1}^{N} p_i k [u_i^*(t)]^2 \cdot \left[1 - \frac{2[2\bar{p}_i x - \alpha_0(\bar{p}_i + \frac{\underline{p}}{x^2})]}{p_i^a} \right].
\end{aligned}$$

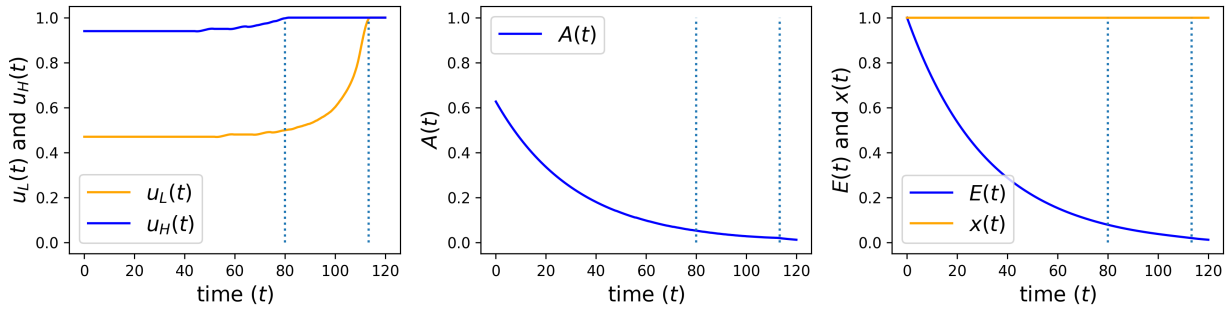
Let $\mathbf{u}_{-i}(t) = \{u_j(t)|j \neq i\}$ denote the optimal DOD levels of all price pairs other than i. Putting it all together, we have:

$$\frac{[u_i^*(t)]'}{u_i^*(t)} = z(x(t), u_i^*(t), \mathbf{u}_{-i}^*(t)), \text{ for}$$

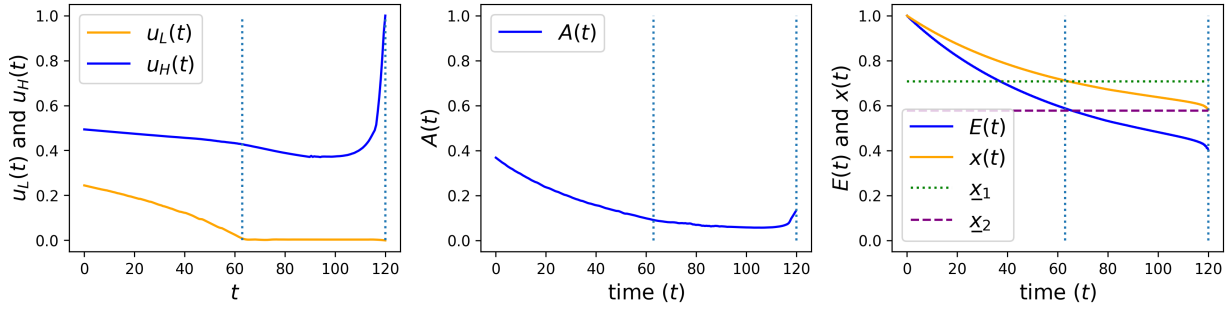
$$\begin{aligned} z(x, u_i, \mathbf{u}_{-i}) &= \frac{1}{p_i^a(x)} \cdot \Big[-(x-\alpha_0)(\bar{p}_i + \frac{\underline{p}}{x^2}) \sum_{j=1}^{N} k p_j u_j^2 - \delta p_i^a(x) \Big] \\ &\quad - \sum_{j=1}^{N} k p_j u_j^2 \big[1 - \frac{2[2\bar{p}_j x - \alpha_0(\bar{p}_j + \frac{\underline{p}}{x^2})]}{p_j^a}\big] \\ &= -\delta + \sum_{j=1}^{N} p_j k u_j^2 \Big[1 + \underbrace{\frac{2(x-\alpha_0)(\bar{p}_j + \underline{p}/x^2)}{p_j^a} - \frac{(x-\alpha_0)(\bar{p}_i + \underline{p}/x^2)}{p_i^a}}_{=h(x)\geq 0 \text{ for any } p_i^a \leq p_j^a} \Big]. \end{aligned}$$

□

Theorem B.10 confirms that the functional form of the discounted revenue rate remains the same as in the single-price case, where it decays exponentially in terms of the discount factor δ. It also shows that the structure of the optimal DOD under the N-price setting remains similar: a battery subject to both capacity and efficiency degradation may exhibit non-monotonic patterns due to the trade-off between time discounting and degradation effects. Also, when time discounting is negligible ($\delta \to 0$), the optimal DOD $u_i^*(t)$ is monotone increasing for all $i \in [N]$. However, relative to the single-price model, $\frac{[u_i^*(t)]'}{u_i^*(t)}$ becomes more nuanced, as it now depends on the utilization of other price pairs $u_j^*(t)$, as shown in (B.55). For example, with multiple prices, even under a finite horizon T, $u_i^*(t)$ may be monotone decreasing for some $i \in [N]$—a behavior that arises only in the infinite-horizon single-price setting (see Theorems 3.4 and 3.6)—as illustrated by $u_L^*(t)$ in Figure B.4(b).



(a) Capacity-degradation-only



(b) Unified degradation

Figure B.4: Optimal system dynamics under multiple prices (Theorems B.8 and B.10): (a) capacity degradation only ($\alpha_0 = 1, \alpha_1 = 0$), and (b) unified degradation ($\alpha_0 = 0.3, \alpha_1 = 0.7$). Other parameters: $\bar{p}_1 = 80, \bar{p}_2 = 120, \underline{p} = 40, p_1 = p_2 = 1/2, \delta = 0.03, k = 0.07, T = 120$.

B.4 Additional Numerical Results

B.4.1 Capacity-Degradation-Only: Hueristics

Fixed-A policy. We next consider the fixed-A policy, in which we provide a constant throughput by selling a fixed amount of energy denoted by A. Many white papers and research articles adopt this fixed throughput policy, assuming representative grid environments when evaluating the value of BESS.

Theorem 3.1 states that a fixed-A policy can be near-optimal under the undiscounted model. In this subsection, we evaluate the performance of the constant throughput policy under a discounted setting. Given some constant energy quantity A, let t_A denote the smallest time $t \in [0, T]$ such that $E(t) = A$ ($t_A := \infty$ if $E(T) > A$). For $t < t_A$, $u(t) = \frac{A}{E(t)} < 1$. Also, the system dynamic of (B.5) implies

$$E(t) = \sqrt{1 - 2ktA^2}. \tag{B.56}$$

For $t_A < t \leq T$, providing A amount of service becomes infeasible due to the limited energy capacity. Thus, we have $u(t) = 1$ and the system dynamic of (B.5) implies

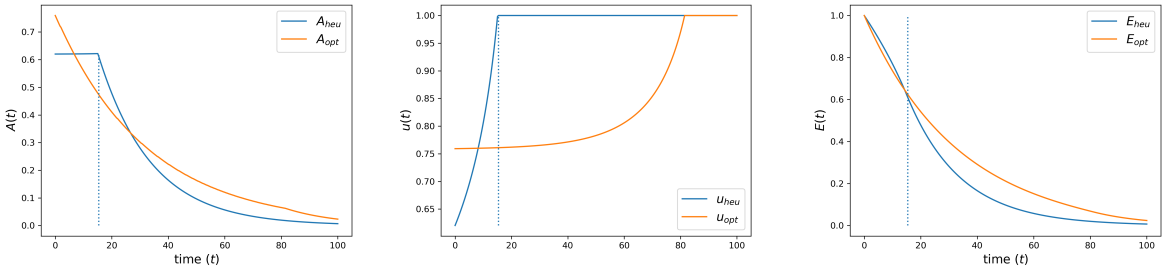
$$E(t) = Ae^{-k(t-t_A)}, \tag{B.57}$$

for

$$t_A = \begin{cases} \frac{1-A^2}{2kA^2}, & \text{if } \frac{1}{\sqrt{1+2kT}} \leq A, \text{ and} \\ \infty, & \text{otherwise.} \end{cases}$$

Plugging (B.56) – (B.57) into the objective function of (B.5), the best service level A can be selected as the constant maximizing the revenue over the full horizon. Note that if $\frac{1}{\sqrt{1+2kT}} > A$, then

$$\max_{0 \leq A \leq \frac{1}{\sqrt{1+2kT}}} \int_0^T e^{-\delta t} p^a A dt = \max_{0 \leq A \leq \frac{1}{\sqrt{1+2kT}}} \frac{p^a A}{\delta}(1 - e^{-\delta T}),$$



(a) $A(t)$ (b) $u(t)$ (c) $E(t)$

Figure B.5: Illustration of the optimal dynamic policy versus the optimal fixed-A heuristic. $T = 100, \delta = 0.03, \alpha_1 = 0.3, \underline{p} = 40, \bar{p} = 100$.

which implies that the optimal service quantity always satisfies $A \geq \frac{1}{\sqrt{1+2kT}}$. Thus, we have

$$\begin{aligned} R^A_{cum} &:= \max_{\frac{1}{\sqrt{1+2kT}} \leq A \leq 1} \left[\int_0^{t_A} e^{-\delta t} p^a A dt + \int_{t_A}^{T} e^{-\delta t} p^a A e^{-k(t-t_A)} dt \right] \\ &= \max_{\frac{1}{\sqrt{1+2kT}} \leq A \leq 1} \underbrace{p^a A \left[\frac{1}{\delta}(1 - e^{-\delta \frac{1-A^2}{2kA^2}}) - \frac{e^{\frac{1-A^2}{2A^2}}}{k+\delta}(e^{-(k+\delta)T} - e^{-(k+\delta)\frac{1-A^2}{2kA^2}}) \right]}_{:=\bar{r}(A)}. \end{aligned}$$

Let $\bar{A} := \arg\max_{0 \leq A \leq 1} \bar{r}(A)$. We can numerically study the performance of the heuristic compared to the optimal policy. Let $S(\delta) := \frac{R^A_{cum}}{R^*_{cum}}$ be the ratio between the cumulative discounted revenues from the fixed-A heuristic at optimal level $\bar{A}$ and optimal dynamic policy, respectively, under some discount factor $\delta > 0$.

Figure B.5 numerically illustrates key differences between the optimal dynamic policy and the optimal fixed-A heuristic under a discounted setting ($\delta = 0.03$). The optimal dynamic policy initially achieves higher arbitrage rates than the optimal fixed-A heuristic (i.e., $A^*(t) > \bar{A}$ for $0 \leq t < 6.3$), generating more revenue upfront. However, over time, the optimal dynamic policy gradually decreases the arbitrage quantity, providing less service and generating less revenue than the heuristic (i.e., $A^*(t) < \bar{A}$ for $6.3 < t < 26.4$) in the middle range. This allows $u^*(t)$ to grow at a slower pace and prevents significant battery capacity degradation. In contrast, the fixed-A policy, by maintaining $\bar{A}$, leads to a rapid increase in DOD (up to full DOD) and incurs significant capacity degradation. As a result, with less capacity degradation, the optimal dynamic policy generates more revenue in the later periods (for $26.4 < t \leq 100$).

APPENDIX C

Proofs in Chapter 4

C.1 Proof of Statements (Main)

Proof of Theorem 4.1

We first consider a linear case ($\beta = 1$). With $x(t) = \alpha_0 + \lambda E(t)$, solving the ODE yields:

$$\begin{aligned} E(t) &= (C + \frac{\alpha_0}{\lambda})e^{-k\lambda S(t)} - \frac{\alpha_0}{\lambda}, \\ x(t) &= (C\lambda + \alpha_0)e^{-k\lambda S(t)}, \\ x(T) &= (C\lambda + \alpha_0)e^{-k\lambda W}, \end{aligned}$$

where $S(t) := \int_0^t R(s)ds$. Then we have:

$$r^{energy}(C) = c^e \int_0^T R(t)x^2(t)dt.$$

Via variable substitution $F = S(t)$, we have:

$$\begin{aligned} r^{energy}(C) &= c^e(C\lambda + \alpha_0)^2 \int_0^W e^{-2k\lambda F}dF \\ &= c^e(C\lambda + \alpha_0)^2 \cdot \frac{1 - e^{-2k\lambda W}}{2k\lambda}, \end{aligned}$$

meaning that any $R(t)$ that performs W total work has an identical revenue $r^{energy}(C)$ under linear degradation.

Next, we consider the case of $\beta > 1$. The Hamiltonian is

$$H(R, E, p, q) = c^e R(\alpha_0 + \lambda E)^2 - pE \cdot \Phi\left(\frac{R(\alpha_0 + \lambda E)}{E}\right) - qR,$$

where $p, q \geq 0$ are the shadow prices of energy capacity and total work completed, respectively. Note that q is constant across the horizon—work completed at any time t counts the same amount against the total workload limit W. The FOC with respect to the control R yields

$$\frac{\partial H}{\partial R} = c^e(\alpha_0 + \lambda E)^2 - p(\alpha_0 + \lambda E)\Phi'\left(\frac{R(\alpha_0 + \lambda E)}{E}\right) - q = 0.$$

Whenever the service rate is set by the FOC,

$$q(t) = c^e(\alpha_0 + \lambda E(t))^2 - p(t)(\alpha_0 + \lambda E(t))\Phi'\left(\frac{R(\alpha_0 + \lambda E(t))}{E(t)}\right).$$

Define the elasticity of the degradation function as:

$$\epsilon(u) := \frac{\Phi'(u)/\Phi(u)}{1/u} \Leftrightarrow \Phi'(u) = \frac{\epsilon(u)}{u}\Phi(u).$$

Then we have $\epsilon(u) = \beta$ for $\Phi(u) = ku^\beta$.

Plugging expressions for $q(t)$ and $\Phi'(u)$ into the Hamiltonian yields

$$H^*(t) = (\beta - 1) \cdot p(t)E(t) \cdot \Phi\left(\frac{R(t)(\alpha_0 + \lambda E(t))}{E(t)}\right).$$

Because the system is autonomous (no explicit t-dependence in the Hamiltonian), $H^*(t)$ is constant over time along the optimal trajectory. This enables us to reason about the trajectory of $R(t)$ through time using the original expression for the Hamiltonian:

$$\underbrace{H^*(t)}_{\text{constant}} = \underbrace{c^e((\alpha_0 + \lambda E(t))^2 - q(t))}_{\text{decreasing}} \cdot R(t) - \underbrace{p(t)E(t)\Phi(\frac{R(\alpha_0 + \lambda E(t))}{E(t)})}_{\text{constant}},$$

meaning $R(t)$ must be an increasing function.

□

Proof of Lemma 4.1

Assume $R^*_{1,L} < \min\{d_L, R^*_{1,H}\}$. We can slightly increase $R^*_{1,L}$ and decrease $R^*_{1,H}$ while keeping the total workload for each battery unchanged. The revenues for both batteries and the cost for the linear battery remain unchanged, whereas the cost for the convex battery decreases, yielding a contradiction. Now assume $R^*_{1,L} > R^*_{1,H}$. An analogous argument leads to a contradiction by slightly decreasing $R^*_{1,L}$ and increasing $R^*_{1,H}$. □

Proof of Theorem 4.2

Fix $R_{1,L}$ and $R_{1,H}$, meaning $R_{2,L} = d_L - R_{1,L}$ and $R_{2,H} = d_H - R_{1,H}$. We consider $\beta_2 > 1$ and take the limit $\beta_2 \to 1$. Then the objective Π becomes:

$$\begin{aligned}\Pi &= r_1^{energy}(n_L R_{1,L} + n_H R_{1,H}) + r_2^{energy}(n_L(d_L - R_{1,L}) + n_H(d_H - R_{1,H})) \\ &\quad - c_1^b C_1 - c_2^b C_2 - c_1^{deg} C_1^{1-\beta_1} W_1(R_{1,L}, R_{1,H}) - c_2^{deg} C_2^{1-\beta_2} W_2(R_{1,L}, R_{1,H}), \quad \text{for} \\ W_1(R_{1,L}, R_{1,H}) &:= n_L R_{1,L}^{\beta_1} + n_H R_{1,H}^{\beta_1}, \\ W_2(R_{1,L}, R_{1,H}) &:= n_L(d_L - R_{1,L})^{\beta_2} + n_H(d_H - R_{1,H})^{\beta_2}.\end{aligned}$$

Next, we endogenize C_1 and C_2 for β_1, β_2. For each battery type i (dropping the arguments on W_i for notational simplicity), we have

$$\frac{\partial \Pi}{\partial C_i} = -c_i^b + (\underbrace{\beta_i - 1}_{>0}) c_i^{deg} W_i C_i^{-\beta_i},$$

so $C_i^* = (\frac{(\beta_i - 1) c_i^{deg} W_i}{c_i^b})^{1/\beta_i}$, $i = 1, 2$. Also, we have:

$$c_i^{deg}(C_i^*)^{1-\beta_i} W_i = \frac{c_i^b C_i^*}{\beta_i - 1} \quad \text{and} \quad c_i^b C_i^* + c_i^{deg}(C_i^*)^{1-\beta_i} W_i = \frac{\beta_i}{\beta_i - 1} c_i^b C_i^*.$$

We now take the limit $\beta_2 \to 1$. Note that $\beta_2 \to 1$ implies $C_2^* \to 0$, $W_2 \to \bar{W}_2 := n_L(d_L - R_{1,L}) + n_H(d_H - R_{1,H})$, and $\lim_{\beta_2 \to 1} \frac{\beta_2}{\beta_2 - 1} c_2^b C_2^* = c_2^{deg} \bar{W}_2$.

Plugging $C_2^* = 0$ and C_1^* into the profit function yields

$$\begin{aligned}\Pi(R_{1,L}, R_{1,H}) &= \Gamma + B(n_L R_{1,L} + n_H R_{1,H}) - A(n_L R_{1,L}^{\beta_1} + n_H R_{1,H}^{\beta_1})^{1/\beta_1}, \text{ for} \\ \Gamma &:= (r_2^{energy} - c_2^{deg})(n_L d_L + n_H d_H), \\ A &:= \beta_1 (\frac{c_1^b}{\beta_1 - 1})^{\frac{\beta_1 - 1}{\beta_1}} (c_1^{deg})^{1/\beta_1}, \text{ and} \\ B &:= r_1^{energy} - r_2^{energy} + c_2^{deg}.\end{aligned}$$

If all work is assigned to battery type i, the profit of each homogeneous battery becomes:

$$\begin{aligned}\Pi_{\text{homo1}} &= r_1^{energy}(n_L d_L + n_H d_H) - A(n_L d_L^{\beta_1} + n_H d_H^{\beta_1})^{1/\beta_1} \text{ and} \\ \Pi_{\text{homo2}} &= \Gamma = (r_2^{energy} - c_2^{deg})(n_L d_L + n_H d_H).\end{aligned}$$

We focus on $\Pi_{\text{homo1}} = \Pi_{\text{homo2}}$ and $\text{AllCost}_{\text{homo1}} = \text{AllCost}_{\text{homo2}}$ (i.e., homogeneous batter-

ies yield the same profit and cost measures):

$$B = r_1^{energy} - r_2^{energy} + c_2^{deg} = A \cdot \frac{(n_L d_L^{\beta_1} + n_H d_H^{\beta_1})^{1/\beta_1}}{n_L d_L + n_H d_H}. \tag{C.1}$$

We first show $R_{1,L}^* = d_L < R_{1,H}^* < d_H$ and then derive the optimal $R_{1,H}^*$.

Step 1. Show $R_{1,L}^* = d_L$. Assume, for a contradiction, that $R_{1,L}^* < d_L$, meaning $R_{1,L}^* = R_{1,H}^*$ via Lemma 4.1. Then the objective becomes

$$\begin{aligned}\Pi(R_{1,H}) &= \Gamma + R_{1,H}(B(n_L + n_H) - A(n_L + n_H)^{1/\beta_1}),\\ \Pi'(R_{1,H}) &= B(n_L + n_H) - A(n_L + n_H)^{1/\beta_1}.\end{aligned}$$

So $\Pi'(R_{1,H}) > 0$ if and only if:

$$B > A(n_L + n_H)^{\frac{1-\beta_1}{\beta_1}}. \tag{C.2}$$

Under $\Pi_{\text{homo1}} = \Pi_{\text{homo2}}$, using (C.1), the inequality (C.2) becomes:

$$\frac{(n_L d_L^{\beta_1} + n_H d_H^{\beta_1})^{1/\beta_1}}{n_L d_L + n_H d_H} > (n_L + n_H)^{1/\beta_1 - 1}. \tag{C.3}$$

This is true by the power-mean inequality, with strict inequality when $d_H > d_L$. We conclude via contradiction that $R_{1,L}^* = d_L$.

Step 2. Show $d_L < R_{1,H}^* < d_H$. Whenever $R_{1,L} = d_L$, we have

$$\begin{aligned}\Pi(R_{1,H}) &= \Gamma + B(n_L d_L + n_H R_{1,H}) - A(n_L d_L^{\beta_1} + n_H R_{1,H}^{\beta_1})^{1/\beta_1} \text{ and}\\ \Pi'(R_{1,H}) &= n_H \left[B - A R_{1,H}^{\beta_1 - 1} (n_L d_L^{\beta_1} + n_H R_{1,H}^{\beta_1})^{\frac{1-\beta_1}{\beta_1}} \right].\end{aligned}$$

Define $g(R_{1,H})$ as

$$\begin{aligned} g(R_{1,H}) &:= R_{1,H}^{\beta_1 - 1} (K + n_H R_{1,H}^{\beta_1})^{\frac{1-\beta_1}{\beta_1}}, \text{ for}\\ K &= n_L d_L^{\beta_1}.\end{aligned}$$

Then

$$\Pi''(R_{1,H}) = -n_H A g'(R_{1,H}).$$

Note that

$$\begin{aligned}
\ln g(R_{1,H}) &= (\beta_1 - 1)\ln R_{1,H} + \frac{1-\beta_1}{\beta_1}\ln(K + n_H R_{1,H}^{\beta_1}) \text{ and} \\
\frac{g'(R_{1,H})}{g(R_{1,H})} &= \frac{\beta_1 - 1}{R_{1,H}} + \frac{1-\beta_1}{\beta_1} \cdot \frac{n_H \beta_1 R_{1,H}^{\beta_1 - 1}}{K + n_H R_{1,H}^{\beta_1}} \\
&= (\beta_1 - 1)\left[\frac{1}{R_{1,H}} - \frac{n_H R_{1,H}^{\beta_1 - 1}}{K + n_H R_{1,H}^{\beta_1}}\right] \\
&= (\beta_1 - 1)\frac{K}{R_{1,H}(K + n_H R_{1,H}^{\beta_1})}.
\end{aligned}$$

Since $g(R_{1,H}) > 0$, we conclude that $g'(R_{1,H}) > 0$ and therefore that $\Pi(R_{1,H})$ is a strictly concave function.

At $R_{1,H} = d_L$,

$$\begin{aligned}
\Pi'(R_{1,H} = d_L) &= n_H\left[B - A d_L^{\beta_1 - 1}(n_L d_L^{\beta_1} + n_H d_L^{\beta_1})^{\frac{1-\beta_1}{\beta_1}}\right] \\
&= n_H\left[\underbrace{B - A(n_L + n_H)^{\frac{1-\beta_1}{\beta_1}}}_{>0 \text{ from (C.3) for } d_H > d_L}\right] > 0.
\end{aligned}$$

At $R_{1,H} = d_H$,

$$\Pi'(R_{1,H} = d_H) = n_H\left[B - A d_H^{\beta_1 - 1}(n_L d_L^{\beta_1} + n_H d_H^{\beta_1})^{\frac{1-\beta_1}{\beta_1}}\right].$$

Using (C.1), $\Pi'(d_H) < 0$ is equivalent to

$$\frac{(n_L d_L^{\beta_1} + n_H d_H^{\beta_1})^{1/\beta_1}}{n_L d_L + n_H d_H} < d_H^{\beta_1 - 1}(n_L d_L^{\beta_1} + n_H d_H^{\beta_1})^{1/\beta_1 - 1},$$

which simplifies to:

$$n_L d_L + n_H d_H > \frac{n_L d_L^{\beta_1} + n_H d_H^{\beta_1}}{d_H^{\beta_1 - 1}} = n_L d_L(\frac{d_L}{d_H})^{\beta_1 - 1} + n_H d_H,$$

which holds strictly whenever $d_H > d_L$. Since $\Pi(R_{1,H})$ is a strictly concave function with a positive derivative at d_L and a negative derivative at d_H, we conclude that

$$R_{1,L}^* = d_L < R_{1,H}^* < d_H.$$

Step 3. Derive $R^*_{1,H}, AllCost_{\textbf{hybrid}}$, and $\Pi^*(R^*_{1,L}, R^*_{1,H})$.

Since $\Pi(R_{1,H})$ is strictly concave in $R_{1,H}$, $R^*_{1,H} \in (d_L, d_H)$ is the unique solution to

$$B = AR_{1,H}^{\beta_1 - 1}(n_L d_L^{\beta_1} + n_H R_{1,H}^{\beta_1})^{\frac{1-\beta_1}{\beta_1}},$$

or equivalently

$$\left(\frac{A}{B}\right)^{\frac{\beta_1}{\beta_1 - 1}} R_{1,H}^{\beta_1} = n_L d_L^{\beta_1} + n_H R_{1,H}^{\beta_1}.$$

This yields:

$$R^*_{1,H} = \left[\frac{n_L d_L^{\beta_1}}{\left(\frac{A}{B}\right)^{\frac{\beta_1}{\beta_1 - 1}} - n_H}\right]^{1/\beta_1}.$$

From (C.1), we can rewrite $R^*_{1,H}$ as a function of battery 1 and workload parameters only:

$$R^*_{1,H} = \left[\frac{n_L d_L^{\beta_1}}{\left(\frac{n_L d_L + n_H d_H}{(n_L d_L^{\beta_1} + n_H d_H^{\beta_1})^{1/\beta_1}}\right)^{\frac{\beta_1}{\beta_1 - 1}} - n_H}\right]^{1/\beta_1}.$$

Plugging this quantity back into $\Pi(d_L, R^*_{1,H})$ yields the optimal profit $\Pi^*(R^*_{1,L}, R^*_{1,H})$. Lastly, for $\text{AllCost}_{\text{hybrid}}$, we use the fact that $C_1^* = \left[\frac{(\beta_1 - 1)c_1^{deg}[n_L d_L^{\beta_1} + n_H (R^*_{1,H})^{\beta_1}]}{c_1^b}\right]^{1/\beta_1}$, $C_2^* = 0$, and

$$R^{\text{benchmark}} = c^e \max(x_1, x_2)^2 (n_L d_L + n_H d_H),$$

where x_1 and x_2 are efficiency of battery types 1 and 2, respectively. For homogeneous batteries, we have the following:

$$\begin{aligned}\text{AllCost}_{\text{homo1}} &= \frac{\beta_1}{\beta_1 - 1} c_1^b \left[\frac{(\beta_1 - 1)c_1^{deg}[n_L d_L^{\beta_1} + n_H d_H^{\beta_1}]}{c_1^b}\right]^{1/\beta_1} \\ &\quad + c^e[\max(x_1, x_2)^2 - x_1^2](n_L d_L + n_H d_H), \quad \text{and} \qquad \text{(C.4)} \\ \text{AllCost}_{\text{homo2}} &= \left[c^e[\max(x_1, x_2)^2 - x_2^2] + c_2^{deg}\right](n_L d_L + n_H d_H). \qquad \text{(C.5)}\end{aligned}$$

□

Proof of Corollary 4.2

From Theorem 4.2,

$$\begin{aligned}\lim_{\beta_1\to\infty}\text{AllCost}_{\text{hybrid}} =& c_1^b d_L + c_2^{deg} n_H(d_H - d_L) \\ &+ c^e[\max(x_1,x_2)^2(n_L d_L + n_H d_H) - x_1^2(n_L+n_H)d_L - x_2^2 n_H(d_H - d_L)].\end{aligned}$$

For homogeneous battery systems, (C.4) and (C.5) imply:

$$\begin{aligned}\lim_{\beta_1\to\infty}\text{AllCost}_{\text{homo1}} &= c_1^b d_H + c^e\big[\max(x_1,x_2)^2 - x_1^2\big](n_L d_L + n_H d_H), \quad \text{and} \\ \text{AllCost}_{\text{homo2}} &= \Big[c^e[\max(x_1,x_2)^2 - x_2^2] + c_2^{deg}\Big](n_L d_L + n_H d_H).\end{aligned}$$

Then $\text{AllCost}_{\text{homo1}} = \text{AllCost}_{\text{homo2}}$ is equivalent to

$$c_1^b d_H = [c_2^{deg} + c^e(x_1^2 - x_2^2)](n_L d_L + n_H d_H). \tag{C.6}$$

If $x_1 \le x_2$, then

$$\lim_{\beta_1\to\infty} S^C = 1 - \frac{c_1^b d_L + c_2^{deg} n_H(d_H - d_L) + c^e(x_2^2 - x_1^2)(n_L + n_H)d_L}{c_1^b d_H + c^e(x_2^2 - x_1^2)(n_L d_L + n_H d_H)}.$$

From (C.6), $c_1^b d_L = \frac{d_L}{d_H}[c_2^{deg} - c^e(x_2^2 - x_1^2)](n_L d_L + n_H d_H)$, and we have:

$$\lim_{\beta_1\to\infty} S^C = \frac{n_L d_L(d_H - d_L)}{d_H(n_L d_L + n_H d_H)}\left(1 - \frac{c^e(x_2^2 - x_1^2)}{c_2^{deg}}\right).$$

If $x_1 \ge x_2$, then

$$\begin{aligned}\lim_{\beta_1\to\infty} S^C &= 1 - \frac{c_1^b d_L + [c_2^{deg} + c^e(x_1^2 - x_2^2)]n_H(d_H - d_L)}{c_1^b d_H} \\ &= 1 - \frac{d_L}{d_H} - \frac{[c_2^{deg} + c^e(x_1^2 - x_2^2)]n_H(d_H - d_L)}{c_1^b d_H} \\ &= 1 - \frac{d_L}{d_H} - \frac{[c_2^{deg} + c^e(x_1^2 - x_2^2)]n_H(d_H - d_L)}{[c_2^{deg} + c^e(x_1^2 - x_2^2)](n_L d_L + n_H d_H)} \quad (\because \text{(C.6)}) \\ &= 1 - \frac{d_L}{d_H} - \frac{n_H(d_H - d_L)}{n_L d_L + n_H d_H} \\ &= \frac{n_L d_L(d_H - d_L)}{d_H(n_L d_L + n_H d_H)}.\end{aligned}$$

□

BIBLIOGRAPHY

[1] Anthony Afful-Dadzie, Eric Afful-Dadzie, Iddrisu Awudu, and Joseph Kwaku Banuro. Power generation capacity planning under budget constraint in developing countries. Applied Energy, 188:71–82, 2017.

[2] Vishal V. Agrawal, L. Beril Toktay, and Şafak Yücel. Non-ownership business models for solar energy. Manufacturing & Service Operations Management, 24(4):2048–2063, 2022.

[3] Vishal V Agrawal and Şafak Yücel. Renewable energy sourcing. Swaminathan J., Deshpande V., eds. In Responsible Business Operations, pages 211–224. Springer, 2021.

[4] Leila Ahmadi, Michael Fowler, Steven B Young, Roydon A Fraser, Ben Gaffney, and Sean B Walker. Energy efficiency of Li-ion battery packs re-used in stationary power applications. Sustainable Energy Technologies and Assessments, 8:9–17, 2014.

[5] Muhammad Bin Fayyaz Ahsan, Saad Mekhilef, Tey Kok Soon, Marizan Binti Mubin, Prashant Shrivastava, and Mehdi Seyedmahmoudian. Lithium-ion battery and supercapacitor-based hybrid energy storage system for electric vehicle applications: A review. International Journal of Energy Research, 46(14):19826–19854, 2022.

[6] Hisham Alharbi and Kankar Bhattacharya. Stochastic optimal planning of battery energy storage systems for isolated microgrids. IEEE Transactions on Sustainable Energy, 9(1):211–227, 2017.

[7] Mohammed I Alizadeh, M Parsa Moghaddam, Nima Amjady, Pierluigi Siano, and Mohammed K Sheikh-El-Eslami. Flexibility in future power systems with high renewable penetration: A review. Renewable and Sustainable Energy Reviews, 57:1186–1193, 2016.

[8] Saed Alizamir, Francis de Véricourt, and Peng Sun. Efficient feed-in-tariff policies for renewable energy technologies. Operations Research, 64(1):52–66, 2016.

[9] Saed Alizamir, Foad Iravani, and Şafak Yücel. Investment in wind energy: The role of subsidies. Georgetown McDonough School of Business Research Paper, (3868573), 2021.

[10] American Clean Power. Clean power quarterly market report. https://cleanpower.org, 2024. Accessed: 2025-12-03.

[11] Jerry Anunrojwong, Santiago R Balseiro, Omar Besbes, and Bolun Xu. Battery operations in electricity markets: Strategic behavior and distortions. arXiv preprint arXiv:2406.18685, 2024.

[12] Masahito Arima, Lei Lin, and Masahiro Fukui. Kalman-filter-based learning of characteristic profiles of lithium-ion batteries. Sensors, 22(14):5156, 2022.

[13] Sant R Arora and PT Lele. A note on optimal maintenance policy and sale date of a machine. Management Science, 17(3):170–173, 1970.

[14] Ava Community Energy. Staff report item 18. https://avaenergy.org, 2024. Accessed: 2025-12-03.

[15] Buket Avci, Karan Girotra, and Serguei Netessine. Electric vehicles with a battery switching station: Adoption and environmental impact. Management Science, 61(4):772–794, 2015.

[16] Sarah Paul Ayeng'o, Toni Schirmer, Kai-Philipp Kairies, Hendrik Axelsen, and Dirk Uwe Sauer. Comparison of off-grid power supply systems using lead-acid and lithium-ion batteries. Solar Energy, 162:140–152, 2018.

[17] Joonho Bae, Roman Kapuscinski, and John Silberholz. Cost-saving synergy: Energy stacking in battery energy storage systems. Management Science, page Forthcoming, 2025.

[18] Mohamed Bahloul and Shafiuzzaman K Khadem. An analytical approach for techno-economic evaluation of hybrid energy storage system for grid services. Journal of Energy Storage, 31:101662, 2020.

[19] I Beil, IA Hiskens, and S Backhaus. Round-trip efficiency of fast demand response in a large commercial air conditioner. Energy and Buildings, 97:47–55, 2015.

[20] Bloomberg. Where 3 million electric vehicle batteries will go when they retire. Bloomberg, 2018. Accessed: 03.03.2023.

[21] BloombergNEF, 2022.

[22] Bonnen. Hybrid battery packs: The future of energy storage with A+B cell integration. https://www.bonnenbatteries.com, 2025. Accessed: 2025-12-03.

[23] Gerald Broneske and David Wozabal. How do contract parameters influence the economics of vehicle-to-grid? Manufacturing & Service Operations Management, 19(1):150–164, 2017.

[24] Michel Broussely, Ph Biensan, F Bonhomme, Ph Blanchard, S Herreyre, K Nechev, and RJ Staniewicz. Main aging mechanisms in Li-ion batteries. Journal of Power Sources, 146(1-2):90–96, 2005.

[25] Burns & McDonnell, 2022.

[26] CAISO. Net demand dataset, 2025. Accessed: 10.09.2025.

[27] CAISO. Q4 2024 report on market issues and performance. https://www.caiso.com/library/2024-quarterly-reports, 2025. Accessed: 2025-12-03.

[28] California Community Choice Association. Cca long-term clean energy power purchase agreements. https://cal-cca.org/cca-renewable-energy-map-and-list-of-ppas/, 2025. Accessed: 2025-12-03.

[29] Nicola Campagna, Vincenzo Castiglia, Alfonso Damiano, Luigi Pio Di Noia, Rosario Miceli, and Antonino Oscar Di Tommaso. A hybrid energy storage sizing for a vertical take-off and landing electric aircraft. In IECON 2021–47th Annual Conference of the IEEE Industrial Electronics Society, pages 1–6. IEEE, 2021.

[30] CEC. Electric generation capacity and energy. https://www.energy.ca.gov/data-reports, 2025. Accessed: 2025-12-03.

[31] Ming-Hui Chang, Han-Pang Huang, and Shu-Wei Chang. A new state of charge estimation method for LiFePO4 battery packs used in robots. Energies, 6(4):2007–2030, 2013.

[32] Jie Chen, Huiping Yang, Tianhao Li, Chaoyang Liu, Hui Tong, Jiaxin Chen, Zengsheng Liu, Lingfeng Xia, Zhaoyong Chen, Junfei Duan, et al. The effects of reversibility of H2-H3 phase transition on Ni-rich layered oxide cathode for high-energy lithium-ion batteries. Frontiers in Chemistry, 7:500, 2019.

[33] Li Chen, Long He, and Yangfang Zhou. An exponential cone programming approach for managing electric vehicle charging. Operations Research., Forthcoming., 2023.

[34] Xinjiang Chen, Yu Yang, Jianxiao Wang, Jie Song, and Guannan He. Battery valuation and management for battery swapping station. Energy, 279:128120, 2023.

[35] Xinjiang Chen, Yu Yang, Zongxian Wang, Jie Song, Jianxiao Wang, and Guannan He. Battery swapping station management with heterogeneous battery functionality degradation. IEEE Transactions on Smart Grid, 16(1):478–490, 2024.

[36] Bolong Cheng and Warren B Powell. Co-optimizing battery storage for the frequency regulation and energy arbitrage using multi-scale dynamic programming. IEEE Transactions on Smart Grid, 9(3):1997–2005, 2016.

[37] Ming Cheng, Xuan Zhang, Aihua Ran, Guodan Wei, and Hongbin Sun. Optimal dispatch approach for second-life batteries considering degradation with online SoH estimation. Renewable and Sustainable Energy Reviews, 173:113053, 2023.

[38] I Chotia and S Chowdhury. Battery storage and hybrid battery supercapacitor storage systems: A comparative critical review. 2015 IEEE Innovative Smart Grid Technologies-Asia (ISGT ASIA), pages 1–6, 2015.

[39] Steven Chung and Olivier Trescases. Hybrid lead-acid/lithium-ion energy storage system with power-mix control for light electric vehicles. In 2016 18th European Conference on Power Electronics and Applications (EPE'16 ECCE Europe), pages 1–10. IEEE, 2016.

[40] Andrew J Clark and Herbert Scarf. Optimal policies for a multi-echelon inventory problem. Management Science, 6(4):475–490, 1960.

[41] James Cruise, Lisa Flatley, Richard Gibbens, and Stan Zachary. Control of energy storage with market impact: Lagrangian approach and horizons. Operations Research, 67(1):1–9, 2019.

[42] Yingzhi Cui, Chunyu Du, Yunzhi Gao, Jie Yang, Lingling Zhang, Ting Guan, Lijie Yang, Xinqun Cheng, Pengjian Zuo, Yulin Ma, et al. Recovery strategy and mechanism of aged lithium ion batteries after shallow depth of discharge at elevated temperature. ACS Applied Materials & Interfaces, 8(8):5234–5242, 2016.

[43] Shantayanan Devarajan and Anthony C Fisher. Hotelling's "Economics of exhaustible resources": Fifty years later. Journal of Economic Literature, 19(1):65–73, 1981.

[44] Francisco Diaz-Gonzalez, Cristian Chillón-Antón, Marc Llonch-Masachs, Samuel Galceran-Arellano, Joan Rull-Duran, Joan Bergas-Jane, and Eduard Bullich-Massagué. A hybrid energy storage solution based on supercapacitors and batteries for the grid integration of utility scale photovoltaic plants. Journal of Energy Storage, 51:104446, 2022.

[45] Collin Drent, Melvin Drent, and Joachim Arts. Condition-based production for stochastically deteriorating systems: Optimal policies and learning. Manufacturing & Service Operations Management, 26(3):1137–1156, 2024.

[46] Collin Drent, Melvin Drent, Joachim Arts, and Stella Kapodistria. Real-time integrated learning and decision making for cumulative shock degradation. Manufacturing & Service Operations Management, 25(1):235–253, 2023.

[47] Easan Drury, Paul Denholm, and Ramteen Sioshansi. The value of compressed air energy storage in energy and reserve markets. Energy, 36(8):4959–4973, 2011.

[48] Deepak P Dubal, Omar Ayyad, Vanesa Ruiz, and Pedro Gomez-Romero. Hybrid energy storage: The merging of battery and supercapacitor chemistries. Chemical Society Reviews, 44(7):1777–1790, 2015.

[49] E3. Minnesota energy storage cost-benefit analysis. Technical report, E3, 2020.

[50] EBCE. Solar power purchase & battery energy storage services agreement. https://avaenergy.org, 2022. Accessed: 2025-12-03.

[51] Madeleine Ecker, Nerea Nieto, Stefan Käbitz, Johannes Schmalstieg, Holger Blanke, Alexander Warnecke, and Dirk Uwe Sauer. Calendar and cycle life study of Li(NiMnCo)O2-based 18650 lithium-ion batteries. Journal of Power Sources, 248:839–851, 2014.

[52] Ali Eftekhari. Energy efficiency: A critically important but neglected factor in battery research. Sustainable Energy & Fuels, 1(10):2053–2060, 2017.

[53] EIA. Capital cost and performance characteristic estimates for utility scale electric power generating technologies. Technical report, Energy Information Administration, 2020. Accessed: 03.03.2023.

[54] EIA. Battery storage in the United States: An update on market trends. Technical report, EIA, 2021.

[55] EIA. Form EIA-860. Technical report, Energy Information Administration, 2021.

[56] EIA. Utility-scale batteries and pumped storage return about 80% of the electricity they store. Technical report, Energy Information Administration, 2021. Accessed: 07.21.2022.

[57] Elektrek, 2020.

[58] Jonas Engels, Bert Claessens, and Geert Deconinck. Combined stochastic optimization of frequency control and self-consumption with a battery. IEEE Transactions on Smart Grid, 10(2):1971–1981, 2017.

[59] Entergy. Appendix C model solar power purchase agreement. https://www.entergy.com/renewable-energy, 2025. Accessed: 2025-12-03.

[60] Stealth EV. Tesla 5.3 kWh Battery Module (85 kWh Pack). https://stealthev.com/product/tesla-module/, 2026. Accessed: 2025-12-03.

[61] Valerie Eveloy and Tesfaldet Gebreegziabher. A review of projected power-to-gas deployment scenarios. Energies, 11(7):1824, 2018.

[62] Ziyu Fang, Jonathan KH Shek, and Wei Sun. A review of grid-connected hybrid energy storage systems: Sizing configurations, control strategies, and future directions. Journal of Energy Storage, 118:116226, 2025.

[63] Garrett Fitzgerald, James Mandel, Jesse Morris, and Hervé Touati. The economics of battery energy storage: How multi-use, customer-sited batteries deliver the most services and value to customers and the grid. Technical report, Rocky Mountain Institute, 2015.

[64] Fluence, 2020.

[65] Frost & Sullivan. Battery energy storage growth opportunities: Renewed governmental support for clean energy transition propels an already fast-growing industry. Technical report, Frost & Sullivan, 2023.

[66] A Geetha and C Subramani. A comprehensive review on energy management strategies of hybrid energy storage system for electric vehicles. International Journal of Energy Research, 41(13):1817–1834, 2017.

[67] Shadi Goodarzi, Sam Aflaki, and Andrea Masini. Optimal feed-in tariff policies: The impact of market structure and technology characteristics. Production and Operations Management, 28(5):1108–1128, 2019.

[68] Guardian. Millions of electric car batteries will retire in the next decade. What happens to them? https://www.theguardian.com/environment/2021/aug/20, 2021. Accessed: 2025-12-03.

[69] Chris Hanna, AJ Jain, and Trisha Sieh, 2024.

[70] Sameer Hasija, Zuo-Jun Max Shen, and Chung-Piaw Teo. Smart city operations: Modeling challenges and opportunities. Manufacturing & Service Operations Management, 22(1):203–213, 2020.

[71] Guannan He, Qixin Chen, Panayiotis Moutis, Soummya Kar, and Jay F Whitacre. An intertemporal decision framework for electrochemical energy storage management. Nature Energy, 3(5):404–412, 2018.

[72] Guannan He, Rebecca Ciez, Panayiotis Moutis, Soummya Kar, and Jay F Whitacre. The economic end of life of electrochemical energy storage. Applied Energy, 273:115151, 2020.

[73] Dominik Heide, Lueder Von Bremen, Martin Greiner, Clemens Hoffmann, Markus Speckmann, and Stefan Bofinger. Seasonal optimal mix of wind and solar power in a future, highly renewable Europe. Renewable Energy, 35(11):2483–2489, 2010.

[74] Anderson Hoke, Alexander Brissette, Dragan Maksimović, Annabelle Pratt, and Kandler Smith. Electric vehicle charge optimization including effects of lithium-ion battery degradation. In 2011 IEEE Vehicle Power and Propulsion Conference, pages 1–8. IEEE, 2011.

[75] Harold Hotelling. The economics of exhaustible resources. Journal of Political Economy, 39(2):137–175, 1931.

[76] Qingchun Hou, Yanghao Yu, Ershun Du, Hongjie He, Ning Zhang, Chongqing Kang, Guojing Liu, and Huan Zhu. Embedding lithium-ion battery scrapping criterion and degradation model in optimal operation of peak-shaving energy storage. arXiv preprint arXiv:1910.04028, 2019.

[77] Jinsol Im, Jieun Lee, Myung-Hyun Ryou, Yong Min Lee, and Kuk Young Cho. Fluorinated carbonate-based electrolyte for high-voltage Li $(Ni_{0.8}Mn_{0.1}Co_{0.1})$ o_2/graphite lithium-ion battery. Journal of The Electrochemical Society, 164(1):A6381, 2017.

[78] International Energy Agency. The cost of capital in clean energy transitions. https://www.iea.org/articles/the-cost-of-capital-in-clean-energy-transitions, 2021. Accessed: 2025-12-03.

[79] IRENA. Electricity storage valuation framework: Assessing system value and ensuring project viability. Technical report, IRENA, 2020.

[80] ISO-NE. ISO-NE simulated automatic generator control setpoint dataset, 2014. Accessed: 06.11.2023.

[81] ISO-NE. ISO-NE operational dataset, 2021. Accessed: 07.21.2022.

[82] ISO-NE. 2022 annual markets report. Technical report, ISO-NE, 2022.

[83] ISO-NE. ISO-NE regulation offer data, 2023. Accessed: 06.21.2023.

[84] ISO-NE. ISO-NE operational dataset, 2025. Accessed: 10.09.2025.

[85] Samppa Jenu, Ari Hentunen, Jari Haavisto, and Mikko Pihlatie. State of health estimation of cycle aged large format lithium-ion cells based on partial charging. Journal of Energy Storage, 46:103855, 2022.

[86] Daniel R Jiang and Warren B Powell. Optimal hour-ahead bidding in the real-time electricity market with battery storage using approximate dynamic programming. INFORMS Journal on Computing, 27(3):525–543, 2015.

[87] Bradley A Johnson and Ralph E White. Characterization of commercially available lithium-ion batteries. Journal of Power Sources, 70(1):48–54, 1998.

[88] Chengquan Ju, Peng Wang, Lalit Goel, and Yan Xu. A two-layer energy management system for microgrids with hybrid energy storage considering degradation costs. IEEE Transactions on Smart Grid, 9(6):6047–6057, 2017.

[89] Sunhyung Jurng, Satu Kristiina Heiskanen, KWD Kaveendi Chandrasiri, Maheeka Yapa Abeywardana, and Brett L Lucht. Minimized metal dissolution from high-energy nickel cobalt manganese oxide cathodes with Al_2O_3 coating and its effects on electrolyte decomposition on graphite anodes. Journal of The Electrochemical Society, 166(13):A2721, 2019.

[90] Soteris Kalogirou. McEvoy's handbook of photovoltaics: Fundamentals and applications. Academic Press, 2017.

[91] Morton I Kamien and Nancy L Schwartz. Optimal maintenance and sale age for a machine subject to failure. Management Science, 17(8):B–495, 1971.

[92] Christian Kaps and Simone Marinesi. When batteries meet hydrogen: Dual-storage investments for load-shifting purposes. Available at SSRN: https://ssrn.com/abstract=4993905, 2024.

[93] Christian Kaps, Simone Marinesi, and Serguei Netessine. When should the off-grid sun shine at night? optimum renewable generation and energy storage investments. Management Science, 69(12):7633–7650, 2023.

[94] Christian Kaps and Serguei Netessine. Residential battery storage – Reshaping the way we do electricity. Available at SSRN: https://ssrn.com/abstract=4219247, 2024.

[95] Roman Kapuscinski and Sridhar Tayur. A capacitated production-inventory model with periodic demand. Operations Research, 46(6):899–911, 1998.

[96] Samuel Karlin. Dynamic inventory policy with varying stochastic demands. Management Science, 6(3):231–258, 1960.

[97] KCE. Key Capture Energy announces launch of KCE NY6 Project with Sungrow and Black and Mcdonald, 2023. Accessed: 07.21.2023.

[98] Joseph J Kelly and Paul G Leahy. Sizing battery energy storage systems: Using multi-objective optimization to overcome the investment scale problem of annual worth. IEEE Transactions on Sustainable Energy, 11(4):2305–2314, 2019.

[99] Willett Kempton and Jasna Tomić. Vehicle-to-grid power fundamentals: Calculating capacity and net revenue. Journal of Power Sources, 144(1):268–279, 2005.

[100] Muhammad Khalid. A review on the selected applications of battery-supercapacitor hybrid energy storage systems for microgrids. Energies, 12(23):4559, 2019.

[101] Jae Ho Kim and Warren B Powell. Optimal energy commitments with storage and intermittent supply. Operations Research, 59(6):1347–1360, 2011.

[102] A Gürhan Kök, Kevin Shang, and Şafak Yücel. Impact of electricity pricing policies on renewable energy investments and carbon emissions. Management Science, 64(1):131–148, 2018.

[103] A Gürhan Kök, Kevin Shang, and Şafak Yücel. Investments in renewable and conventional energy: The role of operational flexibility. Manufacturing & Service Operations Management, 22(5):925–941, 2020.

[104] Mariya Koleva, Ying Shi, Killian McKenna, Michael Craig, and Adarsh Nagarajan. Optimal strategies for hybrid battery-storage systems design. Energy Technology, 11(10):2300115, 2023.

[105] Michael Koller, Theodor Borsche, Andreas Ulbig, and Göran Andersson. Defining a degradation cost function for optimal control of a battery energy storage system. In 2013 IEEE Grenoble Conference, pages 1–6. IEEE, 2013.

[106] Dheepak Krishnamurthy, Canan Uckun, Zhi Zhou, Prakash R Thimmapuram, and Audun Botterud. Energy storage arbitrage under day-ahead and real-time price uncertainty. IEEE Transactions on Power Systems, 33(1):84–93, 2017.

[107] Long Lam and Pavol Bauer. Practical capacity fading model for Li-ion battery cells in electric vehicles. IEEE Transactions on Power Electronics, 28(12):5910–5918, 2012.

[108] Izaro Laresgoiti, Stefan Käbitz, Madeleine Ecker, and Dirk Uwe Sauer. Modeling mechanical degradation in lithium ion batteries during cycling: Solid electrolyte interphase fracture. Journal of Power Sources, 300:112–122, 2015.

[109] Dirk Lauinger, François Vuille, and Daniel Kuhn. Reliable frequency regulation through vehicle-to-grid: Encoding legislation with robust constraints. Manufacturing & Service Operations Management., Forthcoming., 2024.

[110] Lazard. Lazard's levelized cost of storage analysis. Technical report, Lazard, 2021.

[111] Lazard. Lazard's levelized cost of energy. Technical report, Lazard, 2025.

[112] Mpho J Lencwe, Shyama P Daniel Chowdhury, and Thomas O Olwal. Hybrid energy storage system topology approaches for use in transport vehicles: A review. Energy Science & Engineering, 10(4):1449–1477, 2022.

[113] David Levhari and Nissan Liviatan. Notes on hotelling's economics of exhaustible resources. Canadian Journal of Economics, pages 177–192, 1977.

[114] Xialin Li, Zhiwang Li, Li Guo, Jiebei Zhu, Yizhen Wang, and Chengshan Wang. Enhanced dynamic stability control for low-inertia hybrid ac/dc microgrid with distributed energy storage systems. IEEE Access, 7:91234–91242, 2019.

[115] Zihui Lin, Dagang Li, and Yuntao Zou. Energy efficiency of lithium-ion batteries: Influential factors and long-term degradation. Journal of Energy Storage, 74:109386, 2023.

[116] Yu Liu and Hong-Zhong Huang. Optimal replacement policy for multi-state system under imperfect maintenance. IEEE Transactions on Reliability, 59(3):483–495, 2010.

[117] Nils Löhndorf and David Wozabal. The value of coordination in multimarket bidding of grid energy storage. Operations Research, 71(1):1–22, 2022.

[118] Nils Löhndorf and David Wozabal. The value of coordination in multimarket bidding of grid energy storage. Operations Research, 71(1):1–22, 2023.

[119] Nils Löhndorf, David Wozabal, and Stefan Minner. Optimizing trading decisions for hydro storage systems using approximate dual dynamic programming. Operations Research, 61(4):810–823, 2013.

[120] Matthias Luh and Thomas Blank. Comprehensive battery aging dataset: capacity and impedance fade measurements of a lithium-ion nmc/c-sio cell. Scientific Data, 11(1):1004, 2024.

[121] Ho-Yin Mak, Ying Rong, and Zuo-Jun Max Shen. Infrastructure planning for electric vehicles with battery swapping. Management Science, 59(7):1557–1575, 2013.

[122] Egoitz Martinez-Laserna, Iñigo Gandiaga, Elixabet Sarasketa-Zabala, Julia Badeda, D-I Stroe, Maciej Swierczynski, and Ander Goikoetxea. Battery second life: Hype, hope or reality? A critical review of the state of the art. Renewable and Sustainable Energy Reviews, 93:701–718, 2018.

[123] Alan Millner. Modeling lithium ion battery degradation in electric vehicles. In 2010 IEEE Conference on Innovative Technologies for an Efficient and Reliable Electricity Supply, pages 349–356. IEEE, 2010.

[124] Ramin Moghaddass and Ming J Zuo. An integrated framework for online diagnostic and prognostic health monitoring using a multistate deterioration process. Reliability Engineering & System Safety, 124:92–104, 2014.

[125] MonitoringAnalytics. State of the market report for PJM. Technical report, Monitoring Analytics, 2022.

[126] MordorIntelligence. Secondary battery market - Growth, trends, COVID-19 impact, and forecasts (2022 - 2027). Technical report, Mordor Intelligence, 2022.

[127] Seyedabolfazl Mousavihashemi, Katja Lahtinen, and Tanja Kallio. In-situ dilatometry and impedance spectroscopy characterization of single walled carbon nanotubes blended $LiNi_{0.6}Mn_{0.2}Co_{0.2}O_2$ electrode with enhanced performance. Electrochimica Acta, 412:140093, 2022.

[128] MPower. Battery performance characteristics, 2007. Accessed: 07.21.2022.

[129] Paskalis Sahaya Murphin Kumar, Vinothkumar Ponnusamy, Hyoung-il Kim, Martín Adelaido Hernández-Landaverde, Siva Kumar Krishnan, and Umapada Pal. Molybdenum-doped nickel disulfide (NiS_2: Mo) microspheres as an active anode material for high-performance durable lithium-ion batteries. ACS Applied Energy Materials, 5(6):6734–6745, 2022.

[130] Cameron Murray, 2023.

[131] Selvaprabu Nadarajah and Nicola Secomandi. Merchant energy trading in a network. Operations Research, 66(5):1304–1320, 2018.

[132] Tu A Nguyen, Raymond H Byrne, Ricky J Concepcion, and Imre Gyuk. Maximizing revenue from electrical energy storage in MISO energy & frequency regulation markets. In 2017 IEEE Power & Energy Society General Meeting, pages 1–5. IEEE, 2017.

[133] NREL, 2019.

[134] NYISO. Ancillary services manual. NYISO, 2021.

[135] NYISO. NYISO operational dataset, 2022. Accessed: 03.03.2023.

[136] NYISO. NYISO market administration and control area services tariff (MST). Technical report, NYISO, 2023. Accessed: 03.03.2023.

[137] NYISO. Operational dataset, 2025. Accessed: 10.09.2025.

[138] Adem Örsdemir, Vinayak Deshpande, and Ali K Parlaktürk. Is servicization a win-win strategy? Profitability and environmental implications of servicization. Manufacturing & Service Operations Management, 21(3):674–691, 2019.

[139] Amir Ostadi and Mehrdad Kazerani. A comparative analysis of optimal sizing of battery-only, ultracapacitor-only, and battery–ultracapacitor hybrid energy storage systems for a city bus. IEEE Transactions on Vehicular Technology, 64(10):4449–4460, 2014.

[140] PacifiCorp. PPA documents for power purchase agreement with collocated energy storage (Appendix E-2.2). https://www.pacificorp.com, 2022. Accessed: 2025-12-03.

[141] Geoffrey G Parker, Burcu Tan, and Osman Kazan. Electric power industry: Operational and public policy challenges and opportunities. Production and Operations Management, 28(11):2738–2777, 2019.

[142] Barb Peck and Bjarne Hansen. Lithium house battery – impressions after one year. https://currents.bluewatercruising.org, 2021. Accessed: 2025-12-03.

[143] Dario Pelosi, Giacomo Alessandri, Federico Gallorini, and Linda Barelli. Hybrid energy storage systems coupled with renewable power plants for power smoothing applications. In Hybrid Energy Storage: Case Studies for the Energy Transition, pages 121–139. Springer, 2025.

[144] Aramis Perez, Rodrigo Moreno, Roberto Moreira, Marcos Orchard, and Goran Strbac. Effect of battery degradation on multi-service portfolios of energy storage. IEEE Transactions on Sustainable Energy, 7(4):1718–1729, 2016.

[145] Scott B Peterson, Jay Apt, and JF Whitacre. Lithium-ion battery cell degradation resulting from realistic vehicle and vehicle-to-grid utilization. Journal of Power Sources, 195(8):2385–2392, 2010.

[146] Scott B Peterson, JF Whitacre, and Jay Apt. The economics of using plug-in hybrid electric vehicle battery packs for grid storage. Journal of Power Sources, 195(8):2377–2384, 2010.

[147] Heikki Peura and Derek W Bunn. Renewable power and electricity prices: the impact of forward markets. Management Science, 67(8):4772–4788, 2021.

[148] PJM. Implementation and rationale for PJM's conditional neutrality regulation signals. Technical report, PJM, 2017. Accessed: 07.21.2022.

[149] PJM. PJM regulation signal dataset, 2020. Accessed: 06.11.2023.

[150] PJM. PJM operational dataset, 2021. Accessed: 07.21.2022.

[151] PJM. PJM manual 12: Balancing operations. PJM, 2022.

[152] PJM. PJM manual 28: Operating agreement accounting. PJM, 2022.

[153] PJM. Energy & ancillary services market operations, 2023.

[154] Gregory L Plett. Battery Management Systems, Volume I: Battery Modeling. Artech House, 2015.

[155] Gregory L Plett. Battery management systems, Volume II: Equivalent-circuit methods. Artech House, 2015.

[156] S Ali Pourmousavi, Ratnesh K Sharma, and Babak Asghari. A framework for real-time power management of a grid-tied microgrid to extend battery lifetime and reduce cost of energy. In 2012 IEEE PES Innovative Smart Grid Technologies (ISGT), pages 1–8. IEEE, 2012.

[157] PowerTechSystems. Lithium iron phosphate life cycle, 2021. Accessed: 07.21.2022.

[158] Yuliya Preger, Heather M Barkholtz, Armando Fresquez, Daniel L Campbell, Benjamin W Juba, Jessica Romàn-Kustas, Summer R Ferreira, and Babu Chalamala. Degradation of commercial lithium-ion cells as a function of chemistry and cycling conditions. Journal of the Electrochemical Society, 167(12):120532, 2020.

[159] Elian Pusceddu, Behnam Zakeri, and Giorgio Castagneto Gissey. Synergies between energy arbitrage and fast frequency response for battery energy storage systems. Applied Energy, 283:116274, 2021.

[160] PV Magazine, 2022.

[161] Wei Qi, Yong Liang, and Zuo-Jun Max Shen. Joint planning of energy storage and transmission for wind energy generation. Operations Research, 63(6):1280–1293, 2015.

[162] Wei Qi and Zuo-Jun Max Shen. A smart-city scope of operations management. Production and Operations Management, 28(2):393–406, 2019.

[163] Giriraj Rathore, 2024.

[164] Eduardo Redondo-Iglesias, Pascal Venet, and Serge Pelissier. Efficiency degradation model of lithium-ion batteries for electric vehicles. IEEE Transactions on Industry Applications, 55(2):1932–1940, 2018.

[165] Igor Rychlik. A new definition of the rainflow cycle counting method. International Journal of Fatigue, 9(2):119–121, 1987.

[166] Apurba Sakti, Raanan Miller, and Fikile Brushett. What's cost got to do with it? An assessment of Tesla's Powerwall. MIT Energy Initiative, 2015. Accessed: 03.03.2023.

[167] Dirk Uwe Sauer and Heinz Wenzl. Comparison of different approaches for lifetime prediction of electrochemical systems—Using lead-acid batteries as example. Journal of Power Sources, 176(2):534–546, 2008.

[168] Herbert Scarf. The optimality of (S, s) policies in the dynamic inventory problem. Stanford University Press Stanford, 1959.

[169] Nicola Secomandi. Optimal commodity trading with a capacitated storage asset. Management Science, 56(3):449–467, 2010.

[170] Saeed Sepasi. Adaptive state of charge estimation for battery packs. PhD thesis, University of Hawai'i at Manoa, 2014.

[171] Sureth P Sethi. Optimal Control Theory: Applications to Management Science and Economics. Springer, 2022.

[172] Junaid Shah. Top 5: Largest BESS projects in the world in 2025. https://www.saurenergy.com, 2025. Accessed: 2025-12-03.

[173] Jeff Shepard. What are six key considerations when choosing a Li-ion battery chemistry? Battery Power Tips, 2022. Accessed: 03.03.2023.

[174] Yuanyuan Shi, Bolun Xu, Di Wang, and Baosen Zhang. Using battery storage for peak shaving and frequency regulation: Joint optimization for superlinear gains. IEEE Transactions on Power Systems, 33(3):2882–2894, 2017.

[175] Ziyou Song, Jianqiu Li, Jun Hou, Heath Hofmann, Minggao Ouyang, and Jiuyu Du. The battery-supercapacitor hybrid energy storage system in electric vehicle applications: A case study. Energy, 154:433–441, 2018.

[176] Isaac W Soro, Mustapha Nourelfath, and Daoud Ait-Kadi. Performance evaluation of multi-state degraded systems with minimal repairs and imperfect preventive maintenance. Reliability Engineering & System Safety, 95(2):65–69, 2010.

[177] S&P Global. Key Capture Energy installs 20-MW battery energy storage system in New York. S&P Global, 2019. Accessed: 03.03.2023.

[178] Lena Spitthoff, Paul R Shearing, and Odne Stokke Burheim. Temperature, ageing and thermal management of lithium-ion batteries. Energies, 14(5):1248, 2021.

[179] Qiuzhuang Sun, Piao Chen, Xin Wang, and Zhi-Sheng Ye. Robust condition-based production and maintenance planning for degradation management. Production and Operations Management, 32(12):3951–3967, 2023.

[180] Nur Sunar and Jayashankar M Swaminathan. Net-metered distributed renewable energy: A peril for utilities? Management Science, 67(11):6716–6733, 2021.

[181] Tanvir R Tanim, Matthew G Shirk, Randy L Bewley, Eric J Dufek, and Bor Yann Liaw. Fast charge implications: Pack and cell analysis and comparison. Journal of Power Sources, 381:56–65, 2018.

[182] Telegraph, 2024.

[183] George Willard Terborgh. Dynamic Equipment Policy. McGraw-Hill, 1949.

[184] Tesla. Megapack. https://www.tesla.com/megapack, 2026. Accessed: 2025-12-03.

[185] Gerald L Thompson. Optimal maintenance policy and sale date of a machine. Management Science, 14(9):543–550, 1968.

[186] Donald M Topkis. Minimizing a submodular function on a lattice. Operations Research, 26(2):305–321, 1978.

[187] Donald M Topkis. Supermodularity and complementarity. Princeton university press, 1998.

[188] Maryam Torkashvand, Abolfazl Khodadadi, Mehrdad Bagheri Sanjareh, and Muhammad H Nazary. A life cycle-cost analysis of li-ion and lead-acid besss and their actively hybridized esss with supercapacitors for islanded microgrid applications. IEEE Access, 8:153215–153225, 2020.

[189] Michiel AJ uit het Broek, Ruud H Teunter, Bram de Jonge, Jasper Veldman, and Nicky D Van Foreest. Condition-based production planning: Adjusting production rates to balance output and failure risk. Manufacturing & Service Operations Management, 22(4):792–811, 2020.

[190] Ciriaco Valdez-Flores and Richard M Feldman. A survey of preventive maintenance models for stochastically deteriorating single-unit systems. Naval Research Logistics, 36(4):419–446, 1989.

[191] Konstantina Valogianni, Wolfgang Ketter, John Collins, and Dmitry Zhdanov. Sustainable electric vehicle charging using adaptive pricing. Production and Operations Management, 29(6):1550–1572, 2020.

[192] Anton Vykhodtsev. Development of physics-based models of lithium-ion battery energy storage for power system techno-economic studies. Doctoral thesis, University of Calgary, 2023.

[193] Anton V Vykhodtsev, Darren Jang, Qianpu Wang, William Rosehart, and Hamidreza Zareipour. Physics-aware degradation model of lithium-ion battery energy storage for techno-economic studies in power systems. IEEE Transactions on Sustainable Energy, 15(1):316–327, 2023.

[194] Hongzhou Wang. A survey of maintenance policies of deteriorating systems. European Journal of Operational Research, 139(3):469–489, 2002.

[195] Sebastian Wodyk, Maciej Wieczorek, Paweł Witaszek, and Rafał Poliszkiewicz. Design and control of the hybrid lithium-ion/lead–acid battery. Energy Reports, 9:106–115, 2023.

[196] Wood Mackenzie. Can LFP technology retain its battery market share?, 2022. Accessed: 03.03.2023.

[197] Wood Mackenzie. Second life: Carmakers and storage startups get serious about reusing batteries, 2022. Accessed: 03.03.2023.

[198] Owen Q Wu and Roman Kapuscinski. Curtailing intermittent generation in electrical systems. Manufacturing & Service Operations Management, 15(4):578–595, 2013.

[199] Owen Q Wu, Roman Kapuscinski, and Santhosh Suresh. On the distributed energy storage investment and operations. Manufacturing & Service Operations Management, 25(6):2277–2297, 2023.

[200] Owen Q Wu, Derek D Wang, and Zhenwei Qin. Seasonal energy storage operations with limited flexibility: The price-adjusted rolling intrinsic policy. Manufacturing & Service Operations Management, 14(3):455–471, 2012.

[201] Owen Q Wu, Şafak Yücel, and Yangfang Zhou. Smart charging of electric vehicles: An innovative business model for utility firms. Manufacturing & Service Operations Management, 24(5):2481–2499, 2022.

[202] Guoping Xiong, Arpan Kundu, and Timothy S Fisher. Influence of temperature on supercapacitor performance. In Thermal Effects in Supercapacitors, pages 71–114. Springer, 2015.

[203] Bolun Xu. Dynamic valuation of battery lifetime. IEEE Transactions on Power Systems, 37(3):2177–2186, 2022.

[204] Bolun Xu, Alexandre Oudalov, Andreas Ulbig, Göran Andersson, and Daniel S Kirschen. Modeling of lithium-ion battery degradation for cell life assessment. IEEE Transactions on Smart Grid, 9(2):1131–1140, 2018.

[205] Bolun Xu, Yuanyuan Shi, Daniel S Kirschen, and Baosen Zhang. Optimal regulation response of batteries under cycle aging mechanisms. In 2017 IEEE 56th Annual Conference on Decision and Control (CDC), pages 751–756. IEEE, 2017.

[206] Bolun Xu, Yuanyuan Shi, Daniel S Kirschen, and Baosen Zhang. Optimal battery participation in frequency regulation markets. IEEE Transactions on Power Systems, 33(6):6715–6725, 2018.

[207] Bolun Xu, Jinye Zhao, Tongxin Zheng, Eugene Litvinov, and Daniel S Kirschen. Factoring the cycle aging cost of batteries participating in electricity markets. IEEE Transactions on Power Systems, 33(2):2248–2259, 2017.

[208] Bolun Xu, Jinye Zhao, Tongxin Zheng, Eugene Litvinov, and Daniel S Kirschen. Factoring the cycle aging cost of batteries participating in electricity markets. IEEE Transactions on Power Systems, 33(2):2248–2259, 2018.

[209] Candace Arai Yano and Hau L Lee. Lot sizing with random yields: A review. Operations Research, 43(2):311–334, 1995.

[210] Andre T Puati Zau, Mpho J Lencwe, SP Daniel Chowdhury, and Thomas O Olwal. A battery management strategy in a lead-acid and lithium-ion hybrid battery energy storage system for conventional transport vehicles. Energies, 15(7):2577, 2022.

[211] Zelestra. Abastible signs a long-term renewable energy PPA with Zelestra. https://zelestra.energy/en/news/abastibleppa, 2025. Accessed: 2025-12-03.

[212] Lei Zhang, Xiaosong Hu, Zhenpo Wang, Fengchun Sun, Junjun Deng, and David G Dorrell. Multiobjective optimal sizing of hybrid energy storage system for electric vehicles. IEEE Transactions on Vehicular Technology, 67(2):1027–1035, 2017.

[213] Yiling Zhang, Mengshi Lu, and Siqian Shen. On the values of vehicle-to-grid electricity selling in electric vehicle sharing. Manufacturing & Service Operations Management, 23(2):488–507, 2021.

[214] Zhong Zhang, Jianxue Wang, and Xiuli Wang. An improved charging/discharging strategy of lithium batteries considering depreciation cost in day-ahead microgrid scheduling. Energy Conversion and Management, 105:675–684, 2015.

[215] Yangfang Zhou, Alan Scheller-Wolf, Nicola Secomandi, and Stephen Smith. Electricity trading and negative prices: Storage vs. disposal. Management Science, 62(3):880–898, 2016.

[216] Yangfang Zhou, Alan Scheller-Wolf, Nicola Secomandi, and Stephen Smith. Managing wind-based electricity generation in the presence of storage and transmission capacity. Production and Operations Management, 28(4):970–989, 2019.

[217] Juner Zhu, Ian Mathews, Dongsheng Ren, Wei Li, Daniel Cogswell, Bobin Xing, Tobias Sedlatschek, Sai Nithin R Kantareddy, Mengchao Yi, Tao Gao, et al. End-of-life or second-life options for retired electric vehicle batteries. Cell Reports Physical Science, 2(8), 2021.

[218] Wenhua Zuo, Ruizhi Li, Cheng Zhou, Yuanyuan Li, Jianlong Xia, and Jinping Liu. Battery-supercapacitor hybrid devices: Recent progress and future prospects. Advanced Science, 4(7):1600539, 2017.